



ΕΘΝΙΚΟ ΜΕΤΣΟΒΙΟ ΠΟΛΥΤΕΧΝΕΙΟ

ΣΧΟΛΗ ΧΗΜΙΚΩΝ ΜΗΧΑΝΙΚΩΝ

ΔΙΑΤΜΗΜΑΤΙΚΟ ΠΡΟΓΡΑΜΜΑ ΜΕΤΑΠΤΥΧΙΑΚΩΝ ΣΠΟΥΔΩΝ

ΥΠΟΛΟΓΙΣΤΙΚΗ ΜΗΧΑΝΙΚΗ

ΜΕΤΑΠΤΥΧΙΑΚΗ ΕΡΓΑΣΙΑ

«Αλγόριθμοι Επίλυσης Ελαστοπλαστικών Συστημάτων»

ΤΣΟΤΟΥΛΙΔΗ ΒΑΣΙΛΙΚΗ

Επιβλέπων : Κωνσταντίνος Σπηλιόπουλος, Καθηγητής Ε.Μ.Π.

Αθήνα, Φεβρουάριος 2023



NATIONAL TECHNICAL UNIVERSITY OF ATHENS
POST GRADUATE PROGRAM IN COMPUTATIONAL MECHANICS

ALGORITHMS FOR SOLVING ELASTOPLASTIC SYSTEMS

Master Thesis submitted

By

Vasiliki Tsotoulidi

Supervisor: Konstantinos Spiliopoulos, Professor N.T.U.A.,

School of Civil Engineering

Athens, February 2023

Copyright © Βασιλική Τσοτουλίδη, 2023

Με επιφύλαξη παντός δικαιώματος

Απαγορεύεται η αντιγραφή, αποθήκευση σε αρχείο πληροφοριών, διανομή, αναπαραγωγή, μετάφραση ή μετάδοση της παρούσας εργασίας, εξ' ολοκλήρου ή τμήματος αυτής, για εμπορικό σκοπό, υπό οποιαδήποτε μορφή και με οποιοδήποτε μέσο επικοινωνίας, ηλεκτρονικό ή μηχανικό, χωρίς την προηγούμενη έγγραφη άδεια του συγγραφέα. Επιτρέπεται η αναπαραγωγή, αποθήκευση και διανομή για σκοπό μη κερδοσκοπικό, εκπαιδευτικής ή ερευνητικής φύσης, υπό την προϋπόθεση να αναφέρεται η πηγή προέλευσης και να διατηρείται το παρόν μήνυμα. Ερωτήματα που αφορούν στη χρήση της εργασίας για κερδοσκοπικό σκοπό πρέπει να απευθύνονται προς τον συγγραφέα.

Η έγκριση της μεταπτυχιακής διατριβής από τη Σχολή Πολιτικών Μηχανικών του Εθνικού Μετσόβιου Πολυτεχνείου δεν υποδηλώνει αποδοχή των απόψεων του συγγραφέα (Ν. 5343/32 αρ. 202 παρ. 2).

Copyright © Vasiliki Tsotoulidi, 2023

All Rights Reserved

Neither the whole nor any part of this master thesis may be copied, stored in a retrieval system, distributed, reproduced, translated, or transmitted for commercial purposes, in any form or by any means now or here after known, electronic, or mechanical, without the written permission from the author. Reproducing, storing, and distributing this thesis for non-profitable, educational or research purposes is allowed, without prejudice to reference to its source and to inclusion of the present text. Any queries in relation to the use of the present thesis for commercial purposes must be addressed to its author.

Approval of this master thesis by the School of Civil Engineering of the National Technical University of Athens (NTUA) does not constitute in any way an acceptance of the views of the author contained herein by the said academic organization (L. 5343/1932, art. 202).

Βασιλική Τσοτουλίδη (2023)

Αλγόριθμοι Επίλυσης Ελαστοπλαστικών Συστημάτων,
Εργαστήριο Στατικής και Αντισεισμικών Ερευνών, Εθνικό Μετσόβιο
Πολυτεχνείο, Αθήνα.

Vasiliki Tsotoulidi (2023)

Algorithms for Solving Elastoplastic Systems,
Institute of Structural Analysis and Antiseismic Research,
National Technical University of Athens, Greece

ΕΥΧΑΡΙΣΤΙΕΣ

Θα ήθελα καταρχήν να ευχαριστήσω όλους όσους συνέβαλαν με οποιονδήποτε τρόπο στην επιτυχή εκπόνηση αυτής της μεταπτυχιακής εργασίας. Θα πρέπει να ευχαριστήσω θερμά τον κύριο Κωνσταντίνο Σπηλιόπουλο Καθηγητή του τμήματος Πολιτικών Μηχανικών του Εθνικού Μετσόβιου Πολυτεχνείου για την επίβλεψη αυτής της μεταπτυχιακής εργασίας.

Ήταν πάντα διαθέσιμος να μου προσφέρει τις γνώσεις και την εμπειρία της για την βαθύτερη κατανόηση των βασικών εννοιών που διαπραγματεύεται η παρούσα μεταπτυχιακή διατριβή. Η επιμονή του, η καθοδήγηση του και κυρίως η ακεραιότητα του χαρακτήρα του αποτέλεσαν τους βασικούς πυλώνες για την ορθή διεκπεραίωση της εργασίας μου.

Επίσης, θα ήθελα να ευχαριστήσω θερμά τους καθηγητές της σχολής του Τμήματος Πολιτικών Μηχανικών του ΕΜΠ που με καθοδήγησαν τα δύο αυτά χρόνια του μεταπτυχιακού στο πολύ ενδιαφέρον και ευρύ αντικείμενο του πολιτικού μηχανικού.

Σε αυτό το σημείο θέλω να αναφέρω ανθρώπους, εκτός του στενού ακαδημαϊκού περιβάλλοντος, που υπήρξαν σημαντικοί πόλοι στη ζωή μου, προσδίδοντας την απαιτούμενη ισορροπία.

Βέβαια, το μεγαλύτερο ευχαριστώ το οφείλω στους γονείς μου, των οποίων η πίστη στις δυνατότητες μου αποτέλεσε αρωγός σε όλους τους στόχους και τα όνειρά μου. Την παρούσα εργασία την αφιερώνω στη μητέρα μου, η οποία δεν είναι πια εν ζωή.

Φεβρουάριος, 2023
Τσοτουλίδη Βασιλική

CONTENTS

ΕΥΧΑΡΙΣΤΙΕΣ	i
CONTENTS.....	ii
ΠΕΡΙΛΗΨΗ	viii
ABSTRACT	x
CHAPTER 1st - INTRODUCTION	1
1.1 Aim and scope.....	1
1.2 Structure of the dissertation.....	4
CHAPTER 2nd - GENERAL ELASTOPLASTIC CONSTITUTIVE MODEL – FORCE - BASED FIBER ELEMENT.....	5
2.1 The bilinear stress-strain relationship	5
2.2 Cyclic behavior.....	7
2.2.1 Example: hysteretic stress-strain history.....	13
2.3 The model of Menegotto and Pinto for steel reinforcement	15
2.3.1 Uniaxial material laws for concrete.....	18
2.3.2 The modified Kent-Park model.....	19
2.3.3 Force-based fiber element	21
2.3.4 Numerical integration	23
2.3.5 One - dimensional constitutive model	26
CHAPTER 3rd - Ansys Software- Problem Statement and Description..	68
3.1 Introduction.....	68
3.2 Problem Statement	68
3.3 3D Mesh of Classical Finite Elements	81
CHAPTER 4th – OPEN SOURCE CODE MSOLVE.....	84
4.1 General	84
4.1.1 Flow chart	84
4.1.2 Methodology of MSolve Software	88

CHAPTER 5th – BENCHMARK NUMERICAL EXAMPLES	
– RESULTS – COMPARISON	123
5.1 NUMERICAL EXAMPLES.....	123
CHAPTER 6th – CONCLUSIONS.....	158
6.1 GENERAL CONCLUSIONS	158
CHAPTER 7th – APPENDIX	164
7.1 CATALOGUE OF FIGURES.....	164
7.2 NOTATION	166
CHAPTER 8th - REFERENCES	167



ΕΘΝΙΚΟ ΜΕΤΣΟΒΙΟ ΠΟΛΥΤΕΧΝΕΙΟ
ΣΧΟΛΗ ΠΟΛΙΤΙΚΩΝ ΜΗΧΑΝΙΚΩΝ
ΕΡΓΑΣΤΗΡΙΟ ΣΤΑΤΙΚΗΣ ΚΑΙ ΑΝΤΙΣΕΙΣΜΙΚΩΝ ΕΡΕΥΝΩΝ

ΜΕΤΑΠΤΥΧΙΑΚΗ ΔΙΑΤΡΙΒΗ

«Αλγόριθμοι Επίλυσης Ελαστοπλαστικών Συστημάτων»

Βασιλική Τσοτουλίδη

Επιβλέπων: Καθηγητής Κωνσταντίνος Σπηλιόπουλος

ΠΕΡΙΛΗΨΗ

Σκοπός της παρούσας μεταπτυχιακής εργασίας είναι να περιγράψει λεπτομερώς τις αριθμητικές τεχνικές, οι οποίες χρησιμοποιούνται στη θεωρία και ανάλυση μικρών και μεγάλων παραμορφώσεων ελαστικών και ανελαστικών στερεών σωμάτων με τη μέθοδο των πεπερασμένων στοιχείων. Ιδιαίτερη έμφαση δίδεται στην παραγωγή και περιγραφή διάφορων καταστατικών νόμων των μοντέλων λόγω μη γραμμικότητας υλικού- με βάση τη φαινομενολογική ελαστικότητα, ελαστοπλαστικότητα και χρησιμοποιώντας διάφορες περιπτώσεις κριτηρίων διαρροής που χρησιμοποιούνται για τον προσδιορισμό του κατά πόσον ένα υλικό έχει αστοχήσει πλαστικά ή κατά πόσο έχει υπερβεί το πλαστικό όριο διαρροής, καθώς και για τις σχετικές αριθμητικές διαδικασίες και τα πρακτικά ζητήματα που προκύπτουν σε αυτές όταν επιλύονται υπολογιστικά. Το εύρος που εξετάζεται ξεκινάει από το βασικό απειροελάχιστο ισότροπο και συνεχίζει σε πιο περίπλοκες θεωρίες πεπερασμένων παραμορφώσεων, συμπεριλαμβανομένης και της ανισοτροπίας. Οι αριθμητικές αυτές τεχνικές υλοποιούνται με τη βοήθεια του λογισμικού του Ansys, καθώς και του open-source code λογισμικού, MSolve και παρατίθεται σύγκριση των δύο αναλύσεων με τα δύο αυτά λογισμικά.

Η αριθμητική επίλυση του μοντέλου επιλέχθηκε να επιλυθεί και με τη βοήθεια του λογισμικού MSolve, λόγω της πολυπλοκότητας αυτού του προβλήματος και τους αλγόριθμους βελτιστοποίησης, χρησιμοποιήθηκε αυτό το ισχυρό υπολογιστικό εργαλείο, που εξασφάλισε την επίλυση αρκετά πολύπλοκων προβλημάτων με την καλύτερη δυνατή ακρίβεια στα αποτελέσματα και το μικρότερο χρονικό κόστος για

την εύρεση των ζητούμενων μεγεθών. Τελικός στόχος ήταν να γίνει επικύρωση και επαλήθευση των τελικών αποτελεσμάτων για έλεγχο της ορθότητας τους και των παραδοχών που θεωρήθηκαν για την επίλυσή του.

Οι κύριες έννοιες που συνδέονται με τη φαινομενολογική πλαστικότητα που είναι ανεξάρτητη από τον χρόνο εισάγονται εδώ. Αρχικά, μελετούνται τα κριτήρια διαρροής Von Mises, Tresca, Mohr Coulomb, Drucker Prager, μαζί με τους διαδεδομένους κανόνες ροής πλαστιμότητας και νόμους κράτυνσης. Στη συνέχεια, εισάγουμε τις βασικές αριθμητικές μεθόδους που απαιτούνται για τη λύση πεπερασμένων στοιχείων των προβλημάτων αρχικής οριακής τιμής με μοντέλα ελαστοπλαστικών υλικών. Οι εφαρμογές του μοντέλου von Mises τόσο με ισότροπη όσο και με μικτή ισοτροπική/κινητική σκλήρυνση περιγράφονται λεπτομερώς. Έπειτα, η παρούσα μεταπτυχιακή εργασία εστιάζει στη λεπτομερή περιγραφή της εφαρμογής των βασικών μοντέλων πλαστικότητας με βάση τα κριτήρια διαρροής Tresca, Mohr–Coulomb και Drucker–Prager. Όλες αυτές οι περιπτώσεις κριτηρίων διαρροής έχουν εφαρμοστεί σε δοκίμιο κυβικού σχήματος πακτωμένο στη βάση του δοκιμίου και στη διεύθυνση $Z=0$, για $u_x = u_y = u_z = 0$. Η εξωτερική φόρτιση εφαρμόζεται στην άνω επιφάνεια του κύβου κατακόρυφα μέσω 100 μη γραμμικών βημάτων και είναι μονοτονική. Επίσης, οι ίδιες περιπτώσεις χρησιμοποιήθηκαν για να επιλυθεί και με ανακυκλιζόμενη φόρτιση επιβάλλοντας δηλαδή εξωτερική φόρτιση μέσω 400 μη γραμμικών βημάτων (ψευδοδυναμική ανάλυση), καθώς επίσης πραγματοποιήθηκαν και δυναμικές αναλύσεις του ίδιου μοντέλου τόσο για ισοτροπική όσο και για συνδυασμένη περίπτωση κράτυνσης του καταστατικού νόμου του υλικού και εφαρμόζοντας δυναμική τριγωνική δύναμη με χρονικό βήμα $dt=0.1sec$, καθώς και $dt=0.05sec$, με εφαρμογή του μέγιστου κατά απόλυτη τιμή φορτίου τη χρονική στιγμή $T1=10sec$, εκτελώντας ελεύθερη ταλάντωση τη χρονική στιγμή $T2=20sec$ και ολοκλήρωση της ανάλυσης τη χρονική στιγμή $T3=30sec$. Οι δύο αυτές περιπτώσεις δυναμικής φόρτισης, όπου υπάρχει αλλαγή μόνο στο χρονικό βήμα, εξετάστηκαν με σκοπό να συγκριθεί η ακρίβεια των δύο λύσεων χρησιμοποιώντας το λογισμικό ανοιχτού κώδικα MSolve και το εμπορικό λογισμικό Ansys.

Για την εκπόνηση της μεταπτυχιακής διατριβής, στη συνέχεια παρουσιάζονται βασικοί μονοαξονικοί καταστατικοί νόμοι σκυροδέματος και χάλυβα. Τα υλικά αυτά υιοθετούνται συνήθως όταν πρόκειται να αξιολογηθεί η ικανότητα ενός εμβαδού διατομής ή είναι ενσωματωμένα σε στοιχείο δοκού πολυστρωματικής θεώρησης. Ουσιαστικά μελετώνται μη γραμμικές αναλύσεις σε καταστατικούς νόμους υλικών, οι οποίοι είναι κατάλληλοι για την προσομοίωση της κυκλικής απόκρισης χάλυβα και σκυροδέματος για την περίπτωση τρισδιάστατων στοιχείων δοκού πολυστρωματικής θεώρησης βασιζόμενα στη μέθοδο των δυνάμεων. Παρουσιάζουμε πρώτα το διγραμμικό μοντέλο, η οποία είναι η πιο απλή θεώρηση για μοντελοποίηση του ενισχυτικού υλικού του δομικού χάλυβα, ενώ δίνει την απαραίτητη ρύθμιση για την παρουσίαση των θεμελιωδών ιδιοτήτων μιας μονοαξονικής ($\sigma - \epsilon$) σχέσης. Στη συνέχεια, χρησιμοποιούνται πιο προχωρημένοι καταστατικοί νόμοι υλικών για τον χάλυβα ως ενισχυτικό υλικό, οι οποίοι είναι το κριτήριο διαρροής Masing, το Ramberg Osgood, Menegotto Pinto with Filippou isotropic hardening (steel model with damage modulus). Για τις προσομοιώσεις των ινών σκυροδέματος επιλέχθηκε το τροποποιημένο μοντέλο Kent and Park[8], που είναι μια αρκετά απλή σχέση ικανή να παρέχει επαρκή αποτελέσματα για τις

περισσότερες εφαρμογές αντισεισμικής μηχανικής. Συγκεκριμένα, τα μοντέλα που μελετήθηκαν είναι ένας τρισδιάστατος πρόβολος πακτωμένος στη διεύθυνση $Z=0$, για $u_x = u_y = u_z = 0$, τοποθετώντας 5 ίνες χάλυβα στην άνω επιφάνεια και 25 ίνες χάλυβα στην κάτω επιφάνεια. Η διακριτοποίηση αποτελείται από δύο στοιχεία. Η εξωτερική φόρτιση είναι μονοτονική και μονοαξονική εφαρμοζόμενη κατακόρυφα στην άνω επιφάνεια του προβόλου μέσω 20 και 100 βημάτων αντίστοιχα, καθώς και στην περίπτωση της διαξονικής φόρτισης μέσω 20 και 100 βημάτων ομοίως με την προηγούμενη περίπτωση ως τα υπόλοιπα γεωμετρικά χαρακτηριστικά. Ακόμη μελετήθηκε και η περίπτωση της αμφίπακτης δοκού και πάλι με τα ίδια γεωμετρικά χαρακτηριστικά και συννοριακές συνθήκες για τη μονοτονική και μονοαξονική φόρτιση και επιπρόσθετα επιλύθηκαν και οι περιπτώσεις ανακυκλιζόμενης φόρτισης. Οι επιλύσεις έχουν πραγματοποιηθεί χρησιμοποιώντας το λογισμικό MSolve καθώς και το εμπορικό λογισμικό Ansys προκειμένου να συγκριθούν οι δύο λύσεις τόσο στη μονοτονική όσο και στην ανακυκλιζόμενη φόρτιση.

Τέλος, μελετήθηκε ο καταστατικός νόμος ελαστοπλαστικών προμοιωμάτων του Kanvadas and Amorosi, με σκοπό την περιγραφή της μηχανικής συμπεριφοράς των εδαφικών υλικών ανεξαρτήτως του ρυθμού παραμόρφωσης. Η εργαστηριακή διερεύνηση των εδαφικών υλικών φανερώνουν μια έντονα μη-γραμμική, ανισότροπη συμπεριφορά. Αρκετές φορές ενδέχεται να εμφανίσουν χαλάρωση ή ακόμα και κατάρρευση της δομής του εδαφικού ιστού. Η μηχανική συμπεριφορά των γεωυλικών διερευνήθηκε αρχικά σε εργαστηριακό επίπεδο σε αναμοχλευμένα εδαφικά υλικά (με ποσοστό υγρασίας κοντά στο όριο υδαρότητας). Επιπρόσθετα μηχανικά χαρακτηριστικά προτάθηκαν με σκοπό της βελτίωσης της προβλεπόμενης συμπεριφοράς των καταστατικών προσομοιωμάτων, εντοπίζοντας τόσο στην περιγραφή της ανισοτροπίας όσο και στην έντονα ανελαστική συμπεριφορά κατά την διάρκεια ανακυκλικών φορτίσεων. Συγκεκριμένα, τα μοντέλα που μελετήθηκαν είναι ένα μοντέλο κυβικού σχήματος πακτωμένο στη βάση του, χρησιμοποιώντας σαν πεπερασμένα στοιχεία τα εξαεδρικά στοιχεία οχτώ κόμβων. Η εξωτερική φόρτιση που εξετάζεται είναι αρχικά μονοτονική κατακόρυφη και εφαρμοζόμενη στην άνω επιφάνεια του μοντέλου μέσω 100 βημάτων (load steps), καθώς και στην περίπτωση της ανακυκλιζόμενης φόρτισης κατακόρυφη και εφαρμοζόμενη στην άνω επιφάνεια του κύβου μέσω 400 βημάτων (load steps). Οι επιλύσεις έχουν πραγματοποιηθεί χρησιμοποιώντας το λογισμικό MSolve καθώς και το εμπορικό λογισμικό Ansys προκειμένου να συγκριθούν οι δύο λύσεις τόσο στη μονοτονική όσο και στην ανακυκλιζόμενη φόρτιση.

Λέξεις κλειδιά

Καταστατικές σχέσεις, Von Mises isotropic/kinematic hardening, Tresca, Mohr-Coulomb, Drucker-Prager, fiber3Dbeam, Spacone-Filippou Masing, διγραμμικό υλικό Ramberg-Osgood, Menegotto Pinto, Kent and Park



NATIONAL TECHNICAL UNIVERSITY OF ATHENS

SCHOOL OF CIVIL ENGINEERING

INSTITUTE OF STRUCTURAL ANALYSIS AND ANTISEISMIC RESEARCH

MASTER THESIS

«ALGORITHMS FOR SOLVING ELASTOPLASTIC SYSTEMS»

VASILIKI TSOTOLIDI

SUPERVISOR: PROFESSOR KONSTANTINOS SPILIOPOULOS

ABSTRACT

The purpose of this master's thesis is to describe in detail the numerical techniques used in the theory and analysis of small deformations of elastic and inelastic solids using the finite element method. Particular emphasis is placed on the derivation and description of various constitutive laws of the models due to material nonlinearity - based on phenomenological elasticity, elastoplasticity by using various cases of yield criteria where it is determined whether a material has fractured or exceeded yield strength - as well as for the associated numerical procedures and the practical issues that arise in them when solved computationally. The range covered goes from basic infinitesimal isotropic to more sophisticated finite strain theories, including anisotropy. These numerical techniques are implemented with the aid of the commercial software packages, Ansys Workbench, as well as the open-source software code, MSolve, and a comparative study and analysis is presented between Ansys Workbench and MSolve. The results were plotted graphically. For the finite element simulations in nonlinear constitutive relations, the fiber beam - column model for nonlinear analysis of reinforced concrete structures, the commercial software package Ansys Workbench was selected. Due to the complexity of the problem of material nonlinearity and the description of nonlinear constitutive relations as well as the cyclic loading incorporating plasticity and the Bauschinger effect, a powerful computational tool was used, MSolve software, which solved quite complex problems with higher accuracy in the results and less computational time and cost than other commercial software packages.

The main concepts associated with time-independent phenomenological plasticity are introduced here. First, the Von Mises, Tresca, Mohr Coulomb, Drucker Prager yield criteria are studied, along with the popular plastic flow rules and hardening laws. Then, we introduce the basic numerical methods required for the finite element solution of initial boundary value problems with elastoplastic material models. Applications of the von Mises model with both isotropic and mixed isotropic/kinematic hardening are described thoroughly. This master's thesis focuses on the detailed description of the application of the plasticity models based on the Tresca, Mohr–Coulomb and Drucker–Prager yield criteria. All these cases of yield criteria have been applied to a cubic specimen fixed at the base of the specimen and in the $Z=0$ direction, for $u_x = u_y = u_z = 0$. The external loading is applied to the top surface of the cube vertically through 100 non-linear steps and is monotonic. Also, the same cases were used to solve with cyclic loading i.e. imposing external loading through 400 non-linear steps (pseudodynamic analysis), as well as dynamic analyzes of the same model were carried out for both isotropic and combined case of material constitutive law hardening and applying dynamic triangular force with time step $dt=0.1\text{sec}$, as well as $dt=0.05\text{sec}$, applying the maximum absolute value load at time $T1=10\text{sec}$, performing free oscillation at time $T2=20\text{sec}$ and completing the analysis at time moment $T3=30\text{sec}$. These two cases of dynamic loading, where there is only a change in the time step, were examined in order to compare the accuracy of the two solutions using the open-source software MSolve and the commercial software Ansys.

Basic uniaxial constitutive laws of concrete and steel are then presented for the development of the master's thesis. These materials are usually adopted when the capacity of a cross-sectional area is to be evaluated or incorporated into a multi-layer beam element. Essentially, nonlinear analysis in constitutive laws of materials are studied, which are suitable for simulating the cyclic response of steel and concrete for the case of three-dimensional force-based fiber beam elements. We first present the bilinear model, which is the simplest consideration for modeling the reinforcing material of structural steel, while providing the necessary setup to present the fundamental properties of a uniaxial ($\sigma - \epsilon$) relationship. Then, more advanced constitutive laws of materials are used for steel for the case of fiber beam elements, which is the Masing yield criterion, Ramberg Osgood, Menegotto Pinto with Filippou isotropic hardening (steel model with damage modulus). For the simulations of the concrete fibers we present the modified Kent and Park [] model, which is a rather simple relationship able to provide sufficient results for most earthquake engineering applications. Specifically, the studied models are a three-dimensional cantilever fixed in the $Z=0$ direction, for $u_x = u_y = u_z = 0$., with 5 steel fibers on the upper surface and 25 steel fibers on the lower surface. Discretization consists of two elements. The external loading is monotonic and uniaxial applied vertically to the upper surface of the cantilever through 20 and 100 steps respectively, as well as in the case of biaxial loading through 20 and 100 steps similarly to the previous case as the rest of the geometric characteristics. The case of the clamped beam was also studied with the same geometric characteristics and boundary conditions for monotonic and uniaxial loading, and additionally the cases of cyclic loading were also solved. The solutions have been carried out using MSolve software as well as the commercial Ansys

software in order to compare the two solutions under both monotonic and cyclic loading.

Finally, the constitutive law of elastoplastic models of Kavvadas and Amorosi was studied, in order to describe the mechanical behavior of soil materials regardless of the rate of deformation. The experimental investigation of soil materials shows a strongly non-linear, anisotropic behavior. Several times they may show relaxation or even collapse of the soil tissue structure. The mechanical behavior of geomaterials was initially investigated at the experimental level in disturbed soil materials (with a moisture content close to the water limit). Additional mechanical features were proposed in order to improve the predicted behavior of the simulations as far as the constitutive relations are concerned, identifying both the description of the anisotropy and the strongly inelastic behavior during cyclic loading. In particular, the models studied are a cubic model fixed at its base, using eight-node hexahedral elements as finite elements. The external loading considered is initially monotonic vertical and applied to the upper surface of the model through 100 load steps, as well as in the case of the cyclic loading vertical and applied to the upper surface of the cube through 400 load steps. The solutions have been carried out using MSolve software as well as the commercial Ansys software so as to compare the two solutions under both monotonic and cyclic loading.

Keywords

Constitutive relations, Von Mises isotropic/kinematic hardening, Tresca, Mohr-Coulomb, Drucker-Prager, fiber3Dbeam, Spacone-Filippou Masing, bilinear hardening, Ramberg-Osgood, Menegotto Pinto, Kent and Park

CHAPTER 1st

1. INTRODUCTION

1.1 Aim and scope

Recent advances in the field of computation technology and increased requirements in the field of earthquake engineering have led to the development and implementation of highly efficient beam-column elements capable of tracking the hysteretic behavior of Reinforced Concrete (RC) structures. The aim of this dissertation is to model beam-column behavior in a computationally effective manner, reliably revealing the overall response of RC members subjected to cyclic loading. In this respect, plasticity and damage are considered in the predominant longitudinal direction allowing for the derivation of a fiber finite element model.

Constitutive relationships are the heart of material nonlinear analysis. These models provide the mathematical relationships that describe the material and obviously govern the nonlinear analysis. Constitutive relationships is a wide topic and often their mathematical formulation is too complicated since the actual response of a material may also be complicated. The choice of a material model depends on the structure and the type of finite elements chosen to discretized the structure. For example, if three-dimensional solid elements are chosen, the material models should be able to consider all components of the stress tensor. On the other hand, fiber-based beam elements are able to account for only one component of the stress tensor, the longitudinal stress, σ_x , which is parallel to the axis of the element. When it comes to beam elements, lumped plasticity elements are very commonly adopted in engineering practice. In the case of lumped plasticity elements, the constitutive behaviour is expressed through moment-rotation (or moment-curvature) relationships. In this chapter we focus on uniaxial stress-strain ($\sigma - \epsilon$) relationships suitable for fiber elements or section analysis. In the following chapters, basic uniaxial constitutive relationships are presented. These materials are commonly adopted when assessing the capacity of a cross-section or are embedded in fiber beam-column elements. Rather, than discussing all materials available, the aim of the following chapters is to present the underlying concepts and then introduce materials suitable for simulating the cyclic response of steel and concrete. Note that the materials discussed always receive as input the strain ϵ and give as output the stress σ ($\sigma = f(\epsilon)$). Although there is no fundamental restriction to have models of the $\epsilon = f(\sigma)$ form, the structure of FE software make the use of such materials considerably and unnecessarily more complicated. In the sections that follow, we first present the

bilinear model that is available in every nonlinear analysis software. This model is the most common choice when it comes to modelling reinforcing or structural steel, while it gives the necessary setting for presenting the fundamental properties of a uniaxial ($\sigma - \epsilon$) relationship. As a more advance material for steel, we also discuss the model of Menegotto and Pinto []. For the simulations of the concrete fibers we present the modified Kent and Park] model, which is a rather simple relationship able to provide sufficient results for most earthquake engineering applications. . Basically, the theory of plasticity is concerned with solids that, after being subjected to a loading programme, may sustain permanent (or plastic) deformations when completely unloaded. In particular, this theory is restricted to the description of materials (and conditions) for which the permanent deformations do not depend on the rate of application of loads and is often referred to as rate-independent plasticity. Materials whose behaviour can be adequately described by the theory of plasticity are called plastic (or rate-independent plastic) materials. A large number of engineering materials, such as metals, concrete, rocks, clays and soils in general, may be modelled as plastic under a wide range of circumstances of practical interest. The origins of the theory of plasticity can be traced back to the middle of the nineteenth century and, following the substantial development that took place, particularly in the first half of the twentieth century, this theory is today established on sound mathematical foundations and is regarded as one of the most successful phenomenological constitutive models of solid materials. The remainder of the chapters focuses on the detailed description of the plasticity models most commonly used in engineering analysis: the models of Tresca, von Mises, Mohr–Coulomb and Drucker–Prager. The corresponding yield criteria are described in the next chapters. Then, plastic flow rules and hardening laws are addressed, respectively, in the following sections. Obviously, due to the mathematical complexity of such constitutive theories, an exact solution to boundary value problems of practical engineering interest can only be obtained under very simplified conditions. The existing analytical solutions are normally restricted to perfectly plastic models and are used for the determination of limit loads and steady plastic flow of bodies with simple geometries (Chakrabarty, 1987; Hill, 1950; Lubliner, 1990; Prager, 1959; Skrzypek, 1993). The analysis of the behaviour of elastoplastic structures and soils under more realistic conditions requires the adoption of an adequate numerical framework capable of producing approximate solutions within reasonable accuracy. The Finite Element Method is by far the most commonly adopted procedure for the solution of elastoplastic problems. Since the first reported applications of finite elements in plasticity in the mid-1960s, a substantial development of the related numerical techniques has occurred. Today, the Finite Element Method is regarded as the most powerful and reliable tool for the analysis of solid mechanics problems involving elastoplastic materials and is adopted by the vast majority of commercial software packages for elastoplastic stress analysis.

Practical application of the theory and procedures introduced, including a complete description of the algorithms and corresponding subroutines of the Ansys program and open source code Msolve, is then made to the particular case of the von Mises

model with nonlinear isotropic hardening. The choice of this model is motivated here by the simplicity of its computational implementation. A set of numerical examples is also presented. Further application of the theory is made at the end of the chapters to a mixed isotropic/kinematic hardening version of the von Mises model. This model is also included in the Ansys program and Msolve. Application to the Tresca, Mohr–Coulomb and Drucker–Prager models is also examined in this master thesis.

Some general schemes for numerical integration of elastoplastic constitutive equations have been reviewed together with related issues such as the computation of consistent tangent operators and error analysis. To illustrate such concepts, the von Mises model – the simplest of the models discussed in this master thesis – has been used as an example and the corresponding implicit elastic predictor/return-mapping algorithm, together with the associated consistent tangent, have been derived in detail for the isotropic and mixed hardening cases. Namely, the models discussed here are: the Von Mises model with isotropic, kinematic and mixed hardening law with nonlinear constitutive equations (tabular data) the Tresca model, the Mohr-Coulomb model and the Drucker Prager model. The associative plastic flow rule is adopted for the Tresca model whereas, for the Mohr–Coulomb and Drucker–Prager models, the generally non-associated laws are considered. The algorithms for integration of the corresponding elastoplastic constitutive equations derived here are specialisations of the elastic predictor/return mapping scheme based on the fully implicit discretisation of the plastic corrector equations. The associated consistent tangent moduli are also derived in detail and an error analysis based on iso-error maps is presented for each model considered. We remark that the only new concept concerns the computational treatment of singularities (corners) in the yield surface. At the beginning of each of the main sections, a table has been added indicating the location of flowcharts, pseudo-code and MSolve source code of the relevant computational procedures as well as iso-error maps for the particular material model of interest. Applications of the numerical procedures derived in the main sections are illustrated in the last section by means a comprehensive set of benchmarking numerical examples.

Finally, Ansys Workbench was used in this work. Ansys Workbench is a specialized software that is widely used for finite element analysis and offers comprehensive solutions to a wide range of engineering problems. At the same time, due to the complexity of the problem, a powerful computational tool was used, and in particular an open source code that ensured better accuracy in the results with less computational time and cost to find the required quantities and it is MSolve software.

1.2 Structure of the dissertation

In this section, it is presented the structure of the master thesis and the chapters are described concisely as follows:

- **Chapter 2^o : General elastoplastic constitutive model and Force-based fiber element**
- **Chapter 3^o : Ansys Software- Problem Statement and Description**
- **Chapter 4^o : Open source code MSolve**
- **Chapter 5^o : Benchmark Numerical Examples -Results- Comparison Of The Results**
- **Chapter 6^o : Conclusions**
- **Chapter 7^o : Appendix**

CHAPTER 2nd

2. GENERAL ELASTOPLASTIC CONSTITUTIVE MODEL – FORCE - BASED FIBER ELEMENT

2.1 The bilinear stress-strain relationship

Basic material models, such as the bilinear model, can be seen as a set of rules that determine: (i) the elastic behaviour, (ii) when the material yields (yield criterion), (iii) the behaviour of the material in the inelastic range, after yielding (flow rule), and (iv) rules regarding the behaviour of the material under cyclic load reversals. For a simple bilinear model, the behaviour prior yielding is described by Hooke's law with an elastic slope equal to the modulus of elasticity E . The yield point is defined by the yield stress σ_y or the yield strain $\epsilon_y = \sigma_y/E$. After yielding, i.e. when $\sigma > \sigma_y$, the slope of the monotonic $\sigma - \epsilon$ curve is that of the tangent modulus, E_T . When the tangent modulus is equal to zero ($E_T = 0$), the material is called elastic-perfectly plastic. The main advantage of the bilinear model is that its parameters can be easily obtained from simple lab tests, or can be estimated from the nominal material properties¹. The $\sigma - \epsilon$ relationship of the bilinear model is shown in the following figure. The tangent, post-yield modulus E_T is a function of the initial modulus of elasticity E and is defined with the aid of the hardening ratio b :

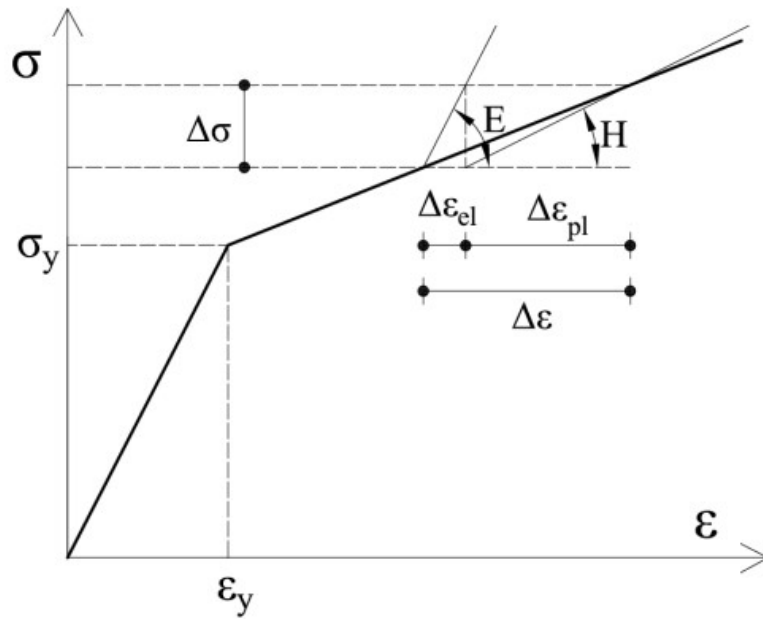
$$E_T = bE$$

thus when $b = 0$ the material is elastic-perfectly plastic. Instead of the hardening ratio b , often the post yield stiffness is determined with the aid of the hardening ratio H . The hardening ratio H is defined as the slope of the curve of the plastic strain ϵ_{pl} versus stress σ . The plastic strain ϵ_{pl} is equal to $\epsilon_{pl} = \epsilon - \epsilon_y$, while $\epsilon_{pl} = 0$ if the material is elastic. Hence, we define:

$$\sigma = H\epsilon_{pl}$$

When the material yields, $\epsilon \geq \epsilon_y$ and $\epsilon_{pl} \neq 0$, a small increment of the strain $\Delta \epsilon$ will produce a stress increment $\Delta \sigma$:

$$\Delta \sigma = E_T \Delta \epsilon$$



Furthermore, the total strain consists of two parts, the elastic and the inelastic strain:

$$\varepsilon = \varepsilon_{el} + \varepsilon_{pl}$$

Then, we have:

$$\frac{\Delta\sigma}{E_T} = \frac{\Delta\sigma}{E} + \frac{\Delta\sigma}{H}$$

and we obtain:

$$H = \frac{E_T}{1-b} = \frac{b}{1-b}E$$

or

$$E_T = E \left(1 - \frac{E}{E-H} \right)$$

The expressions above provide the relationship between E_T , b and H . Once one of these parameters is known we can calculate the rest of them. This is useful since although all software offer the option of a bilinear model, the implementation may be differ and either E_T , b or H may have to be provided as input. Some very useful relationships relating $\Delta\varepsilon$ with $\Delta\sigma$ and $\Delta\varepsilon_{pl}$ can be further derived:

$$\begin{aligned}
\Delta\sigma &= E\Delta\varepsilon_{el} \Leftrightarrow \\
&= E(\Delta\varepsilon - \Delta\varepsilon_{pl}) \Leftrightarrow \\
&= E\Delta\varepsilon - \frac{E}{H}\Delta\sigma \Leftrightarrow \\
\Delta\sigma &= \frac{EH}{E+H}\Delta\varepsilon
\end{aligned}$$

and

$$\Delta\varepsilon_{pl} = \frac{\Delta\sigma}{H} = \frac{E}{E+H}\Delta\varepsilon$$

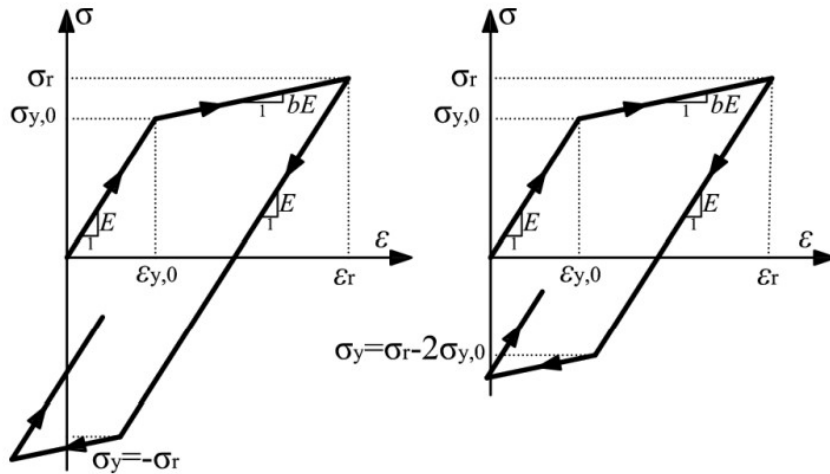
Note that both E and H were assumed linear, but this is merely a simplifying assumption, suitable for many applications. The bilinear stress-strain relationship is also the basis of many constitutive formulations. Another common relationship is the Ramberg-Osgood [1] material. This material is also used extensively and is based on the expression:

$$\varepsilon = \varepsilon_y + \varepsilon_{pl} = \frac{\sigma}{E} + \alpha \left(\frac{\sigma}{\sigma_y} \right)^\beta$$

where α and β are model constants to be calibrated through experimental tests. This expression is nonlinear and hence may be less appealing compared to the bilinear model.

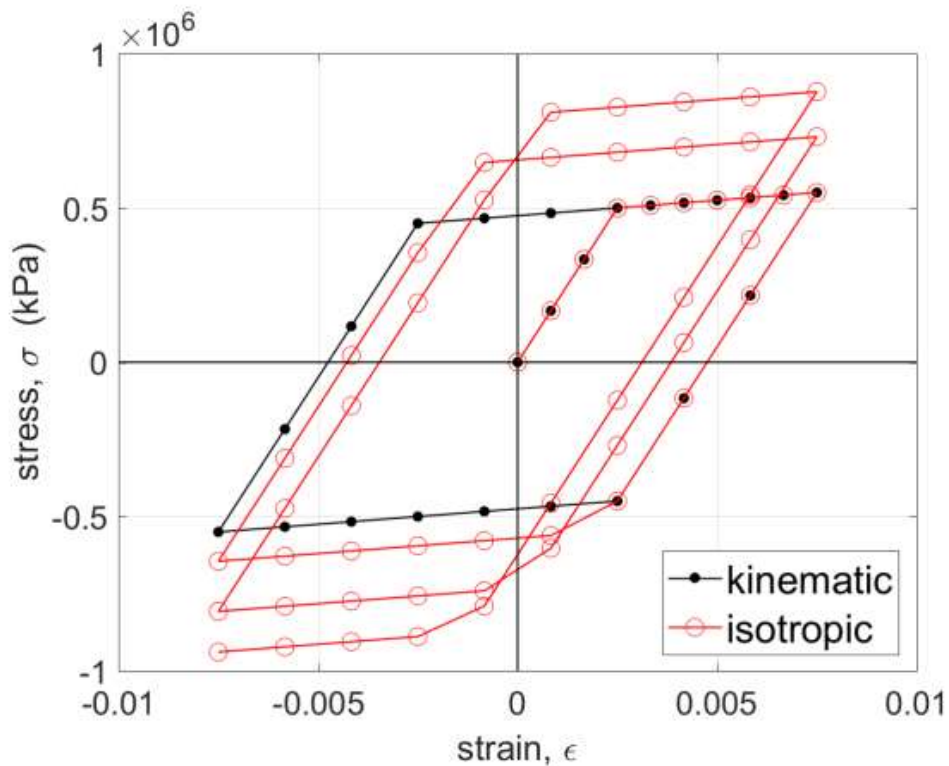
2.2 Cyclic behavior

When the material is in the elastic range ($|\varepsilon| \leq \varepsilon_y$), all strains are reversible, meaning that unloading is also elastic. This means that the material has a “perfect” memory and will unload following the same path as in the loading case. However, after yielding only the elastic part of the strain can be recovered. This implies that once the strain exceeds the yield strain, if unloading occurs then the material will follow a path parallel to the elastic path with slope E. Moreover, once further loading in the opposite direction, the material will yield again, but at a stress lesser than the initial yield stress σ_y . The phenomenon of yielding at a stress less than σ_y when loading in the opposite direction, is known as Bauschinger effect and is a fundamental property of steel materials. Common approaches for modelling the cyclic behaviour of steel materials include the kinematic and the isotropic hardening model. The two models are shown in the following figure. When a pure isotropic material is adopted, the Bauschinger effect is neglected and the yield stress of the last reversal point is used to obtain the yield stress of the subsequent cycles. Isotropic hardening results to constantly increasing the size of the hysteretic loop. On the other hand, kinematic hardening assumes that when loading in the opposite direction, the new yield stress $\bar{\sigma}_y$ is obtained if we subtract from the stress at the point of unloading or the quantity $2\sigma_y$. The pure kinematic hardening model does not change the size of the hysteretic loop but simply translates its centre. A model that combines kinematic and isotropic hardening is a mixed model. The three models are discussed in detail in the sections that follow, but it is the kinematic model that is most commonly adopted for structural and earthquake engineering applications.



Isotropic (left) and kinematic (right) hardening.

The same strain history is applied and the two models produce different stress-strain hysteretic loops. Although in the case of the kinematic model the shape of loop remains unaltered and bounded, in the isotropic model the loops expand and become bigger in every cycle.



Example: stress-strain hysteretic loop using the bilinear model with pure kinematic and pure isotropic hardening.

According to the isotropic hardening model the yield stress $\bar{\sigma}_y$ of every cycle depends on the accumulated plastic strain $\bar{\epsilon}_{pl}$:

$$\bar{\sigma}_y = \sigma_{y0} + H\bar{\epsilon}_{pl}$$

Therefore, the radius of the yield surface increases as function of the effective plastic strain and is proportional to the plastic modulus. When a stress reversal occurs, the yield stress will be:

$$\bar{\sigma}_y = -\sigma_r$$

In order to implement the model, let's assume that at time i the state of the material is known, as we can see it from the following picture. This implies that

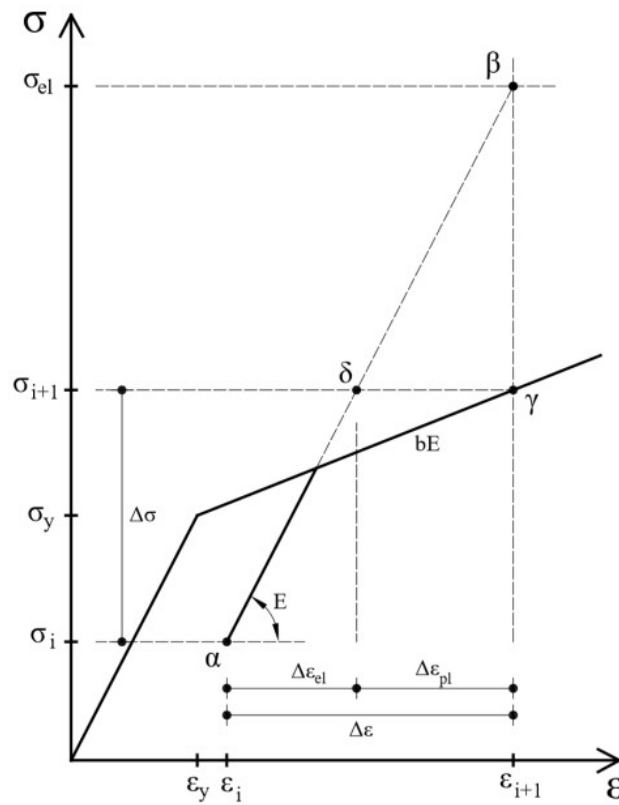


Figure 2.2.1: Elastic trial step and calculation of stress σ_{i+1} .

the strain ε_i and the stress σ_i are known and that we want to determine the stress σ_{i+1} after a strain increment $\Delta\varepsilon$. We also know the fundamental properties of the material, i.e. its yield stress σ_{y0} and the moduli E and H . Furthermore, we define $\varepsilon_{pl,i}$ as a state variable, meaning that it is a variable that is stored and updated in every step. The implementation in a computer code is simple and includes an elastic trial step in order to calculate the elastic stress σ_{el} :

$$\sigma_{el,i} = \sigma_i + E\Delta\varepsilon$$

We also calculate the quantity q :

$$q = |\sigma_{el,i}| - \sigma_{y,i}$$

where

$$\sigma_{y,i} = \sigma_{y,0} + H\varepsilon_{pl,i} = \sigma_{y,0} + \frac{bE}{1-b}\varepsilon_{pl,i}$$

If $q \leq 0$ the material is elastic and it is plastic when $q > 0$. In the elastic case, we simply set $\sigma_i = \sigma_{el,i}$ and $\varepsilon_{pl,i+1} = \varepsilon_{pl,i}$. If the material is plastic, we update the plastic strain and the stress at $i+1$ as:

$$\begin{aligned}\Delta\varepsilon_{pl} &= \frac{q}{E+H} = \frac{q(1-b)}{E} \\ \sigma_{i+1} &= \sigma_{el,i} - E\Delta\varepsilon_{pl,i}\end{aligned}$$

The equation above provides the value of σ_{i+1} and is schematically explained in Figure 2.2.1. Supposing that the state of the material is known at point (α) which has coordinates ε_i, σ_i . After the elastic increment, we calculate the total elastic stress σ_{el} which is shown as (β) in Figure 2.2.1. If the material is elastic, the elastic stress is the correct stress σ_{i+1} , otherwise the elastic stress is corrected subtracting the quantity $E\Delta\varepsilon_{pl}$, which moves us back to point (δ) (Fig. 2.2.1). The stress value at (δ) is σ_{i+1} , equal to the correct stress of point γ that has coordinates $\varepsilon_{i+1}, \sigma_{i+1}$. Furthermore, the plastic strain ε_{pl} is updated ($\varepsilon_{pl,i+1} = \varepsilon_{pl,i} + \Delta\varepsilon_{pl}$) and stored. Finally, the tangent modulus is updated as:

$$E_m = \frac{\partial\sigma}{\partial\varepsilon} = \begin{cases} E, & q \leq 0 \\ bE, & q > 0 \end{cases}$$

The bilinear model with pure kinematic hardening is often used for modelling the cyclic behaviour of steel structures or for modelling the steel reinforcement, since it implicitly considers the Bauschinger effect. According to the kinematic hardening model, in every cycle the yield stress $\bar{\sigma}_y$ depends on the last reversal point σ_r :

$$\bar{\sigma}_y = \sigma_r - 2\sigma_{y0}$$

In the kinematic hardening model, the elastic range remains constant and its center moves parallel to the hardening curve. The equation above implies that the maximum and the minimum stress values lie on two lines parallel with a line with slope equal to bE that passes through the origin. This means that the hysteretic loop will always have the same size and shape and will translate within the bounds of these two lines.

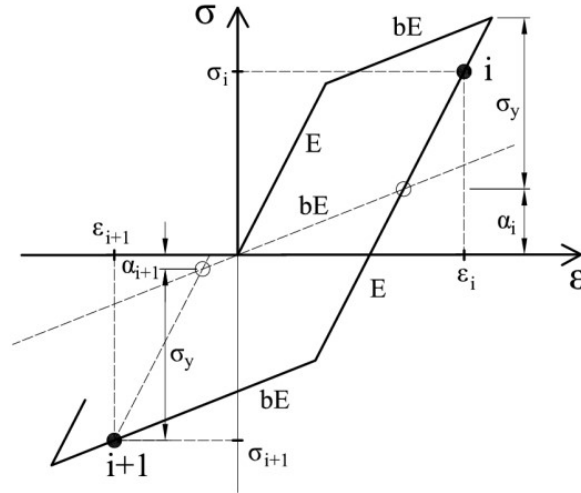


Figure 2.2.2: Bilinear model with kinematic hardening: definition of the back stress α , (center of the elastic region).

In order to implement the model, in every load increment we define the “center” of the elastic region with the aid of a stress value α also termed “back-stress”. The definition of α is shown in Figure 2.2.2 for two different pairs of (ϵ, σ) values. Therefore, the center of the loop lies on a straight line that passes from the origin and its location is updated in every increment using the expression:

$$\begin{aligned}\alpha_{i+1} &= \alpha_i + \text{sgn}(\eta_i) H \Delta \epsilon_{pl,i} \\ &= \alpha_i + \text{sgn}(\eta_i) \frac{bE}{1-b} \Delta \epsilon_{pl,i}\end{aligned}$$

where $\text{sgn}(\eta_i)$ is used to take into consideration the correct sign and is based on η , a parameter discussed a few lines below. We can otherwise calculate α_i if the stress σ_i and the strain ϵ_i are known. When the material is plastic, α_i is equal to the current stress minus the yield stress, i.e. $\alpha_i = \sigma_i - \sigma_{y,0}$ (Fig. 2.2.2, point (i+1)). Furthermore, α_i lies on the intersection of two straight lines. The first line has slope bE and passes from the origin and the second line has slope E and passes from (ϵ_i, σ_i) (Figure 2.2.2). Once we solve the two linear equations we obtain α_i as:

$$\alpha_i = \frac{b}{b-1} (\sigma_i - E \epsilon_i)$$

The first condition is valid only when the material is plastic, while the second condition is always valid. Therefore, α_i is obtained as:

$$\alpha_i = \max \left[\sigma_i - \sigma_{y,0}, \frac{b}{b-1} (\sigma_i - E \epsilon_i) \right]$$

We also define the shifted stress η in order to determine if the material has yielded or not:

$$\eta = \sigma_i - \alpha_i$$

The condition of yielding is defined with the aid of η as follows:

$$q = |\eta_{i+1}| - \sigma_{y0}$$

As in the isotropic model, a trial step is first performed in order to obtain $\sigma_{el,i}$. We then determine if the material has yielded with the aid of the above equation, where $n = \sigma_{el,i} - \alpha_i$. If the material is elastic $\sigma_i = \sigma_{el,i}$ and $E_i = E$, else the current stress is obtained as in the isotropic model, using the formula:

$$\sigma_i = \sigma_{el,i} - E \Delta \varepsilon_{pl}$$

If we prefer storing α , we can use equation $\alpha_{i+1} = \alpha_i + \text{sgn}(\eta_i) \frac{bE}{1-b} \Delta \varepsilon_{pl,i}$ to update its value. The tangent modulus is updated with the aid of equation:

$$E_m = \frac{\partial \sigma}{\partial \varepsilon} = \begin{cases} E, & q \leq 0 \\ bE, & q > 0 \end{cases}$$

Materials in nature often show combined isotropic and kinematic hardening. When this is the case, the yield stress initially increases due to plastic hardening, but it decreases when the direction of strain changes. In order to combine kinematic and isotropic hardening, a new parameter, δ , that varies from 0 to 1 is introduced. δ interpolates the two hardening models with the aid of the expressions:

$$\begin{aligned} \sigma_{y,i+1} &= \sigma_{y,i} + \delta \cdot H \cdot \Delta \varepsilon_{pl} \\ \alpha_{i+1} &= \alpha_i + \text{sgn}(\eta) \cdot (1 - \delta) \cdot H \cdot \Delta \varepsilon_{pl} \end{aligned}$$

When $\delta = 0$ the model becomes pure kinematic, while when $\delta = 1$ it is pure isotropic. In the mixed model, the plastic strain and back stress α are updated and stored at each load increment.

A different approach for combining isotropic and kinematic hardening was proposed by Filippou *et al.* [2]. Isotropic strain hardening is accounted in a pure kinematic hardening formulation by shifting the position of the yield asymptote before evaluating the new asymptote intersection point after a strain reversal. The shift is effected by moving the initial asymptote by a stress shift parallel to its direction. This idea was initially introduced by Stanton and Mc Niven [12], while Filippou *et al.* [2] proposed shifting the yield stress $\bar{\sigma}_y$ by the quantity:

$$\sigma_{sh} = \sigma_y \alpha_1 \left(\frac{\varepsilon_r}{\varepsilon_y} - \alpha_2 \right) > 0$$

where ε_r is the absolute value of the maximum strain at the point of load reversal, α_1 determines the amplitude of isotropic hardening and α_2 is the strain beyond which the isotropic hardening is taken into consideration. Parameters α_1 and α_2 may receive different values in tension and in compression and thus the above equation becomes:

$$\begin{aligned} \sigma_{sh}^{tension} &= \sigma_y \alpha_1 \left(\frac{\varepsilon_{max}}{\varepsilon_y} - \alpha_2 \right) > 0 \\ \sigma_{sh}^{comp.} &= \sigma_y \alpha_3 \left(\left| \frac{\varepsilon_{min}}{\varepsilon_y} \right| - \alpha_4 \right) > 0 \end{aligned}$$

$\alpha_1, \alpha_2, \alpha_3, \alpha_4$ are to be determined experimentally, while the strains ε_{max} and ε_{min} correspond to the strains during a load reversal to a positive or a negative load branch, respectively. Some common values for α_1 and α_3 are $0.01 - 0.025$, while for α_2 and α_4 a possible range of values is $2 - 7$ [3].

2.2.1 Example: hysteretic stress-strain history

Obtain the hysteretic loop for a steel material with $f_y = 500MPa$, $E = 200GPa$ and hardening ratio $b = 3\%$. Assume that the model has only kinematic hardening and use the strain history: $\varepsilon = [0, 0.4\varepsilon_y, 2\varepsilon_y, 1.5\varepsilon_y, -0.5\varepsilon_y] = [0, 0.00100, 0.00500, 0.00375, -0.00125]$.

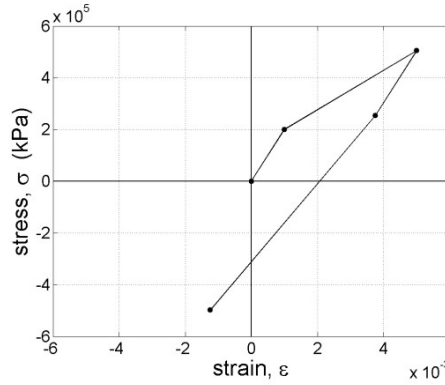


Figure 2.2.1.1: Stress-strain hysteretic loop using the bilinear model with pure kinematic hardening.

The stress-strain curve obtained is shown in Figure 4.6. Every point of the curve refers to a different phenomenon, showing in this very simple example the behaviour of the bilinear model with kinematic hardening.

- *point 1:* the material is elastic, since $\varepsilon_1 \leq \varepsilon_y$, thus $\sigma_1 = E\varepsilon_1 = 0.001 \times 200 = 0.2GPa$.
- *point 2:* the material yields $\varepsilon_2 \geq \varepsilon_y$, thus $\sigma_2 = \sigma_{y,0} + b(\varepsilon_2 - \varepsilon_y) = \sigma_{y,0} + 0.03 \times 200 \times (2 - 1) \times \varepsilon_y = 0.515GPa$.
- *point 3:* the material unloads elastically since $\Delta\varepsilon = \varepsilon_3 - \varepsilon_2 < 0$, therefore $\sigma_3 = \sigma_2 + E \times \Delta\varepsilon = 0.515 + 200 \times (1.5 - 2) \times \varepsilon_y = 0.265GPa$.
- *point 4:* Yielding when loading in the opposite direction is observed in this step. First we calculate the yielding strain and stress for loading in the opposite direction, ε_y^- and σ_y^- , respectively. Therefore, $\varepsilon_y^- = \varepsilon_2 - 2\sigma_y/E$ and $\sigma_y^- = \sigma_2 - 2\sigma_y$. The stress at point 4 will be: $\sigma_4 = \sigma_y^- + bE(\varepsilon_4 - \varepsilon_y^-) = -0.49GPa$.

The Matlab script is shown below, while Figure 2.2.1.1 shows the stress-strain history obtained using the function discussed in Section of kinematic hardening.

We will use a longer strain history: $\varepsilon = [0, 0.5\varepsilon_y, \varepsilon_y, 1.7\varepsilon_y, 0.5\varepsilon_y, 0.2\varepsilon_y, 0.7\varepsilon_y, 0.1\varepsilon_y, -0.2\varepsilon_y, -\varepsilon_y, -1.2\varepsilon_y, -2\varepsilon_y, 0.4\varepsilon_y, 0.9\varepsilon_y, 3\varepsilon_y, 3\varepsilon_y, 1.5\varepsilon_y, 0.5\varepsilon_y, -2\varepsilon_y, -\varepsilon_y, 0, 0.5\varepsilon_y]$.

```
clc; close all; clear;

% input data
Fsy = 500000; Eo = 200*10^6; b = 0.01
ey = Fsy/Eo;
epsilon = [0, 0.5*ey, ey, 1.7*ey, 0.5*ey, 0.2*ey, 0.7*ey, 0.1*ey, ...
-0.2*ey, -ey, -1.2*ey, -2*ey, 0.4*ey, 0.9*ey, 3*ey, 3*ey, 1.5*ey, ...
0.5*ey, -2*ey, -ey, 0, 0.5*ey];

sigs = zeros(size(epsilon));
for i=2:length(epsilon)
    sigsP = sigs(i-1); % strain of previous step
    epssP = epsilon(i-1); % stress of previous step
    depss = epsilon(i) - epssP; % strain of previous step
    [sigs(i), Es(i)] = bilinearKin(Fsy, Eo, b, epssP, sigsP, depss);
end
```

In Opensees the bilinear model can be found as Steel01 model. Otherwise the elastic-perfectly plastic material ElasticPP assuming zero hardening is assumed. The program also offers the option of a linear elastic material using the Elastic material. Steel01 model receives $\alpha_1, \alpha_2, \alpha_3, \alpha_4$ as optional input variables in order to consider combined mixed hardening. These models are offered with the aid of the following commands:

```
uniaxialMaterial Elastic $matTag $E <$eta> <$eneg>
uniaxialMaterial ElasticPP $matTag $E $sepsP <$sepsN $seps0$>
uniaxialMaterial Steel01 $matTag $Fy $E0 $b <$a1 $a2 $a3 $a4>
```

Any computer analysis software can be used for testing any stress-strain material. The idea is simply to introduce a single truss element with unit area $A = 1$ and unit length $L = 1$. One end of the truss element is fixed, while on the end that is free to move we impose a displacement history. Since $A = L = 1$, the imposed displacements can be seen as strains, while the axial forces produced can be seen as stresses. The following script, borrowed from the program manual, can thus be used. The script reads the displacement history from a file named pattern.txt that contains the strain values in a single column.

```
wipe
model BasicBuilder -ndm 1 -ndf 1
# Define nodes
node 1 0.0
node 2 1.0
fix 1 1

#uniaxialMaterial Steel01 $matTag $Fy $E0 $b
uniaxialMaterial Steel01 1 500000 2e8 0.1
```

```
# Define truss element with unit area
# tag ndI ndJ A matTag
element truss 1 1 2 1.0 1

set dt 1.0; # Increment between data points
set filename pattern.txt; # Filename containing data points

pattern Plain 1 "Series -dt $dt -filePath $filename " {
# node dof value
sp 2 1 1.0
}

# Record nodal displacements (same as strains since truss length is 1.0)
recorder Node -file dispOut.txt -time -node 2 -dof 1 disp
# Record truss force (same as stress since truss area is 1.0)
recorder Element -file forceOut.txt -time -ele 1 forces

system UmfPack
constraints Penalty 1.0e12 1.0e12
numberer RCM

# Set increment in load factor used for integration
# Does not have to be the same as dt used to read in displacement pattern
set dl $dt
integrator LoadControl $dl 1 $dl $dl
test NormDispIncr 1.0e-6 10
algorithm Newton
analysis Static
analyze 22
```

2.3 The model of Menegotto and Pinto for steel reinforcement

The bilinear model is the most common option for the analysis of steel structures or for modeling steel reinforcement. We also present the Menegotto-Pinto model [7] which is a more elaborate relationship that is also often used for modelling steel. The Menegotto-Pinto model is an explicit $\sigma = f(\varepsilon)$ relationship that is based on a simple relationship. The model is able to give good results for both steel reinforcement and structural steel, provided that it has been calibrated accordingly.

The backbone of the Menegotto-Pinto model is given by the relationship:

$$\sigma^* = b\varepsilon^* + \frac{(1-b)\varepsilon^*}{(1+\varepsilon^{*R})^{\frac{1}{R}}} \text{ με } \varepsilon^* = \frac{\varepsilon - \varepsilon_r}{\varepsilon_o - \varepsilon_r} \text{ και } \sigma^* = \frac{\sigma - \sigma_r}{\sigma_o - \sigma_r}$$

This equation provides a curved transition from a straight-line asymptote with slope E to another asymptote with slope $E_T = bE$ (Figure 2.3.1, lines (a) and (b) respectively). Parameters ε_o and σ_o are the stress and the strain at the point where two asymptotes of the branch under consideration meet (Figure 2.3.1, point A), while ε_r and σ_r denote the stress and the strain at the point where the last strain reversal with stress of equal sign took place (Figure 2.3.1, point B). This point denotes the beginning of a reloading branch. R is the curvature parameter that controls the transition from the elastic to the hardening branch. At every load reversal ε_o , σ_o , ε_r and σ_r are updated.

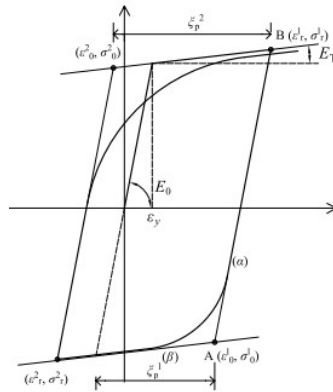


Figure 2.3.1: Stress-strain relationship of the Menegotto-Pinto model.

The curvature parameter R depends on the strain difference between the current asymptote intersection point and the previous load reversal point with maximum or minimum strain depending on the corresponding steel stress [2]. The shape of the transition curve allows a good representation of the Baushinger effect. The expression for R takes the form: $R_i = R_0 - (c_1 \xi_{p,i} / (c_2 + \xi_{p,i}))$, where $\xi_{p,i}$ is the plastic excursion at the current semicycle, defined as: $\xi_{p,i} = \varepsilon_{r,i} - \varepsilon_{0,i}$, where:

$$\varepsilon_{0,i} = \varepsilon_{0,i-1} + \frac{\sigma_{0,i} - \sigma_{r,i-1}}{E}$$

R_0 is the value of R during the first loading and has to be experimentally determined together with c_1 and c_2 . Typical values are $R_0 = 20$, $c_1 = 18.5$ and $c_2 = 0.15$.

The above equations require some further clarification with a set of rules for unloading and reloading for the case of a generalized load history; when partially unloading and then reloading back, often the Menegotto-Pinto relationship may

overestimate the stress value. Since the memory of the model is limited to the previous step, Filippou et al. [2] proposed to limit the memory of the stress–strain history to four controlling curves: (i) the monotonic envelope, (ii) the ascending upper branch curve originating at the reversal point with smallest ε value, (iii) the descending lower branch curve originating at the reversal point with largest ε value, (iv) the current curve originating at the most recent reversal point. The reader interested in the Menegotto-Pinto model can find more details in reference [2]. In OpenSees, the bilinear model can be found as Steel01 model. Otherwise the elastic-perfectly plastic material ElasticPP assuming zero hardening is assumed. The program also offers the option of a linear elastic material using the Elastic material. Steel01 model receives α_1 , α_2 , α_3 , α_4 as optional input variables in order to consider combined mixed hardening. These models are offered with the aid of the following commands: The Menegotto-Pinto model is available in OpenSees as Steel02 model. The model can be adopted using the command:

```
uniaxialMaterial Steel02 $matTag $Fy $E $b $R0 $c1 $c2 <$a1 $a2 $a3 $a4>
```

where F_y , E and b have already been defined for the bilinear steel model and R_0 , c_1 , c_2 are the parameters to control the transition from elastic to plastic branches. OpenSees also gives the option to allow for isotropic hardening using the approach presented in [2]. Isotropic hardening is therefore considered using the optional parameters a_1 , a_2 , a_3 and a_4 discussed in section mixed kinematic and isotropic hardening.

$$R = R_0 - \frac{\alpha_1 \xi}{\alpha_2 + \xi}$$

where ξ is the variable, which is updated in each strain reversal. R_0 comes from R for the case of first load increment only and α_1 , α_2 are the constants, where are measured experimentally together with the R_0 . The variable ξ remains constant when it exists partial unloading.

Furthermore,

E	- elastic modulus
H	- hardening modulus
R_0	- curvature control parameter I
A_1	- curvature control parameter II
A_2	- curvature control parameter III
ξ	- normalized plastic strain variable
σ, ε	- total current stress and strain
σ_x, ε_x	- stress and strain where the asymptotes of the curve intersect
σ_r, ε_r	- stress and strain at the last load reversal

Usually: $b=H= 0.02$

The variable ξ is defined as follows:

$$\xi = \left| (\varepsilon_r - \varepsilon_x) / \varepsilon_0 \right|$$

Where

$$\varepsilon_0 = f_y / E$$

and:

$$(\varepsilon_r - \varepsilon_x)$$

,which is the plastic strain from the previous load step. For the Steel Material we have the following values respectively:

$$\varepsilon_{s_yield} \cong 0.002$$

$$\varepsilon_{s_ultimate} \cong 0.08$$

$$\xi = |0.08/0.002| = 40$$

$$\alpha_1 = 18$$

$$\alpha_2 = 0.13$$

$$R_o = 20$$

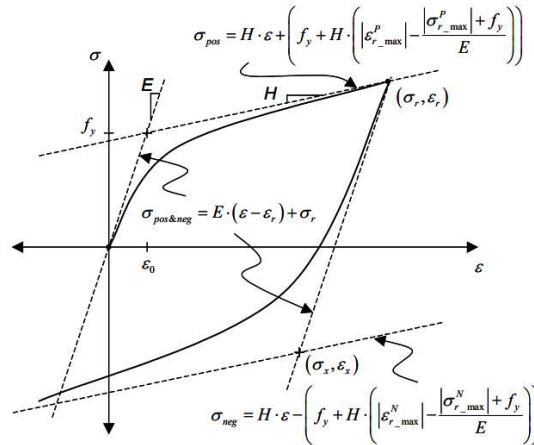
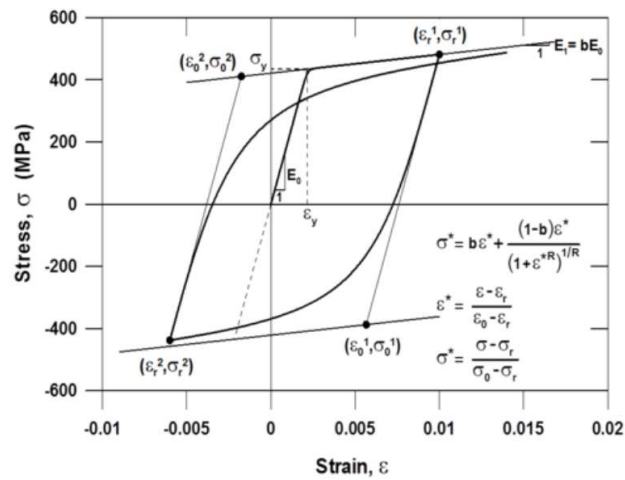


Figure 2: Geometric relations used to obtain the intersect of the asymptotes



Also, it is considered as:

$$\varepsilon_r = \pm 0.001 = \varepsilon_y/2$$

Generally, we have:

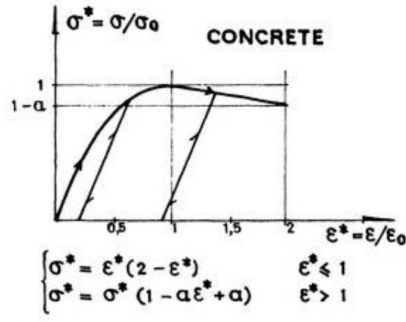


Figure (a)

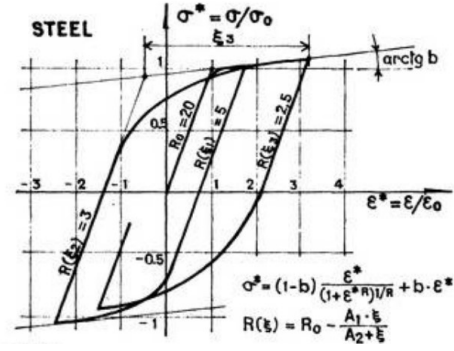
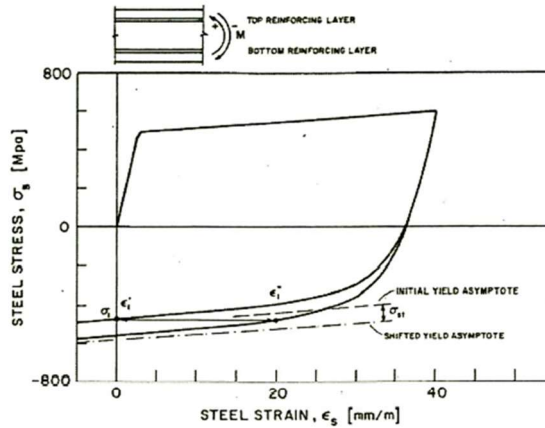


Figure (b)

Also, this simulation is extended by Filippou et al. (1983) with the addition of some permutation of the asymptotes to take into account the isotropic strain hardening. The shift of the asymptote was assumed to depend on the current maximum plastic strain in the form:

$$\frac{\sigma_{st}}{\sigma_y} = \alpha_3 \left(\frac{\varepsilon_{\max}}{\varepsilon_y} - \alpha_4 \right)$$

where ε_{\max} is the absolute maximum strain the time of reverse, ε_y , σ_y the strain and the stress during the yielding and α_3 , α_4 are the constants, which are measured by experiments.



Ισοτροπική κράνση ράβδου (από Filippou et al. 1983).

The specific model according to Menegotto Pinto for steel not considering the isotropic hardening in both compression and tension obtains values, which are equal to $\alpha_1 = \alpha_3 = 0$ and $\alpha_2 = \alpha_4 = 1$. In case isotropic hardening in compression is taken into account, then the usual values are $\alpha_1 = 0.01$ and $\alpha_2 = 7$, while in the case of isotropic hardening in tension, then the proposed values of the parameters experimentally are: $\alpha_3 = 0.01$, as well as $\alpha_4 = 7$.

2.3.1 Uniaxial material laws for concrete

Many of models for modelling the cyclic behaviour of concrete can be found in the literature. We will focus on uniaxial relationships since general-purpose beam elements account only for the principal strain ε_x . Among the various models proposed, some of well-known uniaxial laws are those proposed by Kent and Park [8], Sheikh and Uzumeri [11], Mander

et al. [6], and Madas and Elnashai [5]. These relationships are able to consider the effect of the transverse reinforcement on the uniaxial stress-strain relationship though the passive confinement model of Mander et al. [6] that is also recommended in Eurocode 2 [1]. First, we present a fundamental stress-strain monotonic relationship for concrete derived from first principles. Subsequently we discuss the model proposed by Kent and Park as modified by Scott et al. [10]. This is a relatively simple relationship able to provide sufficient results for a wide range of applications.

2.3.2 The modified Kent-Park model

The modified Kent-Park model is based on the model initially proposed by Kent and Park [8] and latter modified by Scott et al. [10] in order to account for the passive confinement due to the transverse reinforcement. Although there are several models available, the modified Kent-Park model combines simplicity with accurate results and was therefore chosen in order to demonstrate a simple concrete model. The model is also available in the material library of Opensees as the Concrete01 model. Opensees also offers the Concrete02 model which differs from Concrete01 in the sense that it does not consider the tensile strength of concrete. The discussion that follows can be found in reference [2]. According to the Kent-Park model, the stress-strain relationship of concrete in compression consists of three branches:

$$\sigma = \begin{cases} K f'_c \left(2\varepsilon/\varepsilon_0 - (\varepsilon/\varepsilon_0)^2 \right) & \varepsilon \leq \varepsilon_0 \\ K f'_c \left(1 - Z(\varepsilon - \varepsilon_0) \right) \geq 0.2K f'_c & \varepsilon_0 \leq \varepsilon < \varepsilon_u \\ 0.2K f'_c & \varepsilon_u < \varepsilon \end{cases}$$

where $\varepsilon_0 = 0.002K$, and

$$K = 1 + \frac{\rho_s f_{yh}}{f'_c}$$

$$Z = 0.5 / \left(\frac{3 + 0.29 f'_c}{145 f'_c - 1000} + 0.75 \rho_s \sqrt{h'/s_h} - 0.002K \right)$$

where ε_0 is the concrete strain corresponding to the crushing stress (maximum stress), K is a factor that accounts for the effect of passive confinement, multiplying the maximum stress and assumed equal to 1 for the concrete cover. Z is the slope of the descending branch (strain softening), f'_c is the concrete crushing strength in MPa, $f_{y,k}$ is the yield strength of the transverse reinforcement in MPa and ρ_s is the ratio of the volume of the stirrups over the volume of the confined concrete core. h' is the height of the confined concrete core and s_h is the spacing of the transverse reinforcement. For the confined concrete, the ultimate concrete strain ε_u can be conservatively estimated with the aid of Eq. 4.43, setting $\sigma = 0.2K f'_c$. Otherwise the expression that can be used is:

$$\varepsilon_u = 0.004 + \frac{0.9 \rho_s f_{yh}}{300}$$

For the concrete cover, when ε_u is exceeded the stress becomes equal to $0.2 f'_c$, while ε_u can be assumed approximately equal to 0.005 [2]. When unloading and reloading, the stress-strain relationship follows the following rules:

(i) unloading takes place along a straight line that connects ε_r (strain at unloading) with ε_p that lies on the horizontal axis and is calculated as:

$$\frac{\varepsilon_p}{\varepsilon_0} = \begin{cases} 0.145 (\varepsilon_r/\varepsilon_0)^2 + 0.13 \varepsilon_r/\varepsilon_0 & \varepsilon_r/\varepsilon_0 < 2 \\ 0.707 (\varepsilon_r/\varepsilon_0 - 2) + 0.834 & \varepsilon_r/\varepsilon_0 \geq 2 \end{cases}$$

The first branch of Eq. 4.47 was proposed by Karsan and Jirsa [4] and relates the strains along the envelope with a quadratic relationship. The second branch was latter added to Eq. 4.47 since for large strains the initial equation was not producing realistic stress values.

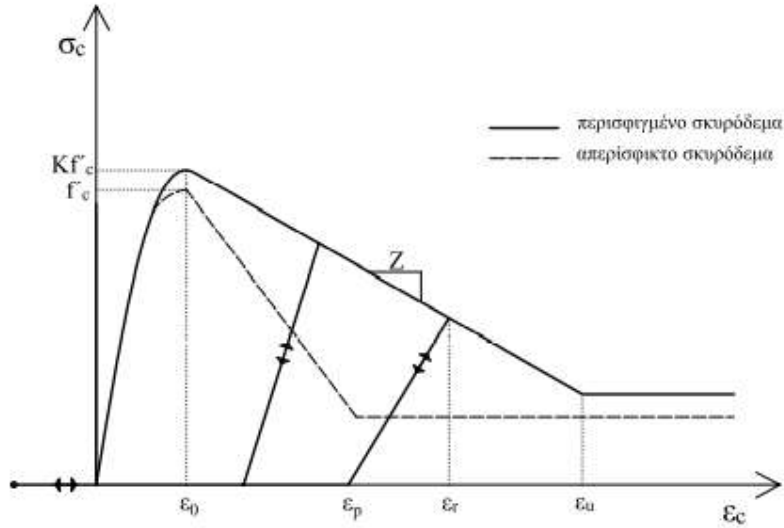


Figure 2.3.2: Behaviour of the concrete model during loading and unloading.

- (ii) The tensile capacity of concrete is neglected, since it does influence the response once concrete cracking occurs.
- (iii) when reloading in compression, the stress is zero as long as the strain is less than the strain of full unloading. Once this value is exceeded, reloading occurs following the path of unloading, but with opposite sign. In real life, the unloading-reloading path is never the same, assuming it is similar has a small effect on the response obtained.

(iv) The slope E of the stress-strain curve is obtained from Eq. 4.43, thus:

$$E = \frac{\partial \sigma}{\partial \varepsilon} = \begin{cases} 2Kf'_c(1 - \varepsilon/\varepsilon_0) & \varepsilon \leq \varepsilon_0 \\ Z & \varepsilon_0 \leq \varepsilon < \varepsilon_u \\ 0 & \varepsilon_u \leq \varepsilon \end{cases}$$

For the first load step, we assume that $E_0 = 2(Kf'_c/\varepsilon_0)$, while for the unloading branch:

$$E = \begin{cases} \sigma_r/(\varepsilon_r - \varepsilon_p) & \varepsilon_r - \varepsilon_p \geq \sigma_r/E_0 \\ E_0 & \varepsilon_r - \varepsilon_p < \sigma_r/E_0 \end{cases}$$

where σ_r is the stress at the point where unloading starts.

Figure 2.3.3 shows the behaviour of the modified Kent-Park model for a sinusoidal strain history of increasing amplitude. This model does not account for the number of cycles and hence does not consider the energy absorbed in every cycle. This parameter is important, but its study is beyond the scope of this book. The parameters assumed for the Concrete01 model in the following examples are: $f_{pc} = 29\text{MPa}$, $\varepsilon_{c0} = 0.2\%$, $f_{pcu} = 0.20 f_c$ and $\varepsilon_{cu} = 0.4\%$. The model is tested in OpenSees using the truss element script and the following lines:


```
#uniaxialMaterial Concrete01 $matTag $fpc $sepsc0 $fpcu $sepsU
uniaxialMaterial Concrete01 1 -29000 -0.002 [expr -0.2*29000] -0.004
```

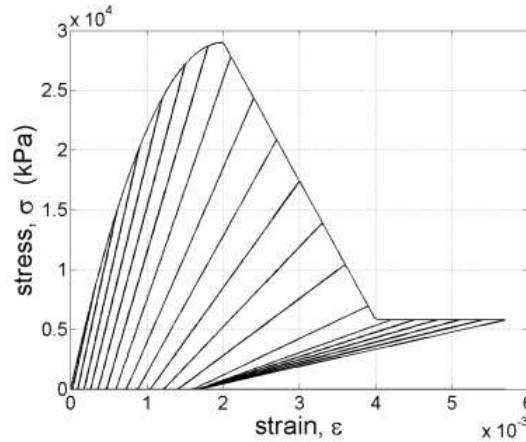


Figure 2.3.3: The modified Kent-Park model.

2.3.3 Force-based fiber element

Force-based elements, also known as flexibility elements, have been proposed by several researchers [18, 19, 15, 21]. This theory allows the use of a single beam-column element per member¹. Compared to the commonly adopted displacement-based elements, this approach improves considerably the accuracy and the efficiency of the analysis. In order to determine the element resisting forces, force-based elements introduce an additional iterative process at the element level, known as element-state determination phase. The element-state determination process complicates the implementation of the force-based concept and, therefore, the formulation is not straightforward as in the case of displacement-based elements.

The accuracy of force-based elements depends on the use of force interpolation functions in order to calculate the section forces from the nodal forces, as opposed to displacement-based elements that calculate section deformations from the nodal displacements. Force interpolation functions (\mathbf{b}_s) are always “exact”, since the axial forces are constant and the bending moments are linear. Compared to rotations which localize when the section yields, this this fundamental difference allows to circumvent the need for a denser mesh at the critical regions. However, all finite element codes are stiffness based, in the sense that we apply forces and we receive as output displacements. This complicates considerably the process since the element forces are not known beforehand. Furthermore, most material laws receive strains as input and not stresses.

In the basic coordinate system, the element forces are denoted \mathbf{S} and \mathbf{v} are the element basic displacements. In the displacement formulation we were calculating the section deformations $\mathbf{d}_{sec}(x)$ from the basic displacements \mathbf{v} . On the other hand, force-based elements calculate, at an arbitrary cross-section x , the section forces $\mathbf{D}_{sec}(x)$ from the element basic forces $\mathbf{S} = \mathbf{K}_N \mathbf{v}$ as follows:

$$\mathbf{D}_{sec} = \mathbf{b}_s(x)\mathbf{S} \Leftrightarrow \begin{bmatrix} N(x) \\ M(x) \end{bmatrix} = \begin{bmatrix} 1 & 0 & 0 \\ 0 & (1-x/L) & (x/L) \end{bmatrix} \begin{bmatrix} N \\ M_1 \\ M_2 \end{bmatrix}$$

where \mathbf{b}_s is the matrix of force interpolation functions, M_1, M_2 are the moments at the beam ends and N is the axial force within the member. Equation 8.2 implies that $M(x) = (1-x/L)M_1 + (x/L)M_2$. Calculating the section forces is preferable compared to section displacements, since the bending moment diagram is always exact along the beam as opposed to displacements and curvatures.

With the aid of the Virtual Work Principle we obtain:

$$W_{basic} = W_{int.} \Rightarrow \delta \mathbf{v}^T \mathbf{S} = \int_L \int_A \delta \varepsilon_x^T \sigma_x dA dx$$

where

$$\int_A \delta \varepsilon_x^T \sigma_x dA = \delta \mathbf{d}_{sec}^T \int_A \mathbf{a}_s^T \sigma dA = \delta \mathbf{d}_{sec}^T \mathbf{D}_{sec} = \delta \mathbf{d}_{sec}^T \mathbf{b}_s(x)\mathbf{S}$$

Eliminating the section forces \mathbf{S} , the element displacements in the basic system will be:

$$\mathbf{v} = \int_L \mathbf{b}_s^T(x) \mathbf{d}_{sec} dx$$

In the displacement-based formulation we integrate the section forces (Eq. 7.10) to obtain the basic forces. Here this operation is not possible since we integrate the displacements \mathbf{v} instead. This complicates the element formulation as the internal forces, necessary for the equilibrium check, are not available. To overcome this problem an additional step known as element-sate determination is necessary.

The stiffness matrix is calculated from the inverse of the basic flexibility matrix $\mathbf{K}_N = \mathbf{F}_N^{-1}$, as follows:

$$\mathbf{F}_N = \frac{\partial \mathbf{v}}{\partial \mathbf{S}} = \frac{\partial \mathbf{v}}{\partial \mathbf{d}_{sec}} \frac{\partial \mathbf{d}_{sec}}{\partial \mathbf{S}} = \frac{\partial \mathbf{v}}{\partial \mathbf{d}_{sec}} \frac{\partial \mathbf{d}_{sec}}{\partial \mathbf{D}_{sec}} \frac{\partial \mathbf{D}_{sec}}{\partial \mathbf{S}} \Leftrightarrow \mathbf{F}_N = \int_L \mathbf{b}_s^T \mathbf{f}_{sec} \mathbf{b}_s dx$$

where \mathbf{f}_{sec} is the section flexibility matrix, $\mathbf{f}_{sec} = \mathbf{k}_{sec}^{-1}$. The stiffness matrix in the local coordinate system is obtained as in the displacement-based element (Eq. 7.15):

$$\mathbf{K}_e = \mathbf{b}_e \mathbf{K}_N \mathbf{b}_e^T$$

When the element is elastic, the flexibility matrix is simplified² to:

$$\mathbf{F}_N = \int_L \mathbf{b}_s^T \mathbf{f}_{sec} \mathbf{b}_s dx = \begin{bmatrix} \frac{L}{EA} & 0 & 0 \\ 0 & \frac{L}{3EI} & -\frac{L}{6EI} \\ 0 & -\frac{L}{6EI} & \frac{L}{3EI} \end{bmatrix}$$

If \mathbf{F}_N is inversed, we obtain the elastic element stiffness matrix of the displacement-based formulation

2.3.4 Numerical integration

For the force-based element we prefer the Gauss-Lobatto quadrature. The commonly adopted Gauss quadrature will also yield sufficient results in most cases, but experience has shown that Gauss-Lobatto quadrature performs better in this case. The primary difference of the two quadrature methods is that the Gauss-Lobatto method introduces as sections of integration the two beam ends where the bending diagram receives its maximum values. This is why Gauss-Lobatto quadrature outperforms Gauss quadrature in the case of force-based elements. The integration is thus written:

$$\int_{-1}^1 f(\xi) d\xi = w_1 f(-1) + w_2 f(1) + \sum_{h=2}^{n_{GP}-1} w_h f(\xi_h)$$

while the weights and the position of the n_{GP} Gauss points are given in Table 8.1. The weight values at the two ends are small, but this is the location that the moment is maximum and therefore this integration scheme is more efficient. The minimum number of integration points is three, while as a rule-of-thumb we use four Gauss-Lobatto points with the force-based element. In principle Gauss-Lobatto quadrature is accurate for polynomials of order up to $3 \times n_{GP} - 2$. Note that in the case of the force-based element, we integrate the element flexibility matrix and the section deformations (rather than the stiffness matrix and the element forces).

Force-based elements suffer from the so-called localization effects, which appear only in the case of softening response (e.g. reinforced concrete members). Localization effects depend on the number of integration points and result to loss of objectivity, which in the case of nonlinear static analysis appears as a loss of objectivity around the limit-point.³ This is because damage localizes at the reference volume of the first control point and as a result denser discretization leads to fictitious steeper softening branches. Several researchers have proposed ([6, 1, 17, 2]) regularization techniques in order to amend the problem and obtain an objective response. In the absence of a more sophisticated regularization scheme, the number of integration points may be selected so that the plastic hinge length is approximately equal to actual plastic hinge length. In force-based elements, we consider the as plastic hinge length the distance of the Gauss points at the member ends with their nearby sections, while several formulas that estimate the plastic hinge length can be found in the literature for both steel and RC sections.

In the standard stiffness approach (displacement-based approach) the section deformations \mathbf{d}_{sec} can be directly obtained from the nodal displacements. In a flexibility-based element this task is performed iteratively:

$$\begin{aligned} \Delta \mathbf{d}_{sec} &= \mathbf{k}_{sec}^{-1} \Delta \mathbf{D}_{sec} \Rightarrow \Delta \mathbf{d}_{sec} = \mathbf{k}_{sec}^{-1} \mathbf{b}_s(x) \Delta \mathbf{S} \Rightarrow \\ &\Delta \mathbf{d}_{sec} = \mathbf{k}_{sec}^{-1} \mathbf{b}_s(x) \mathbf{F}_N \Delta \mathbf{v} \end{aligned}$$

According to Petrangelli and Ciampi [15], different element formulations have been proposed [18, 21], based on Equation 8.9. Early efforts were based on different forms of shape functions, with the “variable shape functions” of

Zeris and Mahin [21] to be a very accurate approach. However, the use of such shape functions does not satisfy strictly the equilibrium along the beam, although the numerical problems that arise are not significant. To overcome this problem, a procedure initially proposed by Ciampi and Carlesimo [5] has been refined by Spacone *et al.* [18, 19] and was applied to a fibre-based, beam-column element. This approach is here discussed, guaranteeing that equilibrium is always strictly satisfied even for highly nonlinear, or softening, problems. An alternative approach that requires a single element iteration and satisfies equilibrium with the aid of the Newton-Raphson scheme was proposed by Neuenhofer and Filippou [12].

The first step of the iterative procedure is to determine the vector of the basic forces from the Cartesian nodal displacements. Then using the force interpolation functions \mathbf{b}_s , the section forces are obtained and subsequently corrected in agreement with the constitutive law of the fibres. The residual section forces are then multiplied with the section flexibility and integrated along the element length to obtain the element residual displacements. The iterative process at the element level is terminated when the residual deformations are minimized following an energy convergence criterion. This procedure is described step-by-step below.

For every element, we calculate the increment of the section forces $\Delta \mathbf{D}_{sec}$ and then the section deformations as

$$\begin{aligned}\Delta \mathbf{d}_i^j(x) &= \mathbf{k}_{sec}^{-1}(x) \Delta \mathbf{D}_i^j(x) \\ \mathbf{d}_i^j(x) &= \mathbf{d}_{i-1}(x) + \Delta \mathbf{d}_i^j(x)\end{aligned}$$

Knowing the section deformations, we update the section forces and the section stiffness and subsequently we calculate for every integration section the residual forces \mathbf{D}_u and deformations \mathbf{r}_u :

$$\begin{aligned}\mathbf{D}_u^j(x) &= \mathbf{D}_i^j(x) - \mathbf{D}_i^{j-1}(x) \\ \mathbf{r}_u^j(x) &= \mathbf{k}_{sec}^{-1}(x) \mathbf{D}_u^j(x)\end{aligned}$$

the section deformations are then integrated to obtain the residual element displacements:

$$\mathbf{v}_r^j = \int_L \mathbf{b}_s(x) \mathbf{r}_u^j(x) dx$$

If \mathbf{v}_r is not zero, we set $\mathbf{v} = -\mathbf{v}_r$ and perform iterations at the member level. Note that in Eq. 8.10 we need to invert the section stiffness and calculate the fiber strains through the section deformations. This is due to the fact that almost all constitutive $\sigma - \varepsilon$ relationships receive as input strains and output stresses.

A comprehensive review on the progress made in the past years on beam element formulations for members subjected to high shear can be found in [4]. One of the early developments was that of Vecchio and Collins [20] who introduced a dual-section analysis procedure where the element is discretized to layers, while iterations are performed for each layer until the internal equilibrium between adjacent sections is satisfied. This approach is limited to 2D problem. Bairan and Mari [3] extended the previous formulation to 3D cases by introducing an asymptotic approximation of the total energy. For RC members, Petrangeli *et al.* [14] proposed a flexibility-based, shear-deformable beam element where the longitudinal strain, ϵ_x , and the shear strain, τ_{xy} , are obtained from the element kinematics, while the transverse strain, ϵ_y , is calculated through lateral equilibrium between steel and concrete fibres. This formulation is combined with a biaxial law for concrete using the components of the two-dimensional strain tensor. Saritas and Filippou [16] presented a force-based formulation for the seismic assessment of steel structures also using a multi-dimensional material law, but their study is limited to two-dimensional problems and has been demonstrated on simple academic examples only, while Navarro *et al.* [11] presented a formulation for concrete beams under combined loading. Marini and Spacone [10] also presented a flexibility-based, shear-deformable beam element where a separate constitutive law for the shear component was adopted. This is clearly a simplifying assumption but maintains all the advantages of fibre beam elements in terms of robustness and simplicity of the material laws. This approach was already discussed in Chapter 5. Below we discuss the generic approach proposed by Papachristidis *et al.* [13].

The implementation of 3D material laws in beam elements is a challenging task. Any material law that refers to the three dimensional case can be used with the beam element formulation that we discussed here. The section kinematics have been already presented in Chapter 5. The constitutive matrix \mathbf{C} relates the increments of strains and stresses as:

$$\delta \boldsymbol{\sigma} = \mathbf{C} \delta \boldsymbol{\epsilon}$$

For the general 3D case the six components of the stress tensor σ_{3D} corresponds to the 6×6 material matrix, \mathbf{C}_{3D} . Finite elements that inherently contain special stress constraints, such as plates, shells and beams usually are restricted to simplified one- or two-dimensional constitutive laws. However, complicated materials are often described in the 3D continuum, thus hampering their application to these "structural" type of elements. In order to incorporate a 3D material law in such elements, local or global algorithms have been proposed in the past [7, 8, 9]. These algorithms impose a zero-stress condition to the components of the stress tensor that according to the element formulation are, or should be, equal to zero. For a beam in space the stress components σ_{yy} , σ_{zz} , τ_{zy} are assumed zero and thus they

are considered not active, while \mathbf{C} is a 3×3 matrix corresponding to the active σ_{xx} , τ_{xy} , τ_{xz} . In this study, we adopt a local iteration algorithm so that for every fibre the non-active stresses are always set to zero. The algorithm is local in the sense that iterations are performed on the fibre level until the unknown stresses are set to zero, thus does not require any additional history variables, as opposed to global iteration procedures, such as the one proposed for shell structures [7], which operates on the element level. Clearly local algorithms can be easily implemented within any general-purpose FE code such as beam-column elements, as shown in [9].

For a beam in space, the non-active stresses are σ_{yy} , σ_{zz} , τ_{zy} , while for a 2D problem σ_{yy} is the only non-active stress. The active components are the remaining elements of the 3D tensor. If the non-active components that need to be set to zero are denoted with the subscript n and the active components with m , the incremental constitutive relationship is partitioned as follows:

$$\delta \boldsymbol{\sigma} = \mathbf{C} \delta \boldsymbol{\epsilon} \Leftrightarrow \begin{bmatrix} \delta \boldsymbol{\sigma}_m \\ \delta \boldsymbol{\sigma}_n \end{bmatrix} = \begin{bmatrix} \mathbf{C}_{mm} & \mathbf{C}_{mn} \\ \mathbf{C}_{nm} & \mathbf{C}_{nn} \end{bmatrix} \begin{bmatrix} \delta \boldsymbol{\epsilon}_m \\ \delta \boldsymbol{\epsilon}_n \end{bmatrix}$$

According to the local plane stress algorithm the \mathbf{C} constitutive matrix of Equation ?? is obtained by condensing \mathbf{C}_{3D} to the active stresses:

$$\mathbf{C} = \mathbf{C}_{mm} - \mathbf{C}_{mn} \mathbf{C}_{nn}^{-1} \mathbf{C}_{nm}$$

The algorithm is iterative and refers to every control point or integration-fibre. The constitutive matrix \mathbf{C} is updated using all the components of the strain vector, $\delta \boldsymbol{\epsilon}_m$ and $\delta \boldsymbol{\epsilon}_n$. The component $\delta \boldsymbol{\epsilon}_m$ is directly calculated through the incremental-iterative analysis, while $\delta \boldsymbol{\epsilon}_n$ is obtained from the second equation of Eq. 8.13, assuming that $\delta \boldsymbol{\sigma}_n = 0$. Thus, for the j^{th} iteration:

$$\begin{aligned} \boldsymbol{\epsilon}_n^j &= \boldsymbol{\epsilon}_n^{j-1} + \delta \boldsymbol{\epsilon}_n^j \\ \delta \boldsymbol{\epsilon}_n &= -\mathbf{C}_{nn}^{-1} \delta \boldsymbol{\epsilon}_m \end{aligned}$$

The above algorithm is general in application and can be combined with every material law that refers to the full engineering stress vector, e.g with a J_2 plasticity material [13].

2.3.5 One -dimensional constitutive model

A simple mathematical model of the uniaxial experiment discussed in the previous section is formulated in what follows. In spite of its simplicity the one-dimensional constitutive model contains all the essential features that form the basis of the mathematical theory of plasticity. At the outset, the original stress–strain curve, that resulted from the loading programme described in the previous section, is approximated by the idealised version. The assumptions involved in the approximation are summarised in the following. Firstly, the difference between unloading and reloading curves (segments Z_0O_1 and O_1Y_1 of Figure 2.3.5.1) is ignored and points Z_0 and Y_1 , that correspond respectively to the beginning of unloading and the onset of plastic yielding upon subsequent reloading, are assumed to coincide. The transition between the elastic region and the elastoplastic regime is now clearly marked by a non-smooth change of slope (points Y_0 and Y_1). During plastic yielding, the stress–strain curve always follows the path defined by $O_0Y_0Y_1Z_1$. This path is normally referred to as the virgin curve and is obtained by a continuous monotonic loading from the initial unstressed state O_0 . Under the above assumptions, after being monotonically loaded from the initial unstressed state to the stress level σ_0 , the behaviour of the bar between states O_1 and Y_1 is considered to be linear elastic, with constant plastic strain, ϵ_p , and yield limit, σ_0 . Thus, within the segment O_1Y_1 , the uniaxial stress corresponding to a configuration with total strain ϵ is given by:

$$\sigma = E (\epsilon - \epsilon^p),$$

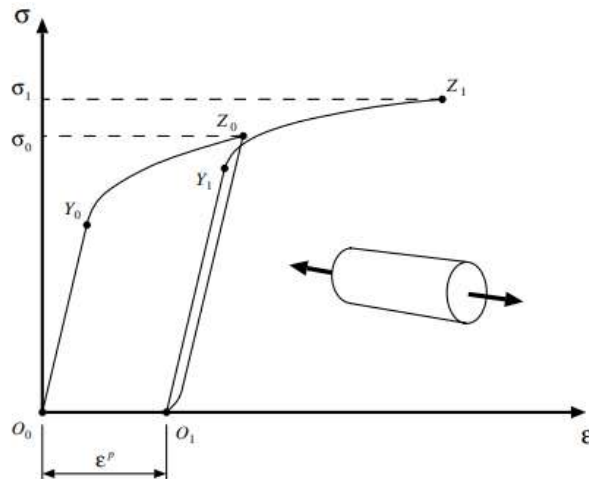


Figure 2.3.5.1: Uniaxial tension experiment with ductile metals.

where E denotes the Young's modulus of the material of the bar. Note that the difference between the total strain and the current plastic strain, $\varepsilon - \varepsilon^p$, is *fully reversible*; that is, upon complete unloading of the bar, $\varepsilon - \varepsilon^p$ is fully recovered without further evolution of plastic strains. This motivates the additive decomposition of the axial strain described in the following section.

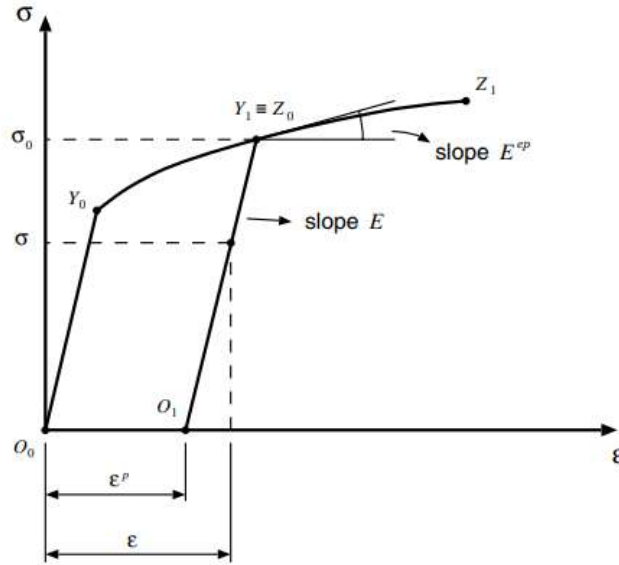


Figure 2.3.5.2: Uniaxial tension experiment. Mathematical model.

One of the chief hypotheses underlying the small strain theory of plasticity is the decomposition of the *total strain*, ε , into the sum of an *elastic* (or reversible) component, ε^e , and a

plastic (or permanent) component, ε^p ,

$$\varepsilon = \varepsilon^e + \varepsilon^p,$$

where the *elastic strain* has been defined as

$$\varepsilon^e = \varepsilon - \varepsilon^p.$$

Following the above definition of the elastic axial strain, the constitutive law for the axial stress can be expressed as

$$\sigma = E \varepsilon^e. \quad (6.4)$$

The next step in the definition of the uniaxial constitutive model is to derive formulae that express mathematically the fundamental phenomenological properties enumerated in Section 6.1. The items 1 and 2 of Section 6.1 are associated with the formulation of a *yield criterion* and a *plastic flow rule*, whereas item 3 requires the formulation of a *hardening law*. These are described in the following.

The existence of an elastic domain delimited by a yield stress has been pointed out in item 1 of Section 6.1. With the introduction of a *yield function*, Φ , of the form

$$\Phi(\sigma, \sigma_y) = |\sigma| - \sigma_y, \quad (6.5)$$

the *elastic domain* at a state with uniaxial yield stress σ_y can be defined in the one-dimensional plasticity model as the set

$$\mathcal{E} = \{\sigma \mid \Phi(\sigma, \sigma_y) < 0\}, \quad (6.6)$$

or, equivalently, the elastic domain is the set of stresses σ that satisfy

$$|\sigma| < \sigma_y. \quad (6.7)$$

Generalising the results of the uniaxial *tension* test discussed, it has been assumed in the above that the yield stress in compression is identical to that in tension. The corresponding idealised elastic domain is illustrated in Figure 6.3.

It should be noted that, at any stage, no stress level is allowed above the current yield stress, i.e. *plastically admissible stresses* lie either in the elastic domain or on its boundary (the yield limit). Thus, any admissible stress must satisfy the restriction

$$\Phi(\sigma, \sigma_y) \leq 0. \quad (6.8)$$

For stress levels within the elastic domain, only elastic straining may occur, whereas on its boundary (at the yield stress), either elastic unloading or plastic yielding (or plastic loading) takes place. This *yield criterion* can be expressed by

$$\begin{aligned} \text{If } \Phi(\sigma, \sigma_y) < 0 &\implies \dot{\varepsilon}^p = 0, \\ \text{If } \Phi(\sigma, \sigma_y) = 0 &\implies \begin{cases} \dot{\varepsilon}^p = 0 & \text{for elastic unloading,} \\ \dot{\varepsilon}^p \neq 0 & \text{for plastic loading.} \end{cases} \end{aligned} \quad (6.9)$$

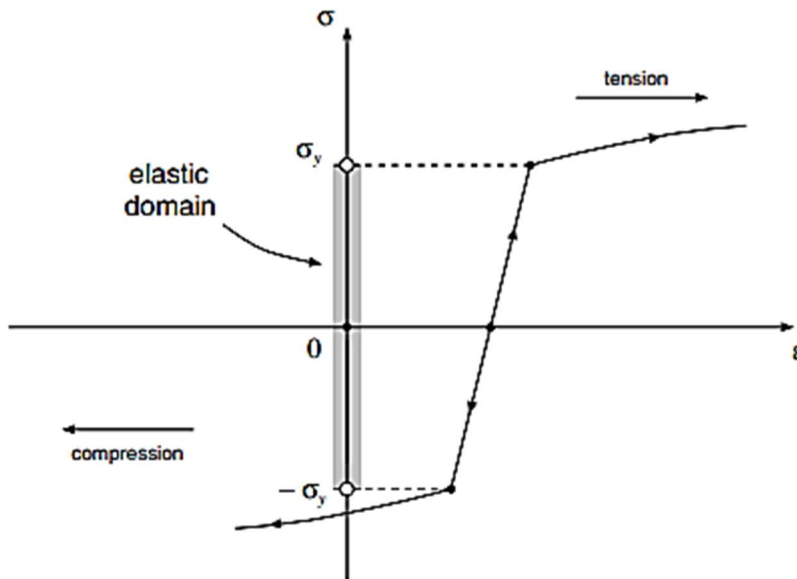


Figure 2.3.5.3: Uniaxial model. Elastic domain.

Expressions (6.9) above have defined a criterion for plastic yielding, i.e. they have set the conditions under which plastic straining may occur. By noting in Figure 6.3 that, upon plastic loading, the plastic strain rate $\dot{\varepsilon}^p$ is positive (stretching) under tension (positive σ) and negative (compressive) under compression (negative σ), the *plastic flow rule* for the uniaxial model can be formally established as

$$\dot{\varepsilon}^p = \dot{\gamma} \text{sign}(\sigma), \quad (6.10)$$

where *sign* is the *signum* function defined as

$$\text{sign}(a) = \begin{cases} +1 & \text{if } a \geq 0 \\ -1 & \text{if } a < 0 \end{cases} \quad (6.11)$$

for any scalar a and the scalar $\dot{\gamma}$ is termed the *plastic multiplier*. The plastic multiplier is *non-negative*,

$$\dot{\gamma} \geq 0, \quad (6.12)$$

and satisfies the *complementarity condition*

$$\Phi \dot{\gamma} = 0. \quad (6.13)$$

The constitutive equations (6.10) to (6.13) imply that, as stated in the yield criterion (6.9), the plastic strain rate vanishes within the elastic domain, i.e.

$$\Phi < 0 \implies \dot{\gamma} = 0 \implies \dot{\varepsilon}^p = 0, \quad (6.14)$$

and plastic flow ($\dot{\varepsilon}^p \neq 0$) may occur only when the stress level σ coincides with the current yield stress

$$|\sigma| = \sigma_y \implies \Phi = 0 \implies \dot{\gamma} \geq 0. \quad (6.15)$$

Expressions (6.8), (6.12) and (6.13) define the so-called *loading/unloading conditions* of the elasticplastic model; that is, the constraints

$$\Phi \leq 0, \quad \dot{\gamma} \geq 0, \quad \dot{\gamma} \Phi = 0, \quad (6.16)$$

establish when plastic flow may occur.

6.2.5. THE HARDENING LAW

Finally, the complete characterisation of the uniaxial model is achieved with the introduction of the *hardening law*. As remarked in item 3 of Section 6.1, an evolution of the yield stress accompanies the evolution of the plastic strain. This phenomenon, known as *hardening*, can be incorporated into the uniaxial model simply by assuming that, in the definition (6.5) of Φ , the yield stress σ_y is a given function

$$\sigma_y = \sigma_y(\bar{\varepsilon}^p) \quad (6.17)$$

of the *accumulated* axial plastic strain, $\bar{\varepsilon}^p$. The accumulated axial plastic strain is defined as

$$\bar{\varepsilon}^p \equiv \int_0^t |\dot{\varepsilon}^p| dt, \quad (6.18)$$

thus ensuring that both tensile and compressive plastic straining contribute to $\bar{\varepsilon}^p$. Clearly, in a monotonic tensile test we have

$$\bar{\varepsilon}^p = \varepsilon^p, \quad (6.19)$$

whereas in a monotonic compressive uniaxial test,

$$\bar{\varepsilon}^p = -\varepsilon^p. \quad (6.20)$$

The curve defined by the hardening function $\sigma_y(\bar{\varepsilon}^p)$ is usually referred to as the *hardening curve* (Figure 6.4).

From the definition of $\bar{\varepsilon}^p$, it follows that its evolution law is given by

$$\dot{\bar{\varepsilon}}^p = |\dot{\varepsilon}^p|, \quad (6.21)$$

which, in view of the plastic flow rule, is equivalent to

$$\dot{\bar{\varepsilon}}^p = \dot{\gamma}. \quad (6.22)$$

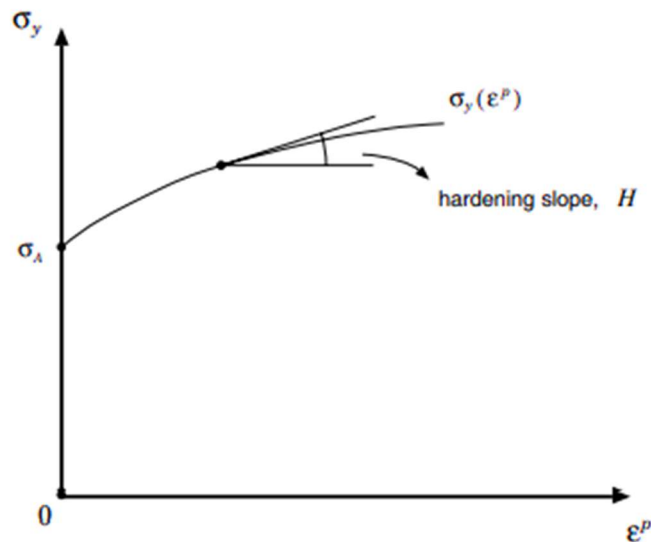


Figure 2.3.5.4: One-dimensional model. Hardening curve.

1. Elastoplastic split of the axial strain

$$\varepsilon = \varepsilon^e + \varepsilon^p$$

2. Uniaxial elastic law

$$\sigma = E \varepsilon^e$$

3. Yield function

$$\Phi(\sigma, \sigma_y) = |\sigma| - \sigma_y$$

4. Plastic flow rule

$$\dot{\varepsilon}^p = \dot{\gamma} \text{sign}(\sigma)$$

5. Hardening law

$$\sigma_y = \sigma_y(\bar{\varepsilon}^p)$$

$$\dot{\bar{\varepsilon}}^p = \dot{\gamma}$$

6. Loading/unloading criterion

$$\Phi \leq 0, \quad \dot{\gamma} \geq 0, \quad \dot{\gamma} \Phi = 0$$

So far, in the uniaxial plasticity model introduced above, the *plastic multiplier*, $\dot{\gamma}$, was left indeterminate during plastic yielding. Indeed, expressions (6.12) and (6.13) just tell us that $\dot{\gamma}$ vanishes during elastic straining but may assume *any* non-negative value during plastic flow. In order to eliminate this indetermination, it should be noted firstly that, *during plastic flow*,

the value of the yield function remains constant

$$\dot{\Phi} = 0, \quad (6.23)$$

as the absolute value of the current stress always coincides with the current yield stress. Therefore, the following additional complementarity condition may be established:

$$\dot{\Phi} \dot{\gamma} = 0 \quad (6.24)$$

which implies that the rate of Φ vanishes whenever plastic yielding occurs ($\dot{\gamma} \neq 0$),

$$\dot{\Phi} = 0, \quad (6.25)$$

and, during elastic straining, ($\dot{\gamma} = 0$), $\dot{\Phi}$ may assume any value. Equation (6.25) is called the *consistency condition*. By taking the time derivative of the yield function (6.5), one obtains

$$\dot{\Phi} = \text{sign}(\sigma) \dot{\sigma} - H \dot{\varepsilon}^p, \quad (6.26)$$

where H is called the *hardening modulus*, or *hardening slope*, and is defined as (refer to Figure 6.4)

$$H = H(\bar{\varepsilon}^p) = \frac{d\sigma_y}{d\bar{\varepsilon}^p}. \quad (6.27)$$

Under plastic yielding, equation (6.25) holds so that one has the following expression for the stress rate

$$\text{sign}(\sigma) \dot{\sigma} = H \dot{\varepsilon}^p. \quad (6.28)$$

From the elastic law, it follows that

$$\dot{\sigma} = E(\dot{\varepsilon} - \dot{\varepsilon}^p). \quad (6.29)$$

Finally, by combining the above expression with (6.22), (6.28) and (6.10), the plastic multiplier, $\dot{\gamma}$, is *uniquely* determined during plastic yielding as

$$\dot{\gamma} = \frac{E}{H + E} \text{sign}(\sigma) \dot{\varepsilon} = \frac{E}{H + E} |\dot{\varepsilon}|. \quad (6.30)$$

6.2.8. THE ELASTOPLASTIC TANGENT MODULUS

Let us now return to the stress-strain curve of Figure 6.2. Plastic flow at a generic yield limit produces the following tangent relation between strain and stress

$$\dot{\sigma} = E^{cp} \dot{\varepsilon}, \quad (6.31)$$

where E^{cp} is called the *elastoplastic tangent modulus*. By combining expressions (6.31), (6.29), the flow rule (6.10) and (6.30) the following expression is obtained for the elastoplastic tangent modulus

$$E^{cp} = \frac{E H}{E + H}. \quad (6.32)$$

Equivalently, the hardening modulus, H , can be expressed in terms of the elastic modulus and the elastoplastic modulus as

$$H = \frac{E^{cp}}{1 - E^{cp}/E}. \quad (6.33)$$

A mathematical model of a uniaxial tension experiment with a ductile metal has been described in the previous section. As already mentioned, the one-dimensional equations contain all basic components of a general elastoplastic constitutive model:

- the elastoplastic strain decomposition;
- an elastic law;
- a yield criterion, stated with the use of a yield function;
- a plastic flow rule defining the evolution of the plastic strain; and
- a hardening law, characterising the evolution of the yield limit.

The generalisation of these concepts for application in two- and three-dimensional situations is described in this section.

Following the decomposition of the uniaxial strain given in the previous section, the corresponding generalisation is obtained by splitting the strain *tensor*, ε , into the sum of an elastic component, ε^e , and a plastic component, ε^p ; that is,

$$\varepsilon = \varepsilon^e + \varepsilon^p. \quad (6.34)$$

The tensors ε^e and ε^p are known, respectively, as the *elastic strain tensor* and the *plastic strain tensor*. The corresponding rate form of the additive split reads

$$\dot{\varepsilon} = \dot{\varepsilon}^e + \dot{\varepsilon}^p. \quad (6.35)$$

Note that (6.35) together with the given initial condition

$$\varepsilon(t_0) = \varepsilon^e(t_0) + \varepsilon^p(t_0) \quad (6.36)$$

at a (pseudo-)time t_0 is equivalent to (6.34).

The formulation of general dissipative models of solids within the framework of thermodynamics with an internal variable has been addressed in Section 3.5 of Chapter 3. Recall that the free energy potential plays a crucial role in the derivation of the model and provides the constitutive law for stress. The starting point of the theories of plasticity treated in this book is the assumption that the free energy, ψ , is a function

$$\psi(\varepsilon, \varepsilon^p, \alpha),$$

of the total strain, the plastic strain (taken as an internal variable) and a set α of internal variables associated with the phenomenon of hardening. It is usual to assume that the free

energy can be split as

$$\begin{aligned}\psi(\boldsymbol{\varepsilon}, \boldsymbol{\varepsilon}^p, \boldsymbol{\alpha}) &= \psi^e(\boldsymbol{\varepsilon} - \boldsymbol{\varepsilon}^p) + \psi^p(\boldsymbol{\alpha}) \\ &= \psi^e(\boldsymbol{\varepsilon}^e) + \psi^p(\boldsymbol{\alpha})\end{aligned}\quad (6.37)$$

into a sum of an elastic contribution, ψ^e , whose dependence upon strains and internal variables appears only through the elastic strain, and a contribution due to hardening, ψ^p .

Following the above expression for the free energy, the Clausius–Duhem inequality reads

$$\left(\boldsymbol{\sigma} - \bar{\rho} \frac{\partial \psi^e}{\partial \boldsymbol{\varepsilon}^e} \right) : \dot{\boldsymbol{\varepsilon}}^e + \boldsymbol{\sigma} : \dot{\boldsymbol{\varepsilon}}^p - \boldsymbol{A} * \dot{\boldsymbol{\alpha}} \geq 0, \quad (6.38)$$

where

$$\boldsymbol{A} \equiv \bar{\rho} \partial \psi^p / \partial \boldsymbol{\alpha} \quad (6.39)$$

is the *hardening thermodynamical force* and we note that $-\boldsymbol{\sigma}$ is the thermodynamical force associated with the plastic strain while the symbol $*$ indicates the appropriate product between \boldsymbol{A} and $\dot{\boldsymbol{\alpha}}$. The above inequality implies a general elastic law of the form

$$\boldsymbol{\sigma} = \bar{\rho} \frac{\partial \psi^e}{\partial \boldsymbol{\varepsilon}^e}, \quad (6.40)$$

so that the requirement of non-negative dissipation can be reduced to

$$\Upsilon^p(\boldsymbol{\sigma}, \boldsymbol{A}; \dot{\boldsymbol{\varepsilon}}^p, \dot{\boldsymbol{\alpha}}) \geq 0, \quad (6.41)$$

where the function Υ^p , defined by

$$\Upsilon^p(\boldsymbol{\sigma}, \boldsymbol{A}; \dot{\boldsymbol{\varepsilon}}^p, \dot{\boldsymbol{\alpha}}) \equiv \boldsymbol{\sigma} : \dot{\boldsymbol{\varepsilon}}^p - \boldsymbol{A} * \dot{\boldsymbol{\alpha}}, \quad (6.42)$$

is called the *plastic dissipation function*.

This chapter is focused on materials whose elastic behaviour is *linear* (as in the uniaxial model of the previous section) and isotropic. In this case, the elastic contribution to the free energy is given by

$$\begin{aligned}\bar{\rho} \psi^e(\boldsymbol{\varepsilon}^e) &= \frac{1}{2} \boldsymbol{\varepsilon}^e : \mathbf{D}^e : \boldsymbol{\varepsilon}^e \\ &= G \boldsymbol{\varepsilon}_d^e : \boldsymbol{\varepsilon}_d^e + \frac{1}{2} K (\boldsymbol{\varepsilon}_v^e)^2\end{aligned}\quad (6.43)$$

where \mathbf{D}^e is the standard isotropic elasticity tensor and G and K are, respectively the shear and bulk moduli. The tensor $\boldsymbol{\varepsilon}_d^e$ is the deviatoric component of the elastic strain and $\boldsymbol{\varepsilon}_v^e \equiv \text{tr}[\boldsymbol{\varepsilon}^e]$ is the volumetric elastic strain. Thus, the general counterpart of uniaxial elastic law (6.4) is given by

$$\begin{aligned}\boldsymbol{\sigma} &= \mathbf{D}^e : \boldsymbol{\varepsilon}^e \\ &= 2G \boldsymbol{\varepsilon}_d^e + K \boldsymbol{\varepsilon}_v^e \mathbf{I}.\end{aligned}\quad (6.44)$$

Recall that in the uniaxial yield criterion it was established that plastic flow may occur when the uniaxial stress attains a critical value. This principle could be expressed by means of a yield function which is negative when only elastic deformations are possible and reaches zero when plastic flow is imminent. Extension of this concept to the three-dimensional case is obtained by stating that plastic flow may occur only when

$$\Phi(\boldsymbol{\sigma}, \mathbf{A}) = 0, \quad (6.45)$$

where the scalar yield function, Φ , is now a function of the stress *tensor* and a set \mathbf{A} of hardening thermodynamical forces. Analogously to the uniaxial case, a yield function defines the *elastic domain* as the set

$$\mathcal{E} = \{\boldsymbol{\sigma} \mid \Phi(\boldsymbol{\sigma}, \mathbf{A}) < 0\} \quad (6.46)$$

of stresses for which plastic yielding is not possible. Any stress lying in the elastic domain or on its boundary is said to be *plastically admissible*. We then define the *set of plastically admissible stresses* (or *plastically admissible domain*) as

$$\bar{\mathcal{E}} = \{\boldsymbol{\sigma} \mid \Phi(\boldsymbol{\sigma}, \mathbf{A}) \leq 0\}. \quad (6.47)$$

The yield locus, i.e. the set of stresses for which plastic yielding may occur, is the boundary of the elastic domain, where $\Phi(\boldsymbol{\sigma}, \mathbf{A}) = 0$. The yield locus in this case is represented by a hypersurface in the space of stresses. This hypersurface is termed the *yield surface* and is defined as

$$\mathcal{Y} = \{\boldsymbol{\sigma} \mid \Phi(\boldsymbol{\sigma}, \mathbf{A}) = 0\}. \quad (6.48)$$

The complete characterisation of the general plasticity model requires the definition of the evolution laws for the internal variables, i.e. the variables associated with the dissipative phenomena. In the present case, the internal variables are the plastic strain tensor and the set $\boldsymbol{\alpha}$ of hardening variables. The following plastic flow rule and hardening law are then postulated

$$\dot{\boldsymbol{\epsilon}}^p = \dot{\gamma} \mathbf{N} \quad (6.49)$$

$$\dot{\boldsymbol{\alpha}} = \dot{\gamma} \mathbf{H}, \quad (6.50)$$

where the tensor

$$\mathbf{N} = \mathbf{N}(\boldsymbol{\sigma}, \mathbf{A}) \quad (6.51)$$

is termed the *flow vector* and the function

$$\mathbf{H} = \mathbf{H}(\boldsymbol{\sigma}, \mathbf{A}) \quad (6.52)$$

is the *generalised hardening modulus* which defines the evolution of the hardening variables. The evolution equations (6.49) and (6.50) are complemented by the loading/unloading conditions

$$\Phi \leq 0, \quad \dot{\gamma} \geq 0, \quad \Phi \dot{\gamma} = 0, \quad (6.53)$$

that define when evolution of plastic strains and internal variables ($\dot{\gamma} \neq 0$) may occur.

1. Additive decomposition of the strain tensor

$$\boldsymbol{\varepsilon} = \boldsymbol{\varepsilon}^e + \boldsymbol{\varepsilon}^p$$

or

$$\dot{\boldsymbol{\varepsilon}} = \dot{\boldsymbol{\varepsilon}}^e + \dot{\boldsymbol{\varepsilon}}^p, \quad \boldsymbol{\varepsilon}(t_0) = \boldsymbol{\varepsilon}^e(t_0) + \boldsymbol{\varepsilon}^p(t_0)$$

2. Free-energy function

$$\psi = \psi(\boldsymbol{\varepsilon}^e, \boldsymbol{\alpha})$$

where $\boldsymbol{\alpha}$ is a set of hardening internal variables

3. Constitutive equation for $\boldsymbol{\sigma}$ and hardening thermodynamic forces \mathbf{A}

$$\boldsymbol{\sigma} = \bar{\rho} \frac{\partial \psi}{\partial \boldsymbol{\varepsilon}^e}, \quad \mathbf{A} = \bar{\rho} \frac{\partial \psi}{\partial \boldsymbol{\alpha}}$$

4. Yield function

$$\Phi = \Phi(\boldsymbol{\sigma}, \mathbf{A})$$

5. Plastic flow rule and hardening law

$$\dot{\boldsymbol{\varepsilon}}^p = \dot{\gamma} \mathbf{N}(\boldsymbol{\sigma}, \mathbf{A})$$

$$\dot{\boldsymbol{\alpha}} = \dot{\gamma} \mathbf{H}(\boldsymbol{\sigma}, \mathbf{A})$$

6. Loading/unloading criterion

$$\Phi \leq 0, \quad \dot{\gamma} \geq 0, \quad \dot{\gamma} \Phi = 0$$

In the formulation of multidimensional plasticity models, it is often convenient to define the flow rule (and possibly the hardening law) in terms of a *flow (or plastic) potential*. The starting point of such an approach is to postulate the existence of a flow potential with general form

$$\Psi = \Psi(\boldsymbol{\sigma}, \mathbf{A}) \quad (6.54)$$

from which the flow vector, \mathbf{N} , is obtained as

$$\mathbf{N} \equiv \frac{\partial \Psi}{\partial \boldsymbol{\sigma}}. \quad (6.55)$$

If the hardening law is assumed to be derived from the same potential, then we have in addition

$$\mathbf{H} \equiv -\frac{\partial \Psi}{\partial \mathbf{A}}. \quad (6.56)$$

When such an approach is adopted, the plastic potential, Ψ , is required to be a non-negative convex function of both $\boldsymbol{\sigma}$ and \mathbf{A} and zero-valued at the origin,

$$\Psi(\mathbf{0}, \mathbf{0}) = 0. \quad (6.57)$$

These restrictions ensure that the dissipation inequality (6.41) is satisfied *a priori* by the evolution equations (6.49) and (6.50).

Associative flow rule

As we shall see later, many plasticity models, particularly for ductile metals, have their yield function, Φ , as a flow potential, i.e.

$$\Psi \equiv \Phi. \quad (6.58)$$

Such models are called associative (or associated) plasticity models.

Here we extend to the multidimensional case the procedure for the determination of the plastic multiplier, $\dot{\gamma}$, described in Section 6.2.7 for the one-dimensional plasticity model. Following the same arguments employed in Section 6.2.7, the starting point in the determination of $\dot{\gamma}$ is the consideration of the additional complementarity equation

$$\dot{\Phi} \dot{\gamma} = 0, \quad (6.59)$$

which implies the *consistency condition*

$$\dot{\Phi} = 0 \quad (6.60)$$

under plastic yielding (when $\dot{\gamma} \neq 0$). By differentiating the yield function with respect to time, we obtain

$$\dot{\Phi} = \frac{\partial \Phi}{\partial \sigma} : \dot{\sigma} + \frac{\partial \Phi}{\partial A} * \dot{A}. \quad (6.61)$$

By taking into account the additive split of the strain tensor, the elastic law and the plastic flow rule (6.49), we promptly find the obvious rate form

$$\dot{\sigma} = \mathbf{D}^e : (\dot{\epsilon} - \dot{\epsilon}^p) = \mathbf{D}^e : (\dot{\epsilon} - \dot{\gamma} \mathbf{N}). \quad (6.62)$$

This, together with the definition of A in terms of the free-energy potential (refer to expression (6.39)) and the evolution law (6.50), allow us to write (6.61) equivalently as

$$\begin{aligned} \dot{\Phi} &= \frac{\partial \Phi}{\partial \sigma} : \mathbf{D}^e : (\dot{\epsilon} - \dot{\epsilon}^p) + \frac{\partial \Phi}{\partial A} * \bar{\rho} \frac{\partial^2 \psi^p}{\partial \alpha^2} * \dot{\alpha} \\ &= \frac{\partial \Phi}{\partial \sigma} : \mathbf{D}^e : (\dot{\epsilon} - \dot{\gamma} \mathbf{N}) + \dot{\gamma} \frac{\partial \Phi}{\partial A} * \bar{\rho} \frac{\partial^2 \psi^p}{\partial \alpha^2} * \mathbf{H}. \end{aligned} \quad (6.63)$$

Finally, the above expression and the consistency condition (6.60) lead to the following closed formula for the plastic multiplier

$$\dot{\gamma} = \frac{\partial \Phi / \partial \sigma : \mathbf{D}^e : \dot{\epsilon}}{\partial \Phi / \partial \sigma : \mathbf{D}^e : \mathbf{N} - \partial \Phi / \partial A * \bar{\rho} \partial^2 \psi^p / \partial \alpha^2 * \mathbf{H}}. \quad (6.64)$$

In the elastic regime, the rate constitutive equation for stress reads simply

$$\dot{\sigma} = \mathbf{D}^e : \dot{\epsilon}. \quad (6.65)$$

Under plastic flow, the corresponding rate relation can be obtained by introducing expression (6.64) into (6.62). The rate equation reads

$$\dot{\sigma} = \mathbf{D}^{ep} : \dot{\epsilon}, \quad (6.66)$$

where \mathbf{D}^{ep} is the *elastoplastic tangent modulus* given by

$$\mathbf{D}^{ep} = \mathbf{D}^e - \frac{(\mathbf{D}^e : \mathbf{N}) \otimes (\mathbf{D}^e : \partial \Phi / \partial \sigma)}{\partial \Phi / \partial \sigma : \mathbf{D}^e : \mathbf{N} - \partial \Phi / \partial A * \bar{\rho} \partial^2 \psi^p / \partial \alpha^2 * \mathbf{H}}. \quad (6.67)$$

In obtaining the above expression, we have made use of the fact that the symmetry (refer to equation (2.87), page 29) of the elasticity tensor implies

$$\partial \Phi / \partial \sigma : \mathbf{D}^e : \dot{\epsilon} = \mathbf{D}^e : \partial \Phi / \partial \sigma : \dot{\epsilon}. \quad (6.68)$$

The fourth-order tensor \mathbf{D}^{ep} is the multidimensional generalisation of the scalar modulus E^{ep} associated with the slope of the uniaxial stress-strain curve under plastic flow. In the computational plasticity literature, \mathbf{D}^{ep} is frequently referred to as the *continuum elastoplastic tangent operator*.

Remark 6.1 (The symmetry of \mathbf{D}^{ep}). Note that if the plastic flow rule is *associative*, i.e. if $\mathbf{N} \equiv \partial \Phi / \partial \sigma$, then the continuum elastoplastic tangent operator is *symmetric*. For models with non-associative plastic flow, \mathbf{D}^{ep} is generally unsymmetric.

It should be noted that expressions (6.55) and (6.56) only make sense if the potential Ψ is differentiable. When that happens, the flow vector, \mathbf{N} , can be interpreted as a vector

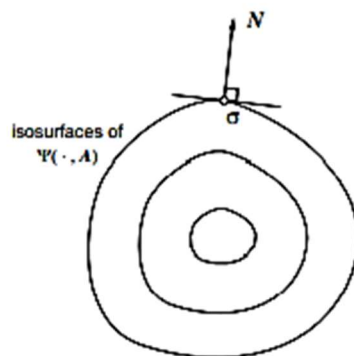


Figure 6.5. The flow vector. Smooth potential.

normal to the iso-surfaces of function Ψ in the space of stresses (with fixed A). A schematic representation of N in this case is shown in Figure 6.5. The generalised modulus, H , can be interpreted in a completely analogous way.

The requirement of differentiability of the flow potential is, however, too restrictive and many practical plasticity models are based on the use of a non-differentiable Ψ . Specific examples are given later in this chapter. For a more comprehensive account of such theories the reader is referred to Duvaut and Lions (1976), Eve *et al.* (1990) and Han and Reddy (1999). In such cases, the function Ψ is called a *pseudo-potential* or *generalised potential* and the formulation of the evolution laws for the internal variables can be dealt with by introducing the concept of *subdifferential sets*, which generalises the classical definition of derivative.[†]

Subgradients and the subdifferential

Let us consider a scalar function $y : \mathcal{R}^n \rightarrow \mathcal{R}$. The *subdifferential* of y at a point \bar{x} is the set

$$\partial y(\bar{x}) = \{s \in \mathcal{R}^n \mid y(x) - y(\bar{x}) \geq s \cdot (x - \bar{x}), \forall x \in \mathcal{R}^n\}. \quad (6.69)$$

If the set ∂y is not empty at \bar{x} , the function y is said to be *subdifferentiable* at \bar{x} . The elements of ∂y are called *subgradients* of y . If the function y is *differentiable*, then the subdifferential contains a *unique* subgradient which coincides with the derivative of y ,

$$\partial y = \left\{ \frac{dy}{dx} \right\}. \quad (6.70)$$

A schematic illustration of the concept of subdifferential is shown in Figure 6.6 for $n = 1$. In this case, when y is subdifferentiable (but not necessarily differentiable) at a point \bar{x} , the subdifferential at that point is composed of all slopes s lying between the slopes on the right and left of \bar{x} (the two one-sided derivatives of y at \bar{x}).

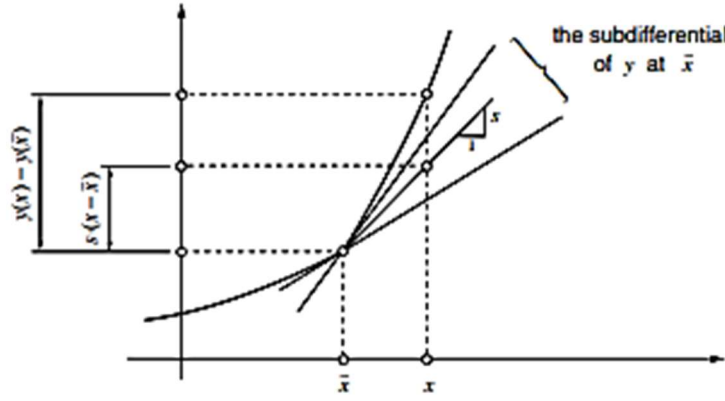


Figure 6.6. The subdifferential of a convex function.

Plastic flow with subdifferentiable flow potentials

Assume now that the (pseudo-) potential Ψ is a subdifferentiable function of σ and A . At points where Ψ is non-differentiable in σ , the isosurfaces of Ψ in the space of stresses contain a singularity (corner) where the normal direction is not uniquely defined. A typical situation is schematically illustrated in Figure 6.7 where two distinct normals, N_1 and N_2 , are assumed to exist. In this case, the subdifferential of Ψ with respect to σ , denoted $\partial_\sigma \Psi$, is the set of vectors contained in the cone defined by all linear combinations (with positive coefficients) of N_1 and N_2 . The generalisation of the plastic flow rule (6.49) is obtained by replacing expression (6.55) for the flow vector with

$$N \in \partial_\sigma \Psi, \quad (6.71)$$

i.e. the flow vector N is now assumed to be a *subgradient* of Ψ . Analogously, the evolution law (6.50) for α can be generalised with the replacement of the definition (6.56) by

$$H \in -\partial_A \Psi. \quad (6.72)$$

At this point, it should be remarked that differentiability of Ψ with respect to the stress tensor is violated for some very basic plasticity models, such as the Tresca, Mohr–Coulomb and Drucker–Prager theories to be seen later. Therefore, the concepts of subgradient and subdifferential sets introduced above are important in the formulation of evolution laws for ε^P .

An alternative definition of the plastic flow rule with non-smooth potentials, which incorporates a wide class of models, is obtained as follows. Firstly assume that a *finite* number, n , of distinct normals (N_1, N_2, \dots, N_n) is defined at a generic singular point of an isosurface of Ψ . In this case, any subgradient of Ψ can be written as a linear combination

$$c_1 N_1 + c_2 N_2 + \dots + c_n N_n,$$

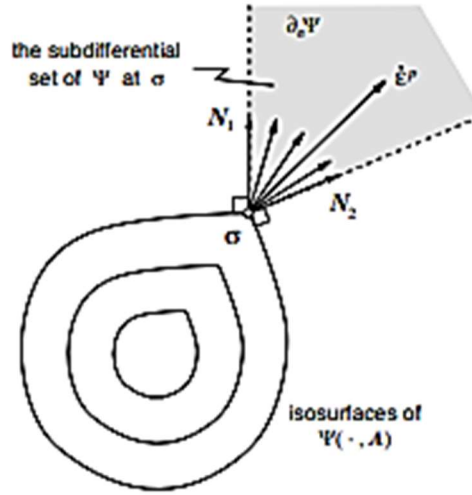


Figure 6.7. The flow vector. Non-smooth potential.

with *non-negative* coefficients c_1, c_2, \dots, c_n .[‡] Based on this observation, the flow rule (6.49) can be generalised as

$$\dot{\epsilon}^p = \sum_{i=1}^n \dot{\gamma}_i N_i, \quad (6.73)$$

with all n plastic multipliers required to be non-negative

$$\dot{\gamma}_i \geq 0, \quad i = 1, \dots, n. \quad (6.74)$$

The generalisation of the plastic flow law, in this format, was originally proposed by Koiter (1953).

Multisurface models

The above concepts are particularly useful in defining evolution laws for *multisurface* plasticity models. In a generic multisurface model, the elastic domain is bound by a *set* of n surfaces in the space of stresses which intersect in a non-smooth fashion. In this case, n yield functions (Φ_i , $i = 1, \dots, n$) are defined so that each bounding surface is given by an equation

$$\Phi_i(\sigma, A) = 0. \quad (6.75)$$

The elastic domain in this case reads

$$\mathcal{E} = \{\sigma \mid \Phi_i(\sigma, A) < 0, \quad i = 1, \dots, n\}, \quad (6.76)$$

and the yield surface, i.e. the boundary of \mathcal{E} , is the set of all stresses such that $\Phi_i(\sigma, A) = 0$ for at least one i and $\Phi_j(\sigma, A) \leq 0$ for all other indices $j \neq i$.

Assuming associativity ($\Psi \equiv \Phi$), the situation discussed previously, where the subgradient of the flow potential is a linear combination of a finite number of normals, is recovered. Thus, the plastic flow rule can be written in the general form (6.73) with the normals being defined here as

$$N_i = \frac{\partial \Phi_i}{\partial \sigma}. \quad (6.77)$$

In the present case, the standard loading/unloading criterion (6.53) is replaced by the generalisation

$$\Phi_i \leq 0, \quad \dot{\gamma}_i \geq 0, \quad \Phi_i \dot{\gamma}_i = 0, \quad (6.78)$$

which must hold for each $i = 1, \dots, n$. Note that summation on repeated indices is not implied in the above law.

The general constitutive model for elastoplastic materials has been established in the previous section. There, the yield criterion has been stated in its general form, without reference to any particular criteria. In this section, some of the most common yield criteria used in engineering practice are described in detail; namely, the criteria of *Tresca*, *von Mises*, *Mohr–Coulomb* and *Drucker–Prager*.

6.4.1. THE TRESCA YIELD CRITERION

This criterion was proposed by Tresca (1868) to describe plastic yielding in metals. The Tresca yield criterion assumes that *plastic yielding begins when the maximum shear stress reaches a critical value*.

Recall the spectral representation of the stress tensor,

$$\boldsymbol{\sigma} = \sum_{i=1}^3 \sigma_i \mathbf{e}_i \otimes \mathbf{e}_i, \quad (6.79)$$

where σ_i are the *principal stresses* and \mathbf{e}_i the associated unit eigenvectors, and let σ_{\max} and σ_{\min} be, respectively, the maximum and minimum principal stresses

$$\begin{aligned} \sigma_{\max} &= \max(\sigma_1, \sigma_2, \sigma_3); \\ \sigma_{\min} &= \min(\sigma_1, \sigma_2, \sigma_3). \end{aligned} \quad (6.80)$$

The *maximum shear stress*, τ_{\max} , is given by

$$\tau_{\max} = \frac{1}{2}(\sigma_{\max} - \sigma_{\min}). \quad (6.81)$$

According to the Tresca criterion, the onset of plastic yielding is defined by the condition

$$\frac{1}{2}(\sigma_{\max} - \sigma_{\min}) = \tau_y(\alpha), \quad (6.82)$$

where τ_y is the *shear yield stress*, here assumed to be a function of a *hardening internal variable*, α , to be defined later. The shear yield stress is the yield limit under a state of pure shear.

In view of (6.82), the yield function associated with the Tresca yield criterion can be represented as

$$\Phi(\sigma) = \frac{1}{2}(\sigma_{\max} - \sigma_{\min}) - \tau_y(\alpha), \quad (6.83)$$

with the onset of yielding characterised by $\Phi = 0$. Alternatively, the Tresca yield function may be defined as

$$\Phi(\sigma) = (\sigma_{\max} - \sigma_{\min}) - \sigma_y(\alpha), \quad (6.84)$$

where σ_y is the *uniaxial* yield stress

$$\sigma_y = 2 \tau_y, \quad (6.85)$$

that is, it is the stress level at which plastic yielding begins under *uniaxial* stress conditions. That σ_y is indeed the uniaxial yield stress for the Tresca theory can be established by noting that, when plastic yielding begins under uniaxial stress conditions, we have

$$\sigma_{\max} = \sigma_y, \quad \sigma_{\min} = 0. \quad (6.86)$$

The substitution of the above into (6.82) gives (6.85). The elastic domain for the Tresca criterion can be defined as

$$\mathcal{E} = \{\sigma \mid \Phi(\sigma, \sigma_y) < 0\}. \quad (6.87)$$

Pressure-insensitivity

Due to its definition exclusively in terms of *shear* stress, the Tresca criterion is *pressure insensitive*, that is, the hydrostatic pressure component,

$$p \equiv \frac{1}{3} \text{tr}[\sigma] = \frac{1}{3} (\sigma_1 + \sigma_2 + \sigma_3), \quad (6.88)$$

of the stress tensor does *not* affect yielding. Indeed, note that the superposition of an arbitrary pressure, p^* , on the stress tensor does not affect the value of the Tresca yield function

$$\Phi(\sigma + p^* \mathbf{I}) = \Phi(\sigma). \quad (6.89)$$

We remark that the von Mises criterion described in Section 6.4.2 below is also pressure-insensitive. This property is particularly relevant in the modelling of metals as, for these materials, the influence of the hydrostatic stress on yielding is usually negligible in practice.

Isotropy

One very important aspect of the Tresca criterion is its *isotropy* (a property shared by the von Mises, Mohr–Coulomb and Drucker–Prager criteria described in the following sections).

Note that, since Φ in (6.83) or (6.84) is defined as a function of the principal stresses, the Tresca yield function is an *isotropic* function of the stress tensor (refer to Section A.1, page 731, for the definition of isotropic scalar functions of a symmetric tensor), i.e. it satisfies

$$\Phi(\sigma) = \Phi(Q\sigma Q^T) \quad (6.90)$$

for all rotations Q ; that is, rotations of the state of stress do not affect the value of the yield function.

At this point, it is convenient to introduce the following definition: *A plastic yield criterion is said to be isotropic if it is defined in terms of an isotropic yield function of the stress tensor.*

Graphical representation

Since any isotropic scalar function of a symmetric tensor can be described as a function of the principal values of its argument, it follows that any iso-surface (i.e. any subset of the function domain with fixed function value) of such functions can be graphically represented as a surface in the space of principal values of the argument. This allows, in particular, the yield surface (refer to expression (6.48), page 150) of any isotropic yield criterion to be represented in a particularly simple and useful format as a three-dimensional surface in the space of principal stresses.

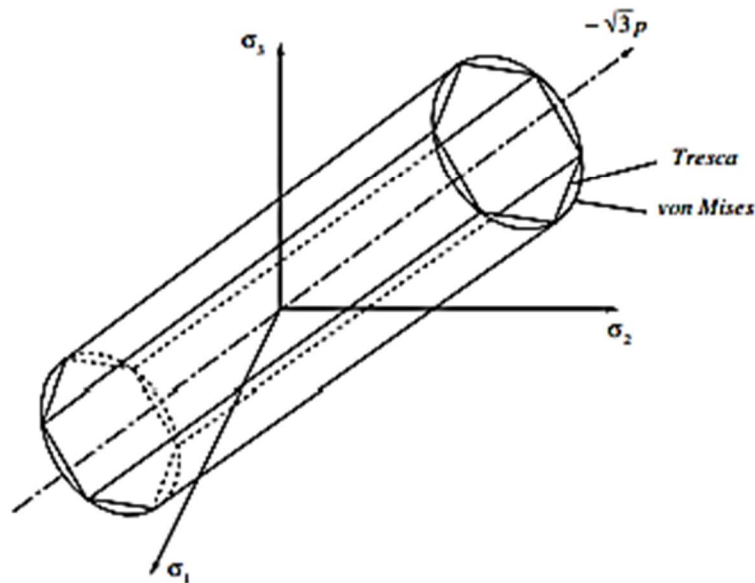


Figure 6.8. The Tresca and von Mises yield surfaces in principal stress space.

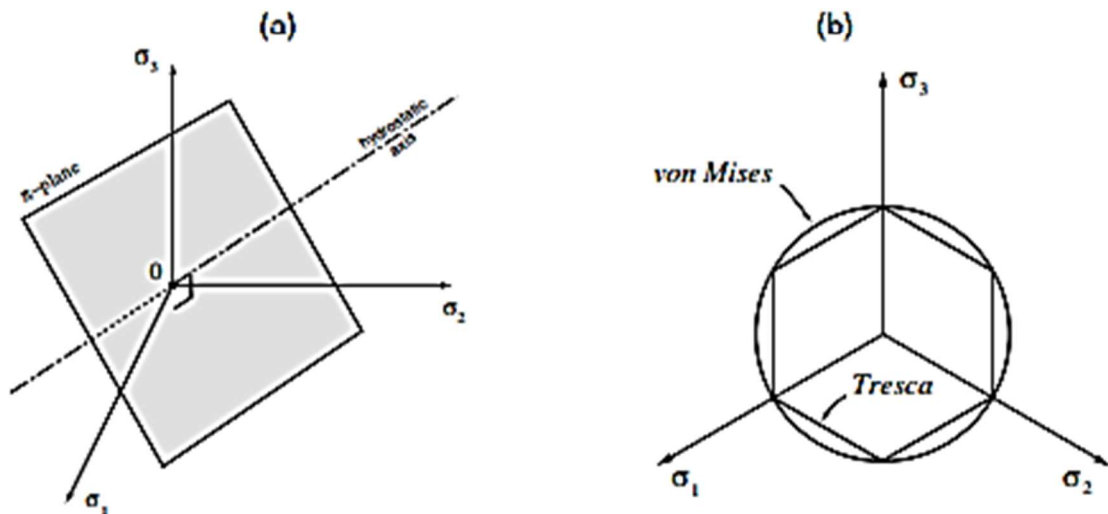


Figure 6.9. (a) The π -plane in principal stress space and, (b) the π -plane representation of the Tresca and von Mises yield surfaces.

In principal stress space, the Tresca yield surface, i.e. the set of stresses for which $\Phi = 0$, is graphically represented by the surface of an infinite hexagonal prism with axis coinciding with the hydrostatic line (also known as the space diagonal), defined by $\sigma_1 = \sigma_2 = \sigma_3$. This is illustrated in Figure 6.8. The elastic domain (for which $\Phi < 0$) corresponds to the interior of the prism. Due to the assumed insensitivity to pressure, a further simplification in the representation of the yield surface is possible in this case. The Tresca yield surface may be represented, without loss of generality, by its projection on the subspace of stresses with zero hydrostatic pressure component ($\sigma_1 + \sigma_2 + \sigma_3 = 0$). This subspace is called the *deviatoric plane*, also referred to as the π -plane. It is graphically illustrated in Figure 6.9(a). Figure 6.9(b) shows the π -plane projection of the Tresca yield surface.

Multisurface representation

Equivalently to the above representation, the Tresca yield criterion can be expressed by means of the following six yield functions

$$\begin{aligned}\Phi_1(\sigma, \sigma_y) &= \sigma_1 - \sigma_3 - \sigma_y \\ \Phi_2(\sigma, \sigma_y) &= \sigma_2 - \sigma_3 - \sigma_y \\ \Phi_3(\sigma, \sigma_y) &= \sigma_2 - \sigma_1 - \sigma_y \\ \Phi_4(\sigma, \sigma_y) &= \sigma_3 - \sigma_1 - \sigma_y \\ \Phi_5(\sigma, \sigma_y) &= \sigma_3 - \sigma_2 - \sigma_y \\ \Phi_6(\sigma, \sigma_y) &= \sigma_1 - \sigma_2 - \sigma_y,\end{aligned}\tag{6.91}$$

so that, for fixed σ_y , the equation

$$\Phi_i(\sigma, \sigma_y) = 0\tag{6.92}$$

corresponds to a *plane* in the space of principal stresses for each $i = 1, \dots, 6$ (Figure 6.10).

In the multisurface representation, the elastic domain for a given σ_y can be defined as

$$\mathcal{E} = \{\sigma \mid \Phi_i(\sigma, \sigma_y) < 0, i = 1, \dots, 6\}.\tag{6.93}$$

Definitions (6.87) and (6.93) are completely equivalent. The yield surface – the boundary of \mathcal{E} – is defined in this case as the set of stresses for which $\Phi_i(\sigma, \sigma_y) = 0$ for at least one i with $\Phi_j(\sigma, \sigma_y) \leq 0$ for $j \neq i$.

Invariant representation

Alternatively to the representations discussed above, it is also possible to describe the yield locus of the Tresca criterion in terms of *stress invariants*. In the invariant representation, proposed by Nayak and Zienkiewicz (1972) (see also Owen and Hinton 1980, and Crisfield 1997), the yield function assumes the format

$$\Phi = 2\sqrt{J_2} \cos \theta - \sigma_y,\tag{6.94}$$

where $J_2 = J_2(s)$ is the invariant of the stress deviator, s , defined by

$$J_2 \equiv -I_2(s) = \frac{1}{2} \text{tr}[s^2] = \frac{1}{2} s : s = \frac{1}{2} \|s\|^2.\tag{6.95}$$

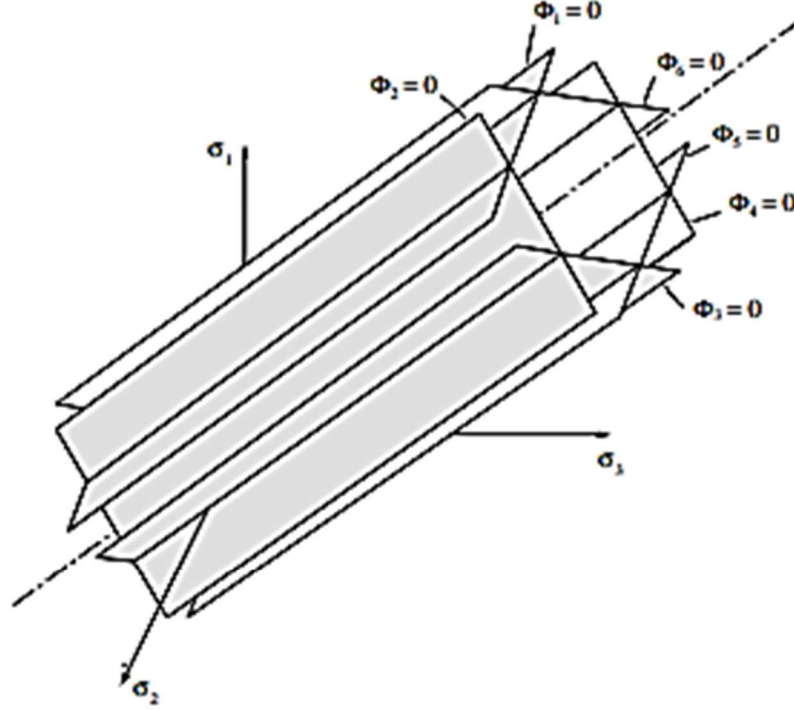


Figure 6.10. The Tresca criterion. Multisurface representation in principal stress space.

Recall that the stress deviator is given by

$$s \equiv \sigma - \frac{1}{3}(\text{tr} \sigma)I. \quad (6.96)$$

The *Lode angle*, θ , is a function of the deviatoric stress defined as

$$\theta \equiv \frac{1}{3} \sin^{-1} \left(\frac{-3\sqrt{3} J_3}{2J_2^{3/2}} \right), \quad (6.97)$$

where J_3 is the third principal invariant of stress deviator[§]

$$J_3 \equiv I_3(s) \equiv \det s = \frac{1}{3} \text{tr}(s)^3. \quad (6.98)$$

The Lode angle is the angle, on the deviatoric plane, between s and the nearest pure shear line (a pure shear line is graphically represented in Figure 6.11). It satisfies

$$-\frac{\pi}{6} \leq \theta \leq \frac{\pi}{6}. \quad (6.99)$$

Despite being used often in computational plasticity, the above invariant representation results in rather cumbersome algorithms for integration of the evolution equations of the Tresca model. This is essentially due to the high degree of nonlinearity introduced by the trigonometric function involved in the definition of the Lode angle. The multisurface representation, on the other hand, is found by the authors to provide an optimal parametrisation of the Tresca surface which results in a simpler numerical algorithm and will be adopted in the computational implementation of the model addressed in Chapter 8.

Also appropriate to describe plastic yielding in metals, this criterion was proposed by von Mises (1913). According to the von Mises criterion, *plastic yielding begins when the J_2 stress deviator invariant reaches a critical value*. This condition is mathematically represented by the equation

$$J_2 = R(\alpha), \quad (6.100)$$

where R is the critical value, here assumed to be a function of a hardening internal variable, α , to be defined later.

The physical interpretation of the von Mises criterion is given in the following. Since the elastic behaviour of the materials described in this chapter is assumed to be linear elastic, the stored elastic strain-energy at the generic state defined by the stress σ can be decomposed as the sum

$$\psi^e = \psi_d^e + \psi_v^e, \quad (6.101)$$

of a *distortional* contribution,

$$\bar{\rho} \psi_d^e = \frac{1}{2G} s : s = \frac{1}{G} J_2, \quad (6.102)$$

and a *volumetric* contribution,

$$\bar{\rho} \psi_v^e = \frac{1}{K} p^2, \quad (6.103)$$

where G and K are, respectively, the shear and bulk modulus. In view of (6.102), the von Mises criterion is equivalent to stating that *plastic yielding begins when the distortional elastic strain-energy reaches a critical value*. The corresponding critical value of the distortional energy is

$$\frac{1}{G} R.$$

It should be noted that, as in the Tresca criterion, the pressure component of the stress tensor does not take part in the definition of the von Mises criterion and only the deviatoric stress can influence plastic yielding. Thus, the von Mises criterion is also *pressure-insensitive*.

In a state of *pure shear*, i.e. a state with stress tensor

$$[\sigma] = \begin{bmatrix} 0 & \tau & 0 \\ \tau & 0 & 0 \\ 0 & 0 & 0 \end{bmatrix}, \quad (6.104)$$

we have, $s = \sigma$ and

$$J_2 = \tau^2. \quad (6.105)$$

Thus, a yield function for the von Mises criterion can be defined as

$$\Phi(\sigma) = \sqrt{J_2(s(\sigma))} - \tau_y, \quad (6.106)$$

where $\tau_y \equiv \sqrt{R}$ is the *shear* yield stress. Let us now consider a state of *uniaxial stress*:

$$[\sigma] = \begin{bmatrix} \sigma & 0 & 0 \\ 0 & 0 & 0 \\ 0 & 0 & 0 \end{bmatrix}. \quad (6.107)$$

In this case, we have

$$[s] = \begin{bmatrix} \frac{2}{3}\sigma & 0 & 0 \\ 0 & -\frac{1}{3}\sigma & 0 \\ 0 & 0 & -\frac{1}{3}\sigma \end{bmatrix} \quad (6.108)$$

and

$$J_2 = \frac{1}{3}\sigma^2. \quad (6.109)$$

The above expression for the J_2 -invariant suggests the following alternative definition of the von Mises yield function:

$$\Phi(\sigma) = q(\sigma) - \sigma_y, \quad (6.110)$$

where $\sigma_y \equiv \sqrt{3}R$ is the *uniaxial* yield stress and

$$q(\sigma) \equiv \sqrt{3 J_2(s(\sigma))} \quad (6.111)$$

is termed the *von Mises effective or equivalent stress*. The uniaxial and shear yield stresses for the von Mises criterion are related by

$$\sigma_y = \sqrt{3} \tau_y. \quad (6.112)$$

Note that this relation differs from that of the Tresca criterion given by (6.85). Obviously, due to its definition in terms of an invariant of the stress tensor, the von Mises yield function is an isotropic function of σ .

The von Mises and Tresca criteria may be set to agree with one another in either uniaxial stress or pure shear states. If they are set by using the yield functions (6.84) and (6.110) so that both predict the same uniaxial yield stress σ_y , then, under pure shear, the von Mises criterion will predict a yield stress $2/\sqrt{3}$ (≈ 1.155) times that given by the Tresca criterion. On the other hand, if both criteria are made to coincide under pure shear (expressions (6.83) and (6.106) with the same τ_y), then, in uniaxial stress states, the von Mises criterion will predict yielding at a stress level $\sqrt{3}/2$ (≈ 0.866) times the level predicted by Tresca's law.

The yield surface ($\Phi = 0$) associated with the von Mises criterion is represented, in the space of principal stresses, by the surface of an infinite circular cylinder, the axis of which coincides with the hydrostatic axis. The von Mises surface is illustrated in Figure 6.8 where it has been set to match the Tresca surface (shown in the same figure) under uniaxial stress. The corresponding π -plane representation is shown in Figure 6.9(b). The von Mises circle intersects the vertices of the Tresca hexagon. The yield surfaces for the von Mises and Tresca criteria set to coincide in shear is shown in Figure 6.11. In this case, the von Mises circle is tangent to the sides of the Tresca hexagon. It is remarked that, for many metals, experimentally determined yield surfaces fall between the von Mises and Tresca surfaces. A more general model, which includes both the Tresca and the von Mises yield surfaces as particular cases (and, in addition, allows for anisotropy of the yield surface), is described in Section 10.3.4 (starting page 427).

6.4.3. THE MOHR-COULOMB YIELD CRITERION

The criteria presented so far are pressure-insensitive and adequate to describe metals. For materials such as soils, rocks and concrete, whose behaviour is generally characterised by

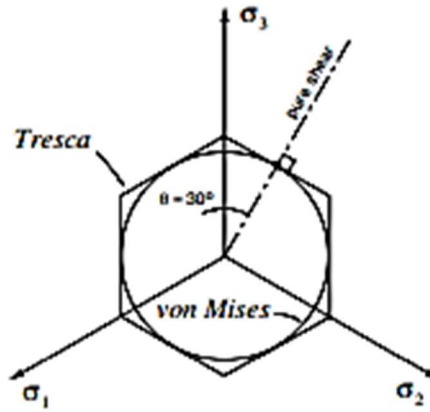


Figure 6.11. Yield surfaces for the Tresca and von Mises criteria coinciding in pure shear.

a strong dependence of the yield limit on the hydrostatic pressure, appropriate description of plastic yielding requires the introduction of *pressure-sensitivity*. A classical example of a pressure-sensitive law is given by the Mohr–Coulomb yield criterion described in the following.

The Mohr–Coulomb criterion is based on the assumption that the phenomenon of macroscopic plastic yielding is, essentially, the result of frictional sliding between material particles. Generalising Coulomb's friction law, this criterion states that *plastic yielding begins when, on a plane in the body, the shearing stress, τ , and the normal stress, σ_n , reach the critical combination*

$$\tau = c - \sigma_n \tan \phi, \quad (6.113)$$

where c is the cohesion and ϕ is the angle of internal friction or frictional angle. In the above, the normal stress, σ_n , was assumed tensile positive.

The yield locus of the Mohr–Coulomb criterion is the set of all stress states such that there exists a plane in which (6.113) holds. The Mohr–Coulomb yield locus can be easily visualised in the Mohr plane representation shown in Figure 6.12. It is the set of all stresses whose largest Mohr circle, i.e. the circle associated with the maximum and minimum principal stresses (σ_{\max} and σ_{\min} , respectively), is tangent to the critical line defined by $\tau = c - \sigma_n \tan \phi$. The elastic domain for the Mohr–Coulomb law is the set of stresses whose all three Mohr circles are below the critical line. From Figure 6.12, the yield condition (6.113) is found to be equivalent to the following form in terms of principal stresses

$$\frac{\sigma_{\max} - \sigma_{\min}}{2} \cos \phi = c - \left(\frac{\sigma_{\max} + \sigma_{\min}}{2} + \frac{\sigma_{\max} - \sigma_{\min}}{2} \sin \phi \right) \tan \phi, \quad (6.114)$$

which, rearranged, gives

$$(\sigma_{\max} - \sigma_{\min}) + (\sigma_{\max} + \sigma_{\min}) \sin \phi = 2c \cos \phi. \quad (6.115)$$

In view of (6.115), a yield function expressed in terms of the principal stresses can be immediately defined for the Mohr–Coulomb criterion as

$$\Phi(\sigma, c) = (\sigma_{\max} - \sigma_{\min}) + (\sigma_{\max} + \sigma_{\min}) \sin \phi - 2c \cos \phi. \quad (6.116)$$

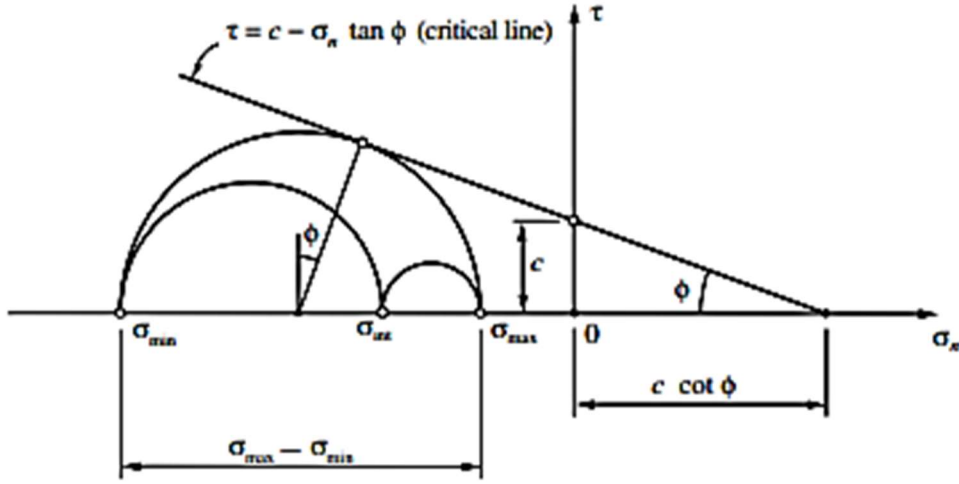


Figure 6.12. The Mohr-Coulomb criterion. Mohr plane representation.

Due to its definition in terms of principal stresses, this yield function is an isotropic function of σ . The corresponding yield surface ($\Phi = 0$) is a hexagonal pyramid aligned with the hydrostatic axis and whose apex is located at

$$p = c \cot \phi \quad (6.117)$$

on the tensile side of the hydrostatic axis. The Mohr-Coulomb surface is illustrated in Figure 6.13. Its pyramidal shape, as opposed to the prismatic shape of the Tresca surface, is a consequence of the *pressure-sensitivity* of the Mohr-Coulomb criterion. It should be noted, however, that both criteria coincide in the absence of internal friction, i.e. when $\phi = 0$. As no stress state is allowed on the outside of the yield surface, the apex of the pyramid (point A in the figure) defines the limit of resistance of the material to tensile pressures. Limited strength under tensile pressure is a typical characteristic of materials such as concrete, rock and soils, to which the Mohr-Coulomb criterion is most applicable.

Multisurface representation

Analogously to the multisurface representation of the Tresca criterion, the Mohr-Coulomb criterion can also be expressed by means of six functions:

$$\begin{aligned} \Phi_1(\sigma, c) &= \sigma_1 - \sigma_3 + (\sigma_1 + \sigma_3) \sin \phi - 2c \cos \phi \\ \Phi_2(\sigma, c) &= \sigma_2 - \sigma_3 + (\sigma_2 + \sigma_3) \sin \phi - 2c \cos \phi \\ \Phi_3(\sigma, c) &= \sigma_2 - \sigma_1 + (\sigma_2 + \sigma_1) \sin \phi - 2c \cos \phi \\ \Phi_4(\sigma, c) &= \sigma_3 - \sigma_1 + (\sigma_3 + \sigma_1) \sin \phi - 2c \cos \phi \\ \Phi_5(\sigma, c) &= \sigma_3 - \sigma_2 + (\sigma_3 + \sigma_2) \sin \phi - 2c \cos \phi \\ \Phi_6(\sigma, c) &= \sigma_1 - \sigma_2 + (\sigma_1 + \sigma_2) \sin \phi - 2c \cos \phi, \end{aligned} \quad (6.118)$$

whose roots, $\Phi_i(\sigma, c) = 0$ (for fixed c), define six planes in the principal stress space. Each plane contains one face of the Mohr-Coulomb pyramid represented in Figure 6.13.

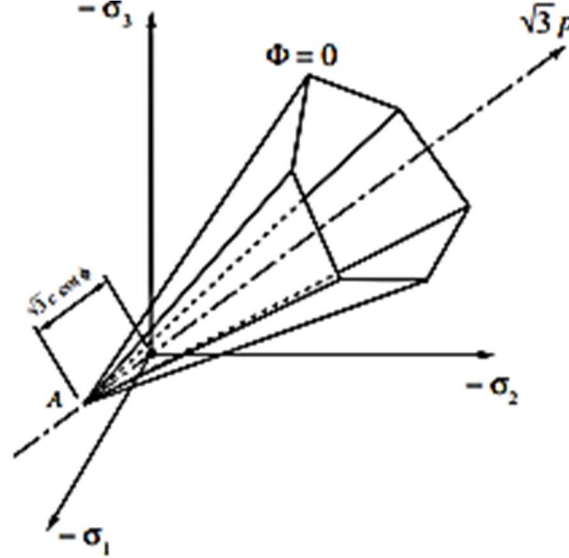


Figure 6.13. The Mohr-Coulomb yield surface in principal stress space.

The definition of the elastic domain and the yield surface in the multisurface representation is completely analogous to that of the Tresca criterion.

Invariant representation

Analogously to the invariant representation (6.94) of the Tresca criterion, the Mohr-Coulomb yield function can be expressed as (Owen and Hinton 1980, and Crisfield 1997):

$$\Phi = \left(\cos \theta - \frac{1}{\sqrt{3}} \sin \theta \sin \phi \right) \sqrt{J_2(s)} + p(\sigma) \sin \phi - c \cos \phi, \quad (6.119)$$

where the Lode angle, θ , is defined in (6.97). As for the Tresca model, in spite of its frequent use in computational plasticity, the invariant representation of the Mohr-Coulomb surface renders more complex numerical algorithms so that the multisurface representation is preferred in the computational implementation of the model described in Chapter 8.

6.4.4. THE DRUCKER-PRAGER YIELD CRITERION

This criterion has been proposed by Drucker and Prager (1952) as a smooth approximation to the Mohr-Coulomb law. It consists of a modification of the von Mises criterion in which an extra term is included to introduce pressure-sensitivity. The Drucker-Prager criterion states that *plastic yielding begins when the J_2 invariant of the deviatoric stress and the hydrostatic stress, p , reach a critical combination*. The onset of plastic yielding occurs when the equation

$$\sqrt{J_2(s)} + \eta p = \bar{c}, \quad (6.120)$$

is satisfied, where η and \bar{c} are material parameters. Represented in the principal stress space, the yield locus of this criterion is a circular cone whose axis is the hydrostatic line. For $\eta = 0$, the von Mises cylinder is recovered. The Drucker-Prager cone is illustrated in Figure 6.14.

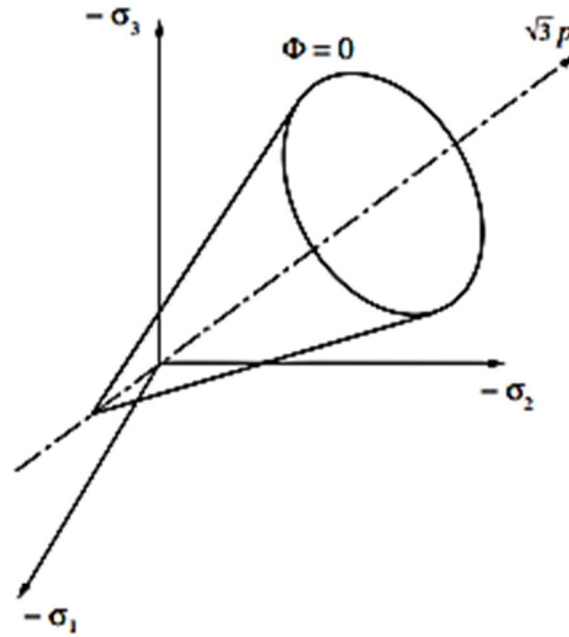


Figure 6.14. The Drucker-Prager yield surface in principal stress space.

In order to approximate the Mohr-Coulomb yield surface, it is convenient to define the Drucker-Prager yield function as

$$\Phi(\sigma, c) = \sqrt{J_2(s(\sigma))} + \eta p(\sigma) - \xi c, \quad (6.121)$$

where c is the *cohesion* and the parameters η and ξ are chosen according to the required approximation to the Mohr-Coulomb criterion. Note that the isotropy of the Mohr-Coulomb yield function follows from the fact that it is defined in terms of invariants of the stress tensor ($J_2(s)$ and p). Two of the most common approximations used are obtained by making the yield surfaces of the Drucker-Prager and Mohr-Coulomb criteria coincident either at the outer or inner edges of the Mohr-Coulomb surface. Coincidence at the *outer* edges is obtained when

$$\eta = \frac{6 \sin \phi}{\sqrt{3} (3 - \sin \phi)}, \quad \xi = \frac{6 \cos \phi}{\sqrt{3} (3 - \sin \phi)}, \quad (6.122)$$

whereas, coincidence at the *inner* edges is given by the choice

$$\eta = \frac{6 \sin \phi}{\sqrt{3} (3 + \sin \phi)}, \quad \xi = \frac{6 \cos \phi}{\sqrt{3} (3 + \sin \phi)}. \quad (6.123)$$

The outer and inner cones are known, respectively, as the *compression cone* and the *extension cone*. The inner cone matches the Mohr-Coulomb criterion in uniaxial tension and biaxial compression. The outer edge approximation matches the Mohr-Coulomb surface in uniaxial compression and biaxial tension. The π -plane section of both surfaces is shown in Figure 6.15. Another popular Drucker-Prager approximation to the Mohr-Coulomb criterion is obtained by forcing both criteria to predict identical collapse loads under *plane strain* conditions. In this case (the reader is referred to Section 4.7 of Chen and Mizuno (1990) for

derivation) the constants η and ξ read

$$\eta = \frac{3 \tan \phi}{\sqrt{9 + 12 \tan^2 \phi}}, \quad \xi = \frac{3}{\sqrt{9 + 12 \tan^2 \phi}}. \quad (6.124)$$

For all three sets of parameters above, the apex of the approximating Drucker–Prager cone coincides with the apex of the corresponding Mohr–Coulomb yield surface. It should be emphasised here that any of the above approximations to the Mohr–Coulomb criterion can give a poor description of the material behaviour for certain states of stress. Thus, according to the dominant stress state in a particular problem to be analysed, other approximations may be more appropriate. For instance, under plane stress, which can be assumed in the analysis of structures such as concrete walls, it may be convenient to use an approximation such that both criteria match under, say, uniaxial tensile and uniaxial compressive stress states. For the Mohr–Coulomb criterion to fit a given uniaxial tensile strength, f'_t , and a given uniaxial compressive strength, f'_c , the parameters ϕ and c have to be chosen as

$$\phi = \sin^{-1} \left(\frac{f'_c - f'_t}{f'_c + f'_t} \right), \quad c = \frac{f'_c f'_t}{f'_c - f'_t} \tan \phi. \quad (6.125)$$

The corresponding Drucker–Prager cone (Figure 6.16) that predicts the same uniaxial failure loads is obtained by setting

$$\eta = \frac{3 \sin \phi}{\sqrt{3}}, \quad \xi = \frac{2 \cos \phi}{\sqrt{3}}. \quad (6.126)$$

Its apex no longer coincides with the apex of the original Mohr–Coulomb pyramid. For problems where the failure mechanism is indeed dominated by uniaxial tension/compression, the above approximation should produce reasonable results. However, if for a particular problem, failure occurs under biaxial compression instead (with stresses near point f'_{bc} of Figure 6.16), then the above approximation will largely overestimate the limit load, particularly for high ratios f'_c/f'_t which are typical for concrete. Under such a condition, a different approximation (such as the inner cone that matches point f'_{bc}) needs to be adopted to produce sensible predictions. Another useful approximation for plane stress, where the Drucker–Prager cone coincides with the Mohr–Coulomb surface in biaxial tension (point f'_{bt}) and biaxial compression (point f'_{bc}), is obtained by setting

$$\eta = \frac{3 \sin \phi}{2\sqrt{3}}, \quad \xi = \frac{2 \cos \phi}{\sqrt{3}}. \quad (6.127)$$

Drucker–Prager approximations to the Mohr–Coulomb criterion are thoroughly discussed by Chen (1982), Chen and Mizuno (1990) and Zienkiewicz *et al.* (1978).

6.5.1. ASSOCIATIVE AND NON-ASSOCIATIVE PLASTICITY

It has already been said that a plasticity model is classed as *associative* if the yield function, Φ , is taken as the flow potential, i.e.

$$\Psi = \Phi. \quad (6.128)$$

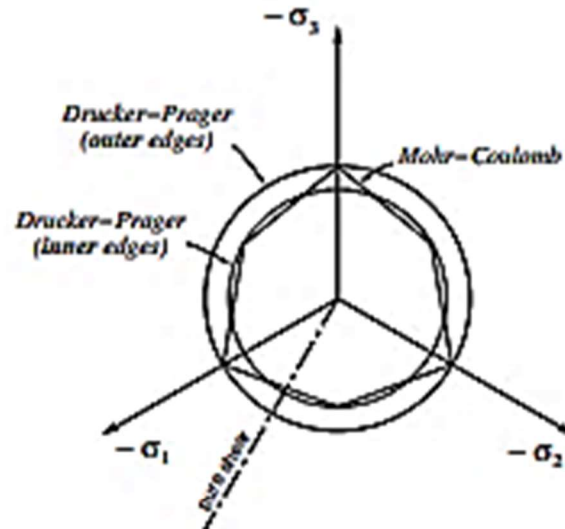


Figure 6.15. The π -plane section of the Mohr-Coulomb surface and the Drucker-Prager approximations.

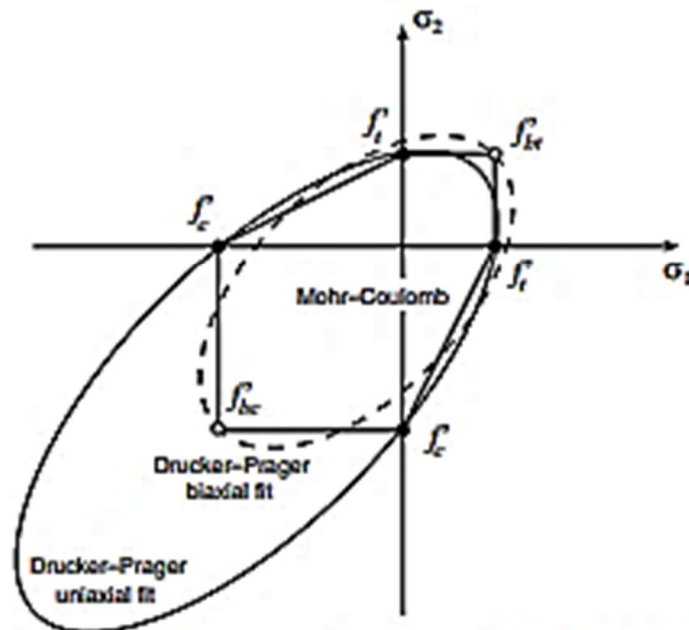


Figure 6.16. Plane stress. Drucker-Prager approximation matching the Mohr-Coulomb surface in uniaxial tension and uniaxial compression.

Any other choice of flow potential characterises a *non-associative* (or *non-associated*) plasticity model.

In associative models, the evolution equations for the plastic strain and hardening variables are given by

$$\dot{\epsilon}^p = \dot{\gamma} \frac{\partial \Phi}{\partial \sigma}, \quad (6.129)$$

and

$$\dot{\alpha} = -\dot{\gamma} \frac{\partial \Phi}{\partial A}. \quad (6.130)$$

Associativity implies that the plastic strain rate is a tensor *normal to the yield surface* in the space of stresses. In the generalised case of non-smooth yield surfaces, the flow vector is a subgradient of the yield function, i.e. we have

$$\dot{\epsilon}^p = \dot{\gamma} N; \quad N \in \partial_{\sigma} \Phi. \quad (6.131)$$

In non-associative models, the plastic strain rate is not normal to the yield surface in general.

6.5.2. ASSOCIATIVE LAWS AND THE PRINCIPLE OF MAXIMUM PLASTIC DISSIPATION

It can be shown that the associative laws are a consequence of the *principle of maximum plastic dissipation*. Before stating the principle of maximum plastic dissipation, recall that for a state defined by a hardening force A , the admissible stress states are those that satisfy $\Phi(\sigma, A) \leq 0$. Thus, it makes sense to define

$$\mathcal{A} = \{(\sigma, A) \mid \Phi(\sigma, A) \leq 0\} \quad (6.132)$$

as the set of all admissible pairs (combinations) of stress and hardening force. The principle of maximum dissipation postulates that *among all admissible pairs $(\sigma^*, A^*) \in \mathcal{A}$, the actual state (σ, A) maximises the dissipation function (6.42) for a given plastic strain rate, $\dot{\epsilon}^p$, and rate $\dot{\alpha}$ of hardening internal variables*. The principle of maximum plastic dissipation requires that, for given $(\dot{\epsilon}^p, \dot{\alpha})$,

$$\Upsilon^p(\sigma, A; \dot{\epsilon}^p, \dot{\alpha}) \geq \Upsilon^p(\sigma^*, A^*; \dot{\epsilon}^p, \dot{\alpha}), \quad \forall (\sigma^*, A^*) \in \mathcal{A}. \quad (6.133)$$

In other words, the actual state (σ, A) of stress and hardening force is a solution to the following constrained optimisation problem:

$$\begin{aligned} & \text{maximise } \Upsilon^p(\sigma^*, A^*; \dot{\epsilon}^p, \dot{\alpha}) \\ & \text{subject to } \Phi(\sigma^*, A^*) \leq 0. \end{aligned} \quad (6.134)$$

The *Kuhn-Tucker optimality conditions* (Luenberger, 1973, Chapter 10) for this optimisation problem are precisely the associative plastic flow rule (6.129), the associative hardening rule (6.130) and the loading/unloading conditions

$$\Phi(\sigma, A) \leq 0, \quad \dot{\gamma} \geq 0, \quad \Phi(\sigma, A)\dot{\gamma} = 0. \quad (6.135)$$

Remark 6.2. The postulate of maximum plastic dissipation, and the corresponding associative laws, are *not* universal. Based on physical considerations, maximum dissipation has been shown to hold in crystal plasticity and is particularly successful when applied to the description of metals. Nevertheless, for many materials, particularly soils and granular materials in general, associative laws frequently do not correspond to experimental evidence. In such cases, the maximum dissipation postulate is clearly not applicable and the use of non-associative laws is essential.

6.5.3. CLASSICAL FLOW RULES

The Prandtl-Reuss equations

The Prandtl-Reuss plasticity law is the flow rule obtained by taking the von Mises yield function (6.110) as the flow potential. The corresponding flow vector is given by

$$N \equiv \frac{\partial \Phi}{\partial \sigma} = \frac{\partial}{\partial \sigma} [\sqrt{3} J_2(s)] = \sqrt{\frac{s}{2}} \frac{s}{\|s\|}, \quad (6.136)$$

and the flow rule results in

$$\dot{\epsilon}^p = \dot{\gamma} \sqrt{\frac{s}{2}} \frac{s}{\|s\|}. \quad (6.137)$$

Here, it should be noted that the Prandtl-Reuss flow vector is the derivative of an isotropic scalar function of a symmetric tensor – the von Mises yield function. Thus (refer to Section A.1.2, page 732, where the derivative of isotropic functions of this type is discussed), N and σ are coaxial, i.e. the principal directions of N coincide with those of σ . Due to the pressure-insensitivity of the von Mises yield function, the plastic flow vector is *deviatoric*. The Prandtl-Reuss flow vector is a tensor parallel to the deviatoric projection s of the stress tensor. Its principal stress representation is depicted in Figure 6.17. The Prandtl-Reuss rule is usually employed in conjunction with the von Mises criterion and the resulting plasticity model is referred to as the von Mises associative model or, simply, the von Mises model.

Associative Tresca

The associative Tresca flow rule utilises the yield function (6.84) as the flow potential. Since Φ here is also an isotropic function of σ , the rate of plastic strain has the same principal directions as σ . The Tresca yield function is differentiable when the three principal stresses are distinct ($\sigma_1 \neq \sigma_2 \neq \sigma_3$) and non-differentiable when two principal stresses coincide (at the edges of the Tresca hexagonal prism). Hence, the Tresca associative plastic flow rule is generally expressed as

$$\dot{\epsilon}^p = \dot{\gamma} N, \quad (6.138)$$

where N is a subgradient of the Tresca function

$$N \in \partial_\sigma \Phi. \quad (6.139)$$

Its multisurface-based representation reads

$$\dot{\epsilon}^p = \sum_{i=1}^n \dot{\gamma}^i N^i = \sum_{i=1}^n \dot{\gamma}^i \frac{\partial \Phi_i}{\partial \sigma}, \quad (6.140)$$

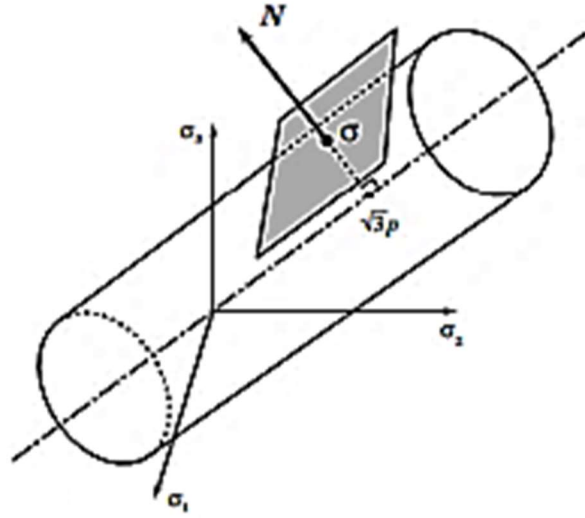


Figure 6.17. The Prandtl-Reuss flow vector.

with the yield functions Φ_i defined by (6.91). Each vector N^i is normal to the plane defined by $\Phi_i = 0$.

The above flow rule can be alternatively expressed as follows. Firstly assume, without loss of generality, that the principal stresses are ordered as $\sigma_1 \geq \sigma_2 \geq \sigma_3$, so that the discussion can be concentrated on the sextant of the π -plane illustrated in Figure 6.18. Three different possibilities have to be considered in this sextant:

- (a) yielding at a stress state on the *side* (main plane) of the Tresca hexagon ($\Phi_1 = 0$, $\Phi_2 < 0$ and $\Phi_3 < 0$);
- (b) yielding from the *right corner*, R ($\Phi_1 = 0$, $\Phi_3 = 0$ and $\Phi_2 < 0$); and
- (c) Yielding from the *left corner*, L ($\Phi_1 = 0$, $\Phi_2 = 0$ and $\Phi_3 < 0$).

When the stress is on the side of the hexagon, only one multiplier may be non-zero and the plastic flow rule reads

$$\dot{\epsilon}^p = \dot{\gamma} N^a, \quad (6.141)$$

where the flow vector is the normal to the plane $\Phi_1 = 0$, given by

$$\begin{aligned} N^a \equiv N^1 &= \frac{\partial \Phi_1}{\partial \sigma} = \frac{\partial}{\partial \sigma}(\sigma_1 - \sigma_3) \\ &= e_1 \otimes e_1 - e_3 \otimes e_3, \end{aligned} \quad (6.142)$$

with e_i denoting the eigenvector of σ associated with the principal stress σ_i . In deriving the last right-hand side of (6.142), use has been made of the expression (A.27) of page 736 for the derivative of an eigenvalue of a symmetric tensor.

At the right and left corners of the hexagon, where two planes intersect, two multipliers may be non-zero. Thus, the plastic flow equation is

$$\dot{\epsilon}^p = \dot{\gamma}^a N^a + \dot{\gamma}^b N^b. \quad (6.143)$$

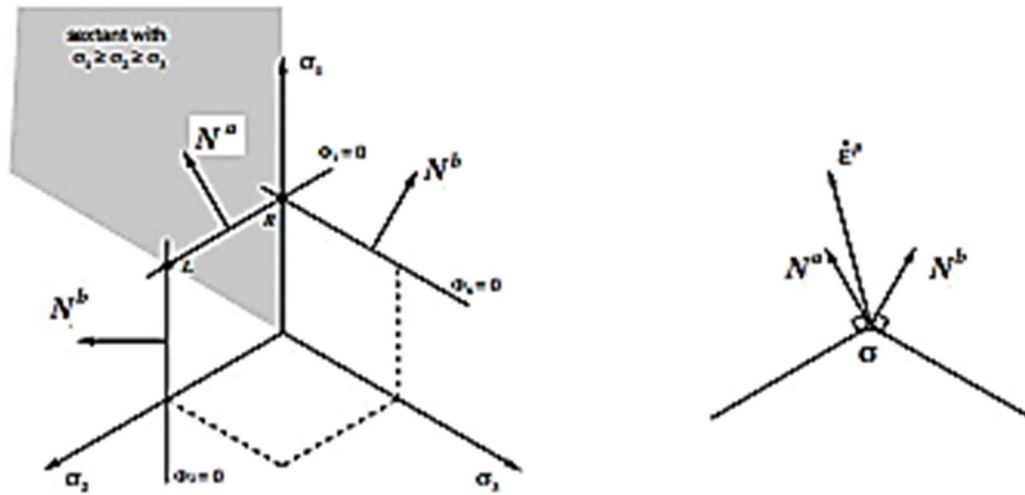


Figure 6.18. The associative Tresca flow rule.

The vector N^a is the normal to the plane $\Phi_1 = 0$, already defined. In the *right corner* (repeated minimum principal stress), the second vector, N^b , is normal to the plane $\Phi_6 = 0$ and is obtained analogously to (6.142) as

$$N^b \equiv N^6 = e_1 \otimes e_1 - e_2 \otimes e_2. \quad (6.144)$$

In the *left corner* (repeated maximum principal stress), N^b , is normal to the plane $\Phi_2 = 0$,

$$N^b \equiv N^2 = e_2 \otimes e_2 - e_3 \otimes e_3. \quad (6.145)$$

It should be noted that, as for the Prandtl-Reuss rule, the plastic flow predicted by the associative Tresca law is *volume-preserving*. Indeed, note that, in the above, we have trivially

$$\text{tr } N^a = \text{tr } N^b = 0. \quad (6.146)$$

This is due to the pressure-insensitivity of the Tresca yield function.

Associative and non-associative Mohr-Coulomb

In the associative Mohr-Coulomb law, the Mohr-Coulomb yield function (6.116) is adopted as the flow potential. Its multisurface representation is based on the yield functions (6.118). The flow rule, which requires consideration of the intersections between the yield surfaces, is derived in a manner analogous to the Tresca law described above. However, it should be noted that in addition to the edge singularities, the present surface has an extra singularity in its apex (Figure 6.13). Plastic yielding may then take place from a face, from an edge or from the apex of the Mohr-Coulomb pyramid.

Again, in the derivation of the flow rules at faces and edges, it is convenient to assume that the principal stresses are ordered as $\sigma_1 \geq \sigma_2 \geq \sigma_3$ so that, without loss of generality, the analysis can be reduced to a single sextant of a cross-section of the Mohr-Coulomb pyramid as illustrated in Figure 6.19. The situation is identical to Tresca's (Figure 6.18) except that

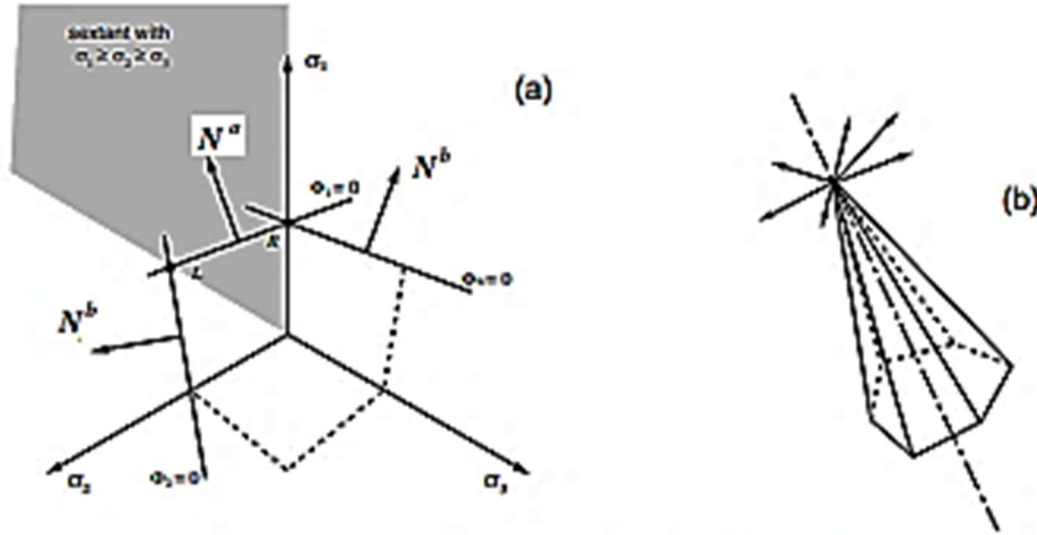


Figure 6.19. The Mohr-Coulomb flow rule; (a) faces and edges, and (b) apex.

the normal vectors N^a and N^b are no longer deviatoric, i.e. they have a non-zero component along the hydrostatic axis (the vectors shown in Figure 6.19 are deviatoric projections of the actual normals). For plastic yielding from the face, the flow rule is given by

$$\dot{\epsilon}^p = \dot{\gamma} N^a, \quad (6.147)$$

where N^a is normal to the plane $\Phi_1 = 0$,

$$\begin{aligned} N^a &= \frac{\partial \Phi_1}{\partial \sigma} = \frac{\partial}{\partial \sigma} [\sigma_1 - \sigma_3 + (\sigma_1 + \sigma_3) \sin \phi] \\ &= (1 + \sin \phi) e_1 \otimes e_1 - (1 - \sin \phi) e_3 \otimes e_3. \end{aligned} \quad (6.148)$$

At the corners, the above flow rule is replaced by

$$\dot{\epsilon}^p = \dot{\gamma}^a N^a + \dot{\gamma}^b N^b. \quad (6.149)$$

At the *right* (extension) corner, R , the second vector, N^b , is normal to the plane $\Phi_6 = 0$ and is given by

$$N^b = (1 + \sin \phi) e_1 \otimes e_1 - (1 - \sin \phi) e_2 \otimes e_2, \quad (6.150)$$

whereas, at the *left* (compression) corner, L , the tensor N^b is normal to the plane $\Phi_2 = 0$,

$$N^b = (1 + \sin \phi) e_2 \otimes e_2 - (1 - \sin \phi) e_3 \otimes e_3. \quad (6.151)$$

At the apex of the Mohr-Coulomb surface, all six planes intersect and, therefore, six normals are defined and up to six plastic multipliers may be non-zero. This situation is schematically illustrated in Figure 6.19(b). The plastic strain rate tensor lies within the pyramid defined by the six normals:

$$\dot{\epsilon}^p = \sum_{i=1}^6 \dot{\gamma}^i N^i. \quad (6.152)$$

It is important to note that, due to the pressure sensitivity of the Mohr–Coulomb criterion, the associative Mohr–Coulomb rule predicts a non-zero *volumetric* plastic straining. This is in contrast to the Prandtl–Reuss and associative Tresca laws. The volumetric component of the plastic strain rate in the associative Mohr–Coulomb law can be obtained by expanding (6.152) in principal stress space taking into account the definitions of N^p . This gives

$$\begin{bmatrix} \dot{\varepsilon}_1^p \\ \dot{\varepsilon}_2^p \\ \dot{\varepsilon}_3^p \end{bmatrix} = \begin{bmatrix} \alpha & 0 & \beta & \beta & 0 & \alpha \\ 0 & \alpha & \alpha & 0 & \beta & \beta \\ \beta & \beta & 0 & \alpha & \alpha & 0 \end{bmatrix} \begin{bmatrix} \dot{\gamma}^1 \\ \dot{\gamma}^2 \\ \dot{\gamma}^3 \\ \dot{\gamma}^4 \\ \dot{\gamma}^5 \\ \dot{\gamma}^6 \end{bmatrix}, \quad (6.153)$$

where

$$\alpha \equiv 1 + \sin \phi, \quad \beta \equiv -1 + \sin \phi. \quad (6.154)$$

The above trivially yields

$$\dot{\varepsilon}_v^p \equiv \dot{\varepsilon}_1^p + \dot{\varepsilon}_2^p + \dot{\varepsilon}_3^p = 2 \sin \phi \sum_{i=1}^6 \dot{\gamma}^i. \quad (6.155)$$

As all $\dot{\gamma}^i$'s are non-negative, the volumetric plastic strain rate is positive and, therefore, *dilatant*. The phenomenon of dilatancy during plastic flow is observed for many materials, particularly geomaterials. However, the dilatancy predicted by the associative Mohr–Coulomb law is often excessive. To overcome this problem, it is necessary to use a *non-associated* flow rule in conjunction with the Mohr–Coulomb criterion. The non-associated Mohr–Coulomb law adopts, as flow potential, a Mohr–Coulomb yield function with the frictional angle ϕ replaced by a different (smaller) angle ψ . The angle ψ is called the *dilatancy angle* and the amount of dilation predicted is proportional to its sine. Note that for $\psi = 0$, the plastic flow becomes purely deviatoric and the flow rule reduces to the associative Tresca law.

Associative and non-associated Drucker–Prager

The associative Drucker–Prager model employs as flow potential the yield function defined by (6.121). To derive the corresponding flow rule, one should note first that the Drucker–Prager function is singular at the apex of the yield surface and is smooth anywhere else. Thus, two situations need to be considered:

- (a) plastic yielding at (smooth portion of) the cone surface; and
- (b) plastic yielding at the apex.

At the cone surface, where the Drucker–Prager yield function is differentiable, the flow vector is obtained by simply differentiating (6.121) which gives (Figure 6.20(a))

$$N = \frac{1}{2 \sqrt{J_2(s)}} s + \frac{\eta}{3} I, \quad (6.156)$$

$\psi < \phi$; that is, we define

$$\Psi(\sigma, c) = \sqrt{J_2(s(\sigma))} + \bar{\eta} p, \quad (6.162)$$

where $\bar{\eta}$ is obtained by replacing ϕ with ψ in the definition of η given by (6.122)₁, (6.123)₁ or (6.124)₁. In other words,

$$\bar{\eta} = \frac{6 \sin \psi}{\sqrt{3} (3 - \sin \psi)}, \quad (6.163)$$

when the outer cone approximation to the Mohr–Coulomb criterion is employed. When the inner cone approximation is used,

$$\bar{\eta} = \frac{6 \sin \psi}{\sqrt{3} (3 + \sin \psi)}, \quad (6.164)$$

whereas, for the plane strain match,

$$\bar{\eta} = \frac{3 \tan \psi}{\sqrt{9 + 12 \tan^2 \psi}}. \quad (6.165)$$

The non-associated Drucker–Prager flow vector differs from its associated counterpart only in the volumetric component which, for the non-associated case, reads

$$N_v = \bar{\eta}. \quad (6.166)$$

If the dilatancy angle of the non-associated potential is chosen as $\psi = 0$, then the volumetric component, N_v , vanishes and the flow rule reduces to the Prandtl–Reuss law that predicts volume-preserving plastic flow (refer to Figure 6.20(a)).

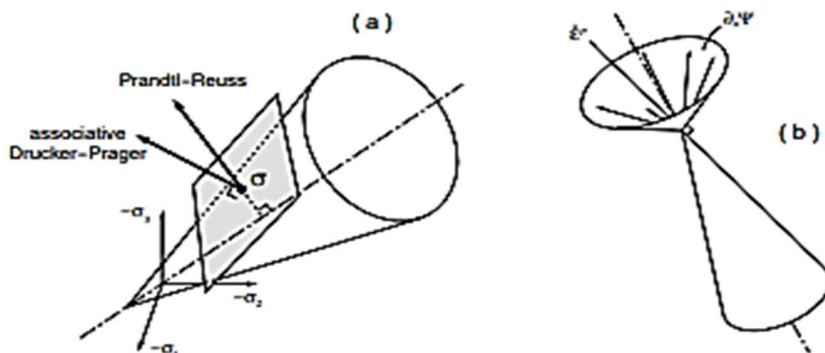


Figure 6.20. The Drucker-Prager flow vector; (a) cone surface, and (b) apex.

where η is given by (6.122)₁, (6.123)₁ or (6.124)₁, according to the chosen approximation to the Mohr-Coulomb surface. The flow rule is then

$$\dot{\varepsilon}^p = \dot{\gamma} N. \quad (6.157)$$

The deviatoric/volumetric decomposition of the Drucker-Prager flow vector gives

$$N_d = \frac{1}{2\sqrt{J_2(s)}} s, \quad N_v = \eta. \quad (6.158)$$

At the apex singularity, the flow vector is an element of the subdifferential of the yield function (6.121):

$$N \in \partial_\sigma \Phi. \quad (6.159)$$

It lies within the complementary cone to the Drucker-Prager yield surface, i.e. the cone whose wall is normal to the Drucker-Prager cone illustrated in Figure 6.20(b). From standard properties of subdifferentials (Rockafellar, 1970; Rockafellar and Wets, 1998) it can be established that the deviatoric/volumetric split of N in this case is given by

$$N_d \in \partial_\sigma \Phi_d, \quad N_v = \eta, \quad (6.160)$$

where $\Phi_d \equiv \sqrt{J_2(s)}$. Expressions (6.157), (6.158) and (6.160) result in the following rate of (dilatant) volumetric plastic strain for the associative Drucker-Prager flow rule:

$$\dot{\varepsilon}_v^p = \dot{\gamma} \eta. \quad (6.161)$$

This expression is analogous to (6.155).

Similarly to the associative Mohr-Coulomb flow rule, the often excessive dilatancy predicted by the associated rule in the present case is avoided by using a non-associated law. The non-associated Drucker-Prager law is obtained by adopting, as the flow potential, a Drucker-Prager yield function with the frictional angle ϕ replaced by a dilatancy angle

$\psi < \phi$; that is, we define

$$\Psi(\sigma, c) = \sqrt{J_2(s(\sigma))} + \bar{\eta} p, \quad (6.162)$$

where $\bar{\eta}$ is obtained by replacing ϕ with ψ in the definition of η given by (6.122)₁, (6.123)₁ or (6.124)₁. In other words,

$$\bar{\eta} = \frac{6 \sin \psi}{\sqrt{3} (3 - \sin \psi)}, \quad (6.163)$$

when the outer cone approximation to the Mohr-Coulomb criterion is employed. When the inner cone approximation is used,

$$\bar{\eta} = \frac{6 \sin \psi}{\sqrt{3} (3 + \sin \psi)}, \quad (6.164)$$

whereas, for the plane strain match,

$$\bar{\eta} = \frac{3 \tan \psi}{\sqrt{9 + 12 \tan^2 \psi}}. \quad (6.165)$$

The non-associated Drucker-Prager flow vector differs from its associated counterpart only in the volumetric component which, for the non-associated case, reads

$$N_v = \bar{\eta}. \quad (6.166)$$

If the dilatancy angle of the non-associated potential is chosen as $\psi = 0$, then the volumetric component, N_v , vanishes and the flow rule reduces to the Prandtl-Reuss law that predicts volume-preserving plastic flow (refer to Figure 6.20(a)).

A material model is said to be *perfectly plastic* if *no hardening* is allowed, that is, the yield stress level does *not* depend in any way on the degree of plastification. In this case, the yield surface remains fixed regardless of any deformation process the material may experience and, in a uniaxial test, the elastoplastic modulus, E^{ep} , vanishes. In the von Mises, Tresca, Drucker–Prager and Mohr–Coulomb models described above, perfect plasticity corresponds to a *constant* uniaxial yield stress, σ_y (or constant cohesion, c). Figure 6.21 shows the stress–strain curve of a typical uniaxial cyclic (tension–compression) test with a perfectly plastic

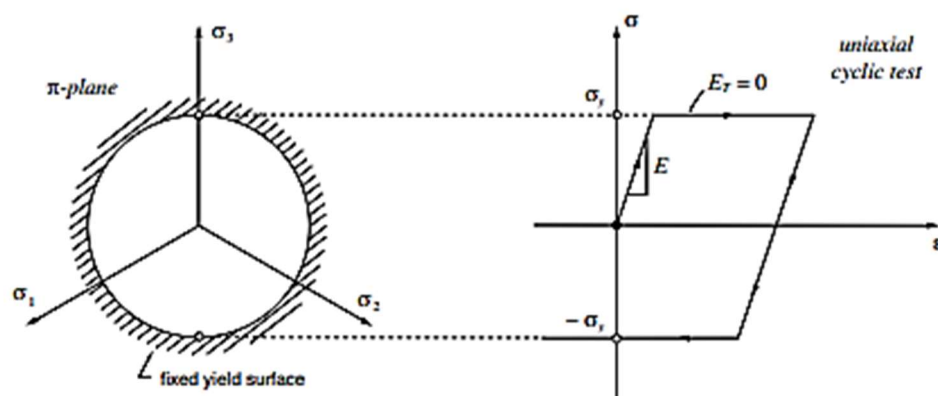


Figure 6.21. Perfect plasticity. Uniaxial test and π -plane representation.

von Mises model along with the corresponding π -plane representation of the yield surface. Perfectly plastic models are particularly suitable for the analysis of the stability of structures and soils and are widely employed in engineering practice for the determination of limit loads and safety factors.

A plasticity model is said to be *isotropic hardening* if the evolution of the yield surface is such that, at any state of hardening, it corresponds to a uniform (isotropic) expansion of the initial yield surface, without translation. The uniaxial model described in Section 6.2 is a typical example of an isotropic hardening model. For that model, the elastic domain expands equally in tension and compression during plastic flow. For a multiaxial plasticity model with a von Mises yield surface, isotropic hardening corresponds to the increase in radius of the von Mises cylinder in principal stress space. This, together with a typical stress–strain curve for a uniaxial cyclic test for an isotropic hardening von Mises model is illustrated in Figure 6.22.

The choice of a suitable set (denoted α in Section 6.3) of hardening internal variables must be obviously dependent on the specific characteristics of the material considered. In metal plasticity, for instance, the hardening internal variable is intrinsically connected with the density of dislocations in the crystallographic microstructure that causes an isotropic increase in resistance to plastic flow. In the constitutive description of isotropic hardening, the set α normally contains a single *scalar* variable, which determines the size of the yield surface. Two approaches, *strain hardening* and *work hardening*, are particularly popular in the treatment of isotropic hardening and are suitable for modelling the behaviour of a wide range of materials. These are described below.

Strain hardening

In this case the hardening internal state variable is some suitably chosen scalar measure of *strain*. A typical example is the von Mises *effective plastic strain*, also referred to as the

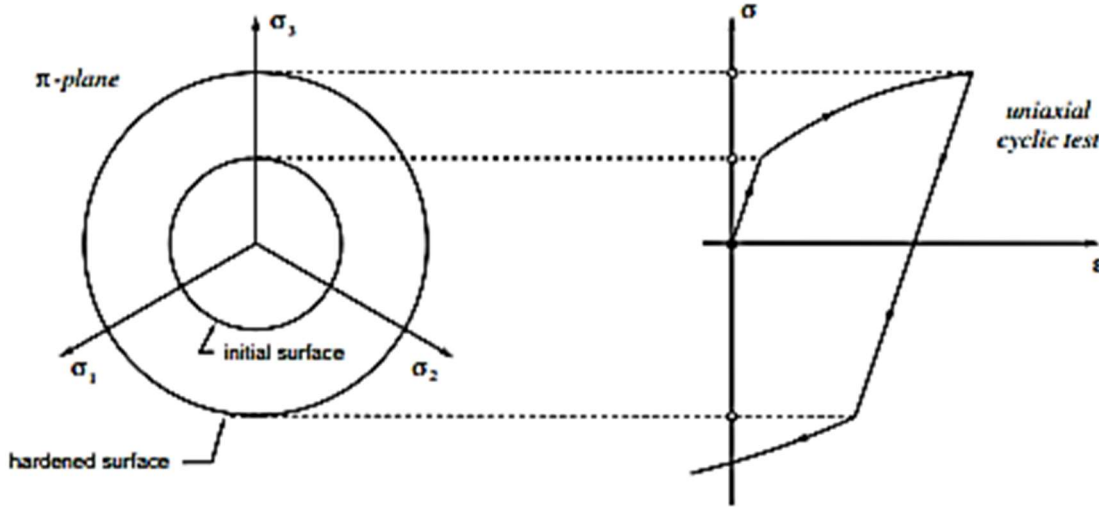


Figure 6.22. Isotropic hardening. Uniaxial test and π -plane representation.

von Mises *equivalent* or *accumulated plastic strain*, defined as

$$\bar{\varepsilon}^P \equiv \int_0^t \sqrt{\frac{2}{3} \dot{\varepsilon}^P : \dot{\varepsilon}^P} dt = \int_0^t \sqrt{\frac{2}{3} \|\dot{\varepsilon}^P\|} dt. \quad (6.167)$$

The above definition generalises the accumulated axial plastic strain (6.18) (page 145) of the one-dimensional model to the multiaxially strained case. Its rate evolution equation reads

$$\dot{\bar{\varepsilon}}^P = \sqrt{\frac{2}{3} \dot{\varepsilon}^P : \dot{\varepsilon}^P} = \sqrt{\frac{2}{3} \|\dot{\varepsilon}^P\|}, \quad (6.168)$$

or, equivalently, in view of the Prandtl–Reuss flow equation (6.137),

$$\dot{\bar{\varepsilon}}^P = \dot{\gamma}. \quad (6.169)$$

Accordingly, a von Mises isotropic *strain-hardening* model is obtained by letting the uniaxial yield stress be a function of the accumulated plastic strain:

$$\sigma_y = \sigma_y(\bar{\varepsilon}^P). \quad (6.170)$$

This function defines the *strain-hardening curve* (or *strain-hardening function*) that can be obtained, for instance, from a uniaxial tensile test.

Behaviour under uniaxial stress conditions

Under uniaxial stress conditions the von Mises model with isotropic strain hardening reproduces the behaviour of the one-dimensional plasticity model discussed in Section 6.2 and summarised in Box 6.1 (page 146). This is demonstrated in the following. Let us assume that both models share the same Young's modulus, E , and hardening function $\sigma_y = \sigma_y(\bar{\varepsilon}^P)$. Clearly, the two models have identical uniaxial elastic behaviour and initial yield stress. Hence, we only need to show next that their behaviour under plastic yielding is also identical.

Under a uniaxial stress state with axial stress σ and axial stress rate $\dot{\sigma}$ in the direction of the base vector \mathbf{e}_1 , the matrix representations of the stress tensor and the stress rate tensor in the three-dimensional model are given by

$$[\boldsymbol{\sigma}] = \sigma \begin{bmatrix} 1 & 0 & 0 \\ 0 & 0 & 0 \\ 0 & 0 & 0 \end{bmatrix}, \quad [\dot{\boldsymbol{\sigma}}] = \dot{\sigma} \begin{bmatrix} 1 & 0 & 0 \\ 0 & 0 & 0 \\ 0 & 0 & 0 \end{bmatrix}. \quad (6.171)$$

The corresponding stress deviator reads

$$[\mathbf{s}] = \frac{2}{3}\sigma \begin{bmatrix} 1 & 0 & 0 \\ 0 & -\frac{1}{2} & 0 \\ 0 & 0 & -\frac{1}{2} \end{bmatrix}. \quad (6.172)$$

In this case, the Prandtl–Reuss flow equation (6.137) gives

$$[\dot{\boldsymbol{\varepsilon}}^P] = \dot{\varepsilon}^P \begin{bmatrix} 1 & 0 & 0 \\ 0 & -\frac{1}{2} & 0 \\ 0 & 0 & -\frac{1}{2} \end{bmatrix}, \quad (6.173)$$

where

$$\dot{\varepsilon}^P = \dot{\gamma} \text{sign}(\sigma) \quad (6.174)$$

is the axial plastic strain rate. Note that the above expression coincides with the one-dimensional plastic flow rule (6.10). Now, we recall the consistency condition (6.60), which must be satisfied under plastic flow. In the present case, by taking the derivatives of the von Mises yield function (6.110), with σ_y defined by (6.170), we obtain

$$\dot{\Phi} = \mathbf{N} : \dot{\boldsymbol{\sigma}} - H \dot{\varepsilon}^P = 0, \quad (6.175)$$

where $\mathbf{N} \equiv \partial\Phi/\partial\boldsymbol{\sigma}$ is the Prandtl–Reuss flow vector (6.136) and $H = H(\varepsilon^P)$ is the hardening modulus defined in (6.27). To conclude the demonstration, we combine (6.175) with (6.136), (6.171)₂ and (6.172) to recover (6.28) and, then, following the same arguments as in the one-dimensional case we find that, under uniaxial stress conditions, the isotropic strain hardening von Mises model predicts the tangential axial stress–strain relation

$$\dot{\sigma} = \frac{EH}{E+H} \dot{\varepsilon}, \quad (6.176)$$

which is identical to equation (6.31) of the one-dimensional model.

Work hardening

In work-hardening models, the variable defining the state of hardening is the dissipated *plastic work*,[†] w^P , defined by

$$w^P \equiv \int_0^t \boldsymbol{\sigma} : \dot{\boldsymbol{\varepsilon}}^P dt. \quad (6.177)$$

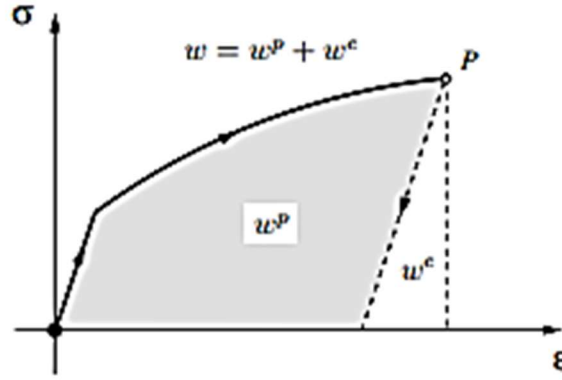


Figure 6.23. The plastic work.

In a uniaxial test, for instance (Figure 6.23), the total work w necessary to deform the material up to point P is given by the total area under the corresponding stress–strain curve. Part of this work, w^e , is stored in the form of elastic energy and is fully recovered upon elastic unloading. The remaining (shaded) area, w^p , is the *plastic work*. It corresponds to the energy dissipated by the plastic mechanisms and cannot be recovered. From the definition of w^p , its evolution equation is given by

$$\dot{w}^p = \sigma : \dot{\varepsilon}^p. \quad (6.178)$$

An isotropic work-hardening von Mises model is obtained by postulating

$$\sigma_y = \sigma_y(w^p). \quad (6.179)$$

This defines the *work-hardening curve* (or *work-hardening function*).

Equivalence between strain and work hardening

Under some circumstances, the strain-hardening and work-hardening descriptions are equivalent. This is shown in the following for the von Mises model with associative flow rule (6.137).

The substitution of (6.137) into (6.178), together with the identity $\sqrt{3/2}\|s\| = \sigma_y$ valid for the von Mises model under plastic flow, gives

$$\dot{w}^p = \sigma_y \dot{\varepsilon}^p, \quad (6.180)$$

or, equivalently,

$$\frac{dw^p}{d\varepsilon^p} = \sigma_y. \quad (6.181)$$

As σ_y is strictly positive ($\sigma_y > 0$), the above differential relation implies that the mapping between w^p and ε^p is one-to-one and, therefore, invertible so that

$$w^p = w^p(\varepsilon^p) \quad (6.182)$$

and

$$\varepsilon^p = \varepsilon^p(w^p). \quad (6.183)$$

This allows any given strain-hardening function of the type (6.170) to be expressed as an equivalent work-hardening function,

$$\sigma_y(\bar{\varepsilon}^p) = \bar{\sigma}_y(w^p) \equiv \sigma_y(\bar{\varepsilon}^p(w^p)), \quad (6.184)$$

and any given work-hardening function of the type (6.179) to be expressed as an equivalent strain-hardening function,

$$\sigma_y(w^p) = \hat{\sigma}_y(\bar{\varepsilon}^p) \equiv \sigma_y(w^p(\bar{\varepsilon}^p)). \quad (6.185)$$

Expressions (6.184) and (6.185) establish the equivalence between the strain and work-hardening descriptions for the von Mises model with associative flow rule.

Linear and nonlinear hardening

A model is said to be *linear hardening* if the strain-hardening function (6.170) is linear, i.e. if it can be expressed as

$$\sigma_y(\bar{\varepsilon}^p) = \sigma_{y0} + H\bar{\varepsilon}^p, \quad (6.186)$$

with constant σ_{y0} and H . The constant σ_{y0} is the *initial yield stress*, i.e. the uniaxial yield stress at the initial (*virgin*) state of the material, and H is called the *linear isotropic hardening modulus*. Any other hardening model is said to be *nonlinear hardening*. Note that perfect plasticity (defined in Section 6.6.1) is obtained if we set $H = 0$ in (6.186).

It should also be noted that a linear work-hardening function corresponds in general to an equivalent *nonlinear* strain-hardening function (i.e. a nonlinear hardening model). This can be easily established by observing that (6.181) defines a nonlinear relation between w^p and $\bar{\varepsilon}^p$ if σ_y is not a constant.

When the yield surfaces preserve their shape and size but *translate* in the stress space as a rigid body, *kinematic hardening* is said to take place. It is frequently observed in experiments that, after being loaded (and hardened) in one direction, many materials show a decreased resistance to plastic yielding in the opposite direction (Lemaitre and Chaboche, 1990). This phenomenon is known as the *Bauschinger effect* and can be modelled with the introduction of kinematic hardening. A number of constitutive models have been proposed to describe elastoplastic behaviour under cyclic loading conditions (Lemaitre and Chaboche, 1990; Mróz, 1967; Skrzypek, 1993). The typical result of a uniaxial cyclic test showing the Bauschinger effect is illustrated in Figure 6.24. The evolution of a kinematically hardening von Mises-type yield surface (in the deviatoric plane) used to model the phenomenon is shown alongside. The yield function for the kinematically hardening model is given by

$$\Phi(\sigma, \beta) = \sqrt{3 J_2(\eta(\sigma, \beta))} - \sigma_y, \quad (6.208)$$

where

$$\eta(\sigma, \beta) \equiv s(\sigma) - \beta \quad (6.209)$$

is the *relative stress* tensor, defined as the difference between the stress deviator and the symmetric deviatoric (stress-like) tensor, β , known as the *back-stress* tensor. Note that, by definition, the relative stress is *deviatoric*. The back-stress tensor is the thermodynamical force associated with kinematic hardening and represents the translation (Figure 6.24) of the yield surface in the space of stresses. The constant σ_y in (6.208) defines the radius of the yield surface. When $\beta = 0$, we have $\eta = s$ and the yield surface defined by $\Phi = 0$ is the isotropic von Mises yield surface with uniaxial yield stress σ_y .

It is important to observe that, unlike the isotropically hardening von Mises model, the yield function Φ defined by (6.208) is *not* an isotropic function of the stress tensor for kinematically hardened states ($\beta \neq 0$). The function (6.208) is an isotropic function of the *relative stress*, η . Analogously to expression (6.208), it is possible to introduce kinematic hardening in other plasticity models simply by replacing σ with a relative stress measure, defined as the difference $\sigma - \beta$, in the definition of the corresponding yield function.

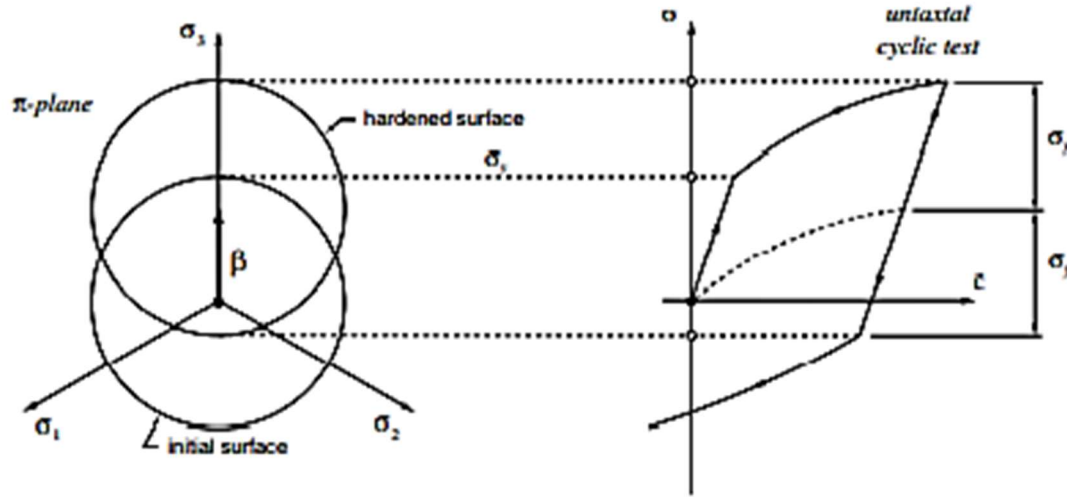


Figure 6.24. Kinematic hardening and the *Bauschinger effect*. Uniaxial test and π -plane representation. Loading in one direction results in decreased resistance to plastic yielding in the opposite direction.

Plastic flow rule with kinematic hardening

The von Mises model with kinematic hardening is used in conjunction with an *associative* flow rule. The flow vector in this case reads

$$N \equiv \frac{\partial \Phi}{\partial \sigma} = \sqrt{\frac{3}{2}} \frac{\eta}{\|\eta\|} \quad (6.210)$$

and we have the following plastic strain rate equation:

$$\dot{\epsilon}^p = \dot{\gamma} N = \dot{\gamma} \sqrt{\frac{3}{2}} \frac{\eta}{\|\eta\|}. \quad (6.211)$$

This rule extends the Prandtl–Reuss equation to account for kinematic hardening. Note that the plastic flow is in the direction of the (deviatoric) relative stress, η , and coincides with the Prandtl–Reuss equation if $\beta = 0$.

Prager's linear kinematic hardening

To complete the definition of the kinematic hardening plasticity model, evolution equations for β are required. One of the most commonly used laws is *Prager's linear kinematic hardening rule*, where the rate evolution equation for β is given by

$$\dot{\beta} = \frac{2}{3} H \dot{\epsilon}^p = \dot{\gamma} \sqrt{\frac{2}{3}} H \frac{\eta}{\|\eta\|}. \quad (6.212)$$

The material constant H is the *linear kinematic hardening modulus*.

Behaviour under monotonic uniaxial stress loading

For monotonic loading under uniaxial stress conditions, the stress–strain behaviour of the model defined by equations (6.208), with constant $\sigma_y = \sigma_{y0}$, (6.211) and (6.212) and initial

state of hardening defined by $\beta = 0$ is identical to the behaviour of the purely isotropic hardening von Mises model with linear hardening curve (6.186) and initial state of hardening $\bar{\varepsilon}^p = 0$. It is assumed in this statement that both models share the same Young's modulus, E . Under the above conditions, it is clear that both models have the same elastic behaviour and uniaxial yield stress, σ_{y0} . To show that their plastic behaviour also coincides, let us consider again a uniaxial test with loading in the direction of the base vector e_1 . In this case, the stress, stress rate and stress deviator tensors have the matrix representations given in (6.171) and (6.172). Now note that the integration of the rate equation (6.212) with initial condition $\beta = 0$ (i.e. $\eta = s$) and s as in (6.172) gives a back-stress tensor of the form

$$[\beta] = \beta \begin{bmatrix} 1 & 0 & 0 \\ 0 & -\frac{1}{2} & 0 \\ 0 & 0 & -\frac{1}{2} \end{bmatrix}, \quad (6.213)$$

where β is the axial back-stress component. With the above, we obtain for the relative stress tensor

$$[\eta] = \eta \begin{bmatrix} 1 & 0 & 0 \\ 0 & -\frac{1}{2} & 0 \\ 0 & 0 & -\frac{1}{2} \end{bmatrix}, \quad (6.214)$$

where

$$\eta = \frac{2}{3}\sigma - \beta \quad (6.215)$$

is the axial relative stress. From (6.212) and (6.214) we obtain

$$[\dot{\beta}] = \frac{2}{3}H\dot{\varepsilon}^p \begin{bmatrix} 1 & 0 & 0 \\ 0 & -\frac{1}{2} & 0 \\ 0 & 0 & -\frac{1}{2} \end{bmatrix}, \quad (6.216)$$

where $\dot{\varepsilon}^p$ is the axial plastic strain rate given by

$$\dot{\varepsilon}^p = \dot{\gamma} \text{sign}(\eta). \quad (6.217)$$

Now, by recalling (6.60) and specialising (6.61) for the present case we have that, under plastic yielding, the following consistency condition must be satisfied:

$$\dot{\Phi} = \frac{\partial \Phi}{\partial \sigma} : \dot{\sigma} + \frac{\partial \Phi}{\partial \beta} : \dot{\beta} = 0. \quad (6.218)$$

After some straightforward tensor algebra, taking into account (6.171)₂ and the above expressions for $\dot{\beta}$, β , the definition of η , and the identity

$$\frac{\partial \Phi}{\partial \beta} = -\frac{\partial \Phi}{\partial \sigma} = -\sqrt{\frac{3}{2}} \frac{\eta}{\|\eta\|}, \quad (6.219)$$

equation (6.218) yields

$$\dot{\sigma} = H\dot{\varepsilon}^p. \quad (6.220)$$

Then, with the introduction of the elastoplastic split of the axial strain rate, together with the equation

$$\dot{\sigma} = E\dot{\varepsilon}^e, \quad (6.221)$$

of the linear elastic model under uniaxial stress conditions, into (6.220), we obtain

$$\dot{\sigma} = \frac{EH}{E + H} \dot{\varepsilon}, \quad (6.222)$$

which coincides with the stress rate equation (6.176) of the von Mises isotropic strain-hardening model with constant H . To complete the demonstration, let us assume that the uniaxial loading is monotonic, i.e. we have either $\dot{\varepsilon} > 0$ or $\dot{\varepsilon} < 0$ throughout the entire loading process. In this case, the integration of (6.222) having the initial yield stress (σ_{y0} for both models) as the initial condition produces the same stress-strain curve as the isotropic model.

CHAPTER 3rd

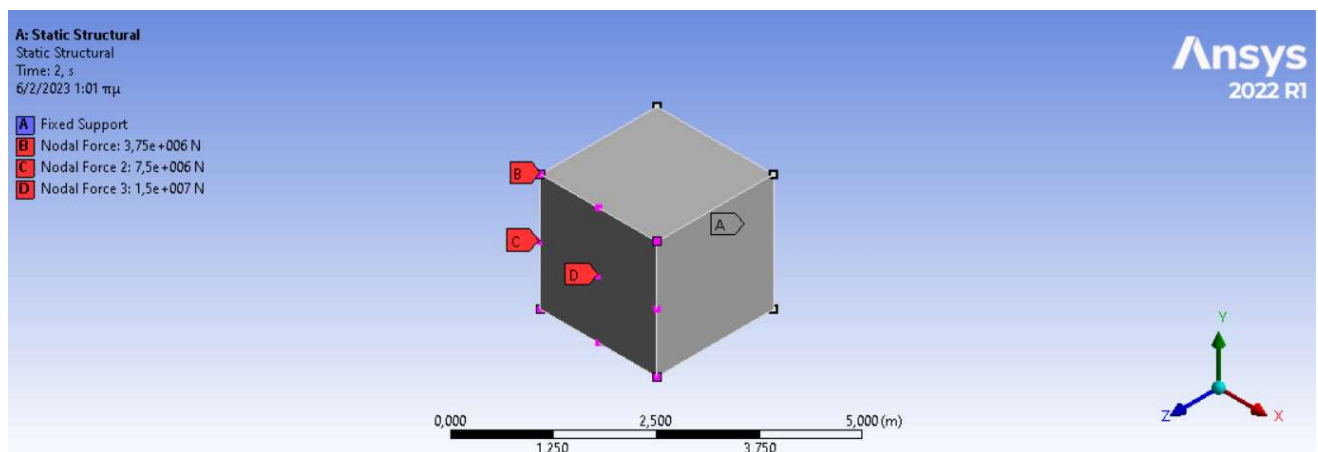
3. Ansys Software- Problem Statement and Description

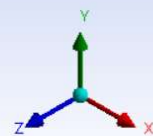
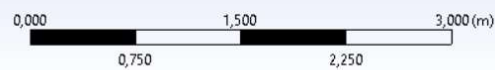
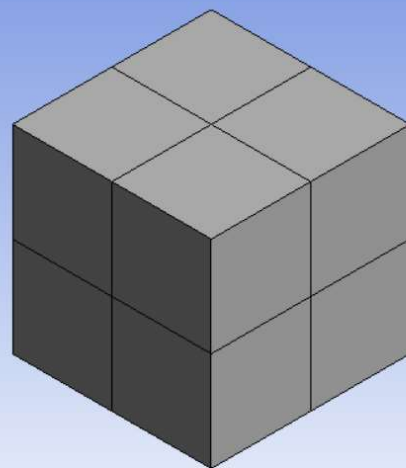
3.1 Introduction

In this chapter, it is represented different cases of nonlinear constitutive laws of the yield criteria of Von Mises with bilinear hardening, isotropic, kinematic and mixed hardening, Tresca, Mohr -Coulomb, Drucker-Prager. Also, it is examined the constitutive model for structured soils (MSS) especially the soil interaction with Kavvadas Clays yield criterion and the uniaxial material for concrete and steel especially the 3d fiber beam and force-based fiber element utilizing Ramberg Osgood, Menegotto Pinto, Kent and Park for both monotonic and cyclic loading cases. Then, it is thoroughly described the way that data given to Ansys Workbench, like the geometry of the structure-model, the boundary conditions, the assumptions of the nonlinear constitutive laws and the solver that used.

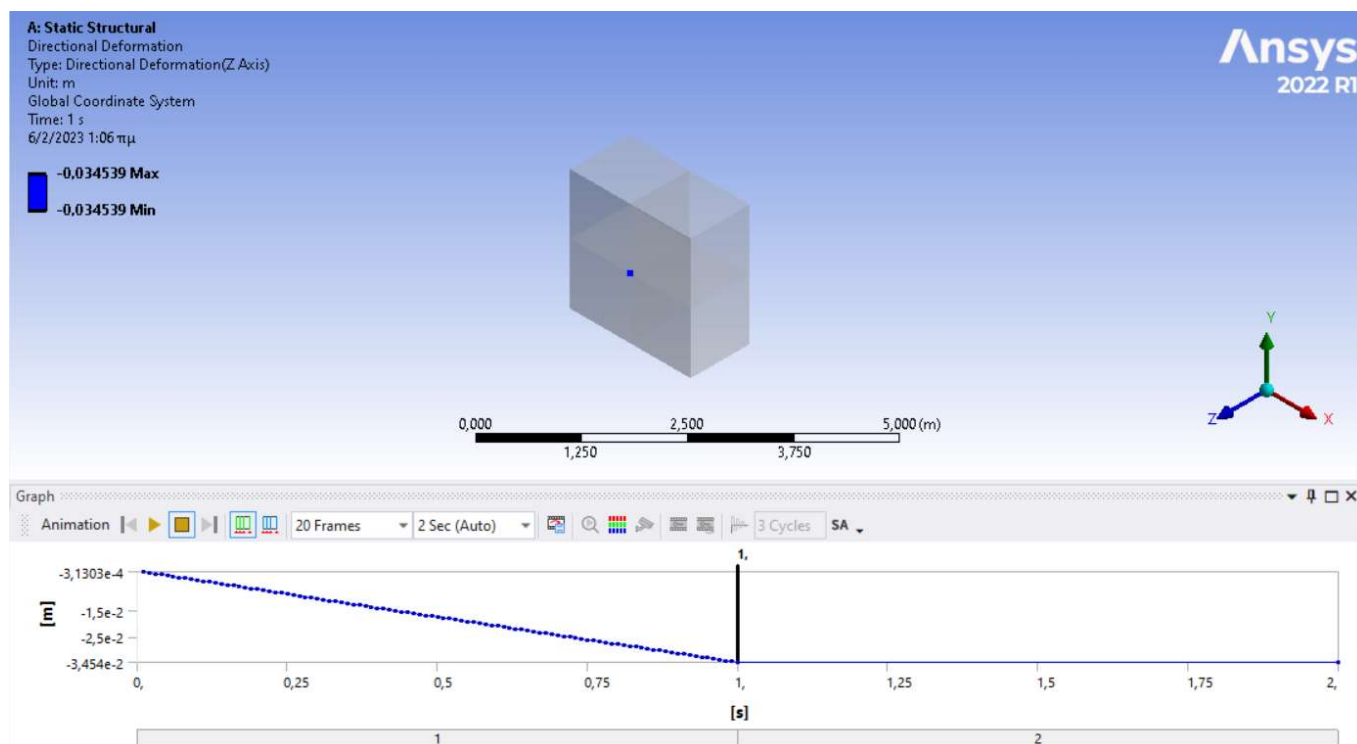
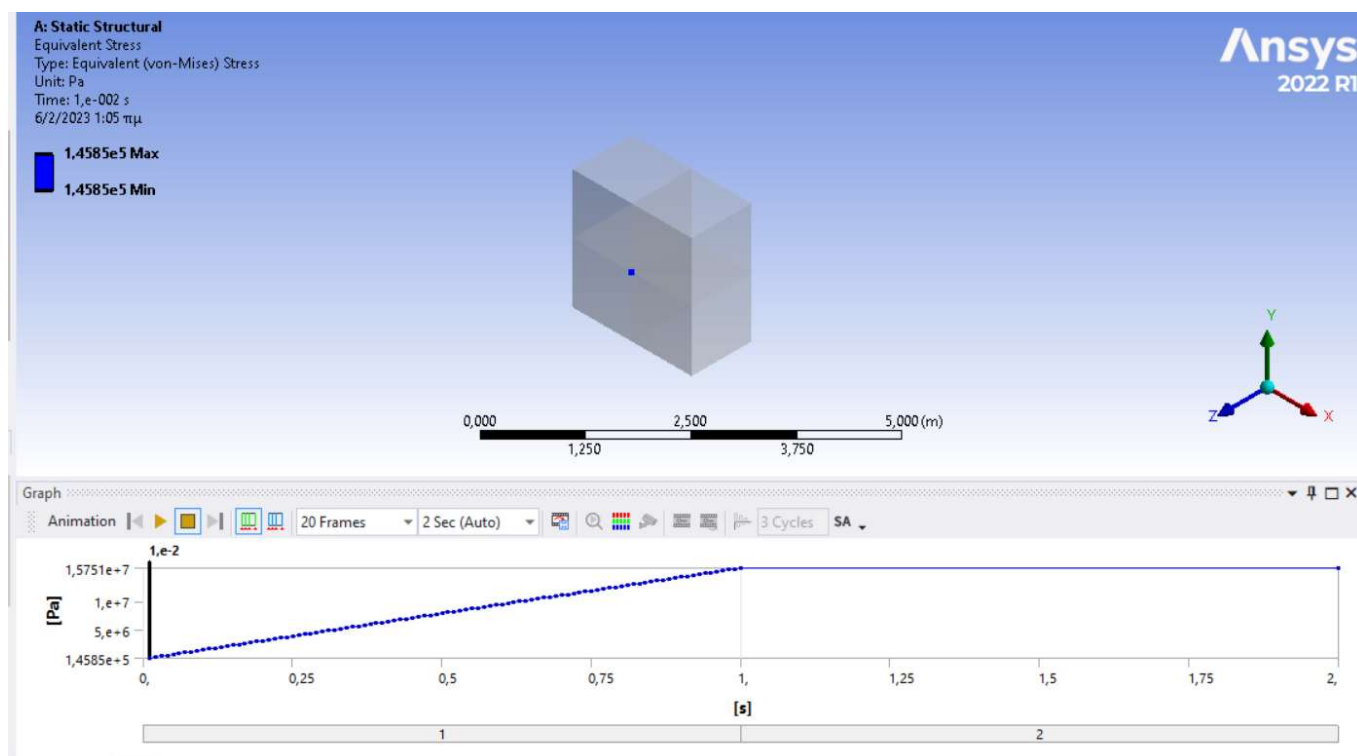
3.2 Problem Statement

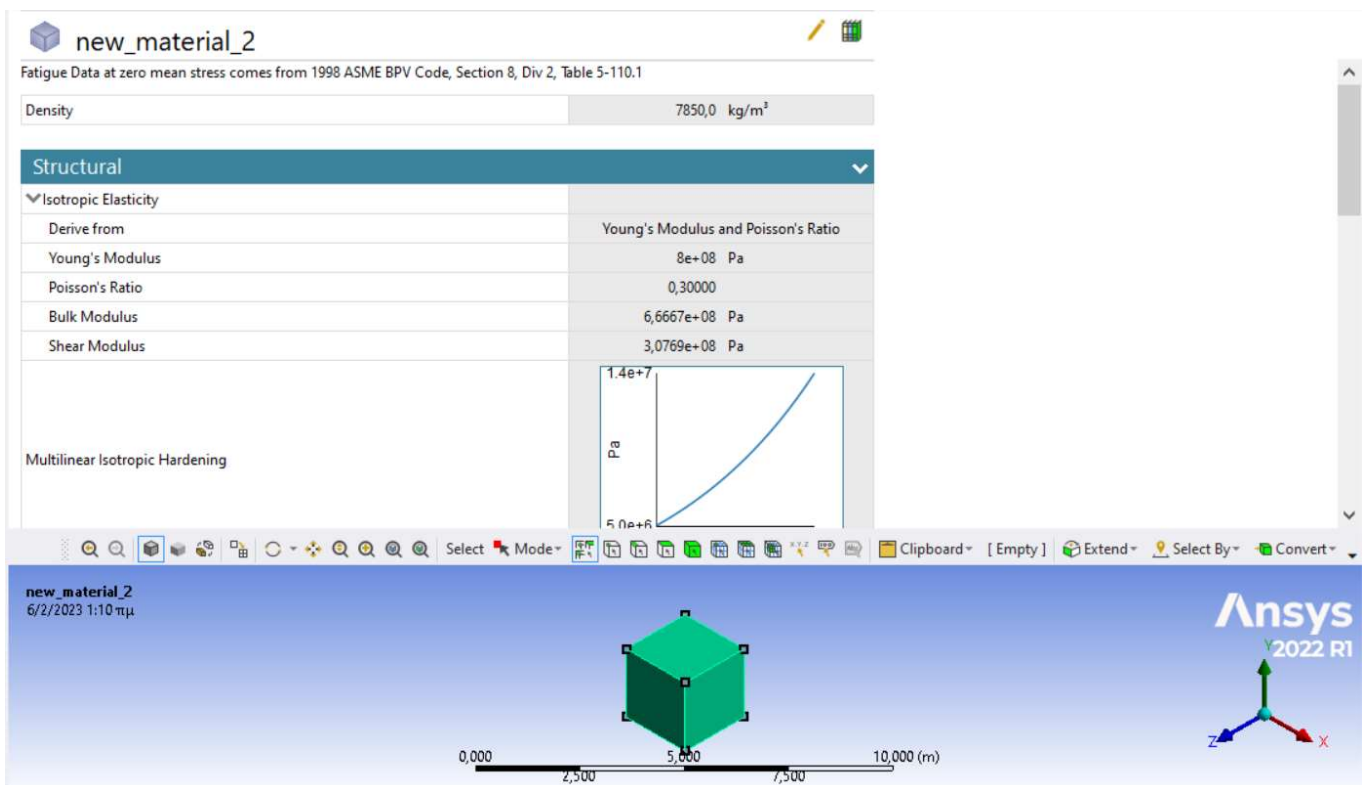
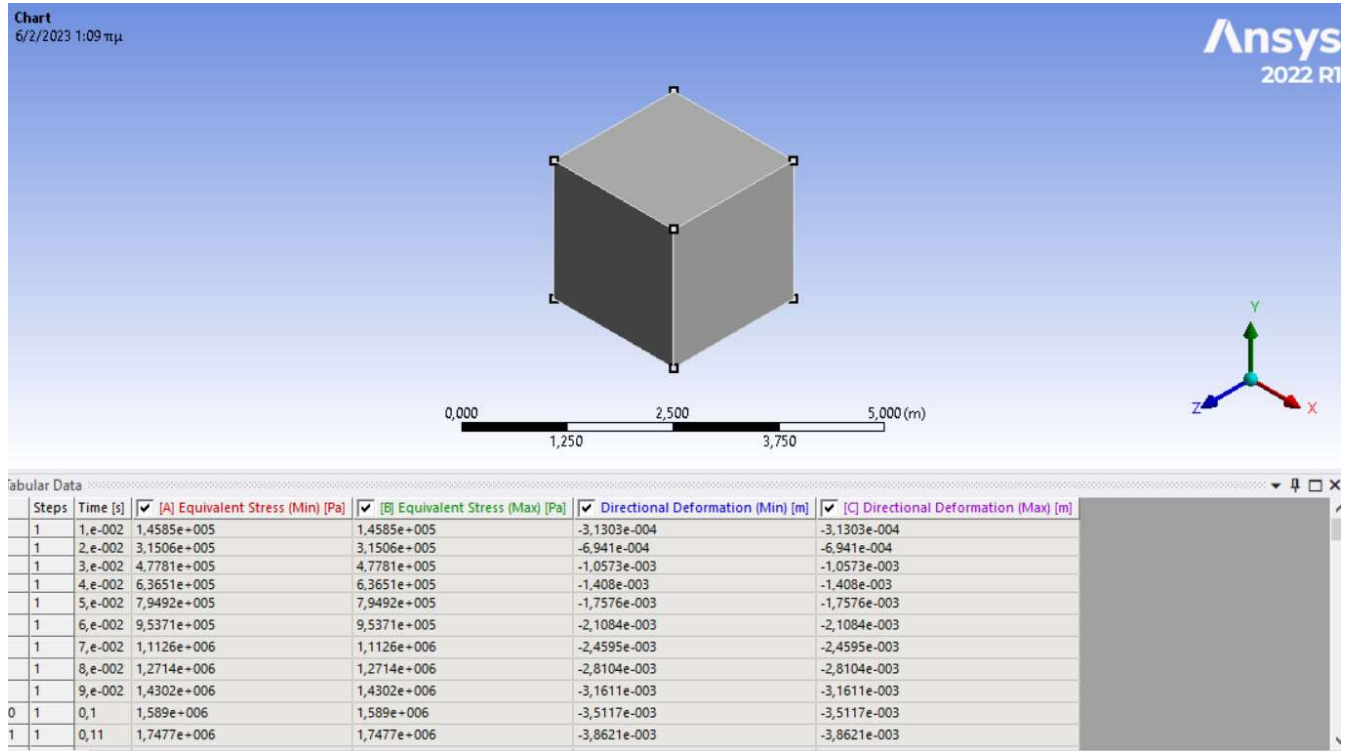
For Von Mises model

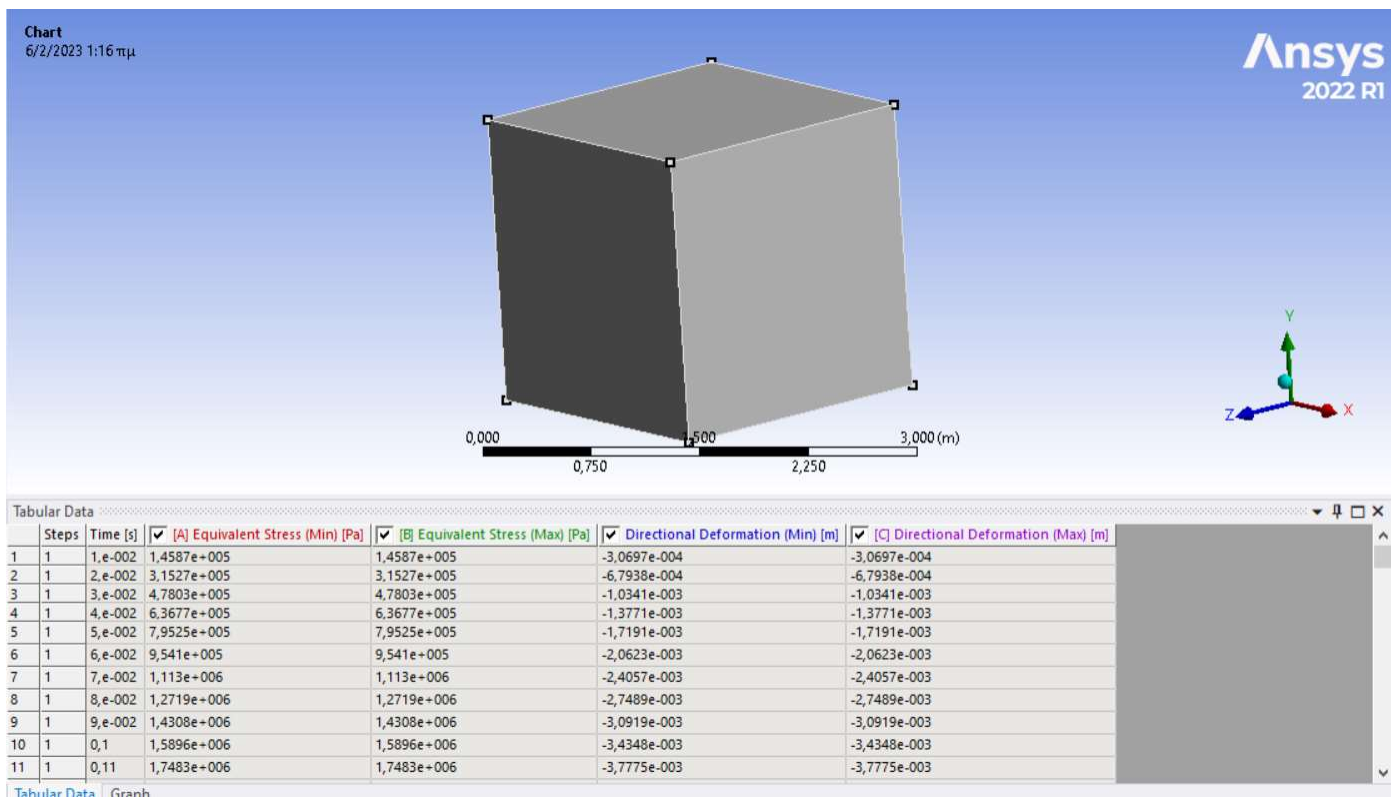
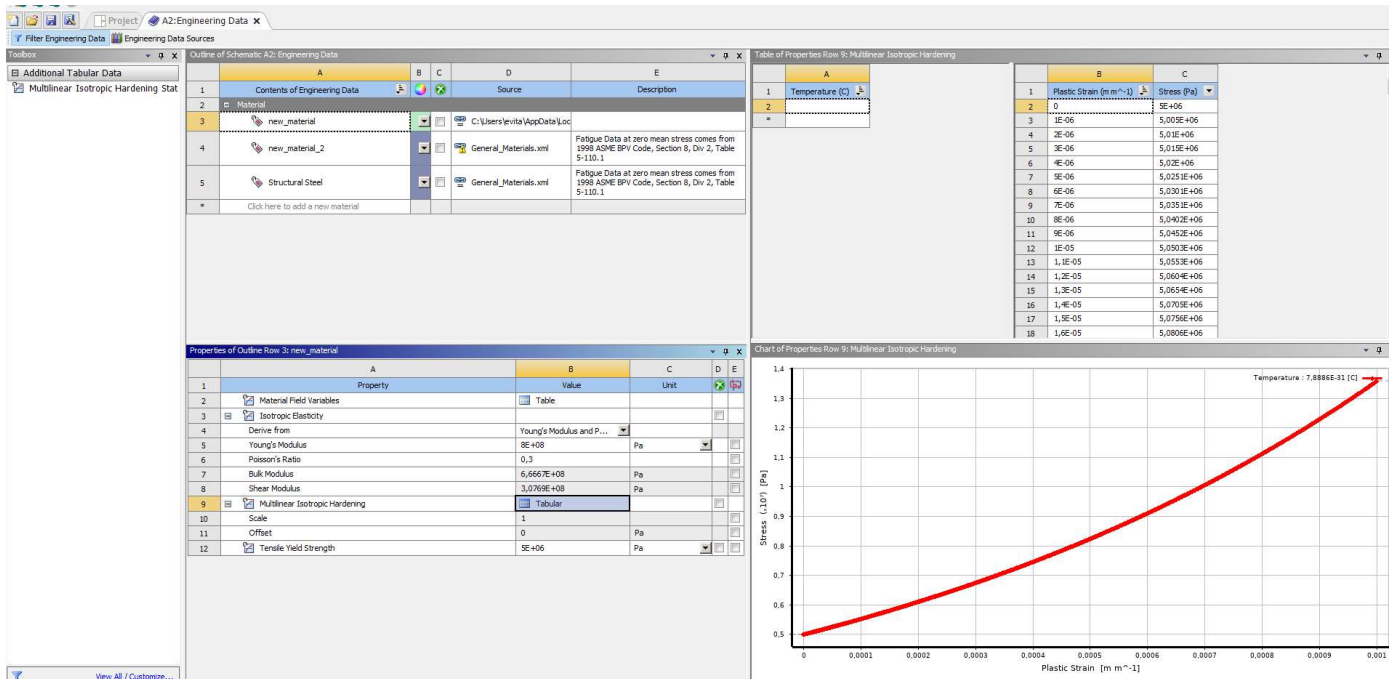




Details of "Mesh"	
Check Mesh Quality	Yes, Errors
Error Limits	Aggressive Mechanical
Target Element Quality	Default (5,e-002)
Smoothing	Medium
Mesh Metric	None
Inflation	
Use Automatic Inflation	None
Inflation Option	Smooth Transition
Transition Ratio	0,272
Maximum Layers	5
Growth Rate	1,2
Inflation Algorithm	Pre
View Advanced Options	No
Advanced	
Number of CPUs for Parallel Part Meshing	Program Controlled
Straight Sided Elements	
Rigid Body Behavior	Dimensionally Reduced
Triangle Surface Mesher	Program Controlled
Topology Checking	Yes
Pinch Tolerance	Please Define
Generate Pinch on Refresh	No
Statistics	
Nodes	27
Elements	8







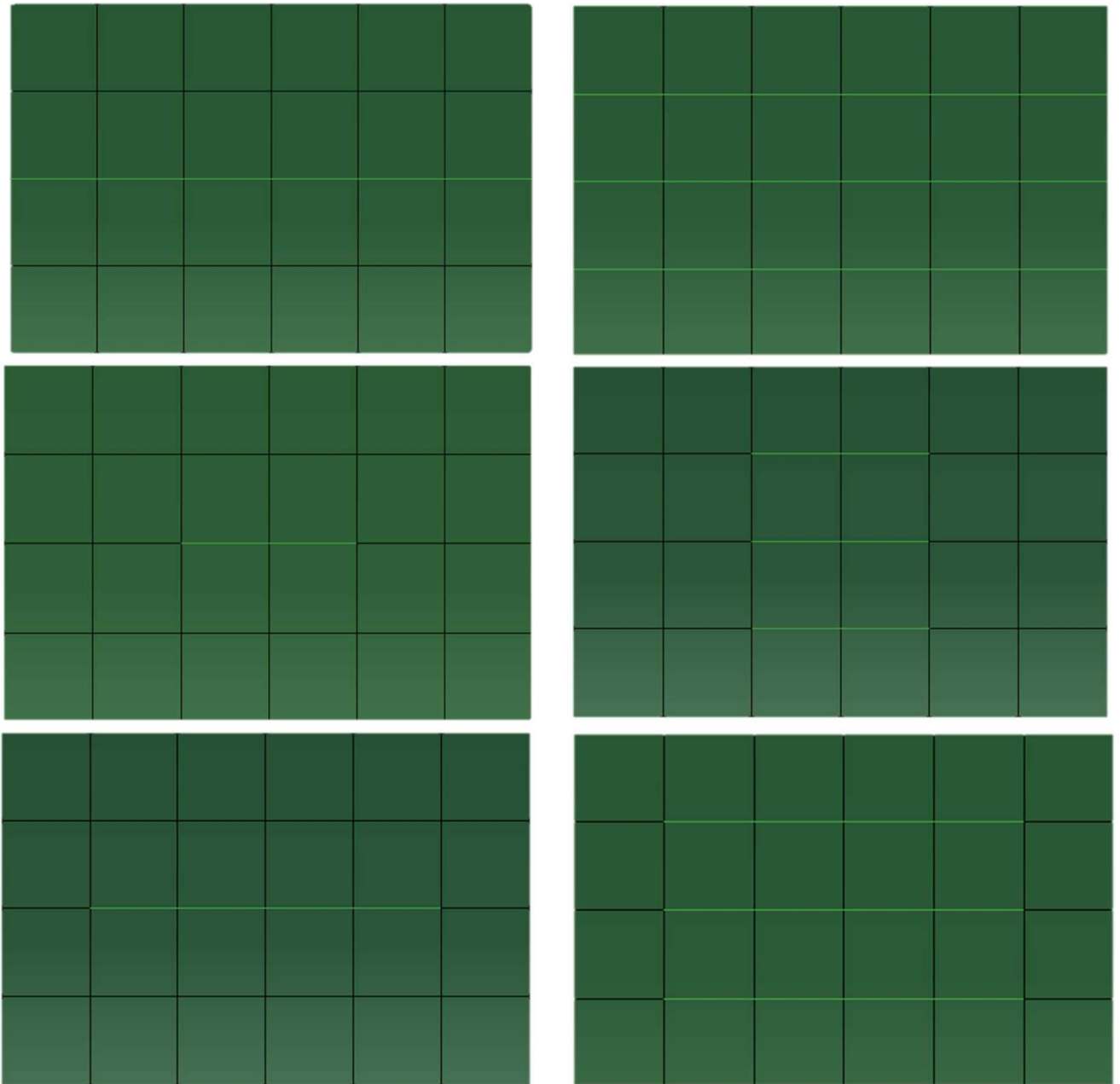
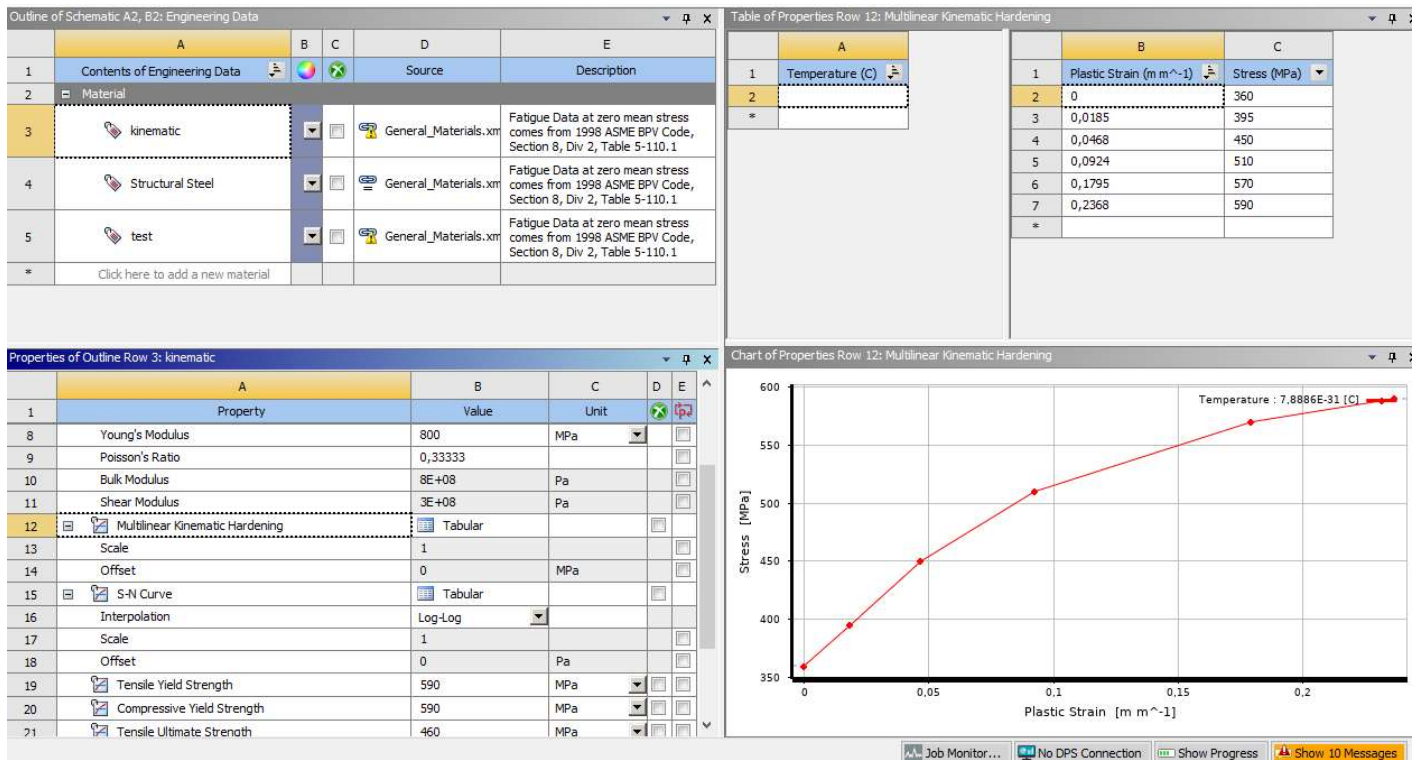


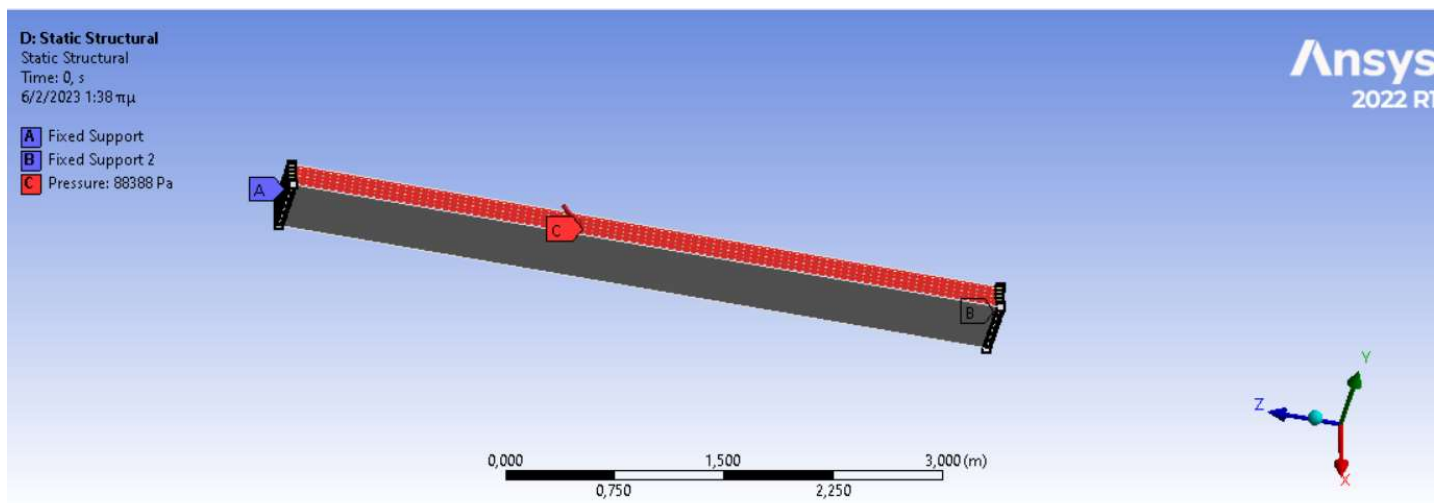
Figure 3.2.1: Geometry of the structure

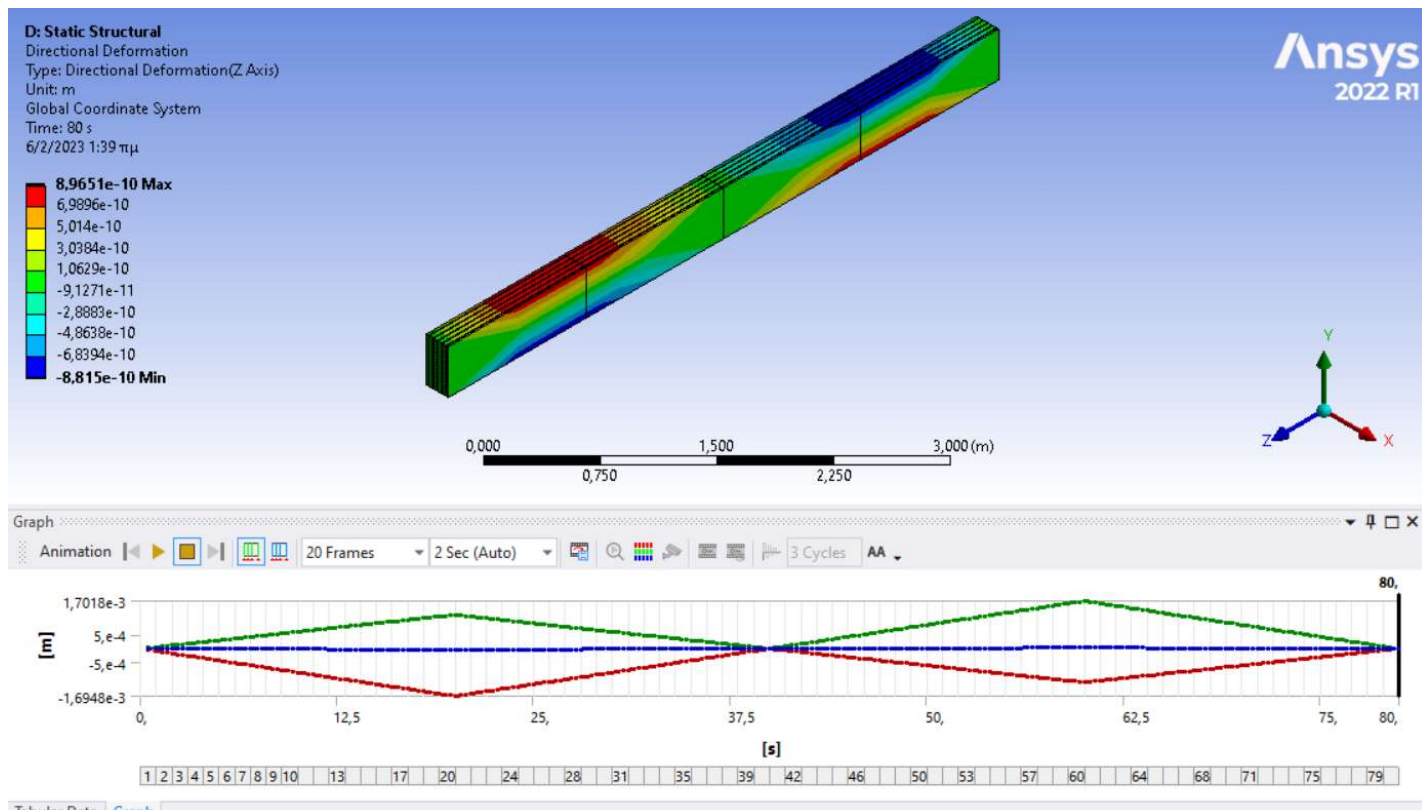
3D Fiber Beam- Force based fiber element

"Αλγόριθμοι Επίλυσης Ελαστοπλαστικών Συστημάτων"

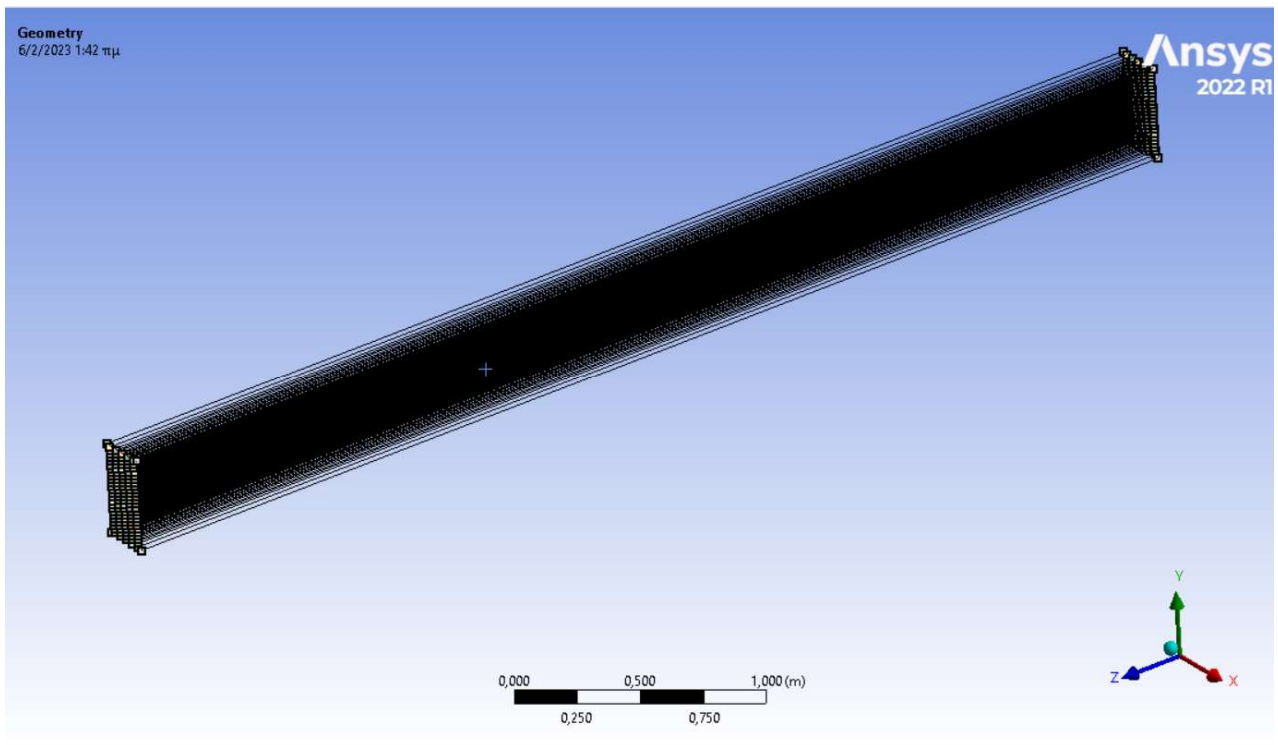
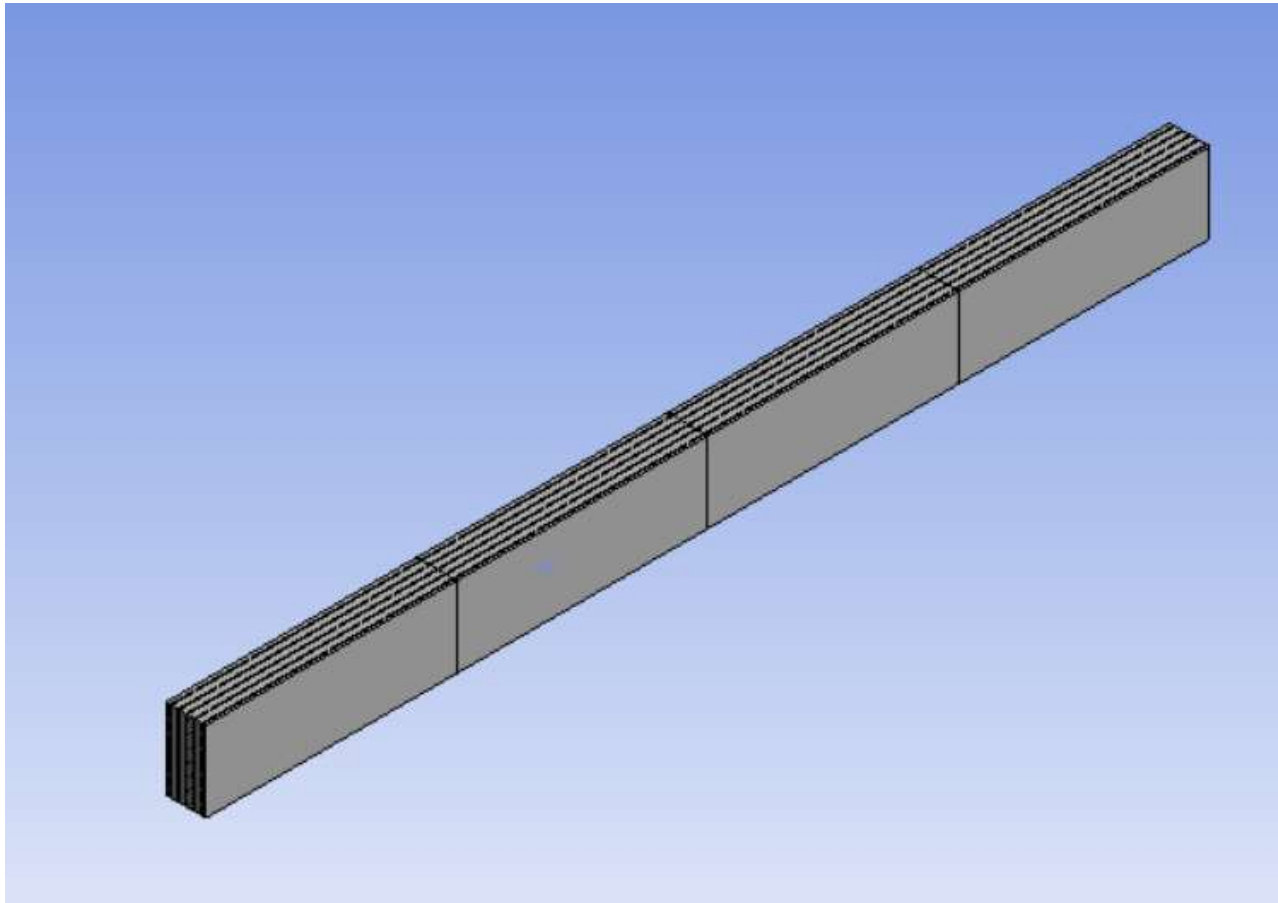


Clamped beam





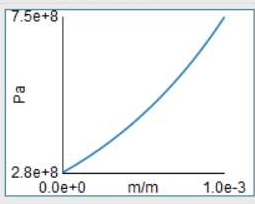
Details of "Mesh"	
Display Style	Use Geometry Setting
Defaults	
Physics Preference	Mechanical
Element Order	Program Controlled
Element Size	10, m
Sizing	
Quality	
Inflation	
Batch Connections	
Advanced	
Statistics	
Nodes	431
Elements	129





Rebars-Non-Linear Steel



Derive from	Young's Modulus and Poisson's Ratio
Young's Modulus	2,1e+11 Pa
Poisson's Ratio	0,30000
Bulk Modulus	1,75e+11 Pa
Shear Modulus	8,0769e+10 Pa
Multilinear Isotropic Hardening	
Isotropic Secant Coefficient of Thermal Expansion	1,2e-05 1/°C
Compressive Ultimate Strength	7,4753e+08 Pa
Compressive Yield Strength	2,75e+08 Pa
	-6.6e-1

Concrete-Linear



Structural

Isotropic Elasticity

Derive from	Young's Modulus and Poisson's Ratio
Young's Modulus	3e+10 Pa
Poisson's Ratio	0,30000
Bulk Modulus	2,5e+10 Pa
Shear Modulus	1,1538e+10 Pa

Additional Tabular Data

Multilinear Isotropic Hardening Stat

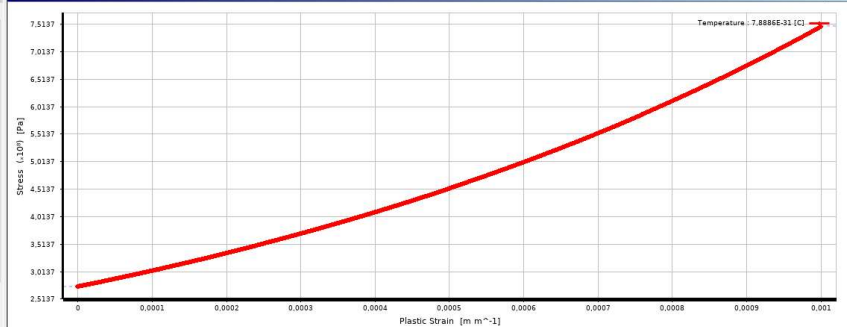
	A	B	C	D	E
1	Contents of Engineering Data		Source		Description
2	Material				
3	Concrete-Linear		C:\Users\evita\		
4	Rebars-Non-Linear Steel		General_Materi		Fatigue Data at zero mean stress comes from 1998 ASME BPV Code, Section 8, Div 2, Table 5-110.1
5	Click here to add a new material				

A
1 Temperature (C)
2 *

B	C
1 Plastic Strain [m m ⁻¹]	Stress (Pa)
2 0	2,79E+08
3 1E-06	2,7528E+08
4 2E-06	2,7555E+08
5 3E-06	2,7583E+08
6 4E-06	2,761E+08
7 5E-06	2,7638E+08
8 6E-06	2,7665E+08
9 7E-06	2,7693E+08
10 8E-06	2,7721E+08
11 9E-06	2,7749E+08
12 1E-05	2,7776E+08
13 1,1E-05	2,7804E+08
14 1,2E-05	2,7832E+08
15 1,3E-05	2,786E+08
16 1,4E-05	2,7888E+08
17 1,5E-05	2,7916E+08
18 1,6E-05	2,7944E+08

A	B	C	D	E
1 Property	Value	Unit		
2 Material Field Variables	Table			
3 Density	7850	kg m ⁻³		
4 Isotropic Secant Coefficient of Thermal Expansion				
5 Coefficient of Thermal Expansion	1,2E-05	C ⁻¹		
6 Isotropic Elasticity				
7 Derive from	Young's Mo...			
8 Young's Modulus	2,1E+11	Pa		
9 Poisson's Ratio	0,3			
10 Bulk Modulus	1,79E+11	Pa		
11 Shear Modulus	8,0769E+10	Pa		
12 Multilinear Isotropic Hardening	Tabular			
13 Scale	1			
14 Offset	0	Pa		
15 Strain-Life Parameters				
23 S-N Curve	Tabular			
24 Interpolation	Log-Log			
25 Scale	1			
26 Offset	0	Pa		
27 Tensile Yield Strength	2,79E+08	Pa		

Chart of Properties Row 12: Multilinear Isotropic Hardening



Analysis Type

Edit Step

Name: Heating Step

Type: Heat transfer

Basic Incrementation Other

Type: ☒ Automatic ☐ Fixed

Maximum number of increments: 100

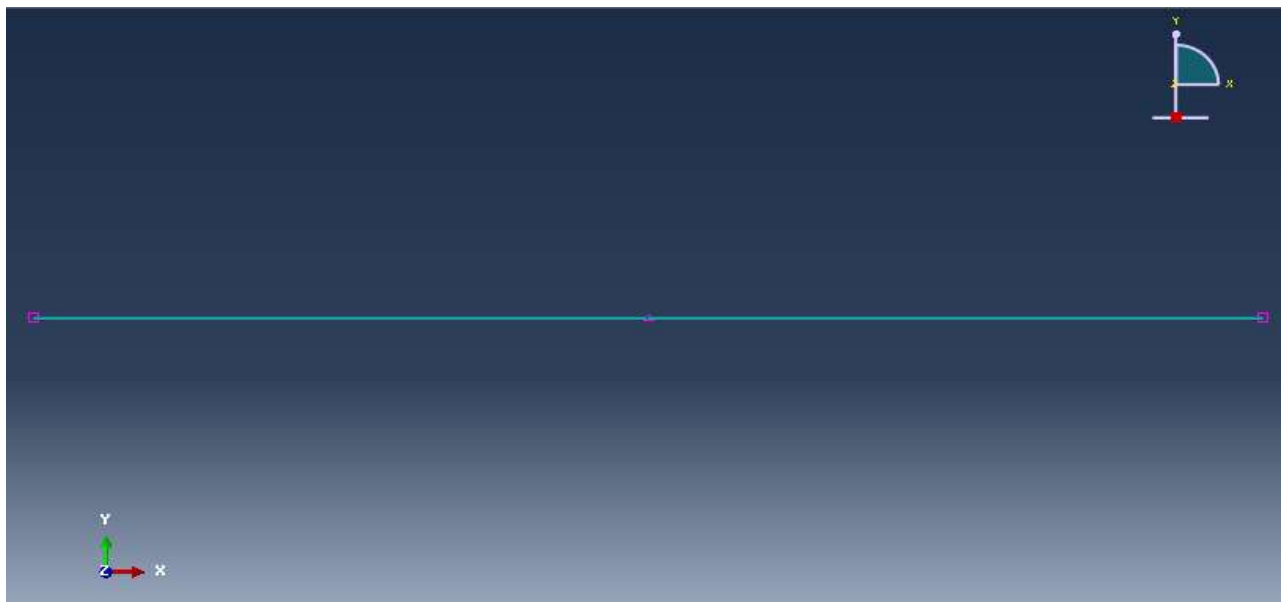
	Initial	Minimum	Maximum
Increment size:	1	1E-005	1

☐ End step when temperature change is less than: []

Max. allowable temperature change per increment: []

Max. allowable emissivity change per increment: 0.1

OK Cancel



Mesh of fiber beam element

3.3 3D Mesh of Classical Finite Elements

Hexa8

The elements used to simulate the structure in the present case are 3D finite elements with linear elastic material properties. The generation of finite elements for the analysis of vectors whose intensive state corresponds to 3D elasticity can easily be used from the 2D elasticity elements by adding the z-coordinate and the corresponding displacement w . Specifically, regarding the modeling of the cubic specimen, three-dimensional 8-node finite elements were used where the reference system and numbering of nodes is shown in Figure 3.3.1 and the coordinates of the nodes as well as the numbering of the nodes is counter-clockwise. Also, Solid 185 type was selected from the Ansys finite element library (Figure 3.3.1).

Hexahedron:

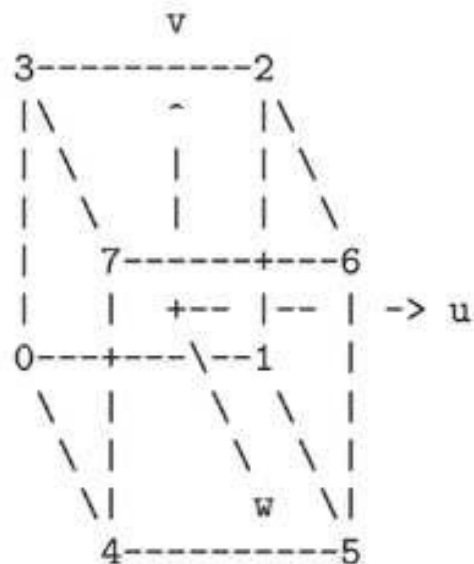
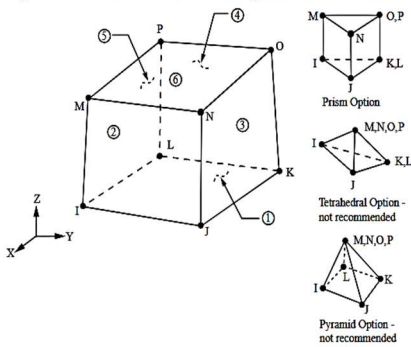


Figure 3.3.1: 3D Hexa8 FE

SOLID185 Homogeneous Structural Solid Element Description

SOLID185 Structural Solid is suitable for modeling general 3-D solid structures. It allows for prism, tetrahedral, and pyramid degenerations when used in irregular regions. Various element technologies such as B-bar, uniformly reduced integration, and enhanced strains are supported.

Figure 185.1: SOLID185 Homogeneous Structural Solid Geometry



KEYOPT(2)

Element technology:

- 0 -- Full integration with \bar{B} method (default)
- 1 -- Uniform reduced integration with hourglass control
- 2 -- Enhanced strain formulation
- 3 -- Simplified enhanced strain formulation

KEYOPT(3)

Layer construction:

- 0 -- Structural Solid (default) -- nonlayered
- 1 -- [Layered Solid](#) (not applicable to SOLID185 Structural Solid)

KEYOPT(6)

Element formulation:

- 0 -- Use pure displacement formulation (default)
- 1 -- Use mixed formulation

KEYOPT(15)

PML absorbing condition:

- 0 -- Do not include PML absorbing condition (default)
- 1 -- Include PML absorbing condition

KEYOPT(16)

Steady state analysis flag:

0 --

Steady state analysis disabled (default)

1 --

Enable steady state analysis

KEYOPT(17)

Extra surface output:

0 --

Basic element solution (default)

4 --

Surface solution for faces with nonzero pressure

SOLID185 Homogeneous Structural Solid Element Technology

SOLID185 Homogeneous Structural Solid uses the full-integration [B₈ method](#) (also known as the selective reduced integration method), [enhanced strain formulation](#), [simplified enhanced strain formulation](#), or [uniform reduced integration](#).

When enhanced strain formulation (KEYOPT(2) = 2) is selected, the element introduces nine *internal* (user-inaccessible) degrees of freedom to handle shear locking, and four internal degrees of freedom to handle volumetric locking.

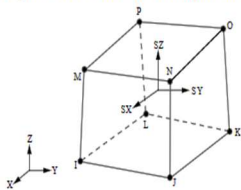
For more information, see [Element Technologies](#).

SOLID185 Homogeneous Structural Solid Output Data

The solution output associated with the element is in two forms:

- Nodal displacements included in the overall nodal solution
- Additional element output as shown in [Table 185.1: SOLID185 Homogeneous Structural Solid Element Output Definitions](#)

Several items are illustrated in [Figure 185.2: SOLID185 Homogeneous Structural Solid Stress Output](#). See [Element Table for Variables Identified By Sequence Number](#) and [The Item and Sequence Number Table](#) in this document for more information.

Figure 185.2: SOLID185 Homogeneous Structural Solid Stress Output

Stress directions shown are for global directions.

The subroutine for Hexa8 from Ansys Apdl Commands is the following:

```
ET,matid,SOLID185
ETCONTROL,off,ON
KEYOPT,matid,1,0
KEYOPT,matid,2,0
KEYOPT,matid,3,0
KEYOPT,matid,4,0
KEYOPT,matid,5,0
KEYOPT,matid,6,0
KEYOPT,matid,7,0
KEYOPT,matid,8,0
```

CHAPTER 4th

4. OPEN SOURCE CODE MSOLVE

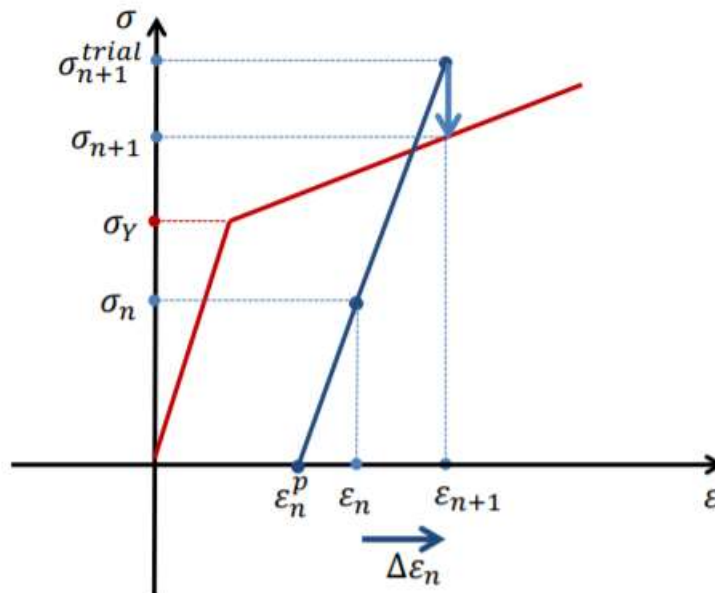
4.1 General

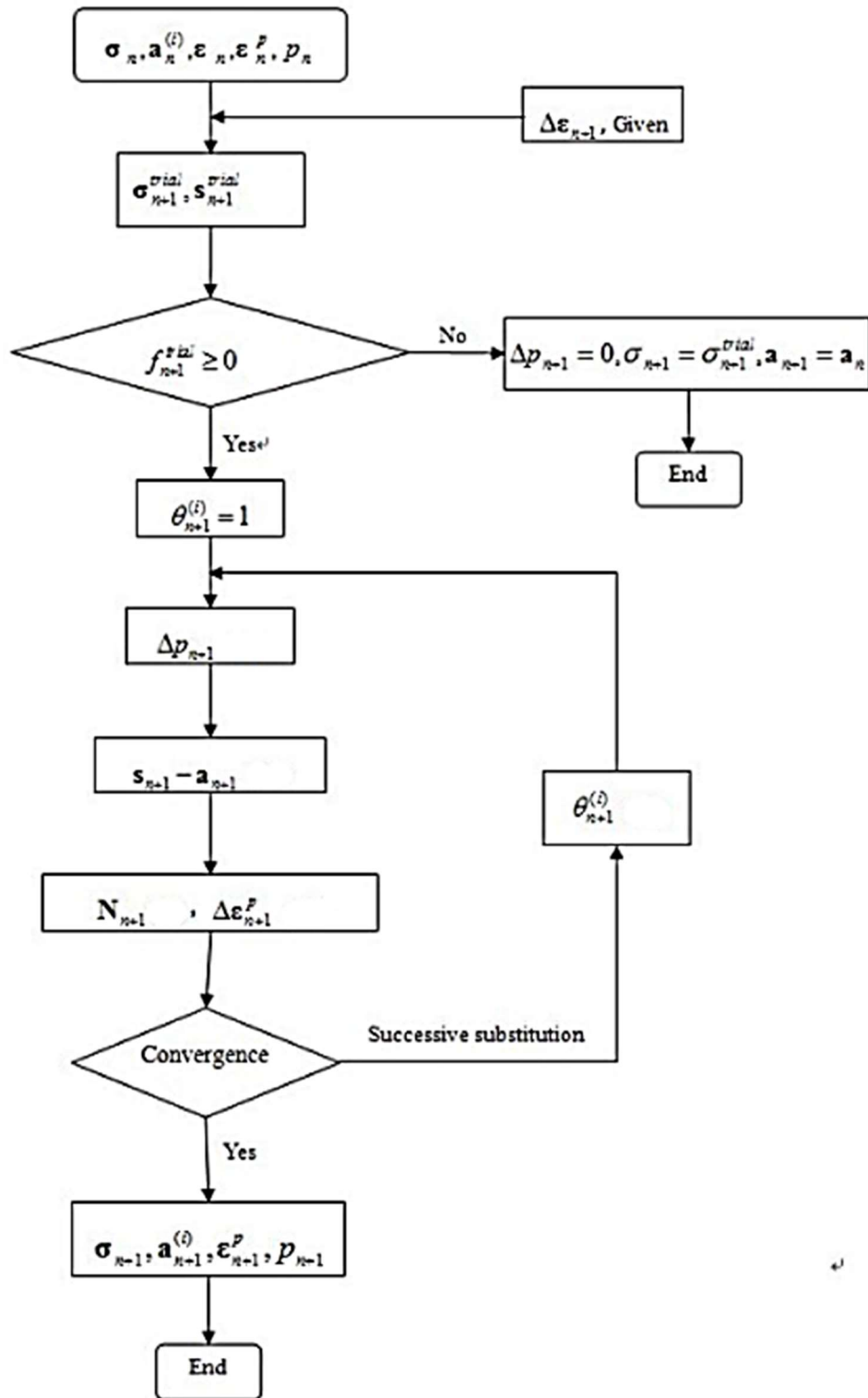
The numerical solution of the composite material model was chosen to be solved with the help of the MSolve software, due to the complexity of this problem, the optimization algorithms as well as the generation of meshes, this powerful computational tool was used, which ensured the solution of quite complex problems with the best possible accuracy in the results and the least time cost to find the requested sizes. The final goal was to validate and verify the final results to check their correctness and the assumptions considered for its solution.

4.1.1 Flow chart

In this section, a general flow chart is presented that summarizes the process – algorithm followed to calculate the force-displacement curve and all the initial conditions and assumptions taken to solve it.

Therefore, it follows:





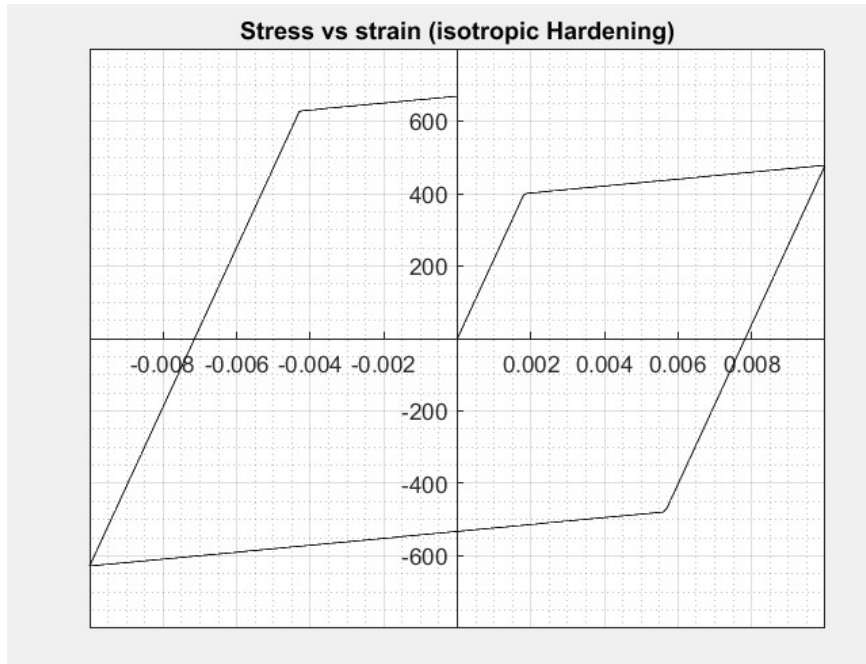
```

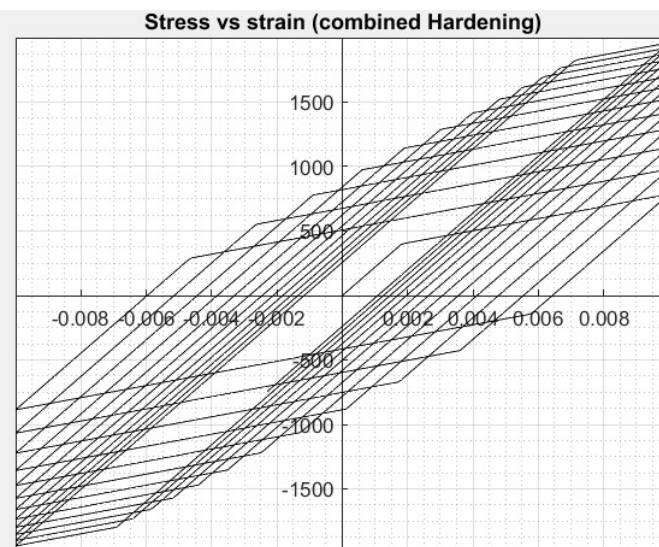
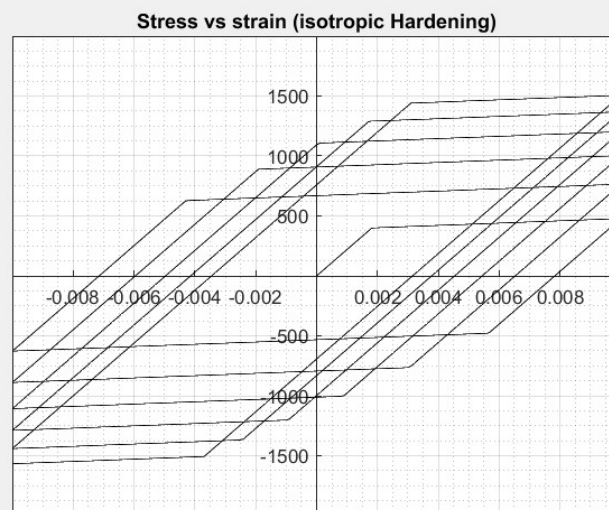
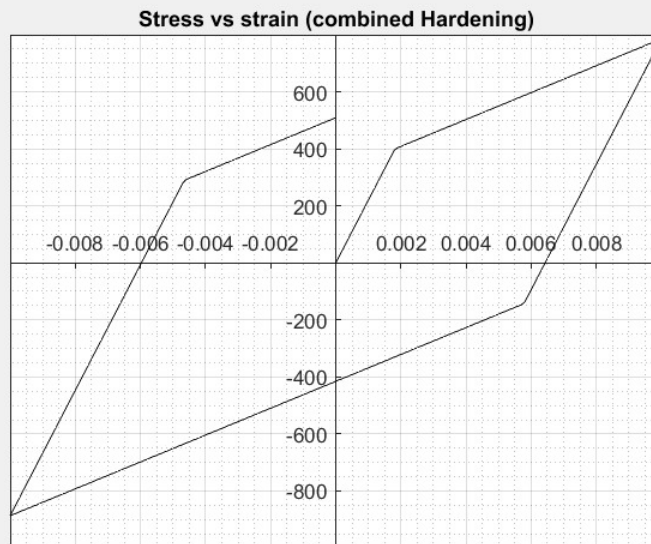
1. Database at  $x \in \mathcal{B} : \{\varepsilon_n^p, \alpha_n, q_n\}$ .
2. Given strain field at  $x \in \mathcal{B} : \varepsilon_{n+1} = \varepsilon_n + \Delta\varepsilon_n$ .
3. Compute elastic trial stress and test for plastic loading
 $\sigma_{n+1}^{\text{trial}} := E (\varepsilon_{n+1} - \varepsilon_n^p)$ 
 $\xi_{n+1}^{\text{trial}} := \sigma_{n+1}^{\text{trial}} - q_n$ 
 $f_{n+1}^{\text{trial}} := |\xi_{n+1}^{\text{trial}}| - [\sigma_Y + K\alpha_n]$ 
IF  $f_{n+1}^{\text{trial}} \leq 0$  THEN
    Elastic step: set  $(\bullet)_{n+1} = (\bullet)_{n+1}^{\text{trial}}$  & EXIT
ELSE
    Plastic step: Proceed to step 4.
ENDIF
4. Return mapping

 $\Delta\gamma := \frac{f_{n+1}^{\text{trial}}}{E + [K + H]} > 0$ 

 $\sigma_{n+1} := \sigma_{n+1}^{\text{trial}} - \Delta\gamma E \text{sign}(\xi_{n+1}^{\text{trial}})$ 
 $\varepsilon_{n+1}^p := \varepsilon_n^p + \Delta\gamma \text{sign}(\xi_{n+1}^{\text{trial}})$ 
 $q_{n+1} := q_n + \Delta\gamma H \text{sign}(\xi_{n+1}^{\text{trial}})$ 
 $\alpha_{n+1} := \alpha_n + \Delta\gamma$ 
    
```

Figure 4.1.1.1: Flow Chart Representation





4.1.2 Methodology of MSolve Software

General numerical integration algorithm for elastoplastic constitutive equations

The importance of the state-updating procedure within the overall finite element scheme has been stressed in Chapter 4. In the case of path-dependent materials, such as elastoplastic materials, the updating scheme usually requires the formulation of a numerical algorithm for integration of the corresponding rate constitutive equations. This requirement stems from the fact that analytical solutions to the initial value problem defined by the elastoplastic equations are generally not known for complex strain paths. An important point that one should bear in mind regarding the formulation of state-updating procedures is that the accuracy of the overall finite element scheme depends crucially on the accuracy of the particular numerical algorithm adopted. This section describes a numerical procedure for integration of the general elastoplastic model of Section 6.3. The strategy presented here is later specialised and applied to the von Mises model in Section 7.3. Specialisation to the other basic plasticity models of Chapter 6, i.e. the Tresca, Mohr–Coulomb and Drucker–Prager models, is presented in Chapter 8 and its plane stress implementation is addressed in Chapter 9. Further applications of the algorithms described in the present chapter are made in Chapter 10, in the context of advanced plasticity models, and in Chapter 12, where the numerical implementation of damage mechanics models is discussed.

7.2.1. THE ELASTOPLASTIC CONSTITUTIVE INITIAL VALUE PROBLEM

Consider a point \mathbf{p} of a body \mathcal{B} with constitutive behaviour described by the general elastoplastic model of Box 6.2 (page 151). Assume that at a given (pseudo-)time t_0 the elastic strain, $\boldsymbol{\varepsilon}^e(t_0)$, the plastic strain tensor, $\boldsymbol{\varepsilon}^p(t_0)$, and all elements of the set $\boldsymbol{\alpha}(t_0)$ of hardening internal variables are known at point \mathbf{p} . Furthermore, let the motion of \mathcal{B} be prescribed between t_0 and a subsequent instant, T . Clearly, the prescribed motion defines the *history* of the strain tensor, $\boldsymbol{\varepsilon}(t)$, at the material point of interest between instants t_0 and T . The basic elastoplastic constitutive initial value problem at point \mathbf{p} is stated in the following.

Problem 7.1 (The elastoplastic constitutive initial value problem). *Given the initial values $\boldsymbol{\varepsilon}^e(t_0)$ and $\boldsymbol{\alpha}(t_0)$ and given the history of the strain tensor, $\boldsymbol{\varepsilon}(t)$, $t \in [t_0, T]$, find the functions $\boldsymbol{\varepsilon}^e(t)$, $\boldsymbol{\alpha}(t)$ and $\dot{\gamma}(t)$ for the elastic strain, hardening internal variables set and plastic multiplier that satisfy the reduced general elastoplastic constitutive equations*

$$\begin{aligned}\dot{\boldsymbol{\varepsilon}}^e(t) &= \dot{\boldsymbol{\varepsilon}}(t) - \dot{\gamma}(t) \mathbf{N}(\boldsymbol{\sigma}(t), \mathbf{A}(t)) \\ \dot{\boldsymbol{\alpha}}(t) &= \dot{\gamma}(t) \mathbf{H}(\boldsymbol{\sigma}(t), \mathbf{A}(t))\end{aligned}\tag{7.6}$$

$$\dot{\gamma}(t) \geq 0, \quad \Phi(\boldsymbol{\sigma}(t), \mathbf{A}(t)) \leq 0, \quad \dot{\gamma}(t) \Phi(\boldsymbol{\sigma}(t), \mathbf{A}(t)) = 0\tag{7.7}$$

for each instant $t \in [t_0, T]$, with

$$\boldsymbol{\sigma}(t) = \bar{\rho} \left. \frac{\partial \psi}{\partial \boldsymbol{\varepsilon}^e} \right|_t, \quad \mathbf{A}(t) = \bar{\rho} \left. \frac{\partial \psi}{\partial \boldsymbol{\alpha}} \right|_t.\tag{7.8}$$

Remark 7.1. We refer to the system of differential equations (7.6) as *reduced* in that it is obtained from the model of Box 6.2 by incorporating the plastic flow equation into the additive strain rate decomposition. In this way, the plastic strain does not appear explicitly in

the system and the only unknowns are the elastic strain, the set of hardening internal variables and the plastic multiplier. Note that with the solution $\varepsilon^e(t)$ of Problem 7.1 at hand, the history of the plastic strain tensor is obtained from the trivial relation

$$\varepsilon^p(t) = \varepsilon(t) - \varepsilon^e(t), \quad (7.9)$$

so that the history of all variables involved in the definition of the elastoplastic model of Box 6.2 is determined.

As already mentioned, exact solutions to Problem 7.1, when yield functions and flow rules such as the ones described in the previous chapter are adopted, may only be obtained for very simple prescribed strain histories. Even in such cases, the derivation of the analytical solutions is normally cumbersome. For complex deformation paths, which are more likely to occur in realistic engineering problems, analytical solutions are not available in general and the adoption of a numerical technique to find an approximate solution becomes absolutely essential. A general framework for the numerical solution of the constitutive initial value problem of elastoplasticity is described below.

Solution of the incremental problem

Due to the presence of the discrete complementarity condition (7.11), the solution of the incremental elastoplastic problem (7.10)–(7.12) does not follow directly the conventional procedure for standard initial value problems (i.e. initial value problems without equations of the type (7.7)). Nevertheless, as we shall see, the solution scheme in the present case remains rather simple with the discrete complementarity condition giving rise to a two-step algorithm derived in the following.

Firstly, note that (7.11)₁ allows only for the two (mutually exclusive) possibilities enumerated below:

1. Null incremental plastic multiplier,

$$\Delta\gamma = 0. \quad (7.15)$$

In this case there is no plastic flow or evolution of internal variables within the considered interval $[t_n, t_{n+1}]$, i.e. the step is purely elastic. The constraint (7.11)₃ is automatically satisfied, ϵ_{n+1}^e and α_{n+1} are given by

$$\begin{aligned} \epsilon_{n+1}^e &= \epsilon_n^e + \Delta\epsilon \\ \alpha_{n+1} &= \alpha_n \end{aligned} \quad (7.16)$$

and, in addition, the constraint

$$\Phi(\sigma_{n+1}, A_{n+1}) \leq 0, \quad (7.17)$$

must hold, where σ_{n+1} and A_{n+1} are functions of ϵ_{n+1}^e and A_{n+1} defined through the potential relations (7.12).

2. Strictly positive plastic multiplier,

$$\Delta\gamma > 0. \quad (7.18)$$

In this case, ϵ_{n+1}^e , α_{n+1} and $\Delta\gamma$ satisfy

$$\begin{aligned} \epsilon_{n+1}^e &= \epsilon_n^e + \Delta\epsilon - \Delta\gamma N(\sigma_{n+1}, A_{n+1}) \\ \alpha_{n+1} &= \alpha_n + \Delta\gamma H(\sigma_{n+1}, A_{n+1}) \end{aligned} \quad (7.19)$$

and (7.11)₂ combined with (7.11)₃ result in the constraint

$$\Phi(\sigma_{n+1}, A_{n+1}) = 0. \quad (7.20)$$

The nature of the above problem motivates the establishment of a (conceptually very simple) two-step algorithm in which the two possible sets of equations are employed sequentially and the final solution is selected as the only valid one. The strategy adopted is the following:

(a) *The Elastic Trial Step.*

Firstly, we assume that the first of the above two situations ($\Delta\gamma = 0$) occurs; that is, we assume that the step $[t_n, t_{n+1}]$ is *elastic*. The solution given by (7.16), which is not necessarily the actual solution to Problem 7.2, will be called the *elastic trial solution*, and will be denoted

$$\begin{aligned}\epsilon_{n+1}^{e \text{ trial}} &= \epsilon_n^e + \Delta\epsilon \\ \alpha_{n+1}^{\text{trial}} &= \alpha_n.\end{aligned}\tag{7.21}$$

The corresponding stress and hardening force will be called the *elastic trial stress* and *elastic trial hardening force*, given by

$$\sigma_{n+1}^{\text{trial}} = \bar{\rho} \frac{\partial \psi}{\partial \epsilon^e} \Big|_{n+1}^{\text{trial}}, \quad A_{n+1}^{\text{trial}} = \bar{\rho} \frac{\partial \psi}{\partial \alpha} \Big|_{n+1}^{\text{trial}}.\tag{7.22}$$

The above variables are collectively called the *elastic trial state*. Now note that, to be the actual solution, the elastic trial state has, in addition, to satisfy (7.17). We then proceed as follows. If

$$\Phi^{\text{trial}} \equiv \Phi(\sigma_{n+1}^{\text{trial}}, A_{n+1}^{\text{trial}}) \leq 0,\tag{7.23}$$

that is, if the *elastic trial state* lies within the elastic domain or on the yield surface, it is accepted as a solution to Problem 7.2. In this case, we update

$$(\cdot)_{n+1} := (\cdot)_{n+1}^{\text{trial}}\tag{7.24}$$

and the algorithm is terminated. Otherwise, the elastic trial state is not plastically admissible and a solution to Problem 7.2 must be obtained from the *plastic corrector step* described below.

(b) *The Plastic Corrector Step (or Return-Mapping Algorithm).*

The only option left now is to solve the system (7.19)–(7.20) of algebraic equations subject to the constraint (7.18). Using the elastic trial state definition above, we rewrite the algebraic system equivalently as

$$\begin{aligned}\epsilon_{n+1}^e &= \epsilon_{n+1}^{e \text{ trial}} - \Delta\gamma N(\sigma_{n+1}, A_{n+1}) \\ \alpha_{n+1} &= \alpha_{n+1}^{\text{trial}} + \Delta\gamma H(\sigma_{n+1}, A_{n+1}) \\ \Phi(\sigma_{n+1}, A_{n+1}) &= 0,\end{aligned}\tag{7.25}$$

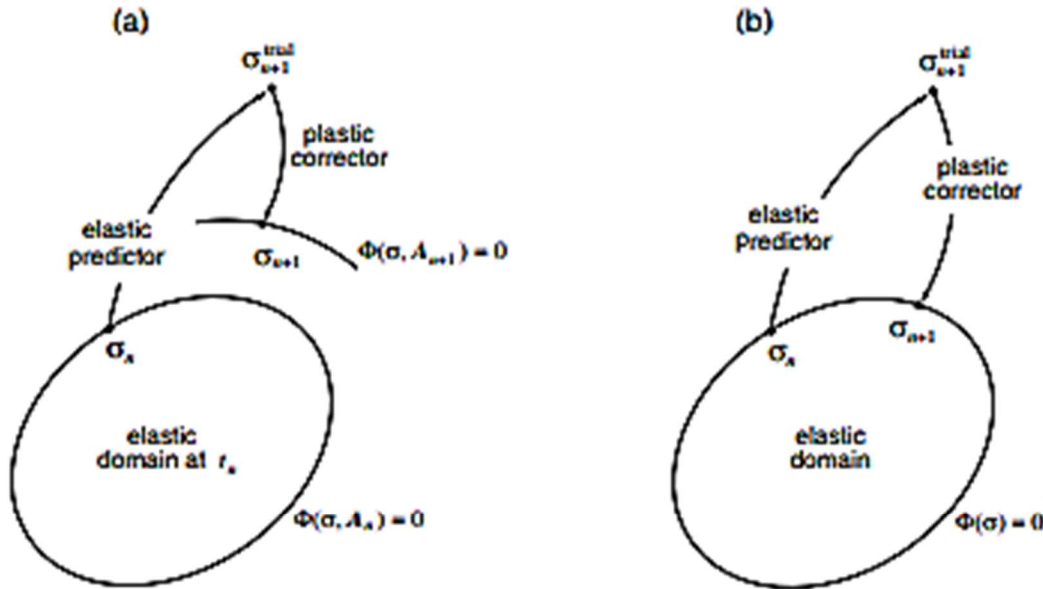


Figure 7.1. General return mapping schemes. Geometric interpretation: (a) hardening plasticity; and (b) perfect plasticity.

which are, of course, complemented with the potential relations (7.12). The plastic corrector stage of the algorithm then consists in finding a solution ϵ_{n+1}^e , α_{n+1} and $\Delta\gamma$ for (7.25) that satisfies

$$\Delta\gamma > 0. \quad (7.26)$$

Remark 7.2. The procedure of item (b) above possesses an appealing geometric interpretation as illustrated in Figure 7.1. Consider the yield surface at the elastic trial state. The elastic trial stress, σ_{n+1}^{trial} , in this case lies outside the plastically admissible domain (i.e. neither in the elastic domain nor on the yield surface). Upon solution of the algebraic system (7.25), equation (7.25)₃, which is commonly referred to as the *plastic consistency equation*, ensures that the stress, σ_{n+1} , at the end of the interval $[t_n, t_{n+1}]$ lies on the updated yield surface; that is, the elastic trial stress *returns* to the yield surface so that plastic consistency is re-established in the updated state. In the case of perfect plasticity, σ_{n+1}^{trial} returns to a *fixed* surface. Due to this interpretation the procedure of item (b) is referred to as the *return mapping algorithm* and (7.25) are called the *return mapping equations*. The first algorithm of this type appears to have been the *radial return method* proposed in the pioneering work of Wilkins (1964).

Summary of the overall procedure

In summary, the application of an Euler difference scheme to find an approximate solution of the constitutive initial value problem of elastoplasticity – Problem 7.1 – has resulted in a numerical algorithm that involves two steps: the *elastic predictor*, in which the evolution problem is solved as if the material were purely elastic within the interval considered, followed by the *return mapping*, which accounts for plastic flow and enforces plastic admissibility. The return mapping procedure is executed only if the elastic trial state violates plastic admissibility. The schematic diagram of Figure 7.2 shows the main steps in the

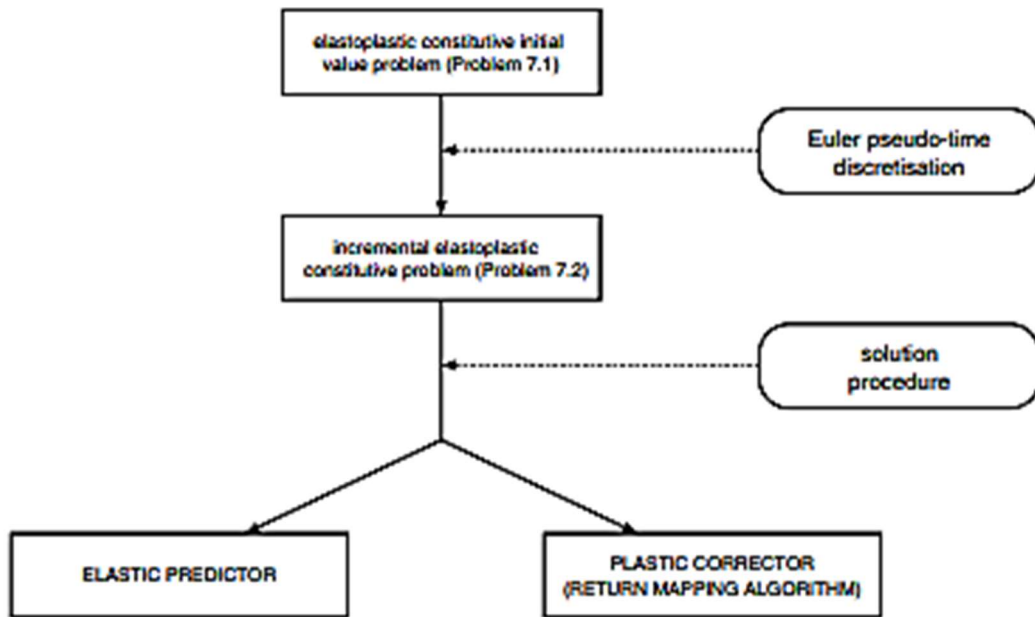


Figure 7.2. From the initial value problem of elastoplasticity to the elastic predictor/return-mapping integration algorithm. Schematic diagram.

derivation of the overall integration algorithm. The algorithm described above has been obtained by adopting, in particular, the backward Euler scheme to discretise elastoplastic constitutive equations and is, therefore, termed the *backward, fully implicit* or simply *implicit* elastic predictor/return mapping scheme. This algorithm is conveniently summarised in Box 7.1 in pseudo-code format. We remark that different discretisation schemes may be used instead, each one resulting in a different return mapping algorithm, but all having the same elastic predictor step. Alternatives to the backward Euler-based algorithm will be discussed in Section 7.2.7.

7.2.4. SOLUTION OF THE RETURN-MAPPING EQUATIONS

Let us now focus on the solution of the return mapping equations. It should be noted that the algebraic system (7.25) is generally nonlinear and, in addition, has to be solved subjected to the constraint (7.26). The procedure commonly adopted in practice is quite simple. Firstly, the algebraic system (7.25) is solved on its own, i.e. without regard for the constraint equation (7.26), by some iterative procedure. If the found solution satisfies (7.26), then it is accepted as a solution to Problem 7.2. Note that if no solution exists with strictly positive incremental plastic multiplier, then Problem 7.2 does not have a solution.

As far as the iterative procedure for the solution of the return-mapping equations is concerned, the standard Newton–Raphson scheme is often an optimal choice and will be adopted *exclusively* throughout this book (and in the elastoplastic implementations of the HYPLAS program). This choice is motivated mainly by the quadratic rates of convergence achieved by this method which, as a general rule, results in very computationally efficient return mapping procedures. Alternative techniques, such as quasi-Newton procedures in general, could be used instead. The main argument in favour of these methods is normally based on

(i) Elastic predictor. Given $\Delta \varepsilon$ and the state variables at t_n , evaluate the *elastic trial state*

$$\varepsilon_{n+1}^{\text{trial}} = \varepsilon_n^e + \Delta \varepsilon$$

$$\alpha_{n+1}^{\text{trial}} = \alpha_n$$

$$\sigma_{n+1}^{\text{trial}} = \bar{\rho} \left. \frac{\partial \psi}{\partial \varepsilon^e} \right|_{n+1}^{\text{trial}}, \quad A_{n+1}^{\text{trial}} = \bar{\rho} \left. \frac{\partial \psi}{\partial \alpha} \right|_{n+1}^{\text{trial}}$$

(ii) Check plastic admissibility

$$\text{IF } \Phi(\sigma_{n+1}^{\text{trial}}, A_{n+1}^{\text{trial}}) \leq 0$$

THEN set $(\cdot)_{n+1} = (\cdot)_{n+1}^{\text{trial}}$ and EXIT

(iii) Return mapping. Solve the system

$$\begin{cases} \varepsilon_{n+1}^e - \varepsilon_{n+1}^{\text{trial}} + \Delta \gamma N_{n+1} \\ \alpha_{n+1} - \alpha_{n+1}^{\text{trial}} - \Delta \gamma H_{n+1} \\ \Phi(\sigma_{n+1}, A_{n+1}) \end{cases} = \begin{Bmatrix} 0 \\ 0 \\ 0 \end{Bmatrix}$$

for ε_{n+1}^e , α_{n+1} and $\Delta \gamma$, with

$$\sigma_{n+1} = \bar{\rho} \left. \frac{\partial \psi}{\partial \varepsilon^e} \right|_{n+1}, \quad A_{n+1} = \bar{\rho} \left. \frac{\partial \psi}{\partial \alpha} \right|_{n+1}$$

(iv) EXIT

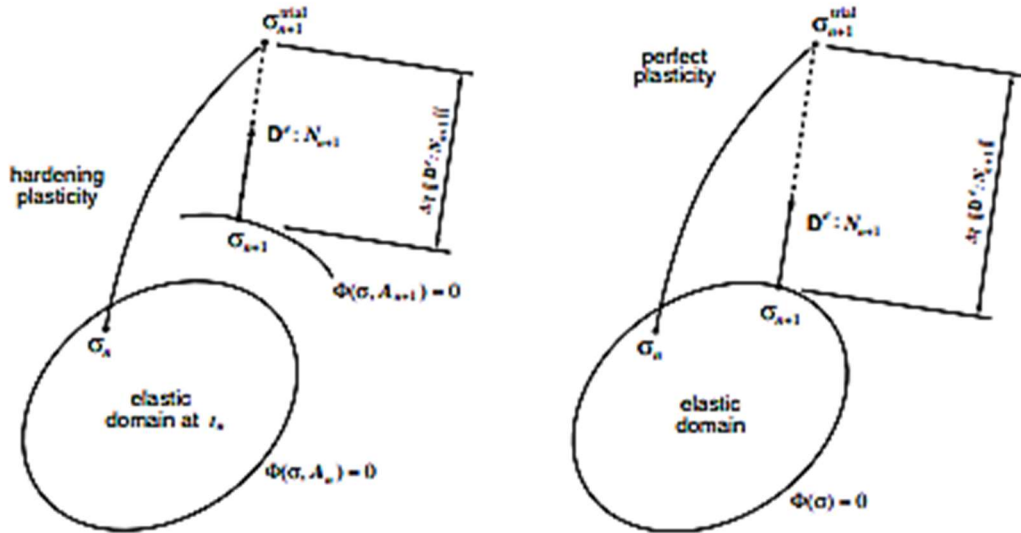


Figure 7.3. The fully implicit return mapping. Geometric interpretation for materials with linear elastic response.

of plastically admissible stresses. With the *energy norm* defined by

$$\|\sigma\|_{\mathbf{D}^e} \equiv \sqrt{\sigma : [\mathbf{D}^e]^{-1} : \sigma}, \quad (7.30)$$

and the associated measure of *distance* between two generic stress states given by

$$d(\sigma_a, \sigma_b) \equiv \|\sigma_a - \sigma_b\|_{\mathbf{D}^e}, \quad (7.31)$$

the updated stress is the admissible stress that lies *closest* to the elastic trial stress, i.e.

$$\sigma_{n+1} = \arg \left\{ \min_{\sigma \in \mathcal{A}} [d(\sigma, \sigma_{n+1}^{\text{trial}})] \right\}. \quad (7.32)$$

The interpretation of the implicit return mapping as a closest point projection of the trial stress remains valid for linearly hardening materials provided that a suitable definition of distance in the space of stress *and* hardening forces is introduced (see Simo *et al.* (1988b) for details).

(i) Given the *elastic trial state*, set $k = 0$ and

$$\sigma_{n+1}^{(0)} = \sigma_{n+1}^{\text{trial}}, \quad A_{n+1}^{(0)} = A_{n+1}^{\text{trial}}$$

(ii) Perform cutting-plane iteration

$$\begin{aligned} \Delta\gamma &= \Phi_{n+1}^{(k)} / \left\{ N_{n+1}^{(k)} : \left[D_{n+1}^{(k)} : N_{n+1}^{(k)} - E_{n+1}^{(k)} * H_{n+1}^{(k)} \right] \right. \\ &\quad \left. + H_{n+1}^{(k)} * \left[F_{n+1}^{(k)} * N_{n+1}^{(k)} - G_{n+1}^{(k)} * H_{n+1}^{(k)} \right] \right\} \\ \sigma_{n+1}^{(k+1)} &= \sigma_{n+1}^{(k)} - \Delta\gamma \left[D_{n+1}^{(k)} : N_{n+1}^{(k)} - E_{n+1}^{(k)} * H_{n+1}^{(k)} \right] \\ A_{n+1}^{(k+1)} &= A_{n+1}^{(k)} - \Delta\gamma \left[F_{n+1}^{(k)} * N_{n+1}^{(k)} - G_{n+1}^{(k)} * H_{n+1}^{(k)} \right] \end{aligned}$$

(iii) Check convergence

IF $\Phi(\sigma_{n+1}^{(k)}, A_{n+1}^{(k)}) \leq \epsilon_{\text{tol}}$ THEN update

$$\begin{aligned} \sigma_{n+1} &= \sigma_{n+1}^{(k)}, & A_{n+1} &= A_{n+1}^{(k)}, \\ \epsilon_{n+1}^e &= \epsilon^e(\sigma_{n+1}^{(k)}, A_{n+1}^{(k)}), & \alpha_{n+1} &= \alpha(\sigma_{n+1}^{(k)}, A_{n+1}^{(k)}), \\ \epsilon_{n+1}^p &= \epsilon_{n+1}^e - \epsilon_{n+1}^e, & & \text{and EXIT} \end{aligned}$$

ELSE
set $k := k + 1$ and GO TO (ii)

(i) Elastic predictor. Given $\Delta\epsilon$ and the state variables at t_n , evaluate the *elastic trial state*

$$\begin{aligned} \epsilon_{n+1}^{\text{trial}} &:= \epsilon_n^e + \Delta\epsilon \\ \bar{\epsilon}_{n+1}^{\text{trial}} &:= \bar{\epsilon}_n^p \\ p_{n+1}^{\text{trial}} &:= K \bar{\epsilon}_{n+1}^{\text{trial}}; \quad s_{n+1}^{\text{trial}} := 2G \epsilon_{n+1}^{\text{trial}} \\ q_{n+1}^{\text{trial}} &:= \sqrt{\frac{3}{2} s_{n+1}^{\text{trial}} : s_{n+1}^{\text{trial}}} \end{aligned}$$

(ii) Check plastic admissibility

$$\begin{aligned} \text{IF } q_{n+1}^{\text{trial}} - \sigma_y(\bar{\epsilon}_{n+1}^{\text{trial}}) &\leq 0 \\ \text{THEN set } (\cdot)_{n+1} &:= (\cdot)_{n+1}^{\text{trial}} \text{ and EXIT} \end{aligned}$$

(iii) Return mapping. Solve the equation

$$\tilde{\Phi}(\Delta\gamma) \equiv q_{n+1}^{\text{trial}} - 3G \Delta\gamma - \sigma_y(\bar{\epsilon}_n^p + \Delta\gamma) = 0$$

for $\Delta\gamma$ using the Newton-Raphson method – GOTO Box 7.4 – and update the state variables

$$\begin{aligned} p_{n+1} &:= p_{n+1}^{\text{trial}}; \quad s_{n+1} := \left(1 - \frac{\Delta\gamma 3G}{q_{n+1}^{\text{trial}}} \right) s_{n+1}^{\text{trial}} \\ \sigma_{n+1} &:= s_{n+1} + p_{n+1} I \\ \epsilon_{n+1}^e &= \frac{1}{2G} s_{n+1} + \frac{1}{3} \bar{\epsilon}_{n+1}^p I \\ \bar{\epsilon}_{n+1}^p &:= \bar{\epsilon}_n^p + \Delta\gamma \end{aligned}$$

(iv) EXIT

$\epsilon_{n+1}^{\text{trial}}$ by means of the following *incremental constitutive function*:

$$\sigma_{n+1} = \sigma_{n+1}(\bar{\epsilon}_n^p, \epsilon_{n+1}^{\text{trial}}) \equiv \left[D^e - \hat{H}(\Phi_{n+1}^{\text{trial}}) \frac{\Delta\gamma 6G^2}{q_{n+1}^{\text{trial}}} I_d \right] : \epsilon_{n+1}^{\text{trial}}, \quad (7.93)$$

where \hat{H} is the *Heaviside step function* defined as

$$\hat{H}(a) \equiv \begin{cases} 1 & \text{if } a > 0 \\ 0 & \text{if } a \leq 0 \end{cases}, \quad \text{for any scalar } a, \quad (7.94)$$

I_d is the deviatoric projection tensor defined by (3.94) (page 59),

$$\begin{aligned} q_{n+1}^{\text{trial}} &= \sqrt{\frac{3}{2}} \|s_{n+1}^{\text{trial}}\| = 2G \sqrt{\frac{3}{2}} \|\epsilon_{n+1}^{\text{trial}}\| \\ &= q_{n+1}^{\text{trial}}(\epsilon_{n+1}^{\text{trial}}) \equiv 2G \sqrt{\frac{3}{2}} \|I_d : \epsilon_{n+1}^{\text{trial}}\|, \end{aligned} \quad (7.95)$$

(i) Initialise iteration counter, $k := 0$, set initial guess for $\Delta\gamma$

$$\Delta\gamma^{(0)} := 0$$

and corresponding residual (yield function value)

$$\tilde{\Phi} := q_{n+1}^{\text{trial}} - \sigma_y(\varepsilon_n^p)$$

(ii) Perform Newton-Raphson iteration

$$H := \left. \frac{d\sigma_y}{d\varepsilon^p} \right|_{\varepsilon_n^p + \Delta\gamma} \quad (\text{hardening slope})$$

$$d := \frac{d\tilde{\Phi}}{d\Delta\gamma} = -3G - H \quad (\text{residual derivative})$$

$$\Delta\gamma := \Delta\gamma - \frac{\tilde{\Phi}}{d} \quad (\text{new guess for } \Delta\gamma)$$

(iii) Check for convergence

$$\tilde{\Phi} := q_{n+1}^{\text{trial}} - 3G \Delta\gamma - \sigma_y(\varepsilon_n^p + \Delta\gamma)$$

IF $|\tilde{\Phi}| \leq \epsilon_{\text{tol}}$ THEN RETURN to Box 7.3

(iv) GOTO (ii)

Φ^{trial} is the value of the yield function at the elastic trial state:

$$\Phi^{\text{trial}} = \Phi^{\text{trial}}(\varepsilon_n^p, \varepsilon_{n+1}^{\text{e trial}}) \equiv q_{n+1}^{\text{trial}}(\varepsilon_{n+1}^{\text{e trial}}) - \sigma_y(\varepsilon_n^p), \quad (7.96)$$

and

$$\Delta\gamma = \Delta\gamma(\varepsilon_n^p, \varepsilon_{n+1}^{\text{e trial}}) \quad (7.97)$$

is the *implicit* function of $\varepsilon_{n+1}^{\text{e trial}}$ and ε_n^p defined as the solution of the consistency equation (7.91).

Clearly, (7.93) defines σ_{n+1} as an *implicit* function of the elastic trial strain and ε_n^p . Equivalently, since $\varepsilon_{n+1}^{\text{e trial}} = \varepsilon_{n+1} - \varepsilon_n^p$, we may write

$$\sigma_{n+1} = \tilde{\sigma}_{n+1}(\varepsilon_n^p, \varepsilon_{n+1}) \equiv \tilde{\sigma}_{n+1}(\varepsilon_n^p, \varepsilon_{n+1} - \varepsilon_n^p). \quad (7.98)$$

For a given state at t_n , the functions (7.93) and (7.98) express the updated stress as implicit functions, respectively, of the elastic trial stress and the total elastic strain at t_{n+1} .

It should be noted that the only source of nonlinearity in the von Mises return-mapping equation (7.91) is the *hardening curve*, defined by the given function $\sigma_y = \sigma_y(\bar{\varepsilon}^p)$. For *linear hardening* materials, this function is linear and is expressed by

$$\sigma_y(\bar{\varepsilon}^p) = \sigma_0 + H \bar{\varepsilon}^p, \quad (7.99)$$

where σ_0 is the initial yield stress of the virgin material and H is the (constant) hardening modulus. In such cases, (7.91) reads

$$\bar{\Phi}(\Delta\gamma) \equiv q_{n+1}^{\text{trial}} - 3G \Delta\gamma - [\sigma_0 + (\bar{\varepsilon}_n^p + \Delta\gamma) H] = 0 \quad (7.100)$$

and the incremental plastic multiplier can be obtained in *closed form* as

$$\Delta\gamma = \frac{\Phi^{\text{trial}}}{3G + H}. \quad (7.101)$$

Thus, for linearly hardening von Mises materials, the above closed expression replaces the Newton–Raphson algorithm of Box 7.4 in the return-mapping procedure.

In the case of *perfect plasticity* ($H = 0$), the expression for $\Delta\gamma$ reads

$$\Delta\gamma = \frac{\Phi^{\text{trial}}}{3G}. \quad (7.102)$$

The geometric interpretation of the fully implicit algorithm for the perfectly plastic von Mises model is illustrated in Figure 7.10. In this case, the updated stress is simply the projection of the elastic trial stress onto the fixed yield surface along its *radial* direction. It is the *closest point* projection of the trial stress onto the yield surface.

d

The explicit incremental constitutive function

Under the assumption of linear hardening, we substitute the explicit formula (7.101) for $\Delta\gamma$ into (7.93) and obtain, after a straightforward manipulation, the following incremental constitutive function for the updated stress:

$$\begin{aligned} \sigma_{n+1} &= \bar{\sigma}_{n+1}(\varepsilon_{n+1}^{\text{trial}}, \bar{\varepsilon}_n^p) \\ &\equiv \left[\mathbf{D}^e - \hat{H}(\Phi^{\text{trial}}) \frac{6G^2}{3G + H} \left(1 - \frac{\sigma_y(\bar{\varepsilon}_n^p)}{q_{n+1}^{\text{trial}}} \right) \mathbf{I}_d \right] : \varepsilon_{n+1}^{\text{trial}}. \end{aligned} \quad (7.103)$$

In contrast to the general case (7.93), $\bar{\sigma}_{n+1}$ in the above definition is an *explicit* function. We remark, however, that explicit incremental constitutive functions are obtainable in the context of implicit integration algorithms only under very special circumstances (such as linear hardening in the present case). For more realistic models, such functions are usually implicit.

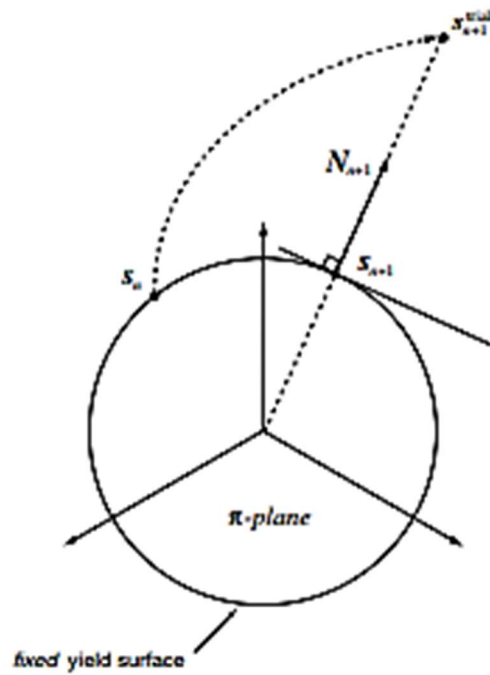


Figure 7.10. The perfectly plastic von Mises model. Geometric interpretation of the implicit return-mapping scheme as the *closest point projection algorithm*.

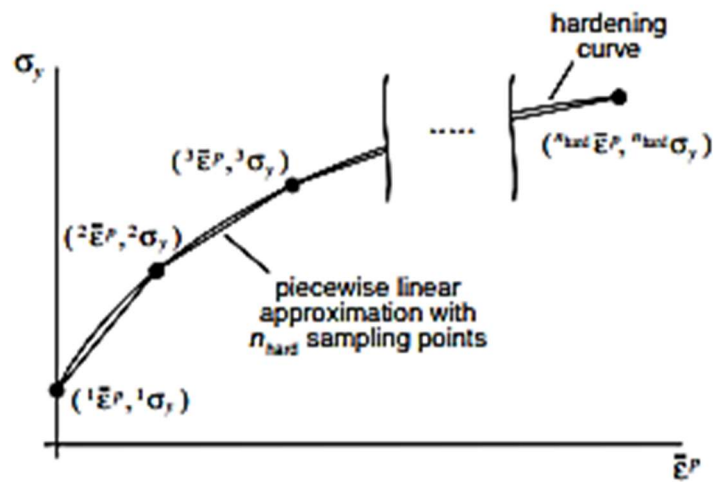


Figure 7.11. Piecewise linear hardening.

7.4.1. CONSISTENT TANGENT OPERATORS IN ELASTOPLASTICITY

As shown in Section 7.2, elastoplastic materials require in general some kind of numerical integration algorithm to update the stress tensor. Basically, given the known internal variable set α_n and the new prescribed total strain ε_{n+1} as input, each of the general integration procedures described in Section 7.2 will deliver the updated stress σ_{n+1} as the result of the application of a particular numerical algorithm (see diagram of Figure 7.12). This defines an *algorithmic* incremental constitutive function, $\hat{\sigma}$, for the stress tensor with general form

$$\sigma_{n+1} = \hat{\sigma}(\alpha_n, \varepsilon_{n+1}). \quad (7.108)$$

Algorithmic functions of this type have been first referred to in Section 4.2.1 (page 95), in the formulation of incremental boundary value problems with general path-dependent material models. Specific examples of incremental constitutive functions have been obtained earlier in this chapter for the fully implicit elastic predictor/return-mapping implementation of the von Mises model with isotropic strain hardening. Expressions (7.93, 7.98) show the corresponding (implicit) incremental constitutive function for the model with nonlinear hardening and expression (7.103) shows the particular (explicit) format obtained under linear hardening.

Within a load increment $[t_n, t_{n+1}]$, the internal variable set α_n given as argument of $\hat{\sigma}$ is *fixed*. Only the guesses for the total strain, ε_{n+1} – associated with the guesses for the displacement field, u_{n+1} – change during the global Newton–Raphson equilibrium iterations (refer to Section 4.2, from page 94 for details on the global Newton–Raphson procedure). In other words, within each global load increment, the stress σ_{n+1} delivered by the integration algorithm is a function of the total strain tensor *only*. This function – $\hat{\sigma}(\alpha_n, \varepsilon_{n+1})$ with fixed α_n – defines a *path-independent* stress/strain relation within the interval $[t_n, t_{n+1}]$, equivalent to a (nonlinear) elastic law. The consistent tangent modulus in this case is precisely the derivative of this equivalent nonlinear elastic law:

$$\mathbf{D} \equiv \frac{d\sigma_{n+1}}{d\varepsilon_{n+1}} = \left. \frac{\partial \hat{\sigma}}{\partial \varepsilon_{n+1}} \right|_{\alpha_n}, \quad (7.109)$$

i.e. it is the derivative of the algorithmic function $\hat{\sigma}$ with respect to ε_{n+1} with α_n held constant.

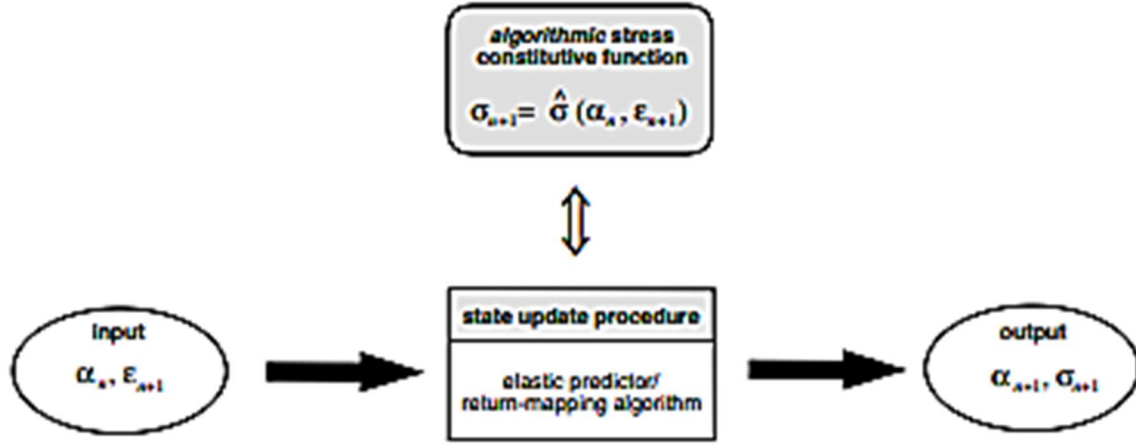


Figure 7.12. The algorithmic constitutive function for the stress tensor.

At this point, it is worth remarking that, in the context of the multiplicative finite strain plasticity framework discussed in Chapter 14, no measure of *total* nonlinear strain analogous to ϵ_{n+1} is used (or needed) in the definition of elastoplastic constitutive models. An *elastic trial* strain measure (analogous to the infinitesimal tensor $\epsilon_{n+1}^{e \text{ trial}}$), however, does appear naturally in the formulation of the corresponding elastic predictor/return-mapping schemes. Clearly, since $\epsilon_{n+1}^{e \text{ trial}} = \epsilon_{n+1} - \epsilon_n^p$, the incremental constitutive function for σ_{n+1} can always be expressed equivalently as¹¹

$$\sigma_{n+1} = \bar{\sigma}(\alpha_n, \epsilon_{n+1}^{e \text{ trial}}) \equiv \bar{\sigma}(\alpha_n, \epsilon_{n+1}^{e \text{ trial}} + \epsilon_n^p), \quad (7.110)$$

in terms of the elastic trial strain and the internal variable set at t_n , and we also have the trivial identity

$$\mathbf{D} = \frac{\partial \bar{\sigma}}{\partial \epsilon_{n+1}} = \frac{\partial \bar{\sigma}}{\partial \epsilon_{n+1}^{e \text{ trial}}} \quad (7.111)$$

for the consistent tangent operator. To make the material presented here formally valid also for the large-strain case addressed in Chapter 14 (where a total strain tensor is not defined), we shall adopt in what follows the rightmost term of (7.111) as the definition of consistent tangent operator.¹²

The elastic and elastoplastic tangents

Before going into further details, it is worth remarking at this point that the algorithmic function $\bar{\sigma}$ is *non-differentiable* in general. This is clearly seen by noting the presence of the Heaviside step function – a non-differentiable function – in definition (7.93), (7.98) of the incremental constitutive law for the implicitly integrated von Mises model with nonlinear isotropic strain hardening. For states lying within the elastic domain, i.e. states corresponding

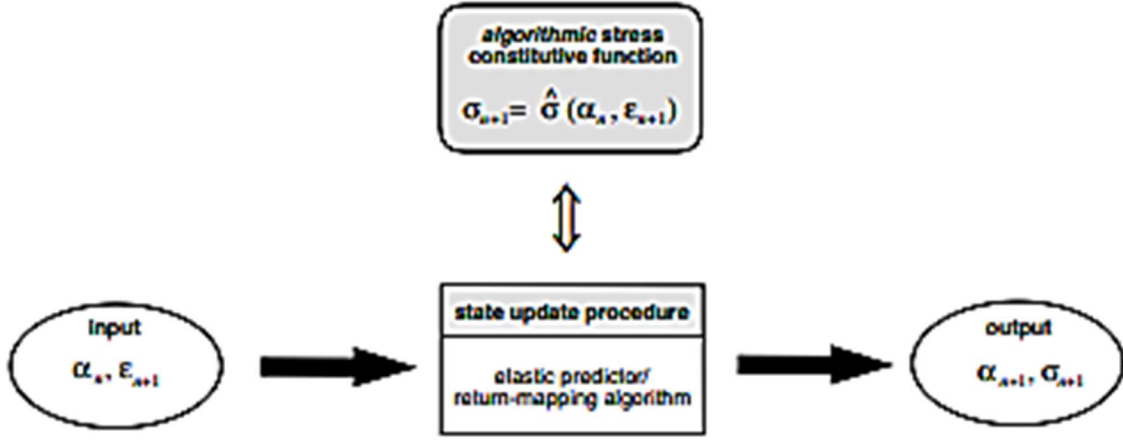


Figure 7.12. The algorithmic constitutive function for the stress tensor.

At this point, it is worth remarking that, in the context of the multiplicative finite strain plasticity framework discussed in Chapter 14, no measure of *total* nonlinear strain analogous to ϵ_{n+1} is used (or needed) in the definition of elastoplastic constitutive models. An *elastic trial* strain measure (analogous to the infinitesimal tensor $\epsilon_{n+1}^{e \text{ trial}}$), however, does appear naturally in the formulation of the corresponding elastic predictor/return-mapping schemes. Clearly, since $\epsilon_{n+1}^{e \text{ trial}} = \epsilon_{n+1} - \epsilon_n^p$, the incremental constitutive function for σ_{n+1} can always be expressed equivalently as^{††}

$$\sigma_{n+1} = \bar{\sigma}(\alpha_n, \epsilon_{n+1}^{e \text{ trial}}) \equiv \bar{\sigma}(\alpha_n, \epsilon_{n+1}^{e \text{ trial}} + \epsilon_n^p), \quad (7.110)$$

in terms of the elastic trial strain and the internal variable set at t_n , and we also have the trivial identity

$$\mathbf{D} = \frac{\partial \bar{\sigma}}{\partial \epsilon_{n+1}} = \frac{\partial \bar{\sigma}}{\partial \epsilon_{n+1}^{e \text{ trial}}} \quad (7.111)$$

for the consistent tangent operator. To make the material presented here formally valid also for the large-strain case addressed in Chapter 14 (where a total strain tensor is not defined), we shall adopt in what follows the rightmost term of (7.111) as the definition of consistent tangent operator.^{‡‡}

The elastic and elastoplastic tangents

Before going into further details, it is worth remarking at this point that the algorithmic function $\bar{\sigma}$ is *non-differentiable* in general. This is clearly seen by noting the presence of the Heaviside step function – a non-differentiable function – in definition (7.93), (7.98) of the incremental constitutive law for the implicitly integrated von Mises model with nonlinear isotropic strain hardening. For states lying within the elastic domain, i.e. states corresponding

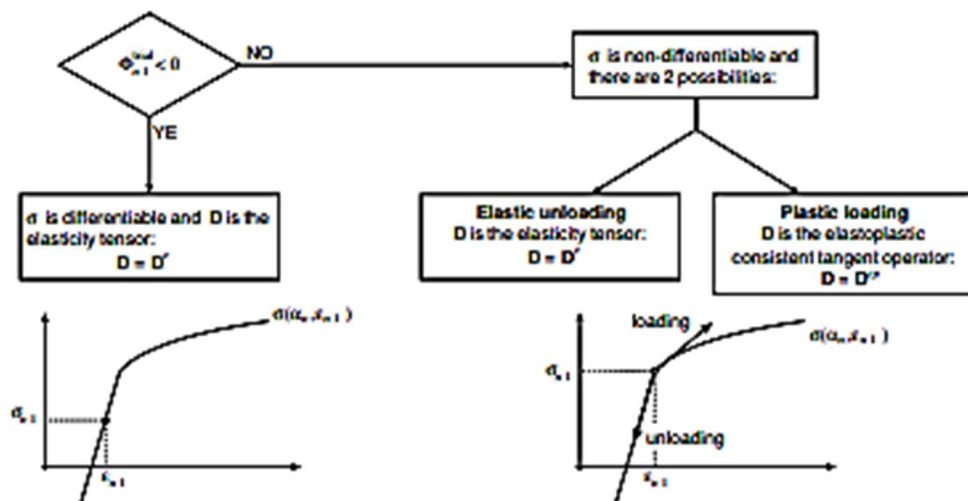


Figure 7.13. The tangent moduli consistent with elastic predictor/return-mapping integration algorithms.

to $\Phi^{trial} < 0$ in (7.93), (7.98), any infinitesimal change of total strain can only be elastic, with the stress σ_{n+1} evolving along the (smooth) elastic curve (see graphical representation of the uniaxial stress case in Figure 7.13). In this case the function $\bar{\sigma}$ is differentiable. At states with $\Phi^{trial} > 0$, the function $\bar{\sigma}$ is also differentiable if the hardening curve is smooth. Infinitesimal changes of ϵ_{n+1} will move the stress along the elastoplastic part of the incremental stress-strain curve. However, at states with $\Phi^{trial} = 0$ in (7.93, 7.98) – where the Heaviside step function is non-differentiable – either elastic unloading or plastic straining may occur in the incremental constitutive law. The incremental constitutive function is obviously *non-differentiable* in this case. The tangent modulus D is not uniquely defined and two tangent stress-strain relations exist: an *elastic* tangent relation, defined for elastic unloading, and an *elastoplastic* tangent relation, defined for plastic loading. Consider the one-dimensional case illustrated in Figure 7.13. Even though $\bar{\sigma}$ is non-differentiable its two *one-sided derivatives* – the *elastic* and the *elastoplastic* tangents – are well defined. In the multidimensional case, these are generalised respectively as the elastic tangent modulus, D^e , and the elastoplastic consistent tangent modulus, D^{ep} . The elastic tangent is associated with the elastic predictor procedure whereas the elastoplastic tangent is related to the plastic corrector (return-mapping) procedure. Clearly, when assembling the tangent stiffness matrix required by the Newton-Raphson iterative procedure for the global incremental equilibrium problem, the appropriate choice of tangent operator must be made.

The elastic tangent

If the stress is inside the elastic domain ($\Phi^{trial} < 0$) or if it is on the yield surface ($\Phi^{trial} = 0$) and elastic unloading is assumed to occur, the tangent modulus D consistent with any of the integration algorithms previously discussed is simply given by

$$D = D^e \equiv \bar{\rho} \frac{\partial^2 \psi}{\partial \epsilon^2}, \quad (7.112)$$

For elastoplastic materials whose elastic response is linear, such as the von Mises model and all other models described in Chapter 6, the *elastic consistent tangent* is the standard elasticity operator (7.107).

The elastoplastic tangent: the derivative of an implicit function

If the stress is on the yield surface, i.e. $\Phi^{\text{trial}} > 0$ or $\Phi^{\text{trial}} = 0$ and it is assumed that further plastic loading is going to occur, then the tangent operator is called the *elastoplastic consistent tangent* and is denoted \mathbf{D}^{ep} . It is important to emphasise here that elastoplastic consistent tangent operators cannot be derived for the cutting-plane algorithm (refer to Remark 7.6, page 208) so that the discussion that follows is restricted to the families of elastic predictor/return-mapping procedures based on the generalised midpoint and trapezoidal algorithms.

Crucial to the derivation of the elastoplastic consistent tangent moduli is the observation that under plastic yielding, the outcome σ_{n+1} of any member of the families of generalised midpoint and trapezoidal integration algorithms is the solution of a nonlinear system of algebraic equations in the plastic corrector (return-mapping) procedure. The system solved in the return mapping depends on the particular algorithm adopted. In this case, it is clear that σ_{n+1} is defined *implicitly* through the corresponding nonlinear system. Note, for example, that the term $\Delta\gamma$ in (7.93) is an implicit function of $\varepsilon_{n+1}^{\text{trial}}$ (or ε_{n+1}) defined as the solution of an algebraic nonlinear equation. In other words, the updated stress σ_{n+1} is an *implicit function* of the elastic trial strain $\varepsilon_{n+1}^{\text{trial}}$ in this case. Thus, the consistent tangent operator

$$\mathbf{D}^{\text{ep}} = \frac{\partial \dot{\sigma}}{\partial \varepsilon_{n+1}^{\text{trial}}}$$

is simply the *derivative of the implicit function defined by the return-mapping equations* and is derived by following the standard procedure for differentiation of implicit functions.

As an illustration of the above concepts, the elastoplastic tangent consistent with the fully implicit algorithm for the von Mises model is derived below.

7.4.2. THE ELASTOPLASTIC CONSISTENT TANGENT FOR THE VON MISES MODEL WITH ISOTROPIC HARDENING

The implicit elastic predictor/return-mapping algorithm for the von Mises model has been described in detail in Section 7.3. There, it was remarked that from the computational point of view the implementation of the von Mises model is the simplest described in this book. In this section, the elastoplastic tangent operator consistent with the von Mises implicit return mapping is derived step by step. The idea is to use this algorithm as an example to provide the reader with a clear picture of the procedure for the derivation of elastoplastic consistent tangent operators. The simplicity of this particular return-mapping scheme avoids the complications associated with more complex models/algorithms. The derivation of elastoplastic tangent operators consistent with the implicit return mapping for *general* plasticity models is addressed later, in Section 7.4.4. The application of the generic

procedure to the isotropically hardening von Mises model, which offers an alternative route to the derivation presented below, is described in Section 7.4.5.

The incremental algorithmic constitutive function for the implicitly integrated von Mises model with nonlinear isotropic strain hardening is given by (7.93). Under plastic flow, i.e. when the return-mapping procedure is used, the update formula for σ_{n+1} reads

$$\sigma_{n+1} = \left[\mathbf{D}^e - \frac{\Delta\gamma}{q_{n+1}^{\text{trial}}} \mathbf{I}_d \right] : \varepsilon_{n+1}^{\text{e trial}}, \quad (7.113)$$

where $\Delta\gamma$ is the solution of the return-mapping equation of the algorithm (Box 7.3),

$$\tilde{\Phi}(\Delta\gamma) \equiv q_{n+1}^{\text{trial}} - 3G \Delta\gamma - \sigma_y(\varepsilon_n^p + \Delta\gamma) = 0. \quad (7.114)$$

In the above, the elastic trial von Mises effective stress, q_{n+1}^{trial} , is the function of the elastic trial strain defined by (7.95). The elastoplastic consistent tangent modulus for the present model/algorithm combination is obtained by differentiating (7.113).

A straightforward application of tensor differentiation rules to (7.113) gives

$$\begin{aligned} \frac{\partial \sigma_{n+1}}{\partial \varepsilon_{n+1}^{\text{e trial}}} &= \mathbf{D}^e - \frac{\Delta\gamma}{q_{n+1}^{\text{trial}}} \mathbf{I}_d - \frac{6G^2}{q_{n+1}^{\text{trial}}} \varepsilon_{d\,n+1}^{\text{e trial}} \otimes \frac{\partial \Delta\gamma}{\partial \varepsilon_{n+1}^{\text{e trial}}} \\ &\quad + \frac{\Delta\gamma}{(q_{n+1}^{\text{trial}})^2} \varepsilon_{d\,n+1}^{\text{e trial}} \otimes \frac{\partial q_{n+1}^{\text{trial}}}{\partial \varepsilon_{n+1}^{\text{e trial}}}. \end{aligned} \quad (7.115)$$

From (7.95) and relation (2.139) (page 36), for the tensor norm derivative, we obtain

$$\frac{\partial q_{n+1}^{\text{trial}}}{\partial \varepsilon_{n+1}^{\text{e trial}}} = 2G \sqrt{\frac{3}{2}} \tilde{N}_{n+1}, \quad (7.116)$$

where we have conveniently defined the *unit* flow vector

$$\tilde{N}_{n+1} \equiv \sqrt{\frac{2}{3}} N_{n+1} = \frac{s_{n+1}^{\text{trial}}}{\|s_{n+1}^{\text{trial}}\|} = \frac{\varepsilon_{d\,n+1}^{\text{e trial}}}{\|\varepsilon_{d\,n+1}^{\text{e trial}}\|} \quad (7.117)$$

and we have made use of the trivial identity: $\varepsilon_{d\,n+1}^{\text{e trial}} : \mathbf{I}_d = \varepsilon_{d\,n+1}^{\text{e trial}}$, when applying the chain rule. Further, the differentiation of the implicit equation (7.114) for $\Delta\gamma$, taking (7.116) into account gives

$$\begin{aligned} \frac{\partial \Delta\gamma}{\partial \varepsilon_{n+1}^{\text{e trial}}} &= \frac{1}{3G + H} \frac{\partial q_{n+1}^{\text{trial}}}{\partial \varepsilon_{n+1}^{\text{e trial}}} \\ &= \frac{2G}{3G + H} \sqrt{\frac{3}{2}} \tilde{N}_{n+1}, \end{aligned} \quad (7.118)$$

where H is the slope of the hardening curve:

$$H \equiv \left. \frac{d\sigma_y}{d\varepsilon^p} \right|_{\varepsilon_n^p + \Delta\gamma}. \quad (7.119)$$

Finally, by substituting (7.116) and (7.118) into (7.115), we obtain, after a straightforward manipulation making use of (7.95) and definition (7.117), the following expression for the

elastoplastic tangent operator consistent with the implicit return-mapping scheme for the isotropically hardening von Mises model:

$$\begin{aligned} \mathbf{D}^{ep} &= \mathbf{D}^e - \frac{\Delta\gamma}{q_{n+1}^{\text{trial}}} \mathbf{I}_d + 6G^2 \left(\frac{\Delta\gamma}{q_{n+1}^{\text{trial}}} - \frac{1}{3G+H} \right) \tilde{\mathbf{N}}_{n+1} \otimes \tilde{\mathbf{N}}_{n+1} \\ &= 2G \left(1 - \frac{\Delta\gamma}{q_{n+1}^{\text{trial}}} \right) \mathbf{I}_d \\ &\quad + 6G^2 \left(\frac{\Delta\gamma}{q_{n+1}^{\text{trial}}} - \frac{1}{3G+H} \right) \tilde{\mathbf{N}}_{n+1} \otimes \tilde{\mathbf{N}}_{n+1} + K \mathbf{I} \otimes \mathbf{I}. \end{aligned} \quad (7.120)$$

It should be noted that the operator \mathbf{D}^{ep} in the present case, i.e. for this particular model and numerical integration algorithm is *symmetric*. The symmetry of consistent elastoplastic tangent operators will be further commented upon in Section 7.4.6. In the HYPLAS program, the above tangent operator is computed in subroutine CTVM. Its implementation is described in detail in Section 7.4.3.

Remark 7.8. Within the global (equilibrium) Newton–Raphson scheme, the value of $\Delta\gamma$, q^{trial} and H , as well as the incremental unit flow vector, $\tilde{\mathbf{N}}_{n+1}$, that take part in (7.120) are those obtained for the Gauss point of interest in the return-mapping procedure of the *previous global iteration*. For the first iteration of any global load increment, $\Delta\gamma$ is zero.

The continuum tangent operator

The concept of tangent operators in plasticity has been initially discussed in Sections 6.2.8 and 6.3.8 (from pages 147 and 153, respectively) in the time-continuum setting. In Section 6.3.8, the corresponding elastoplastic *continuum* tangent operator has been derived for the generic multi-dimensional plasticity model. Its closed form is given by expression (6.67). Let us now particularise this formula for the von Mises model with isotropic strain hardening. Firstly we consider (6.187)–(6.192). In this case we have

$$\bar{\rho} \frac{\partial^2 \psi^p}{\partial \alpha^2} = \bar{\rho} \frac{\partial^2 \psi^p}{\partial \varepsilon^p{}^2} = \frac{\partial \kappa}{\partial \varepsilon^p} = H. \quad (7.121)$$

With the above, together with (6.194) and the associative flow vector definition (6.136) for the von Mises model, we find that expression (6.67) particularises in the following format:

$$\mathbf{D}_c^{ep} = \mathbf{D}^e - \frac{(\mathbf{D}^e : \mathbf{N}) \otimes (\mathbf{D}^e : \mathbf{N})}{\mathbf{N} : \mathbf{D}^e : \mathbf{N} + H}, \quad (7.122)$$

where we have used the subscript ‘c’ to emphasise that the above operator is the *continuum* tangent modulus. With \mathbf{D}^e defined by (7.107), and taking into consideration the fact that for the von Mises model \mathbf{N} is a deviatoric tensor, we have

$$\mathbf{D}^e : \mathbf{N} = 2G \mathbf{N}. \quad (7.123)$$

In addition, using (6.136), it follows that

$$\mathbf{N} : \mathbf{D}^e : \mathbf{N} = 3G. \quad (7.124)$$

By introducing these results into (7.122), we obtain the following explicit expression for the continuum tangent operator for the von Mises model with isotropic strain hardening:

$$\mathbf{D}_e^{ep} = \mathbf{D}^e - \frac{6G^2}{3G + H} \tilde{\mathbf{N}} \otimes \tilde{\mathbf{N}}, \quad (7.125)$$

where $\tilde{\mathbf{N}}$ is the unit flow vector at the current state.

Remark 7.9. The difference between the elastoplastic consistent tangent operator and its continuum counterpart above lies only in the terms that contain $\Delta\gamma$ in expression (7.120). Note that we may write

$$\mathbf{D}_e^{ep} = \mathbf{D}_e^{ep} - \frac{\Delta\gamma}{q_{n+1}^{\text{trial}}} \frac{6G^2}{3G + H} [\mathbf{I}_d - \tilde{\mathbf{N}}_{n+1} \otimes \tilde{\mathbf{N}}_{n+1}]. \quad (7.126)$$

If $\Delta\gamma$ is set to zero (as in the first iteration of any load increment), the continuum tangent is recovered. This fact (Ortiz and Martin, 1989) is a mere consequence of the consistency of the numerical method (backward Euler-based in the present case) adopted in the discretisation of the time-continuum elastoplasticity equations. For large steps, when the value of $\Delta\gamma$ is large, the difference between the continuum and the consistent operator can be substantial. In such cases, the use of the continuum tangent in the assemblage of the stiffness matrix results in a dramatic degradation of the convergence rate of the global iterative procedure. Clearly, if the continuum tangent is used in conjunction with the return-mapping scheme, then the global iterative procedure is *not* the Newton–Raphson algorithm. In this case, the global iterations are a form of approximation to the Newton–Raphson scheme. Early implicit elastoplastic implementations (Owen and Hinton, 1980) relied exclusively on the use of the continuum tangent operator. The use of the consistent tangent operator in this context was introduced by Simo and Taylor (1985).

(i) Elastic predictor. Given $\Delta\epsilon$ and the state variables at t_n , evaluate the *elastic trial state*

$$\begin{aligned} \epsilon_{n+1}^{\text{trial}} &:= \epsilon_n^e + \Delta\epsilon \\ \bar{\epsilon}_{n+1}^{\text{trial}} &:= \bar{\epsilon}_n^p; & \beta_{n+1}^{\text{trial}} &:= \beta_n \\ p_{n+1}^{\text{trial}} &:= K \epsilon_{n+1}^{\text{trial}}; & s_{n+1}^{\text{trial}} &:= 2G \epsilon_{n+1}^{\text{trial}} \\ \eta_{n+1}^{\text{trial}} &:= s_{n+1}^{\text{trial}} - \beta_n; & \bar{q}_{n+1}^{\text{trial}} &:= \sqrt{\frac{3}{2}} \|\eta_{n+1}^{\text{trial}}\| \end{aligned}$$

(ii) Check plastic admissibility

$$\text{IF } \bar{q}_{n+1}^{\text{trial}} - \sigma_y(\bar{\epsilon}_{n+1}^{\text{trial}}) \leq 0$$

THEN set $(\cdot)_{n+1} := (\cdot)_{n+1}^{\text{trial}}$ and EXIT

(iii) Return mapping. Solve the equation for $\Delta\gamma$

$$\bar{q}_{n+1}^{\text{trial}} - 3G\Delta\gamma - \bar{\beta}(\bar{\epsilon}_n^p + \Delta\gamma) + \beta_n - \sigma_y(\bar{\epsilon}_n^p + \Delta\gamma) = 0$$

where $\bar{\beta}_n = \bar{\beta}(\bar{\epsilon}_n^p)$ and update

$$\begin{aligned} \bar{\epsilon}_{n+1}^p &:= \bar{\epsilon}_n^p + \Delta\gamma; & \bar{\beta}_{n+1} &:= \bar{\beta}(\bar{\epsilon}_{n+1}^p) \\ \beta_{n+1} &:= \beta_n + \sqrt{\frac{2}{3}}(\bar{\beta}_{n+1} - \beta_n) \frac{\eta_{n+1}^{\text{trial}}}{\|\eta_{n+1}^{\text{trial}}\|} \\ p_{n+1} &:= p_{n+1}^{\text{trial}}; & s_{n+1} &:= s_{n+1}^{\text{trial}} - 2G\Delta\gamma \sqrt{\frac{3}{2}} \frac{\eta_{n+1}^{\text{trial}}}{\|\eta_{n+1}^{\text{trial}}\|} \\ \sigma_{n+1} &:= s_{n+1} + p_{n+1} \mathbf{I}; & \epsilon_{n+1}^e &:= \frac{1}{2G} s_{n+1} + \frac{1}{3} \epsilon_{n+1}^{\text{trial}} \mathbf{I} \end{aligned}$$

(iv) EXIT

Under plastic flow ($\Phi^{\text{trial}} > 0$), the algorithmic incremental constitutive function (7.202) gives

$$\sigma_{n+1} = \left[\mathbf{D}^e - \frac{\Delta\gamma}{\bar{q}_{n+1}^{\text{trial}}} \mathbf{I}_d \right] : \varepsilon_{n+1}^{\text{trial}} + \frac{\Delta\gamma}{\bar{q}_{n+1}^{\text{trial}}} \beta_n. \quad (7.208)$$

The elastoplastic consistent tangent operator for the present case is obtained by differentiating the above relation. The derivation follows closely that presented in Section 7.4.2 (from page 232) for the isotropic hardening-only model.

The differentiation of (7.208) gives

$$\begin{aligned} \frac{\partial \sigma_{n+1}}{\partial \varepsilon_{n+1}^{\text{trial}}} &= \mathbf{D}^e - \frac{\Delta\gamma}{\bar{q}_{n+1}^{\text{trial}}} \mathbf{I}_d - \frac{3G}{\bar{q}_{n+1}^{\text{trial}}} \eta_{n+1}^{\text{trial}} \otimes \frac{\partial \Delta\gamma}{\partial \varepsilon_{n+1}^{\text{trial}}} \\ &\quad + \frac{\Delta\gamma}{(\bar{q}_{n+1}^{\text{trial}})^2} \eta_{n+1}^{\text{trial}} \otimes \frac{\partial \bar{q}_{n+1}^{\text{trial}}}{\partial \varepsilon_{n+1}^{\text{trial}}}, \end{aligned} \quad (7.209)$$

where we have made use of the connection $\eta_{n+1}^{\text{trial}} = 2G \mathbf{I}_d : \varepsilon_{n+1}^{\text{trial}} - \beta_n$. The derivative of the trial relative effective stress is obtained analogously to (7.116). The corresponding expression in the present case has the same format as (7.116), i.e.

$$\frac{\partial \bar{q}_{n+1}^{\text{trial}}}{\partial \varepsilon_{n+1}^{\text{trial}}} = 2G \sqrt{\frac{2}{3}} \bar{N}_{n+1}, \quad (7.210)$$

with the unit flow vector here defined as

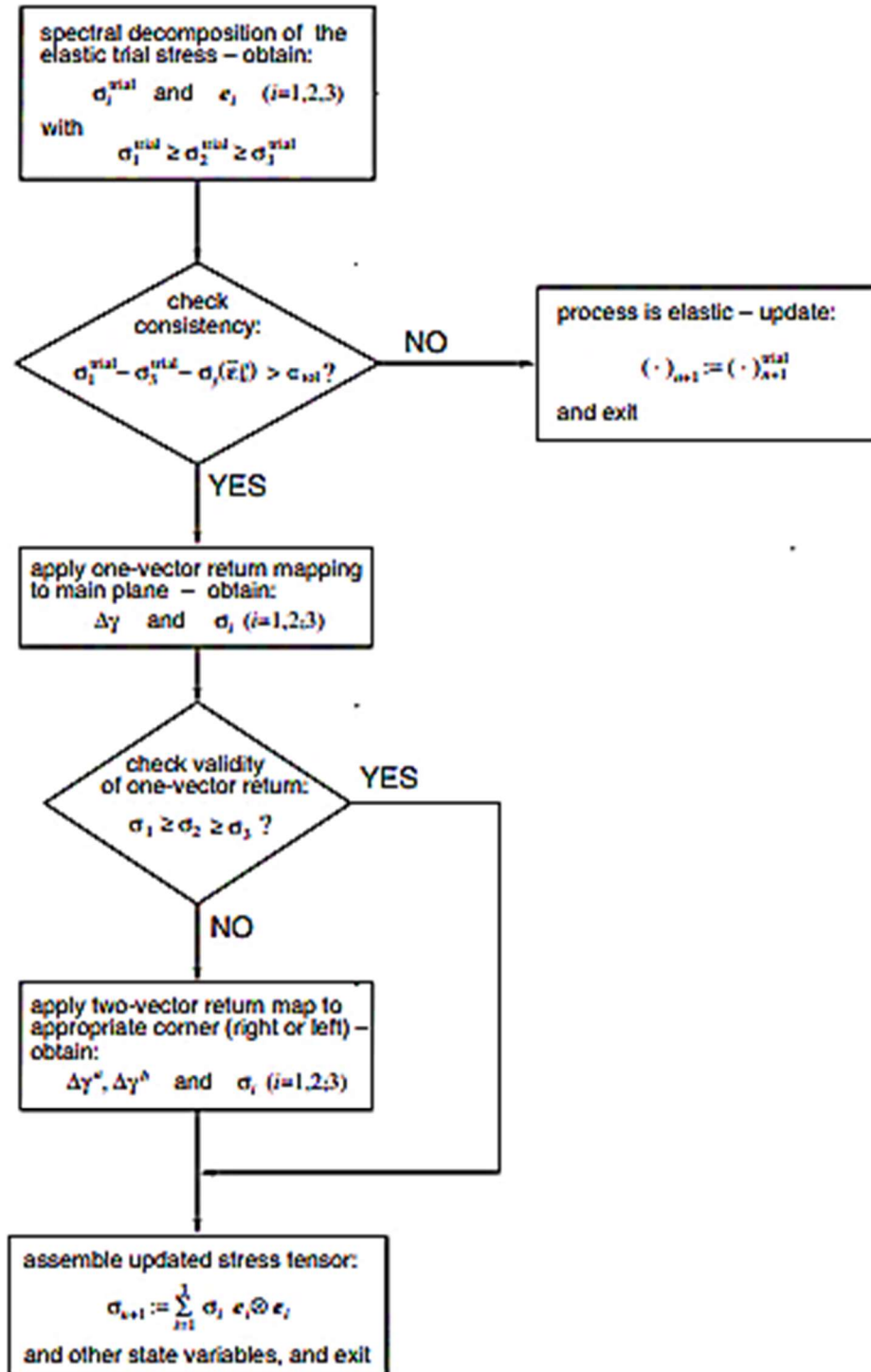
$$\bar{N}_{n+1} \equiv \frac{\eta_{n+1}^{\text{trial}}}{\|\eta_{n+1}^{\text{trial}}\|}. \quad (7.211)$$

The incremental plastic multiplier derivative is obtained by differentiating the return-mapping equation (7.199) with respect to $\varepsilon_{n+1}^{\text{trial}}$. This gives

$$\begin{aligned} \frac{\partial \Delta\gamma}{\partial \varepsilon_{n+1}^{\text{trial}}} &= \frac{1}{3G + H^k + H^i} \frac{\partial \bar{q}_{n+1}^{\text{trial}}}{\partial \varepsilon_{n+1}^{\text{trial}}} \\ &= \frac{2G}{3G + H^k + H^i} \sqrt{\frac{3}{2}} \bar{N}_{n+1}. \end{aligned} \quad (7.212)$$

Then, with the substitution of (7.210) and (7.212) into (7.209) we obtain, after a straightforward algebra taking (7.194) and (7.211) into account, the following closed-form expression for the elastoplastic consistent tangent operator:

$$\begin{aligned} \mathbf{D}^{\text{ep}} &= \mathbf{D}^e - \frac{\Delta\gamma}{\bar{q}_{n+1}^{\text{trial}}} \mathbf{I}_d + 6G^2 \left(\frac{\Delta\gamma}{\bar{q}_{n+1}^{\text{trial}}} - \frac{1}{3G + H^k + H^i} \right) \bar{N}_{n+1} \otimes \bar{N}_{n+1} \\ &= 2G \left(1 - \frac{\Delta\gamma}{\bar{q}_{n+1}^{\text{trial}}} \right) \mathbf{I}_d \\ &\quad + 6G^2 \left(\frac{\Delta\gamma}{\bar{q}_{n+1}^{\text{trial}}} - \frac{1}{3G + H^k + H^i} \right) \bar{N}_{n+1} \otimes \bar{N}_{n+1} + K \mathbf{I} \otimes \mathbf{I}. \end{aligned} \quad (7.213)$$



(i) Elastic predictor. Given $\Delta \varepsilon$ and the state variables at t_n , evaluate the *elastic trial state*

$$\varepsilon_{n+1}^{e, \text{trial}} := \varepsilon_n^e + \Delta \varepsilon; \quad \varepsilon_{n+1}^{p, \text{trial}} := \varepsilon_n^p$$

$$p_{n+1}^{\text{trial}} := K \varepsilon_{n+1}^{e, \text{trial}}; \quad s_{n+1}^{\text{trial}} := 2G \varepsilon_{n+1}^{e, \text{trial}}$$

(ii) Spectral decomposition of s^{trial} (routine SPDEC2). Compute

$$s_1^{\text{trial}} \geq s_2^{\text{trial}} \geq s_3^{\text{trial}} \quad \text{and} \quad e_i \quad (i = 1, 2, 3)$$

(iii) Check plastic admissibility

$$\text{IF } s_1^{\text{trial}} - s_3^{\text{trial}} - \sigma_y(\varepsilon_{n+1}^{p, \text{trial}}) \leq 0$$

$$\text{THEN set } (\cdot)_{n+1} := (\cdot)_{n+1}^{\text{trial}} \text{ and EXIT}$$

(iv) Return mapping

(iv.a) Return to main plane – GOTO Box 8.2

(iv.b) Check validity of main plane return

$$\text{IF } s_1 \geq s_2 \geq s_3 \text{ THEN return is valid – GOTO (v)}$$

(iv.c) Return to corner

$$\text{IF } s_1^{\text{trial}} + s_3^{\text{trial}} - 2 s_2^{\text{trial}} > 0$$

THEN apply return to right corner – GOTO Box 8.3

ELSE apply return to left corner – GOTO Box 8.3

(v) Assemble updated stress

$$p_{n+1} := p_{n+1}^{\text{trial}}$$

$$\sigma_{n+1} := \sum_{i=1}^3 (s_i + p_{n+1}) e_i \otimes e_i$$

and update elastic strain

$$\varepsilon_{n+1}^e := \frac{1}{2G} s_{n+1} + \frac{1}{3} \varepsilon_{n+1}^{e, \text{trial}} I$$

(vi) EXIT

(i) Set initial guess for $\Delta \gamma$

$$\Delta \gamma := 0$$

and corresponding residual (yield function value)

$$\tilde{\Phi} := s_1^{\text{trial}} - s_3^{\text{trial}} - \sigma_y(\varepsilon_n^p)$$

(ii) Perform Newton–Raphson iteration

$$H := \left. \frac{d\sigma_y}{d\varepsilon^p} \right|_{\varepsilon_n^p + \Delta \gamma} \quad (\text{hardening slope})$$

$$d := \frac{d\tilde{\Phi}}{d\Delta \gamma} = -4G - H \quad (\text{residual derivative})$$

$$\Delta \gamma := \Delta \gamma - \frac{\tilde{\Phi}}{d} \quad (\text{new guess for } \Delta \gamma)$$

(iii) Check for convergence

$$\tilde{\Phi} := s_1^{\text{trial}} - s_3^{\text{trial}} - 4G \Delta \gamma - \sigma_y(\varepsilon_n^p + \Delta \gamma)$$

IF $|\tilde{\Phi}| \leq \varepsilon_{\text{tol}}$ THEN update

$$s_1 := s_1^{\text{trial}} - 2G \Delta \gamma$$

$$s_2 := s_2^{\text{trial}}$$

$$s_3 := s_3^{\text{trial}} + 2G \Delta \gamma$$

$$\varepsilon_{n+1}^p := \varepsilon_n^p + \Delta \gamma$$

and RETURN to Box 8.1

(iv) GOTO (ii)

(i) Set initial guess for $\Delta\gamma^a$ and $\Delta\gamma^b$

$$\Delta\gamma^a := 0 \quad \Delta\gamma^b := 0$$

and corresponding residual

$$\begin{bmatrix} \tilde{\Phi}^a \\ \tilde{\Phi}^b \end{bmatrix} := \begin{bmatrix} \tilde{s}^a - \sigma_y(\tilde{\varepsilon}_n^p) \\ \tilde{s}^b - \sigma_y(\tilde{\varepsilon}_n^p) \end{bmatrix}$$

where

$$s^a = s_1^{\text{trial}} - s_3^{\text{trial}}, \quad s^b = \begin{cases} s_1^{\text{trial}} - s_2^{\text{trial}}, & \text{for right corner} \\ s_2^{\text{trial}} - s_3^{\text{trial}}, & \text{for left corner} \end{cases}$$

(ii) Perform Newton-Raphson iteration

$$\overline{\Delta\gamma} := \Delta\gamma^a + \Delta\gamma^b$$

$$\tilde{\varepsilon}_{n+1}^p := \tilde{\varepsilon}_n^p + \overline{\Delta\gamma} \quad (\text{update } \tilde{\varepsilon}^p)$$

$$H := \left. \frac{d\sigma_y}{d\varepsilon^p} \right|_{\varepsilon_{n+1}^p} \quad (\text{hardening slope})$$

residual derivative:

$$d := \begin{bmatrix} \frac{d\tilde{\Phi}^a}{d\Delta\gamma^a} & \frac{d\tilde{\Phi}^a}{d\Delta\gamma^b} \\ \frac{d\tilde{\Phi}^b}{d\Delta\gamma^a} & \frac{d\tilde{\Phi}^b}{d\Delta\gamma^b} \end{bmatrix} = \begin{bmatrix} -4G - H & -2G - H \\ -2G - H & -4G - H \end{bmatrix}$$

new guess for $\Delta\gamma^a$ and $\Delta\gamma^b$:

$$\begin{bmatrix} \Delta\gamma^a \\ \Delta\gamma^b \end{bmatrix} := \begin{bmatrix} \Delta\gamma^a \\ \Delta\gamma^b \end{bmatrix} - d^{-1} \begin{bmatrix} \tilde{\Phi}^a \\ \tilde{\Phi}^b \end{bmatrix}$$

(iii) Check for convergence

$$\begin{bmatrix} \tilde{\Phi}^a \\ \tilde{\Phi}^b \end{bmatrix} := \begin{bmatrix} \tilde{s}^a - 2G(2\Delta\gamma^a + \Delta\gamma^b) - \sigma_y(\tilde{\varepsilon}_{n+1}^p) \\ \tilde{s}^b - 2G(\Delta\gamma^a + 2\Delta\gamma^b) - \sigma_y(\tilde{\varepsilon}_{n+1}^p) \end{bmatrix}$$

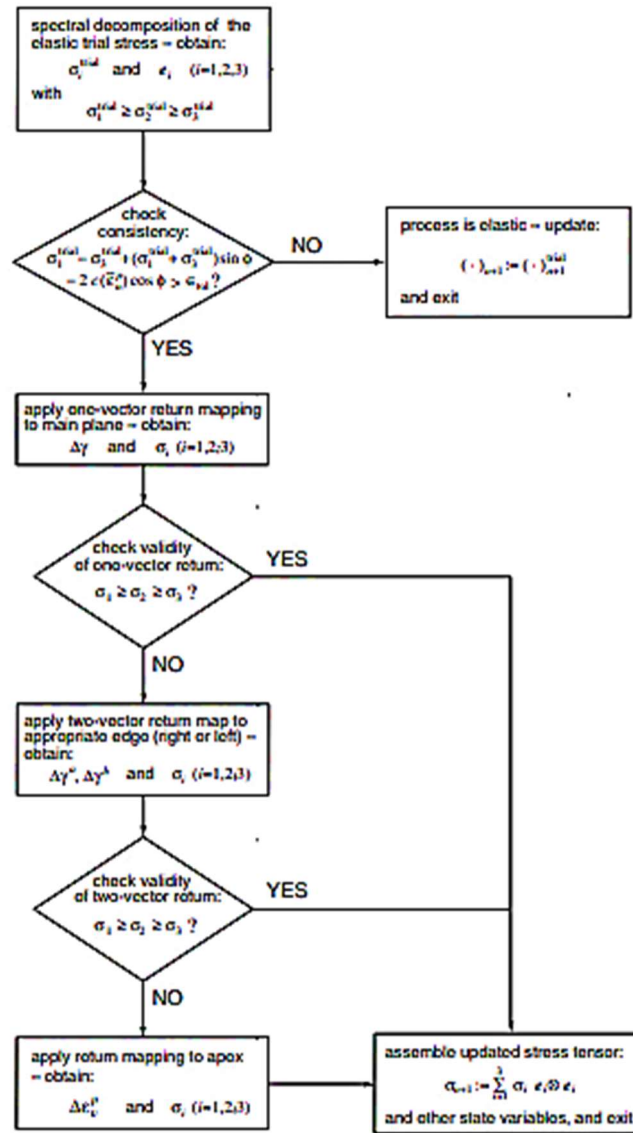
IF $|\tilde{\Phi}^a| + |\tilde{\Phi}^b| \leq \epsilon_{\text{tol}}$ THEN update

$$\left. \begin{aligned} s_1 &:= s_1^{\text{trial}} - 2G(\Delta\gamma^a + \Delta\gamma^b) \\ s_2 &:= s_2^{\text{trial}} + 2G\Delta\gamma^b \\ s_3 &:= s_3^{\text{trial}} + 2G\Delta\gamma^a \end{aligned} \right\} \text{for right corner}$$

$$\left. \begin{aligned} s_1 &:= s_1^{\text{trial}} - 2G\Delta\gamma^a \\ s_2 &:= s_2^{\text{trial}} - 2G\Delta\gamma^b \\ s_3 &:= s_3^{\text{trial}} + 2G(\Delta\gamma^a + \Delta\gamma^b) \end{aligned} \right\} \text{for left corner}$$

and RETURN to Box 8.1

(iv) GOTO (ii)



(i) Elastic predictor. Given $\Delta \varepsilon$ and the state variables at t_n , evaluate the *elastic trial state*

$$\varepsilon_{n+1}^{\text{trial}} := \varepsilon_n^e + \Delta \varepsilon; \quad \varepsilon_{n+1}^p := \varepsilon_n^p$$

$$\sigma_{n+1}^{\text{trial}} := 2G \varepsilon_{n+1}^{\text{trial}} + K \varepsilon_{n+1}^{\text{trial}} \mathbf{I}$$

(ii) Spectral decomposition of σ^{trial} (routine SPDEC2). Compute

$$\sigma_1^{\text{trial}} \geq \sigma_2^{\text{trial}} \geq \sigma_3^{\text{trial}} \quad \text{and} \quad \mathbf{e}_i \quad (i = 1, 2, 3)$$

(iii) Check plastic admissibility

$$\text{IF } \sigma_1^{\text{trial}} - \sigma_3^{\text{trial}} + (\sigma_1^{\text{trial}} + \sigma_3^{\text{trial}}) \sin \phi - 2 c(\varepsilon_{n+1}^p) \cos \phi \leq 0$$

$$\text{THEN set } (\cdot)_{n+1} := (\cdot)_{n+1}^{\text{trial}} \text{ and EXIT}$$

(iv) Return mapping

(iv.a) Return to main plane – GOTO Box 8.5

(iv.b) Check validity of main plane return

IF $\sigma_1 \geq \sigma_2 \geq \sigma_3$ THEN return is valid – GOTO (v)

(iv.c) Return to edge

$$\text{IF } (1 - \sin \psi) \sigma_1^{\text{trial}} - 2 \sigma_3^{\text{trial}} + (1 + \sin \psi) \sigma_2^{\text{trial}} > 0$$

THEN apply return to **right** edge – GOTO Box 8.6

ELSE apply return to **left** edge – GOTO Box 8.6

(iv.d) Check validity of edge return

IF $\sigma_1 \geq \sigma_2 \geq \sigma_3$ THEN return is valid – GOTO (v)

(iv.e) Return to apex – GOTO Box 8.7

(v) Assemble updated stress tensor

$$\sigma_{n+1} := \sum_{i=1}^3 \sigma_i \mathbf{e}_i \otimes \mathbf{e}_i$$

and update elastic strain

$$\varepsilon_{n+1}^e := \frac{1}{2G} s_{n+1} + \frac{p_{n+1}}{3K} \mathbf{I}$$

(vi) EXIT

(i) Set initial guess for $\Delta \gamma$

$$\Delta \gamma := 0; \quad \varepsilon_{n+1}^p := \varepsilon_n^p$$

and corresponding residual (yield function value)

$$\Phi := \sigma_1^{\text{trial}} - \sigma_3^{\text{trial}} + (\sigma_1^{\text{trial}} + \sigma_3^{\text{trial}}) \sin \phi - 2 c(\varepsilon_n^p) \cos \phi$$

(ii) Perform Newton–Raphson iteration for $\Delta \gamma$

$$H := \left. \frac{d\Phi}{d\varepsilon^p} \right|_{\varepsilon_{n+1}^p} \quad (\text{hardening slope})$$

$$d := \frac{d\Phi}{d\Delta \gamma} = -4G(1 + \frac{1}{3} \sin \psi \sin \phi) - 4K \sin \psi \sin \phi - 4H \cos^2 \phi \quad (\text{residual derivative})$$

$$\Delta \gamma := \Delta \gamma - \Phi/d \quad (\text{update } \Delta \gamma)$$

(iii) Check for convergence

$$\varepsilon_{n+1}^p := \varepsilon_n^p + 2 \cos \phi \Delta \gamma$$

$$\Phi := \sigma_1^{\text{trial}} - \sigma_3^{\text{trial}} + (\sigma_1^{\text{trial}} + \sigma_3^{\text{trial}}) \sin \phi - [4G(1 + \frac{1}{3} \sin \psi \sin \phi) + 4K \sin \phi \sin \psi] \Delta \gamma - 2 c(\varepsilon_{n+1}^p) \cos \phi$$

IF $|\Phi| \leq \epsilon_{\text{tol}}$ THEN update

$$\sigma_1 := \sigma_1^{\text{trial}} - [2G(1 + \frac{1}{3} \sin \psi) + 2K \sin \psi] \Delta \gamma$$

$$\sigma_2 := \sigma_2^{\text{trial}} + (\frac{4}{3}G - 2K) \sin \psi \Delta \gamma$$

$$\sigma_3 := \sigma_3^{\text{trial}} + [2G(1 - \frac{1}{3} \sin \psi) - 2K \sin \psi] \Delta \gamma$$

and RETURN to Box 8.4

(iv) GOTO (ii)

(i) Set initial guess for $\Delta \gamma^a$ and $\Delta \gamma^b$

$$\Delta \gamma^a := 0, \quad \Delta \gamma^b := 0; \quad \varepsilon_{n+1}^p := \varepsilon_n^p$$

and corresponding residual

$$\begin{bmatrix} \tilde{\Phi}^a \\ \tilde{\Phi}^b \end{bmatrix} := \begin{bmatrix} \tilde{\sigma}^a - 2 c(\varepsilon_n^p) \cos \phi \\ \tilde{\sigma}^b - 2 c(\varepsilon_n^p) \cos \phi \end{bmatrix}$$

where

$$\tilde{\sigma}^a = \sigma_1^{\text{trial}} - \sigma_3^{\text{trial}} + (\sigma_1^{\text{trial}} + \sigma_3^{\text{trial}}) \sin \phi$$

$$\tilde{\sigma}^b = \begin{cases} \sigma_1^{\text{trial}} - \sigma_2^{\text{trial}} + (\sigma_1^{\text{trial}} + \sigma_2^{\text{trial}}) \sin \phi & \text{right edge} \\ \sigma_2^{\text{trial}} - \sigma_3^{\text{trial}} + (\sigma_2^{\text{trial}} + \sigma_3^{\text{trial}}) \sin \phi & \text{left edge} \end{cases}$$

(ii) Perform Newton–Raphson iteration for $\Delta \gamma^a$ and $\Delta \gamma^b$

$$H := \left. \frac{d\Phi}{d\varepsilon^p} \right|_{\varepsilon_{n+1}^p}$$

$$a := 4G(1 + \frac{1}{3} \sin \phi \sin \psi) + 4K \sin \phi \sin \psi$$

$$b := \begin{cases} 2G(1 + \sin \phi + \sin \psi - \frac{1}{3} \sin \phi \sin \psi) + 4K \sin \phi \sin \psi & \text{right edge} \\ 2G(1 - \sin \phi - \sin \psi - \frac{1}{3} \sin \phi \sin \psi) + 4K \sin \phi \sin \psi & \text{left edge} \end{cases}$$

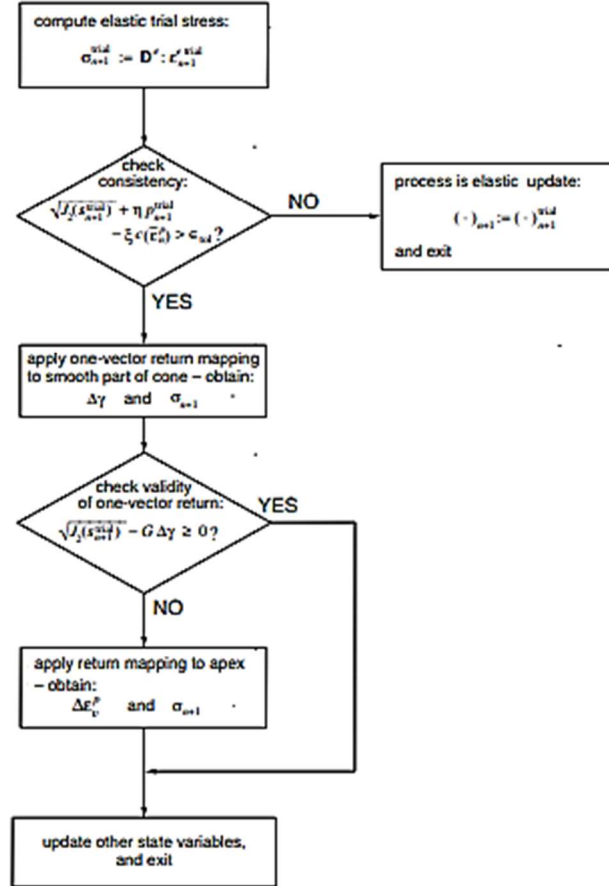
residual derivative matrix:

$$\mathbf{d} := \begin{bmatrix} \frac{\partial \tilde{\Phi}^a}{\partial \Delta \gamma^a} & \frac{\partial \tilde{\Phi}^a}{\partial \Delta \gamma^b} \\ \frac{\partial \tilde{\Phi}^b}{\partial \Delta \gamma^a} & \frac{\partial \tilde{\Phi}^b}{\partial \Delta \gamma^b} \end{bmatrix} = \begin{bmatrix} -a - 4H \cos^2 \phi & -b - 4H \cos^2 \phi \\ -b - 4H \cos^2 \phi & -a - 4H \cos^2 \phi \end{bmatrix}$$

new guess for $\Delta \gamma^a$ and $\Delta \gamma^b$:

$$\begin{bmatrix} \Delta \gamma^a \\ \Delta \gamma^b \end{bmatrix} := \begin{bmatrix} \Delta \gamma^a \\ \Delta \gamma^b \end{bmatrix} - \mathbf{d}^{-1} \begin{bmatrix} \tilde{\Phi}^a \\ \tilde{\Phi}^b \end{bmatrix}$$

- (i) Set initial guess for $\Delta \varepsilon_v^p$
 $\Delta \varepsilon_v^p := 0$; $\varepsilon_{n+1}^p := \varepsilon_n^p$
 and corresponding residual (refer to equation (8.85))
 $r := c(\varepsilon_n^p) \cot \phi - p_{n+1}^{\text{trial}}$
- (ii) Perform Newton-Raphson iteration
 $H := \left. \frac{dc}{d\varepsilon^p} \right|_{\varepsilon_{n+1}^p}$ (hardening slope)
 $d := \frac{H \cos \phi \cot \phi}{\sin \psi} + K$ (residual derivative)
 $\Delta \varepsilon_v^p := \Delta \varepsilon_v^p - r/d$ (update $\Delta \varepsilon_v^p$)
- (iii) Compute new residual and check for convergence
 $\varepsilon_{n+1}^p := \varepsilon_n^p + \frac{\cos \phi}{\sin \psi} \Delta \varepsilon_v^p$
 $p_{n+1} := p_{n+1}^{\text{trial}} - K \Delta \varepsilon_v^p$
 $r := c(\varepsilon_{n+1}^p) \cot \phi - p_{n+1}$
 IF $|r| \leq \epsilon_{\text{tol}}$ THEN update
 $\sigma_1 := \sigma_2 := \sigma_3 := p_{n+1}$
 and RETURN to Box 8.4
- (iv) GOTO (ii)



```

(i) Set initial guess for  $\Delta\gamma$ 

$$\Delta\gamma := 0, \quad \varepsilon_{n+1}^p := \varepsilon_n^p$$

and corresponding residual (yield function value)

$$\Phi := \sqrt{J_2(s_{n+1}^{trial})} + \eta p_{n+1}^{trial} - \xi c(\varepsilon_n^p)$$


(ii) Perform Newton-Raphson iteration for  $\Delta\gamma$ 

$$H := \left. \frac{d\Phi}{d\varepsilon^p} \right|_{\varepsilon_{n+1}^p} \quad (\text{hardening slope})$$


$$d := \frac{d\Phi}{d\Delta\gamma} = -G - K\bar{\eta}\eta - \xi^2 H \quad (\text{residual derivative})$$


$$\Delta\gamma := \Delta\gamma - \Phi/d \quad (\text{new guess for } \Delta\gamma)$$


(iii) Check convergence

$$\varepsilon_{n+1}^p := \varepsilon_n^p + \xi \Delta\gamma$$


$$\Phi := \sqrt{J_2(s_{n+1}^{trial})} - G\Delta\gamma + \eta(p_{n+1}^{trial} - K\bar{\eta}\Delta\gamma) - \xi c(\varepsilon_{n+1}^p)$$

IF  $|\Phi| \leq \epsilon_{tol}$  THEN update

$$s_{n+1} := \left(1 - \frac{G\Delta\gamma}{\sqrt{J_2(s_{n+1}^{trial})}}\right) s_{n+1}^{trial}$$


$$p_{n+1} := p_{n+1}^{trial} - K\bar{\eta}\Delta\gamma$$

and RETURN to Box 8.8

(iv) GOTO (ii)

```

```

(i) Elastic predictor. Given  $\Delta\varepsilon$  and the state variables at  $t_n$ , evaluate the elastic trial state

$$\varepsilon_{n+1}^{e\,trial} := \varepsilon_n^e + \Delta\varepsilon \quad \varepsilon_{n+1}^{p\,trial} := \varepsilon_n^p$$


$$s_{n+1}^{trial} := 2G \varepsilon_{n+1}^{e\,trial} \quad p_{n+1}^{trial} := K \varepsilon_{n+1}^{e\,trial}$$


(ii) Check plastic admissibility
IF  $\sqrt{J_2(s_{n+1}^{trial})} + \eta p_{n+1}^{trial} - \xi c(\varepsilon_{n+1}^{p\,trial}) \leq 0$ 
THEN set  $(\cdot)_{n+1} := (\cdot)_{n+1}^{trial}$  and EXIT

(iii) Return mapping
(a) Return to smooth portion of cone – GOTO Box 8.9
(b) Check validity

$$\text{IF } \sqrt{J_2(s_{n+1}^{trial})} - G\Delta\gamma \geq 0$$

THEN return is valid – GOTO (iv)
(c) Return to apex – GOTO Box 8.10

(iv) Update elastic strain

$$\varepsilon_{n+1}^e := \frac{1}{2G} s_{n+1} + \frac{p_{n+1}}{3K} \mathbf{I}$$


(v) EXIT

```

A. THE MENEGOTTO-PINTO WITH FILIPPOU ISOTROPIC HARDENING MODEL

```

C-----
c      MENEGOTTO-PINTO STEEL MODEL
c      WITH FILIPPOU ISOTROPIC HARDENING
c      steel model with damage modulus
C-----

```

implicit none

```

C-----
c      calling and return arguments
C-----

```

```

real*8 sfixpr(10),shstvP(10),shstv(10)
real*8 epssP,sigsP,depss,sigs,Est

```

```
C-----
c   fixed properties
C-----
    real*8  fsy,es1,b,r0,a1,a2,a3,a4,es2,epy
C-----
c   history variables
C-----
    real*8  epmin,epmax,epex,ep0,s0,epr,sr
    integer kon
C-----
c   local variables
C-----

    integer i,j
    real*8  epss,sst,qi,r,e,dsde,epm

c   clear output variables
    sigs = 0.d0
    Est = 0.d0
C-----
c   retrieve steel fixed material properties
C-----
    fsy = sfixpr(2)
    es1 = sfixpr(3)
    b   = sfixpr(4)
    r0  = sfixpr(5)
    a1  = sfixpr(6)
    a2  = sfixpr(7)
    a3  = sfixpr(8)
    a4  = sfixpr(9)
C-----
c   calculate other fixed material properties
C-----
    es2 = b*es1
    epy = fsy/es1

C-----
c   retrieve steel history variables
C-----
    epmin = shstvP(1)
    epmax = shstvP(2)
    epm   = dmax1(dabs(epmin),dabs(epmax))
    epex  = shstvP(3)
    ep0   = shstvP(4)
    s0    = shstvP(5)
    epr   = shstvP(6)
    sr    = shstvP(7)
    kon   = int(shstvP(8))

c   calculate current strain
    epss = epssP + depss

C-----
c   Menegotto-Pinto model
C-----
c-----check for virgin steel-----
    if(kon.eq.0) then
        if(depss.eq.0.0d0) then
```

```

sigs = 0.d0
est = es1
goto 200
endif
epmax = epy
epmin = -epy
epm = epy
if(depss.lt.0.0d0) then
    kon = 2
    ep0 = -epm
    s0 = -fsy
    epex = -epm
endif
if(depss.gt.0.0d0) then
    kon = 1
    ep0 = epm
    s0 = fsy
    epex = epm
endif
endif

if(depss.eq.0.0d0) goto 100

if(kon.eq.2.and.depss.gt.0.0d0) then
    kon = 1
    epr = epss-depss
    sr = sigsp
    if(epr.lt.epmin) epmin = epr
    epm = dmax1(dabs(epmin),dabs(epmax))
    sst = fsy*a3*(epm/epy-a4)
    sst = dmax1(sst,0.0d0)
    ep0 = (sr + es2*epy - (es1*epr + fsy + sst))/(es2-es1)
    s0 = fsy + sst + es2*(ep0-epy)
    epex = epmax
endif

if(kon.eq.1.and.depss.lt.0.0d0) then
    kon = 2
    epr = epss-depss
    sr = sigsp
    if(epr.gt.epmax) epmax = epr
    epm = dmax1(dabs(epmin),dabs(epmax))
    sst = fsy*a3*(epm/epy-a4)
    sst = dmax1(sst,0.0d0)
    ep0 = (sr + fsy + sst - (es1*epr + es2*epy))/(es2-es1)
    s0 = es2*(ep0+epy) - fsy - sst
    epex = epmin
endif

c-----calculate stress and modulus-----
100 continue
qi = dabs((epex-ep0)/epy)
r = r0 - (a1*qi)/(a2+qi)
e = (epss-epr)/(ep0-epr)
sigs = b*e + (1.0d0-b)*e/(1.0d0+dabs(e)**r)**(1/r)
sigs = sigs*(s0-sr)+sr
dsde = b + (1.0d0-b)*(1.0d0-dabs(e)**r)/(1.0d0+dabs(e)**r)
& /(1.0d0+dabs(e)**r)**(1/r)
est = dsde*(s0-sr)/(ep0-epr)

c-----
c transfer all variables to history vector
c-----

```



```
200 continue
    shstv(1) = epmin
    shstv(2) = epmax
    shstv(3) = epex
    shstv(4) = ep0
    shstv(5) = s0
    shstv(6) = epr
    shstv(7) = sr
    shstv(8) = dble(kon)

    return
end
```

B. MONTI – NUTI MODEL (modified for the case of partial unloading)

```
SUBROUTINE STMDL9
C
C *****
C This subroutine calculates the stress at a monitoring point for
C the material model of Monti and Nuti [1992].
C *****
C
C IMPLICIT UNDEFINED (A-Z)
C
C .....[ ARRAYS AND POINTERS ].....
C
C
C .....[ SUBROUTINE VARIABLES ].....
C
    REAL*8 Fsy,Es0,b0p,L,D,R0,A1,A2,P      ! material properties
    REAL*8 b0n                          ! dependent on material properties
    REAL*8 epssP,sigsP,epss0,sigs0,csimax,dsigsK,dsigsl,epssr,sigsr,R,kon,epss,sigs,Est
    REAL*8 alpha,beta,eoa,soa,era,sra,eob,sob,erb,srb,Ra,Rb,omega
    logical corr

C local variables
    REAL*8 zero,one,dum1,dum2,a5,a6
    REAL*8 depss,csi,epsrat
    REAL*8 Esh,b
    REAL*8 gammap,fi,dsigsKI
    REAL*8 FR,epscor

    INTEGER i,j

C .....[ COMMON BLOCKS ].....
C
    COMMON /M_S9/ Fsy,Es0,b0p,L,D,R0,A1,A2,P,b0n,
+      epssP,sigsP,epss0,sigs0,csimax,dsigsK,dsigsl,epssr,sigsr,R,kon,epss,sigs,Est,Corr
    COMMON /M_S91/ alpha,beta,eoa,soa,era,sra,eob,sob,erb,srb,Ra,Rb,omega
C
C .....

C normalise A2
    A2 = A2*Fsy/Es0

C calculate other fixed material properties
    if (L/D.gt.5) then
        b0n = 3d-3*(5-L/D)
```

```
else
  b0n = b0p
end if
```

```
zero = 0.d0
one  = 1.d0
```

```
C-----
c  calculate increment of current strain
```

```
C-----
  depss = epss - epssP
```

```
C-----
c  assign the current value for hardening ratio
```

```
C-----
  if (depss.gt.zero) then
    b = b0p
  else
    b = b0n
  endif
```

```
C-----
c  check for virgin steel:
```

```
c  if kon=0 set the initial yield stress and strain
```

```
C-----
  if (kon.eq.0) then
    if (depss.gt.zero) then
      kon = 1
    else
      kon = -1
    endif
    epss0 = kon*Fsy/Es0TMP
    sigs0 = kon*Fsy
    R      = R0
  endif
```

```
C-----
c  correction in case of partial unloading
```

```
C-----
  if (corr) then
```

```
    epscor = 0.05*abs(epssr)
    if (omega.eq.0) then
```

```
      if (abs(depss).lt.(epscor).and.kon*depss.lt.0)then
        omega=1
        eoa=epss0
        soa=sigs0
        alpha=epssP
        era=epssr
        sra=sigsr
        Ra=R
        goto 1400
      endif
    endif
```

```
    if (omega.eq.1) then
      if (kon*depss.lt.0) then
        omega=3
        eob=epss0
        sob=sigs0
        beta=epssP
        erb=epssp
```

```
srb=sigsp
Rb=R
else
if (abs(alpha-epss).gt.(epscor)) omega = 0
    goto 1400
endif
endif

if (omega.gt.1) then
    if (omega.eq.3) then
        omega=4
        goto 20
    endif
    if (kon*depss.lt.zero) omega=omega+1
20  continue
        kon=depss/abs(depss)
    if (int(omega/2.) .eq. omega/2.) then

        if (kon.lt.0) then

            if (epss.lt.alpha) then

                epss0=eoα
                sigs0=soα
                epssr=era
                sigsr=sra
                omega=0
                R=Ra
                goto 1500
            endif
            if (epss.gt.beta) then
                epss0=eob
                sigs0=sob
                epssr=erb
                sigsr=srb
                omega=0
                R=Rb
                goto 1500
            endif
            sigs=sigsp+depss*Est
            goto 2000
        endif

        if (kon.gt.0) then

            if (epss.gt.alpha) then
                epss0=eoα
                sigs0=soα
                epssr=era
                sigsr=sra
                omega=0
                R=Ra
                goto 1500
            endif

            if (epss.lt.beta) then
                epss0=eob
                sigs0=sob
                epssr=erb
                sigsr=srb
                omega=0
                R=Rb
```

```
        goto 1500
    endif

    sigs=sigsp+depss*Est
    goto 2000

endif
    else
    if (kon.lt.0) then
    if (epss.gt.alpha) then

        epss0=eoα
        sigs0=soα
        epssr=era
        sigsr=sra
        omega=0
        R=Ra
        goto 1500
    endif

    if (epss.lt.beta) then
        epss0=eob
        sigs0=sob
        epssr=erb
        sigsr=srb
        omega=0
        R=Rb
        goto 1500
    endif

    sigs=sigsp+depss*Est
    goto 2000
    endif

    if (kon.gt.0) then

    if (epss.lt.alpha) then
        epss0=eoα
        sigs0=soα
        epssr=era
        sigsr=sra
        omega=0
        R=Ra
    goto 1500
    endif

    if (epss.gt.beta) then
        epss0=eob
        sigs0=sob
        epssr=erb
        sigsr=srb
        omega=0
        R=Rb
        goto 1500
    endif

    sigs=sigsp+depss*Est
    goto 2000

endif
endif
endif
```



```
endif
1400 continue
c-----
c   in case of load reversal: store the last load reversal point
c   and calculate the stress and strain (sigs0 and epss0) at the
c   new intersection between elastic and strain hardening asymptote
c-----
  if (depss*kon.le.zero) then

c     update index for loading/unloading
    if (kon.eq.1) then
      kon = -1
      Esh = b0p*Es0TMP
    else
      kon = 1
      Esh = b0n*Es0TMP
    endif

c     plastic excursion
    csi = epssP - epss0
    if (csi*kon.gt.0.d0) csi=0.d0  !!non funziona per la prova ciclica!!

c     additional plastic excursion
    if (dabs(csi).gt.csimax) then
      gammap = (dabs(csi) - csimax)*dsign(1d0,csi)
    else
      gammap = 0.d0
    end if

c     update last inversion point
    epssr = epssP
    sigsr = sigsP

c     double plastic work during previous semicycle
    fi = csi*(sigsr-sigs0)

c     maximum plastic excursion of previous semicycle
    csimax = dmax1(csimax,dabs(csi))

c     stress variation due to csi and gammap
c     accounting for the presence of buckling
    if (L/D.le.5) then
      dsigsK = dsigsK + Esh*csi
      dsigsI = dsigsI + dabs(Esh*gammap)*dsign(1d0,fi)
      dsigsKI = P*dsigsK + (1-P)*dsigsI*dsign(1d0,-csi)
    else
      dsigsK = dsigsK + Esh*gammap
      dsigsI = dsigsI + dabs(Esh*csi)*dsign(1d0,fi)
      dsigsKI = P*dsigsK + (1-P)*dsigsI*dsign(1d0,-csi)
    end if

c     calculate degrading stiffness due to buckling
    if (depss.gt.zero) then
      if (L/D.gt.5) then
        a5 = 1 + (5-L/D)/7.5
        a6 = -1000*csi**2
        Es0TMP = Es0TMP*(a5 + (1-a5)*exp(a6))
      end if
    endif

c     calculate new yield stress
    sigs0 = Fsy*dsign(1d0,-csi) + dsigsKI

c     calculate new yield strain
    epss0 = epssr + (sigs0-sigsr)/Es0TMP
```

```
c    update curvature of branch
c    accounting for the presence of buckling
    R = fR(L/D,depss,R0,A1,A2,csimax)
    endif
```

```
C-----
c    calculate current stress sigs
C-----
1500 continue
```

```
c    normalized strain
    epsrat = (epss-epssr)/(epss0-epssr)

c    current stress
    dum1 = one + dabs(epsrat)**R
    dum2 = dum1**(1/R)
    sigs = b*epsrat + (one-b)*epsrat/dum2
    sigs = sigs*(sigs0-sigsr) + sigsr
```

```
C-----
c    calculate appropriate stiffness
C-----
    Est = b + (one-b)/(dum1*dum2)
    Est = Est*(sigs0-sigsr)/(epss0-epssr)
```

```
2000 continue
```

```
    RETURN
    END
```

```
C-----
c    function for variation of R
C-----
    function fR (snell,depss,R0,A1,A2,csimax)
```

```
    implicit none
```

```
    real*8 snell,depss,R0,A1,A2,csimax,fR,fr1
    real*8 Rb,R0b,R1b,A1b,A2b,dum1
```

```
    dum1=A2+csimax
    if (dum1.eq.0.d0) then
        fR = R0
    else
        fR = R0 - (A1*csimax)/(A2+csimax)
    endif
    if (snell.gt.5.and.depss.lt.0) then
        R0b = 0.2*(snell-5)      ! minimum value
        A1b = A1 + 1
        A2b = A2*1000
        R1b = R0 - 2*(snell-5)   ! maximum value
        if (R1b.lt.R0b) R1b = R0b
        if (dum1.eq.0.d0) then
            fR1= R0b
        else
            Rb = R0b + (A1b*csimax)/(A2b+csimax)
            fR1= dmin1(Rb,R1b)
        endif
    end if
    if (fR1.gt.fR) fR = fR1
end
```

ΚΕΦΑΛΑΙΟ 5th

5. NUMERICAL EXAMPLES RESULTS – COMPARISON

5.1 NUMERICAL EXAMPLES

Von Mises yield criterion Examples

Example 1

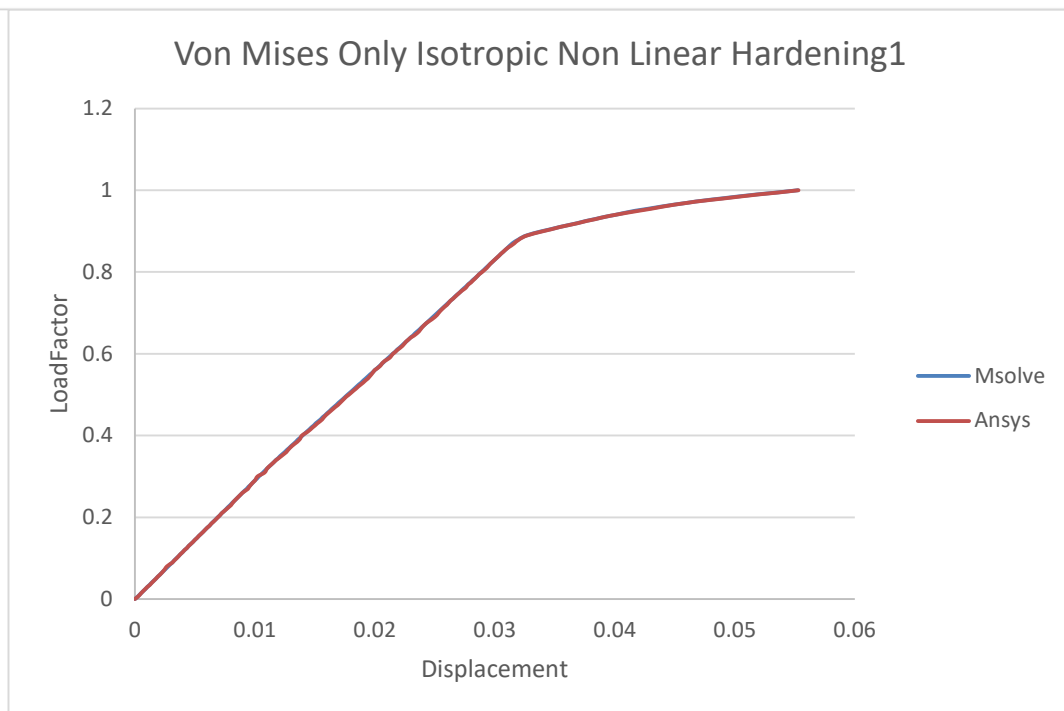
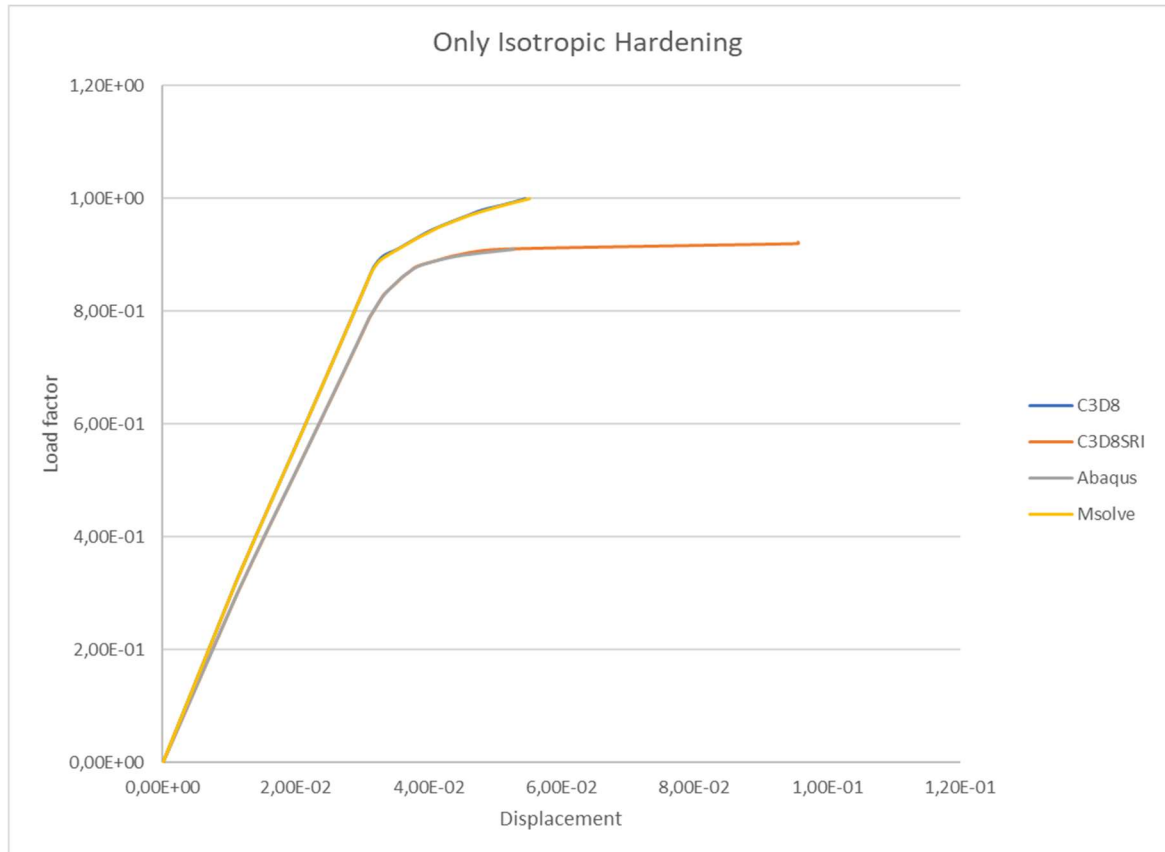
Hexa 8 Box 2mX2mX2m with elements 1mX1mX1m, $E=800000$ Kpa, $\nu=1/3$, $\sigma_{y0}=5000$ Kpa, Only isotropic hardening with curve $\sigma_y = \sigma_{y0} e^{\frac{\varepsilon_{pl}}{0.001}}$ discrete for values of ε_{pl} $[0,0,001]$ with step 10^{-6} . Boundary conditions full fixed supports in the bottom of the box (i. e. for $Z=0$ $u_x = u_y = u_z = 0$). Loading in the upper surface of the box in the vertical direction (100 Non linear increments) as follows

X	Y	Z	Amount (KN)
0	0	2	-3750
0	1	2	-7500
0	2	2	-3750
1	0	2	-7500
1	1	2	-15000
1	2	2	-7500
2	0	2	-3750
2	1	2	-7500
2	2	2	-3750

Monitor output dof is for point

X	Y	Z
1	1	2

In Z direction (Number 41 of Dof and number 52 in suitesparse solver)
Load Displacement Curve (Max Relative Divergence from Ansys 6% found
in 1st step the rest are in the vicinity of 1%)

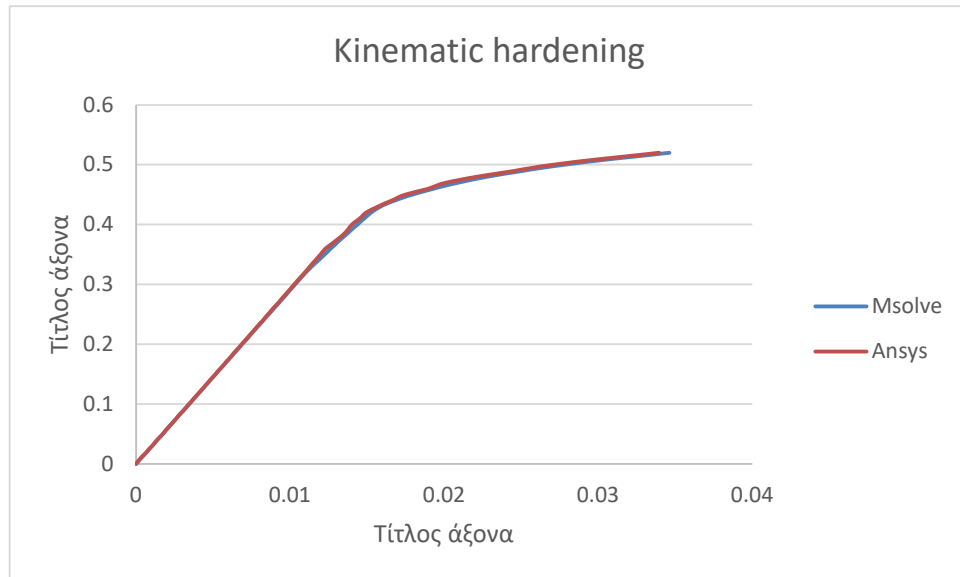


Example 2

The hardening now is kinematic hardening with the formula (kPa)

$$\alpha = \frac{C}{\gamma} * \left(1 - e^{-\gamma \bar{\varepsilon}^{pl}}\right) = 180808.11517296 * \left(1 - e^{-8.97 * \bar{\varepsilon}^{pl}}\right)$$

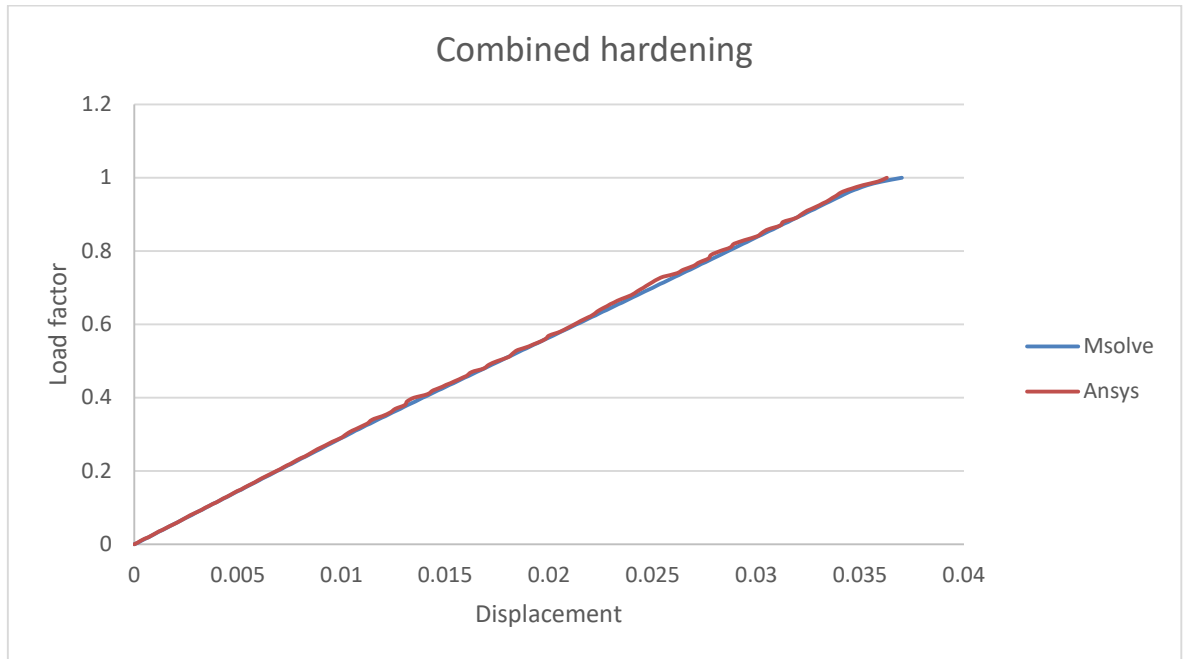
Load Displacement Curve (Max Relative Divergence from Ansys 12% found in 1st step the rest are in the vicinity of 4%)



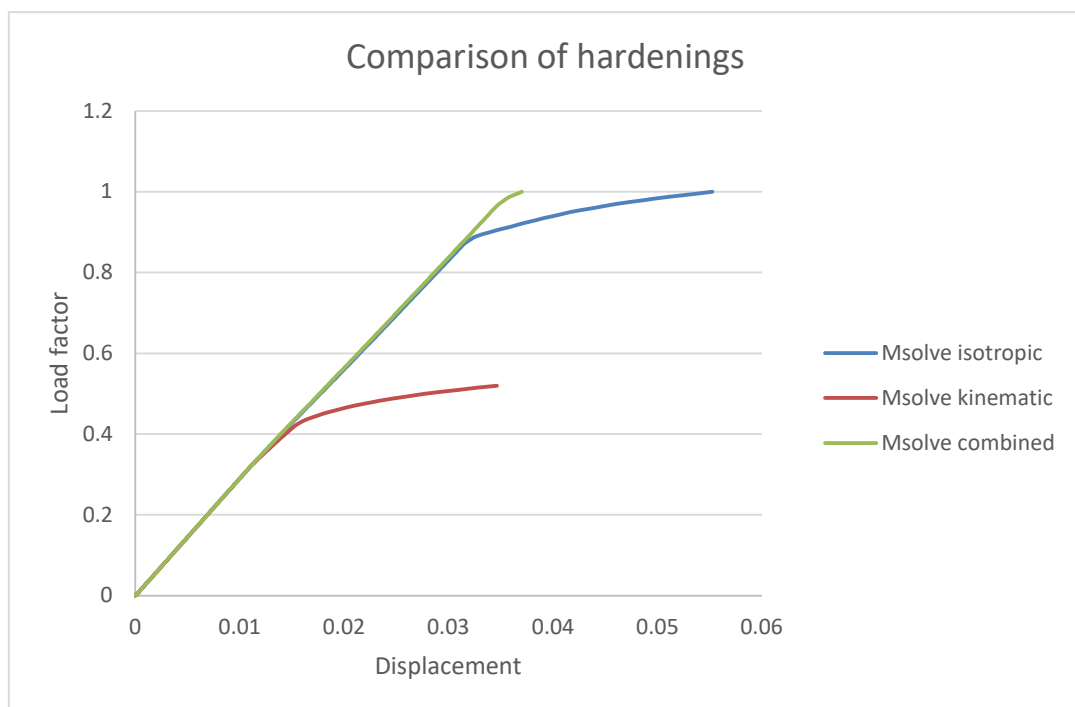
Example 3

The hardening is now the combined hardening of the isotropic hardening law and the kinematic hardening law of the examples 1 and 2

Load Displacement Curve (Max Relative Divergence from Ansys 13% found in 1st step the rest are in the vicinity of 2%)



Comparison of hardenings



Example 4

Hexa 8 Box 2mX2mX2m with elements 1mX1mX1m, E=800000 Kpa, $\nu=1/3$, $\sigma_{y0}=5000$ Kpa, Combined isotropic hardening with curve $\sigma_y = \sigma_{y0} e^{\frac{\varepsilon_{pl}}{0,001}}$ discrete for values of ε_{pl} [0,0,005] with step 10^{-6} . The kinematic hardening with the formula (kPa)

$$\alpha = \frac{C}{\gamma} * \left(1 - e^{-\gamma \varepsilon_{pl}}\right) = 180808.11517296 * (1 - e^{-8.97 * \varepsilon_{pl}})$$

Boundary conditions full fixed supports in the bottom of the box (i. e. for $Z=0$ $u_x = u_y = u_z = 0$). Dynamic symmetric triangle with time step $dt=0,1$ s, time of peak load $T1=10s$, time of free oscillation $T2=20s$ and end of analysis at $T3=30s$. Consistent mass matrix with density $\rho=25$ Mgr/m³ and Rayleigh Coefficients $a=0,35$ (mass matrix), $b=0,003$. Loading in the upper surface of the box in the vertical direction (100 Non linear increments) as follows

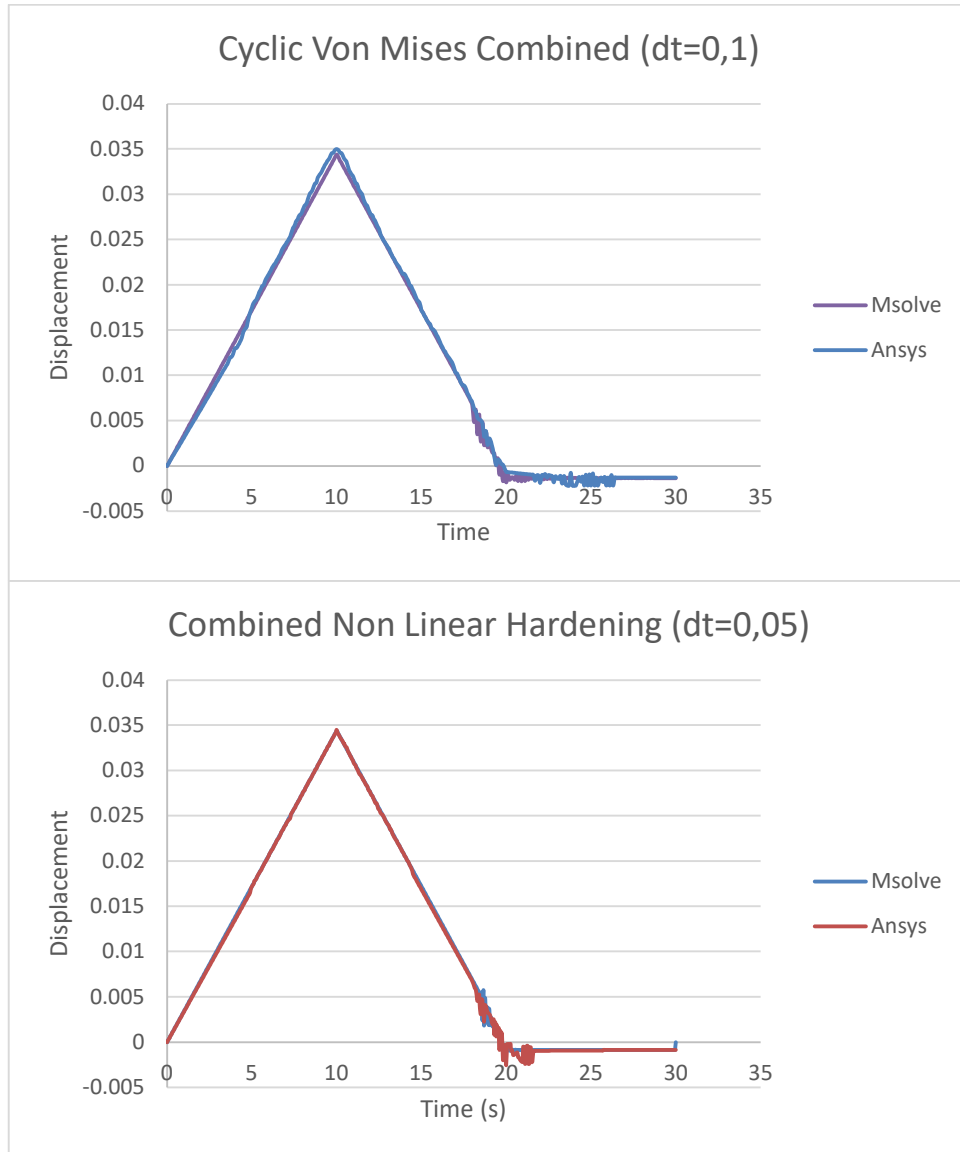
X	Y	Z	Amount (KN)
0	0	2	-3750
0	1	2	-7500
0	2	2	-3750
1	0	2	-7500
1	1	2	-15000
1	2	2	-7500
2	0	2	-3750
2	1	2	-7500
2	2	2	-3750

Monitor output dof is for point

X	Y	Z
1	1	2

In Z direction (Number 41 of Dof and number 52 in suitesparse solver)

Time history Curve



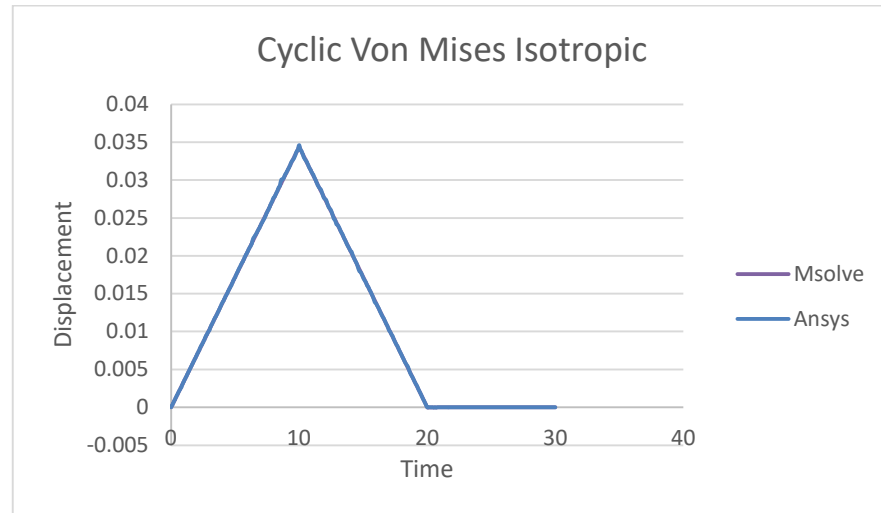
Comparison of time steps accuracy

	Msolve	Ansys	
Peak			
0,1	0,034404	0,035	1,703179
0,05	0,034404	0,034512	0,313358
End			
0,1	0,00134	0,001286	-4,17941
0,05	0,000868	0,000851	-1,94076

Example 5

As the example 4 but with only isotropic hardening

Time history Curve



Example 6

Hexa 8 Box 2mX2mX2m with elements 1mX1mX1m, $E=800000$ Kpa, $\nu=1/3$, $\sigma_{y0}=5000$ Kpa, Combined isotropic hardening with curve $\sigma_y = \sigma_{y0} e^{\frac{\varepsilon_{pl}}{0,001}}$ discrete for values of ε_{pl} $[0,0,001]$ with step 10^{-6} . The kinematic hardening with the formula (kPa)

$$\alpha = \frac{C}{\gamma} * \left(1 - e^{-\gamma \varepsilon^{pl}}\right) = 180808.11517296 * (1 - e^{-8.97 * \varepsilon^{pl}})$$

Boundary conditions full fixed supports in the bottom of the box (i. e. for $Z=0$ $u_x = u_y = u_z = 0$). Dynamic symmetric triangle with time step $dt=0,1$ s, time of peak load $T1=10$ s, time of free oscillation $T2=20$ s and end of analysis at $T3=30$ s. Consistent mass matrix with density $\rho=25$ Mgr/m³ and Rayleigh Coefficients $a=0,35$ (mass matrix), $b=0,003$. Loading in the upper surface of the box in the vertical direction (100 Non linear increments) as follows

X	Y	Z	Amount (KN)
0	0	2	-3750
0	1	2	-7500
0	2	2	-3750
1	0	2	-7500
1	1	2	-15000
1	2	2	-7500
2	0	2	-3750
2	1	2	-7500
2	2	2	-3750

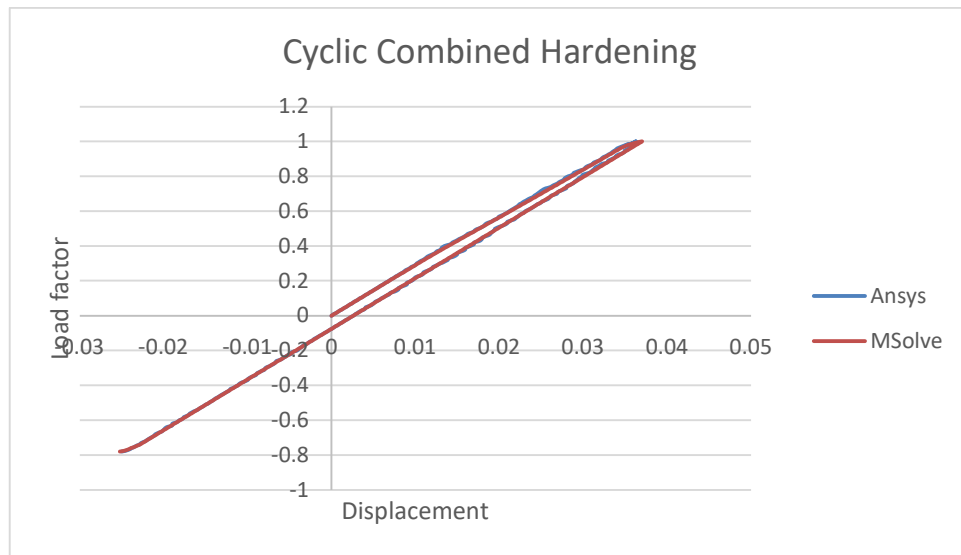
The aforementioned static loads are subjected to pressure loading-unloading-reverse loading-reverse unloading

Monitor output dof is for point

X	Y	Z
1	1	2

In Z direction (Number 41 of Dof and number 52 in suitesparse solver)

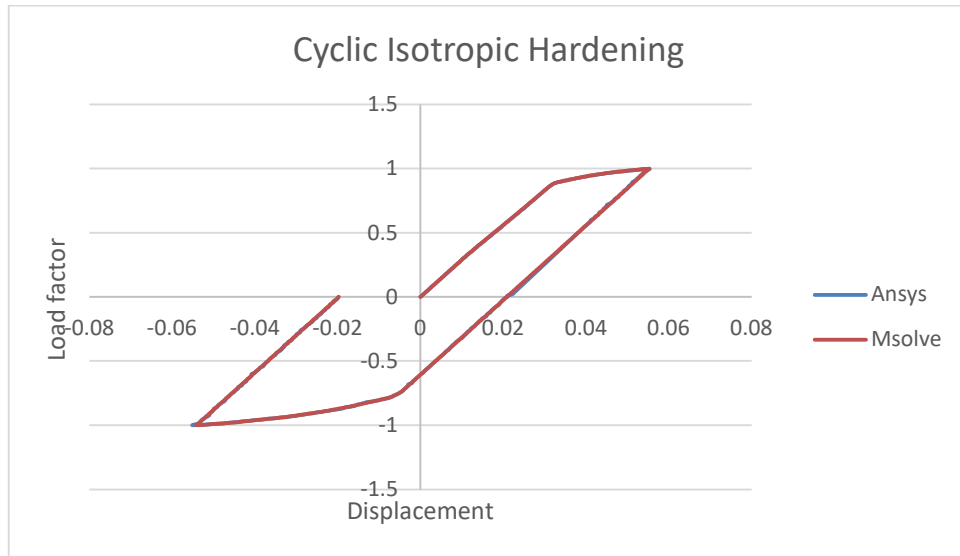
Load Displacement Curve (Max Relative Divergence from Ansys 13% found in 1st step the rest are in the vicinity of 5%)



Example 7

As Example 6 but with only isotropic hardening and no kinematic hardening

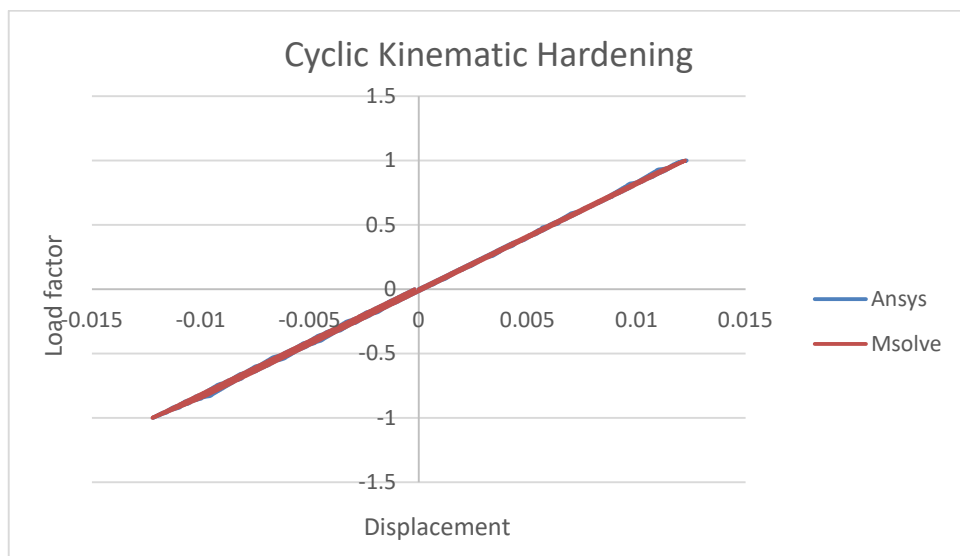
Load Displacement Curve (Max Relative Divergence from Ansys 19% found in Cyclic reverse the rest are in the vicinity of 1%)



Example 8

As Example 6 but with only kinematic hardening and the peak nodal loads are the ones of Example 6 multiplied by 0.35

Load Displacement Curve (Max Relative Divergence from Ansys 10% found in 1st step the rest are in the vicinity of 4%)



Tresca yield criterion Examples

Example 1

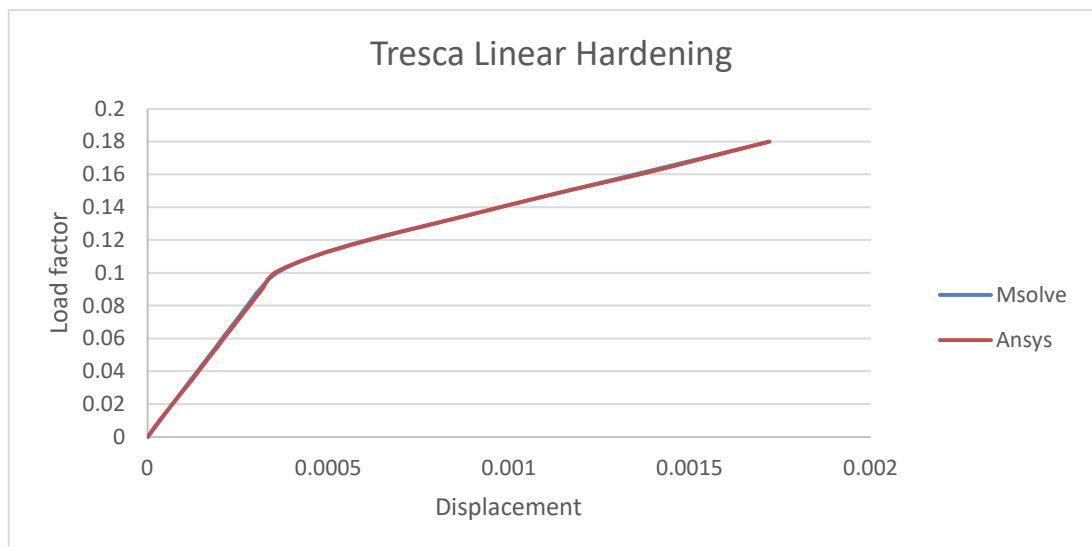
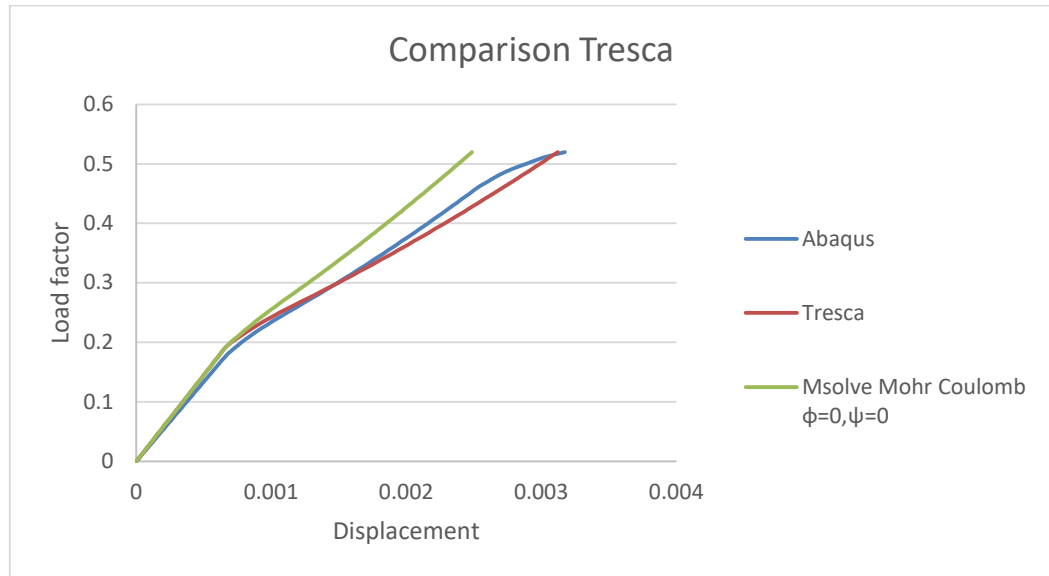
Hexa 8 Box 2mX2mX2m with elements 1mX1mX1m, $E=800000$ Kpa, $\nu=1/3$, $\sigma_{y0}=150$ Kpa, Only isotropic hardening with curve $\sigma_y = 2\sigma_{y0}e^{\frac{\varepsilon_{pl}}{0,001}}$ discrete for values of ε_{pl} $[0,0,001]$ with step 10^{-6} . Boundary conditions full fixed supports in the bottom of the box (i. e. for $Z=0$ $u_x = u_y = u_z = 0$). Loading in the upper surface of the box in the vertical direction (100 Non linear increments) as follows

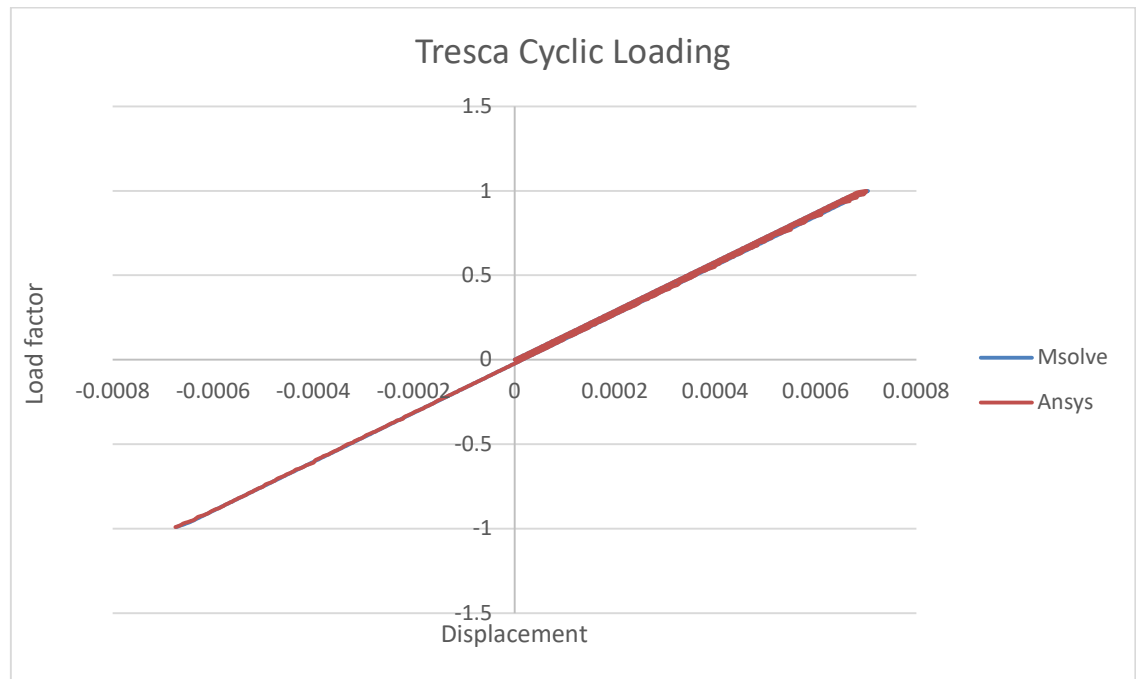
X	Y	Z	Amount (KN)
0	0	2	-375
0	1	2	-750
0	2	2	-375
1	0	2	-750
1	1	2	-1500
1	2	2	-750
2	0	2	-375
2	1	2	-750
2	2	2	-375

Monitor output dof is for point

X	Y	Z
1	1	2

In Z direction (Number 41 of Dof and number 52 in suitesparse solver)
Load Displacement Curve and Comparison with Mohr Coulomb with $\phi=\psi=0$
which should be very close referring to the yield surfaces





Mohr Coulomb yield criterion Examples

Example 1

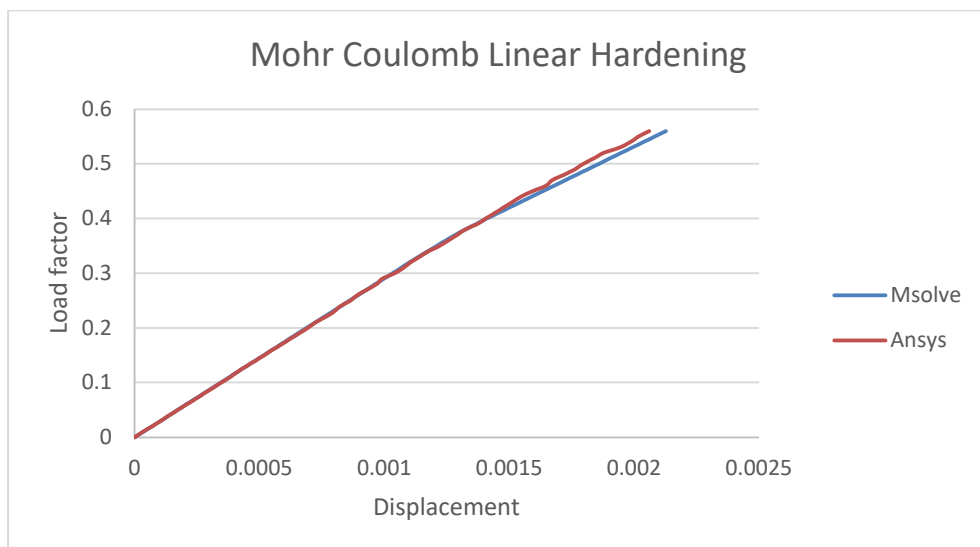
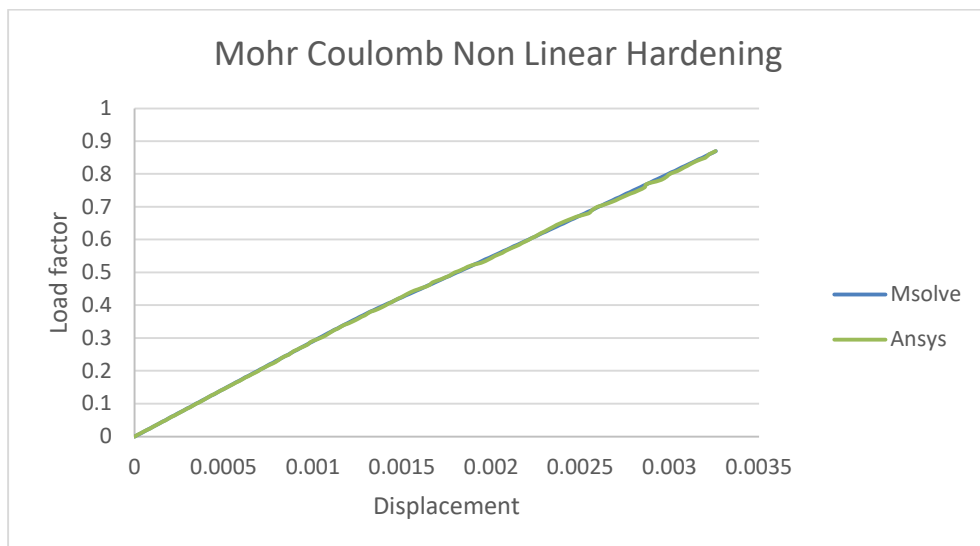
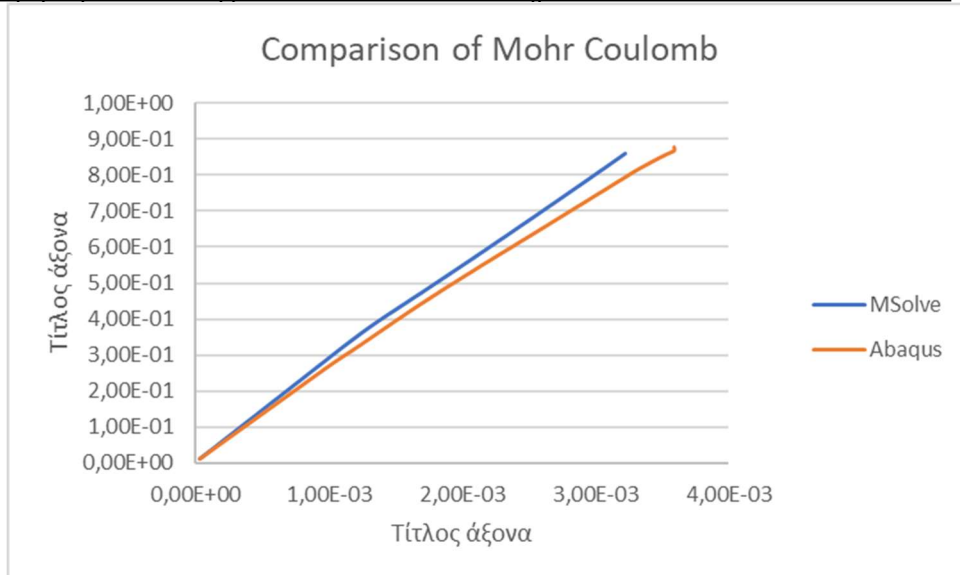
Hexa 8 Box 2mX2mX2m with elements 1mX1mX1m, $E=800000$ Kpa, $\nu=1/3$, $\psi=30^\circ$, $\phi=30^\circ$ $c_0=150$ Kpa, Only isotropic hardening with curve $c = c_0 e^{\frac{\varepsilon_{pl}}{0,001}}$ discrete for values of ε_{pl} $[0,0,001]$ with step 10^{-6} . Boundary conditions full fixed supports in the bottom of the box (i. e. for $Z=0$ $u_x = u_y = u_z = 0$). Loading in the upper surface of the box in the vertical direction (100 Non linear increments) as follows

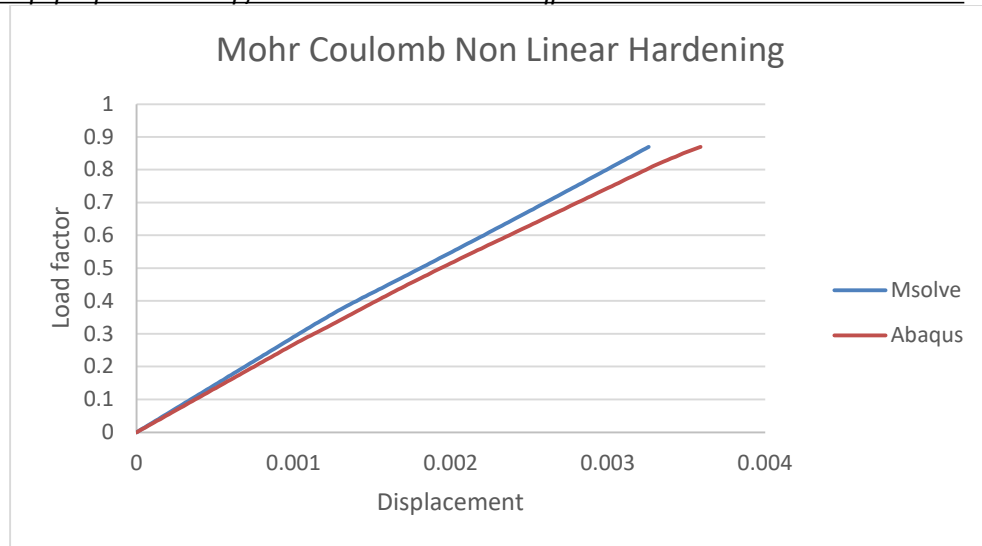
X	Y	Z	Amount (KN)
0	0	2	-375
0	1	2	-750
0	2	2	-375
1	0	2	-750
1	1	2	-1500
1	2	2	-750
2	0	2	-375
2	1	2	-750
2	2	2	-375

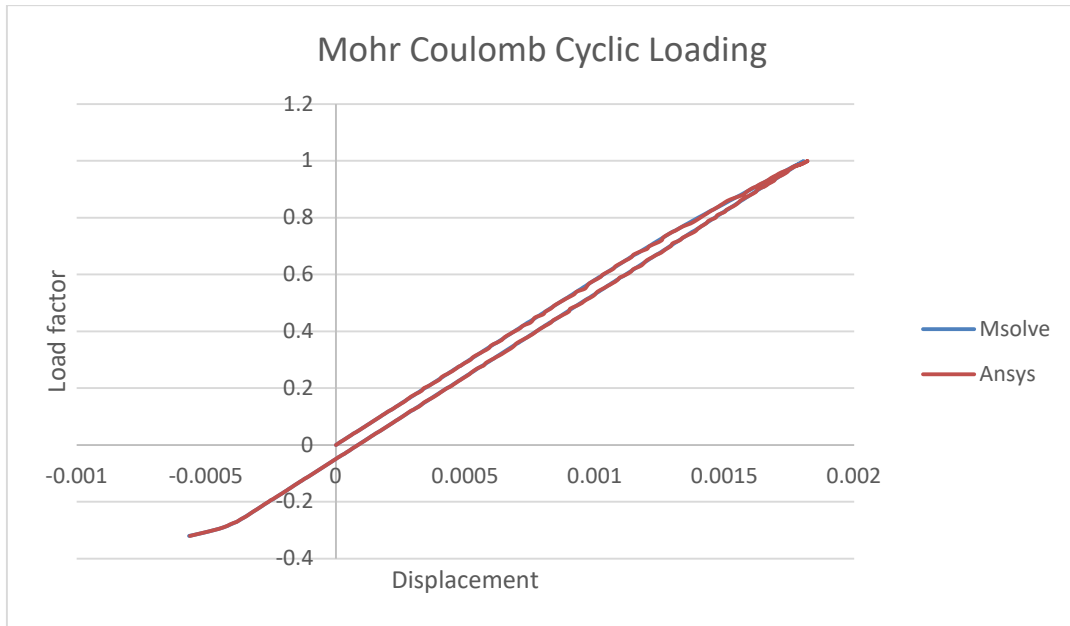
Monitor output dof is for point

X	Y	Z
1	1	2

In Z direction (Number 41 of Dof and number 52 in suitesparse solver)
Load Displacement Curve







Drucker Prager yield criterion Examples

Example 1

Hexa 8 Box 2mX2mX2m with elements 1mX1mX1m, $E=800000$ Kpa, $\nu=1/3$, $\psi=30^\circ$, $\phi=30^\circ$, $c_0=150$ Kpa, Outer Cone approximation of Mohr Coulomb,

that is $n = \frac{6 \sin \psi}{\sqrt{3}(3-\sin \psi)} = \frac{2\sqrt{3}}{5}$, $\bar{n} = \frac{6 \sin \psi}{\sqrt{3}(3-\sin \psi)} = \frac{2\sqrt{3}}{5}$, $\xi = \frac{6 \cos \phi}{\sqrt{3}(3-\sin \psi)} = \frac{6}{5}$

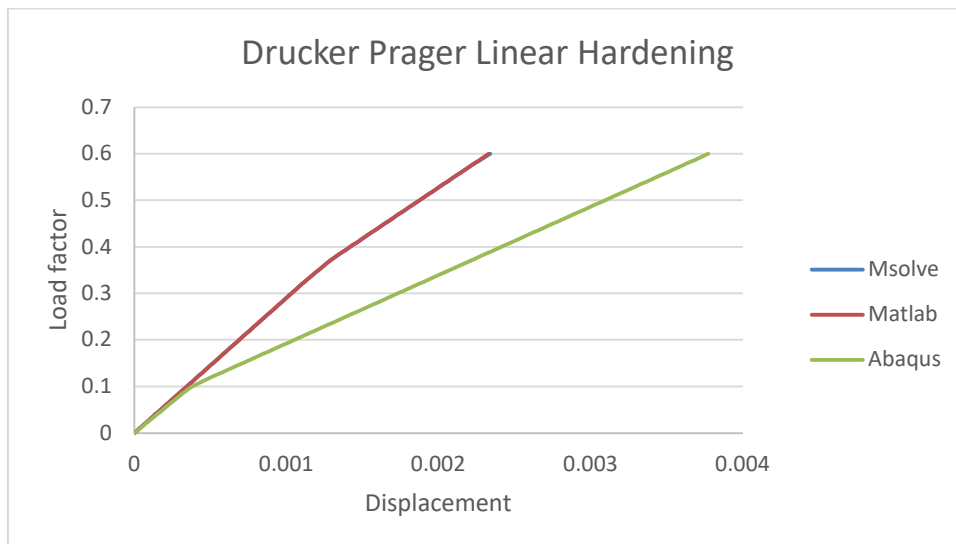
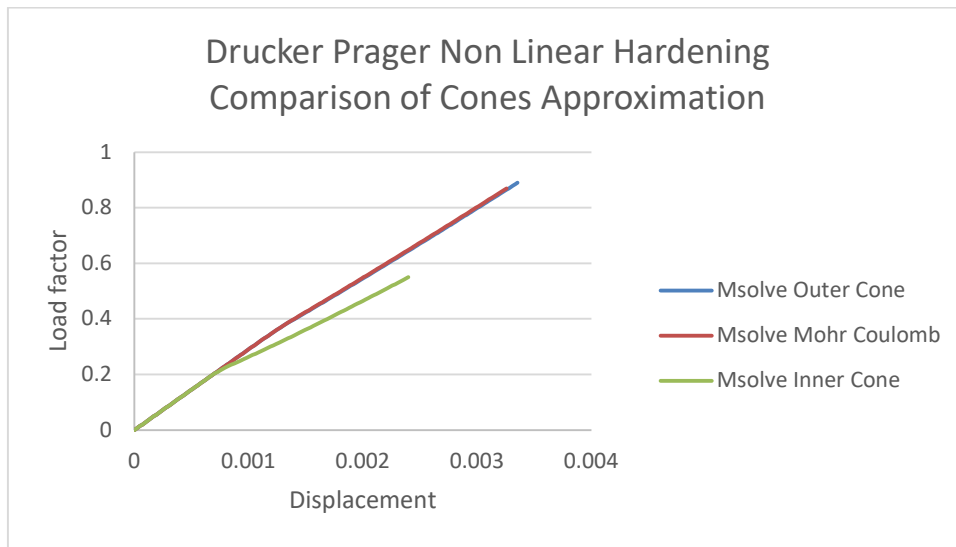
Only isotropic linear hardening with curve hardening modulus $H = 100000$ Kpa Boundary conditions full fixed supports in the bottom of the box (i. e. for $Z=0$ $u_x = u_y = u_z = 0$). Loading in the upper surface of the box in the vertical direction (100 Non linear increments) as follows

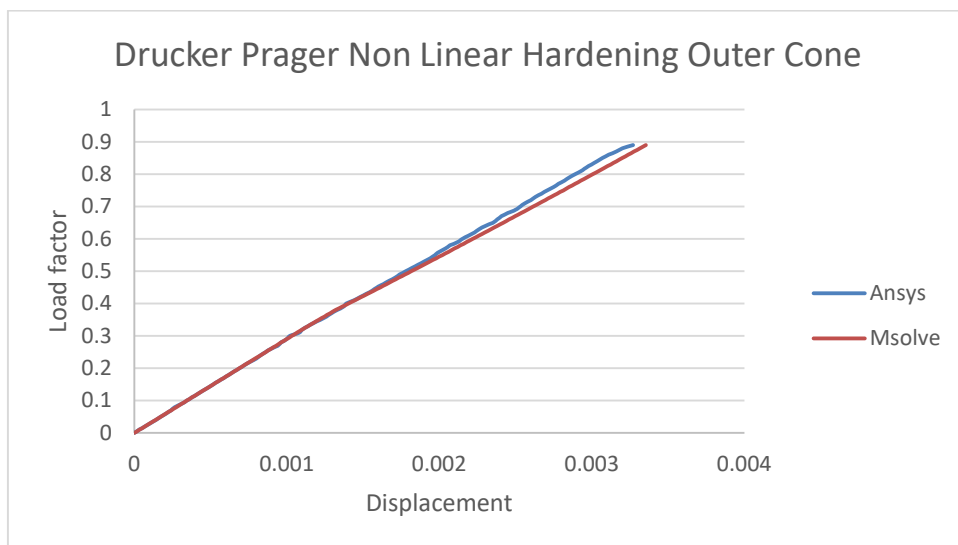
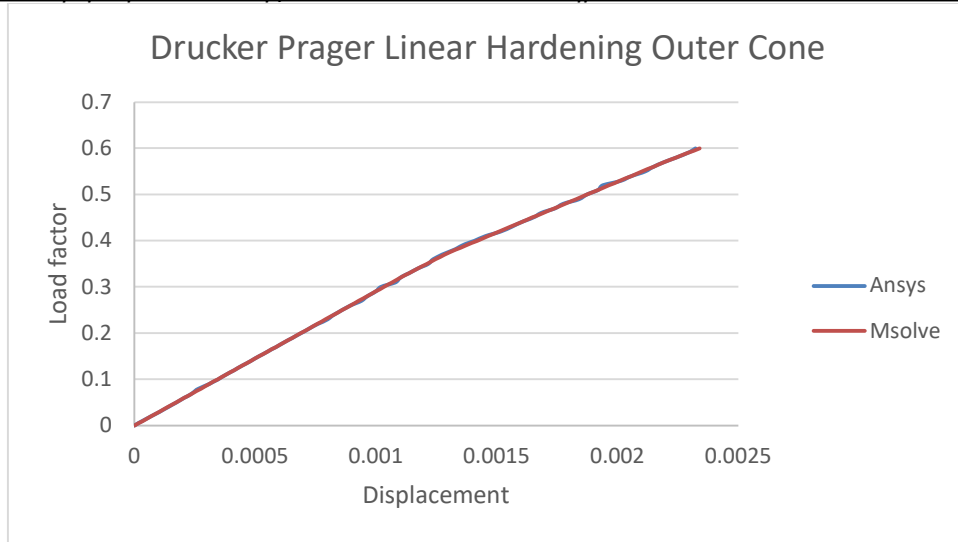
X	Y	Z	Amount (KN)
0	0	2	-375
0	1	2	-750
0	2	2	-375
1	0	2	-750
1	1	2	-1500
1	2	2	-750
2	0	2	-375
2	1	2	-750
2	2	2	-375

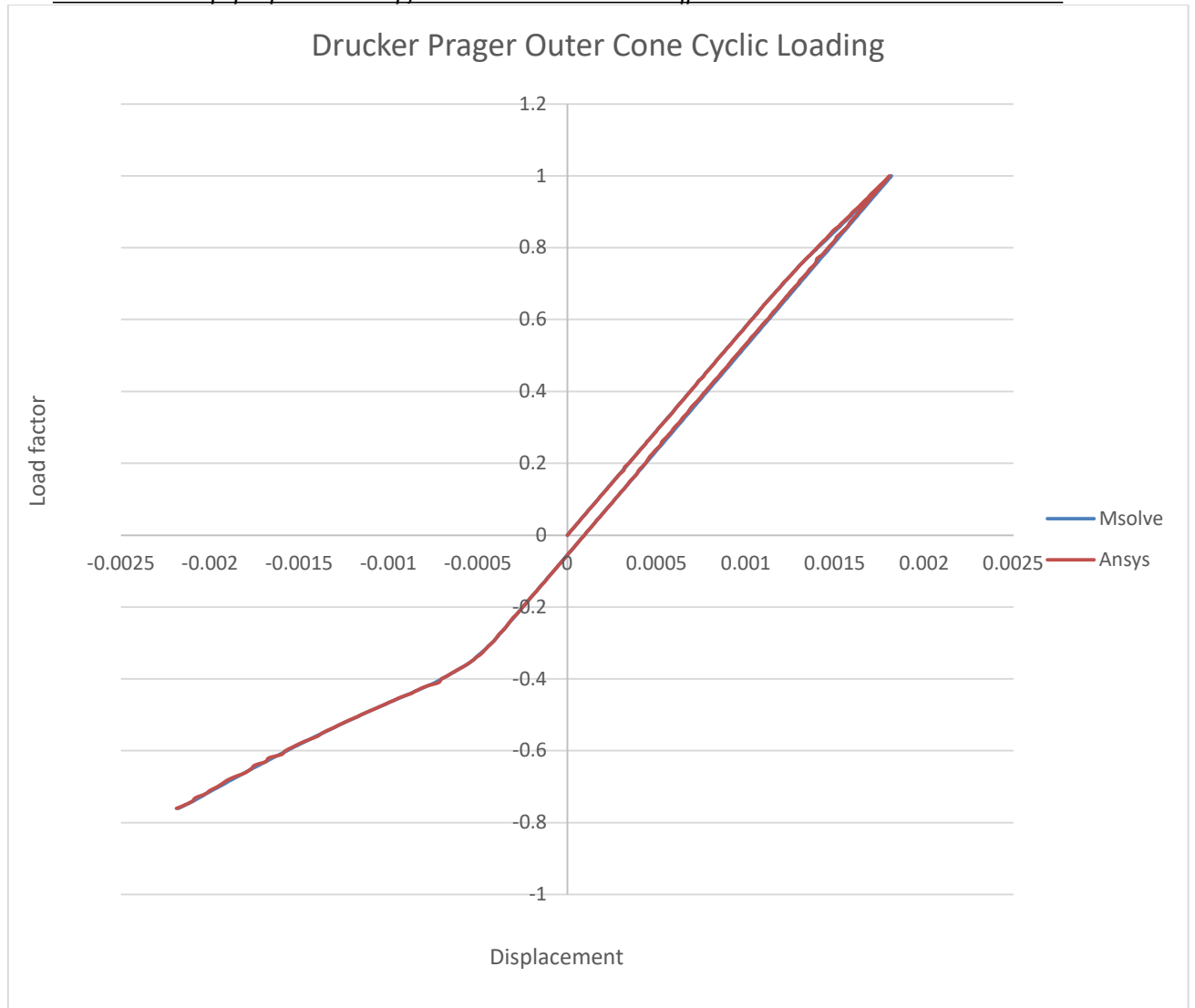
Monitor output dof is for point

X	Y	Z
1	1	2

In Z direction (Number 41 of Dof and number 52 in suitesparse solver)
Load Displacement Curve







Kavvadas Clays yield criterion Examples

Example 1

Hexa 8 Box 2mX2mX2m with elements 1mX1mX1m, compressibility factor $\kappa=0.5*0.008686$, critical state line inclination $c=0.733609251$, $\xi=0.05$, Initial Stresses only hydrostatic -1000 KPa (compression), $N_{iso}=2.15$, virgin inclination factor $\lambda=10*\kappa$ constant, $n=1/3 \rightarrow 2G/K_{bulk}=0,75$, $a^*=400$ Kpa, $a_{initial}=1600$ Kpa, that means $B_{initial}=4$ and $B_{res}=1$. Tuning factors $n_{vp}, n_{qp}=75$ $z_{vp}, z_{qp}=0$. Λ_{1} and γ that are constants employed for the interpolation of the Plastic Yield Envelope Plastic hardening modulus are $\Lambda_{1}=5$ and $\gamma=1$. Also, $v=1.627$ (specific volume) and the initial stresses are the ones of the center of PYE in the beginning of the loading. Center of yield surface is the initial stresses of hydrostatic component only. Boundary conditions full fixed supports in the bottom of the box (i. e. for $Z=0$ $u_x = u_y = u_z = 0$). Loading in the upper surface of the box in the vertical direction (100 Non linear increments) as follows

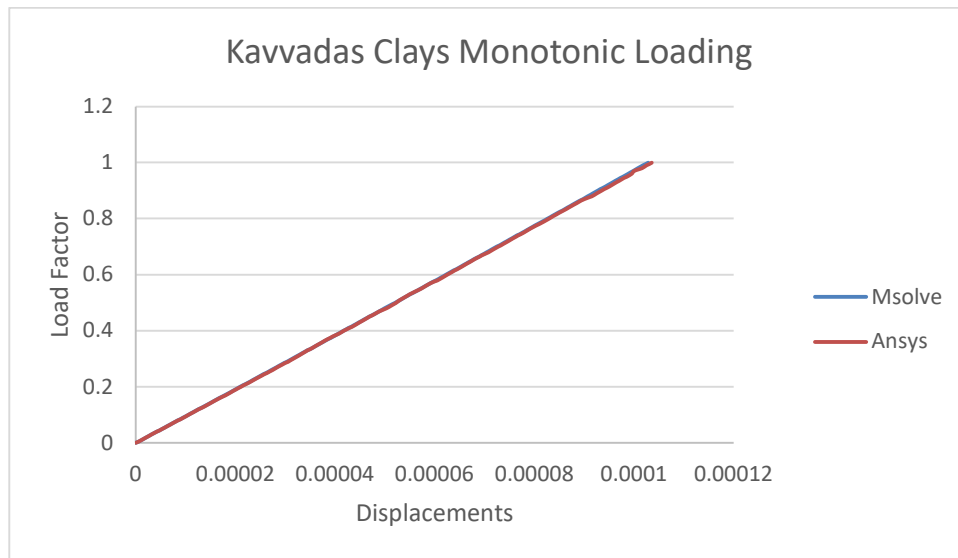
X	Y	Z	Amount (KN)
0	0	2	-0,375
0	1	2	-0,750
0	2	2	-0,375
1	0	2	-0,750
1	1	2	-1,500
1	2	2	-0,750
2	0	2	-0,375
2	1	2	-0,750
2	2	2	-0,375

Monitor output dof is for point

X	Y	Z
1	1	2

In Z direction (Number 41 of Dof and number 52 in suitesparse solver)

Load Displacement Curve and Comparison with Mohr Coulomb with $\phi=\psi=0$ which should be very close referring to the yield surfaces. (Max Relative Divergence from Ansys %)



Example 2

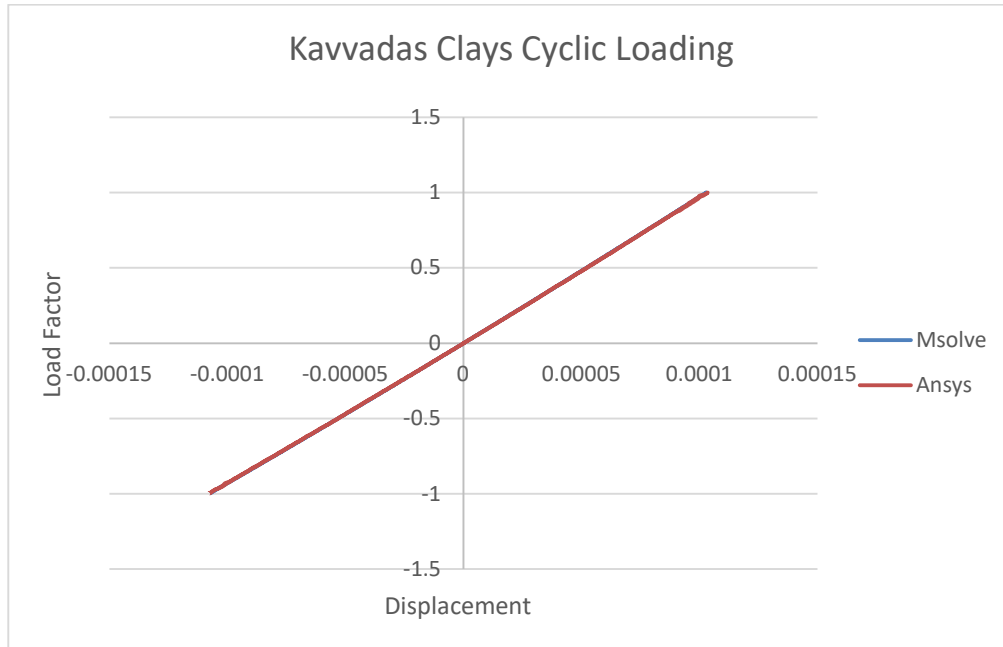
Exactly as Example 1 but with Cyclic loading in the upper surface of the box in the vertical direction (100 Non linear increments/path total 400 increments) with Load-Unload-Reverse load-Reverse unload path as follows

X	Y	Z	Amount (KN)
0	0	2	-0,375
0	1	2	-0,750
0	2	2	-0,375
1	0	2	-0,750
1	1	2	-1,500
1	2	2	-0,750
2	0	2	-0,375
2	1	2	-0,750
2	2	2	-0,375

Monitor output dof is for point

X	Y	Z
1	1	2

In Z direction (Number 41 of Dof and number 52 in suitesparse solver)
Load Displacement Curve. (Max Relative Divergence from Ansys %)



FiberBeam3D with Masing yield criterion Examples

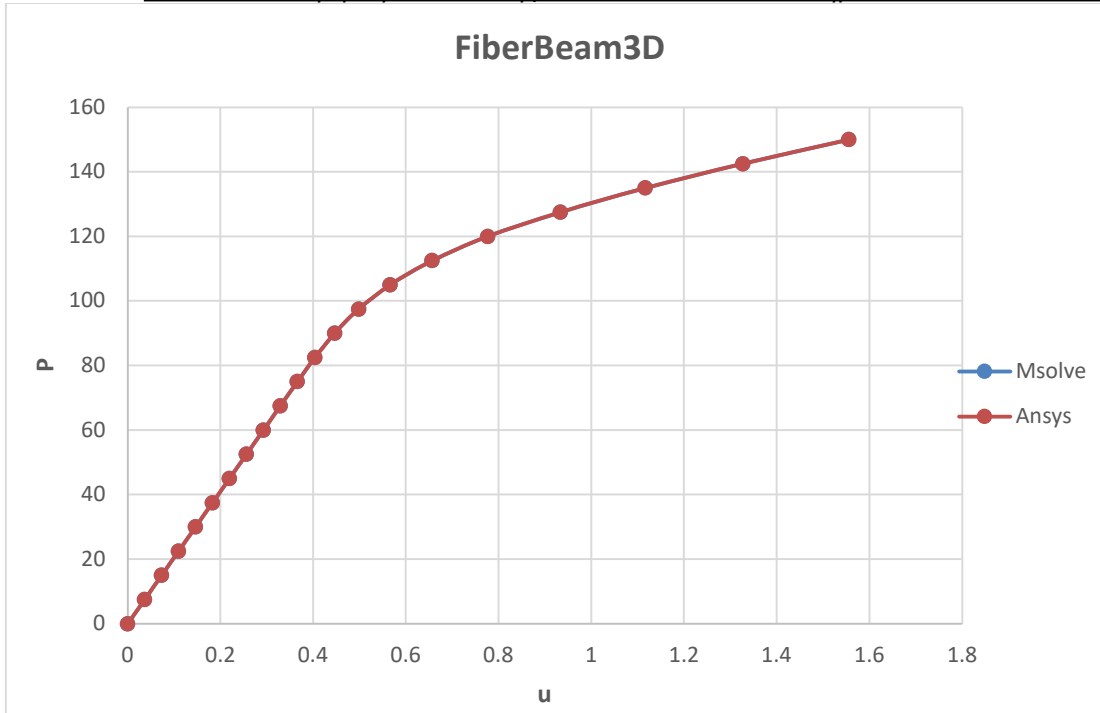
Example 1

Cantilever with $L=10\text{m}$, Section Area $A=b \times h=0,25 \times 0,25$. Upper Fibers with thickness of b $t_b=0.05$ (5 fibers) and Fibers with thickness of h $t_h=0.01$ (25 Fibers). The discretization consists of two elements of 5 m each with Young's modulus $E=210 \text{ GPa}$, tangent Young's modulus $E_t=21\text{GPa}$, $\nu=0,3$, $\sigma_y=275 \text{ MPa}$. The loading is monotonic, uniaxial in the upper surface of the cantilever in the vertical direction (20 increments and 100 increments respectively) with magnitude of $P=150 \text{ KN}$.

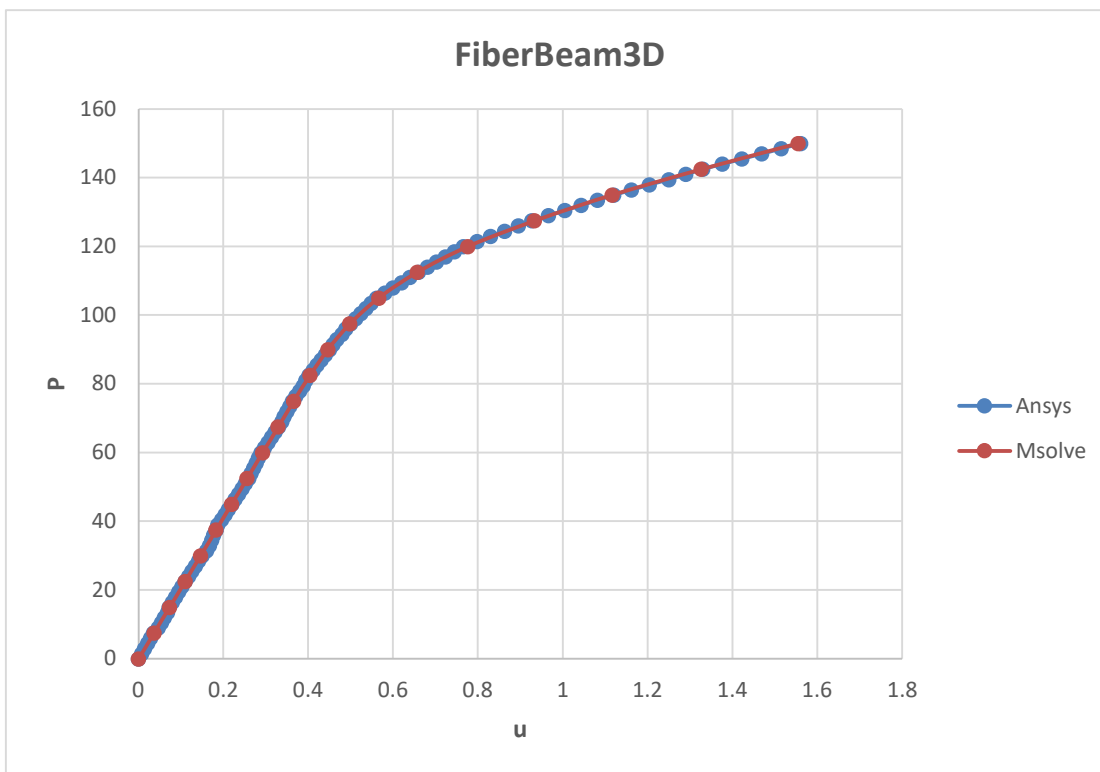
The Masing yield criterion is actually a pure kinematic hardening

Boundary conditions full fixed supports at the left of the beam (i. e. for $Z=0$ $u_x = u_y = u_z = 0$).

Load Displacement Curve (Max Relative Divergence from Ansys 0.9% found in comparison to MSolve).



Σχήμα 1: P - u with 20 increments as loading



Σχήμα 2: P - u with 100 increments as loading

Example 2

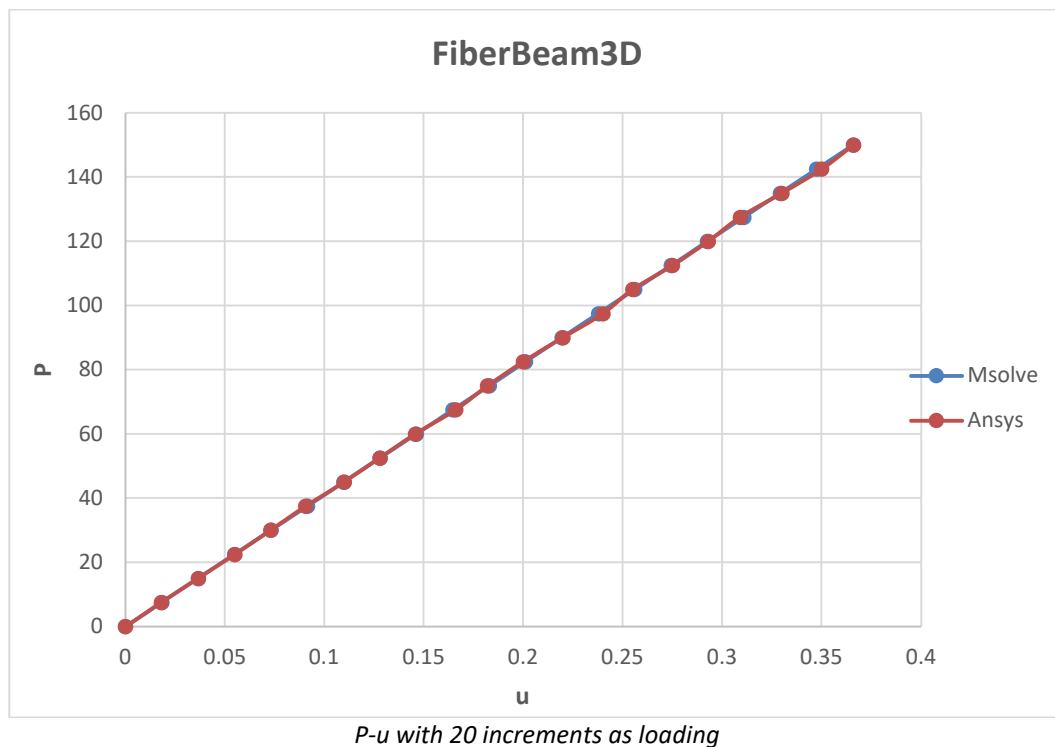
Cantilever with $L=10\text{m}$, Section Area $A=b \times h=0,25 \times 0,25$. Upper Fibers with thickness of b $t_b=0.05$ (5 fibers) and Fibers with thickness of h $t_h=0.01$ (25 Fibers). The discretization consists of two elements of 5 m each with Young's modulus $E=210 \text{ GPa}$, tangent Young's modulus $E_t=21\text{GPa}$, $\nu=0,3$, $\sigma_y=275$

MPa. The loading is monotonic, biaxial in the upper surface of the cantilever in the horizontal and vertical direction (20 increments and 100 increments respectively) with magnitude of $P_x=75\text{KN}=P_y$ at its right edge.

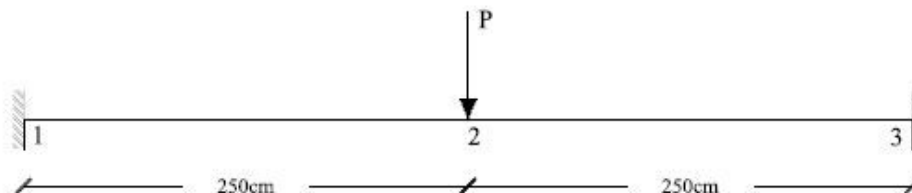
The Masing yield criterion is actually a pure kinematic hardening

Boundary conditions full fixed supports at the left of the beam (i. e. for $Z=0$ $u_x = u_y = u_z = 0$).

Load Displacement Curve (Max Relative Divergence from Ansys 1.5% found in comparison to MSolve).



Example 3

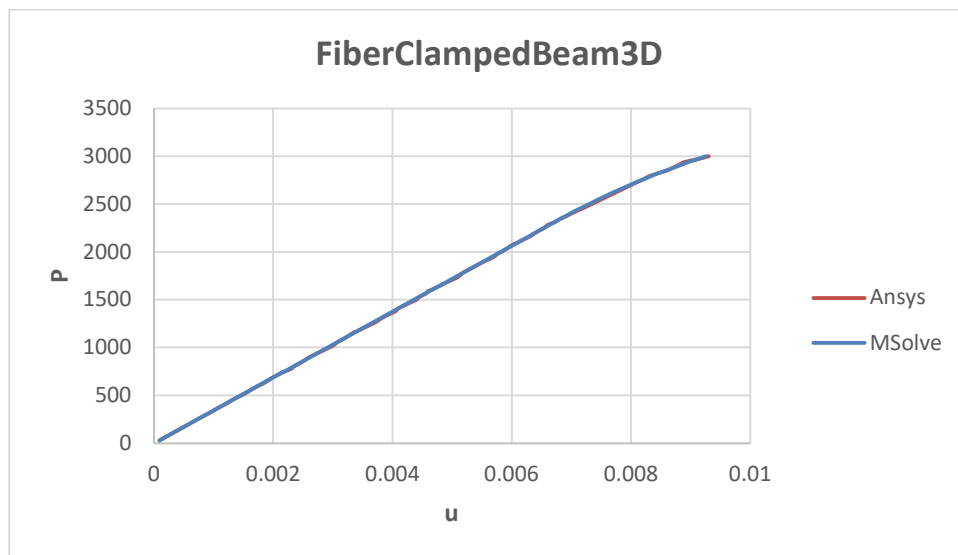
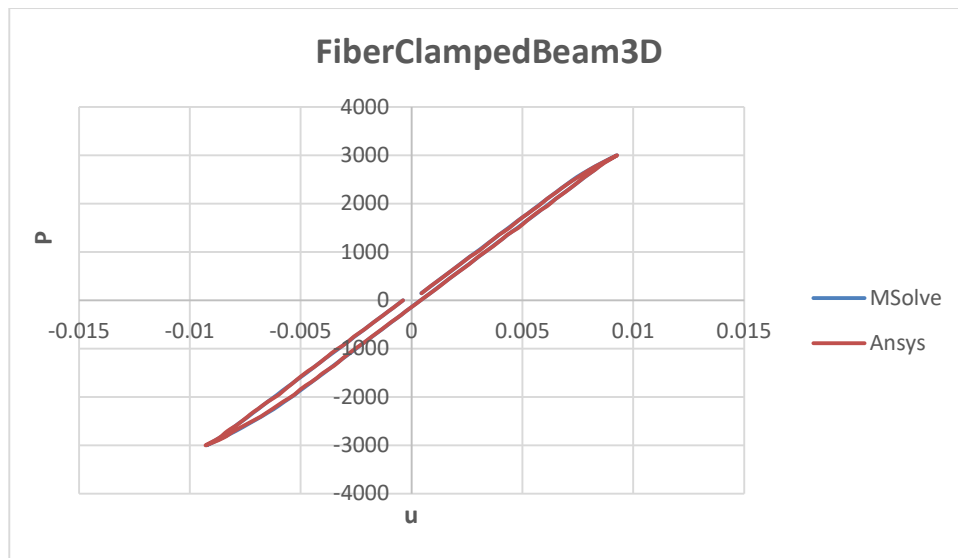


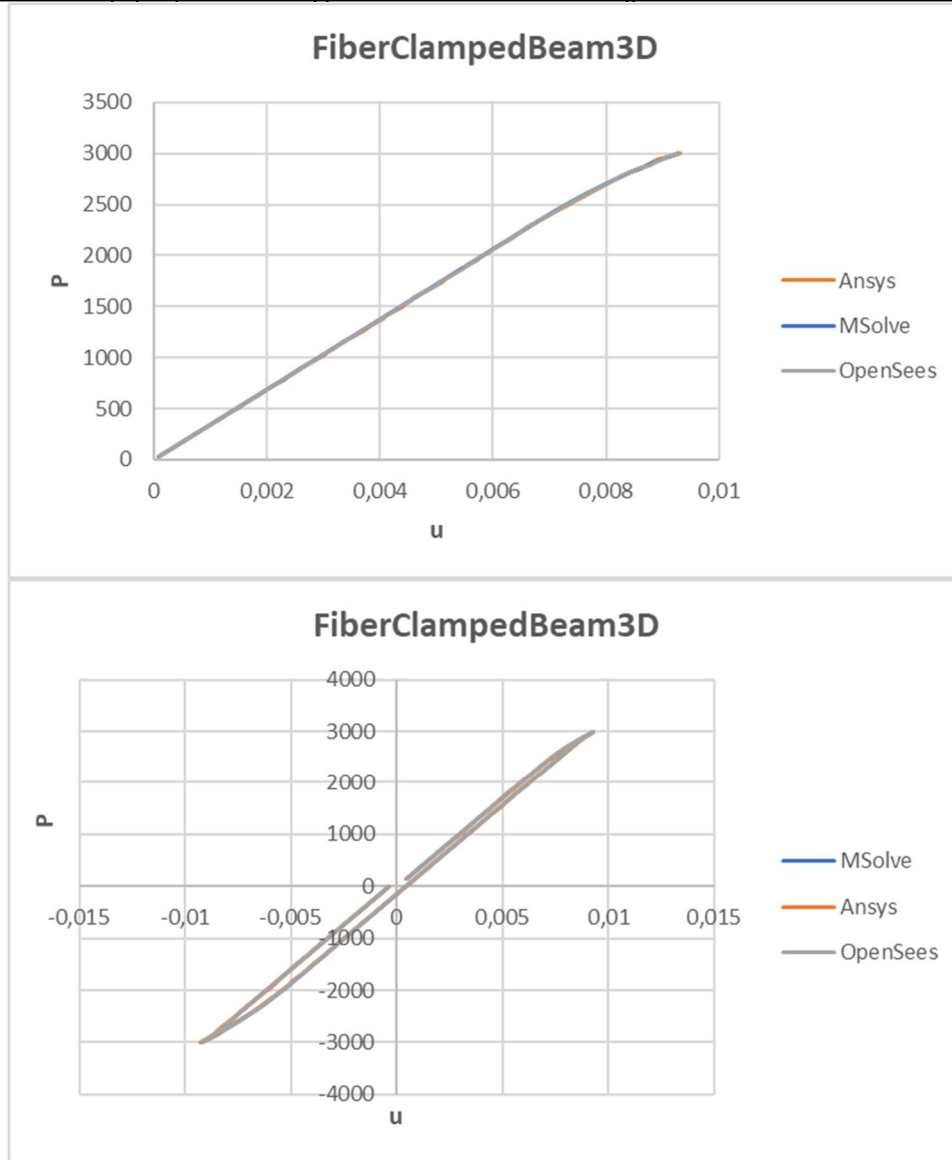
For the clamped beam of the figure with rectangular shape $b \times h = 0,2 \times 0,4$ m. Fibers with thickness of b $t_b = 0.04$ (5 fibers) and Fibers with thickness of h $t_h = 0,016$ (25 Fibers). The discretization consists of two elements of 2,5 m each with Young's modulus $E = 210$ GPa, tangent Young's modulus $E_t = 21$ GPa, $\nu = 0,3$, $\sigma_y = 275$ MPa. Monotonic loading and cyclic loading of 3000

KN with 100 increments The Masing yield criterion is actually a pure kinematic hardening

Boundary conditions full fixed supports (i. e. for $x=0$ and $x=5$ m $u_x = u_y = u_z = 0$).

Load Displacement Curve (Max Relative Divergence from Ansys 1,43% and 1,59% respectively found in comparison to MSolve less than 1% the corresponding errors for Opensees).





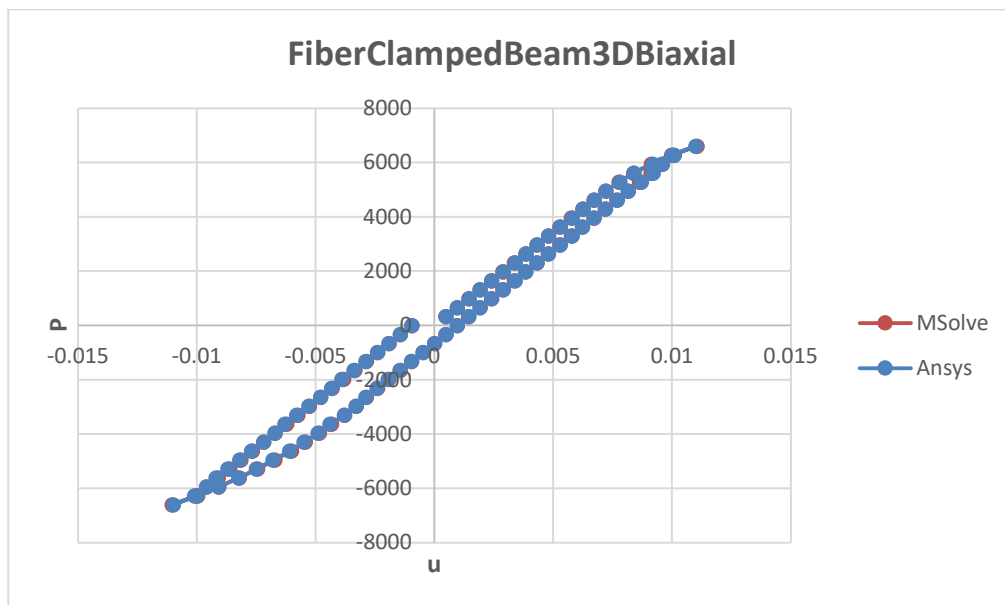
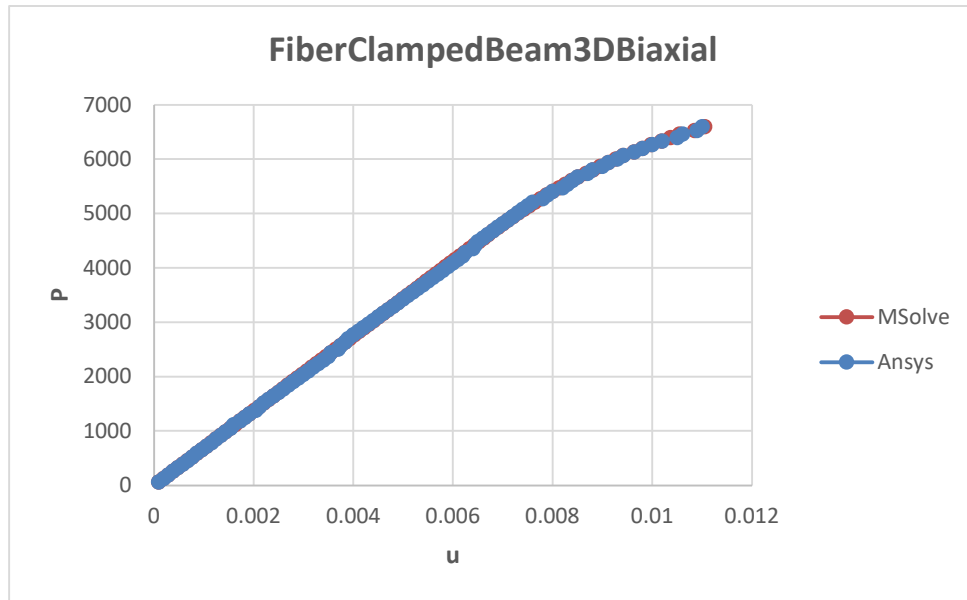
Example 4

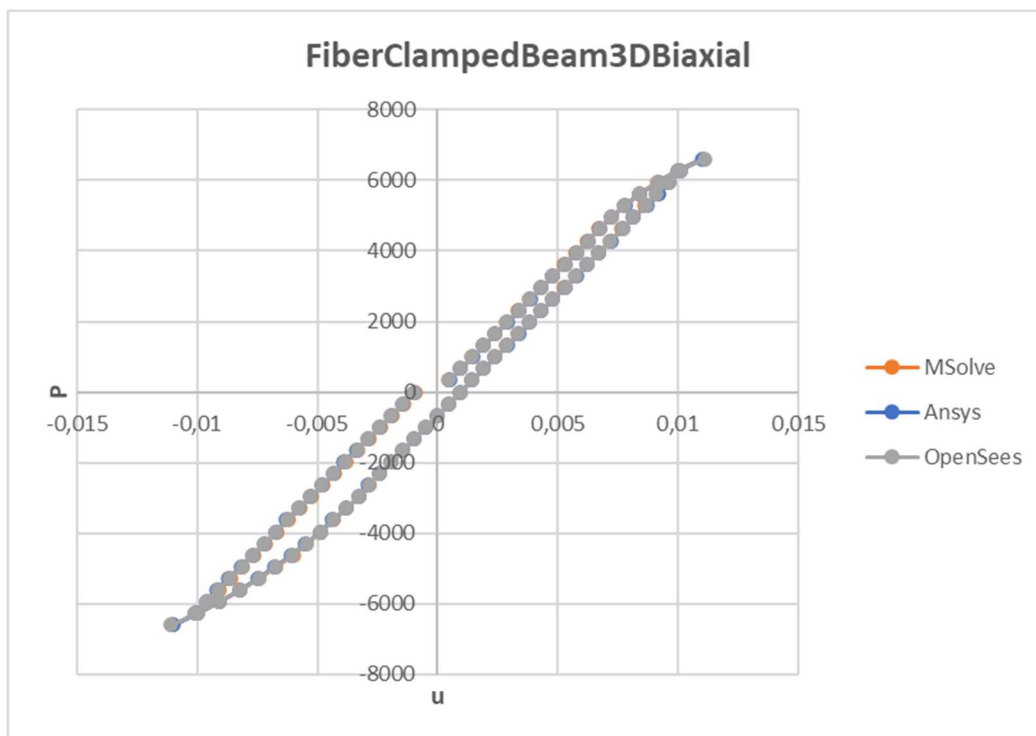
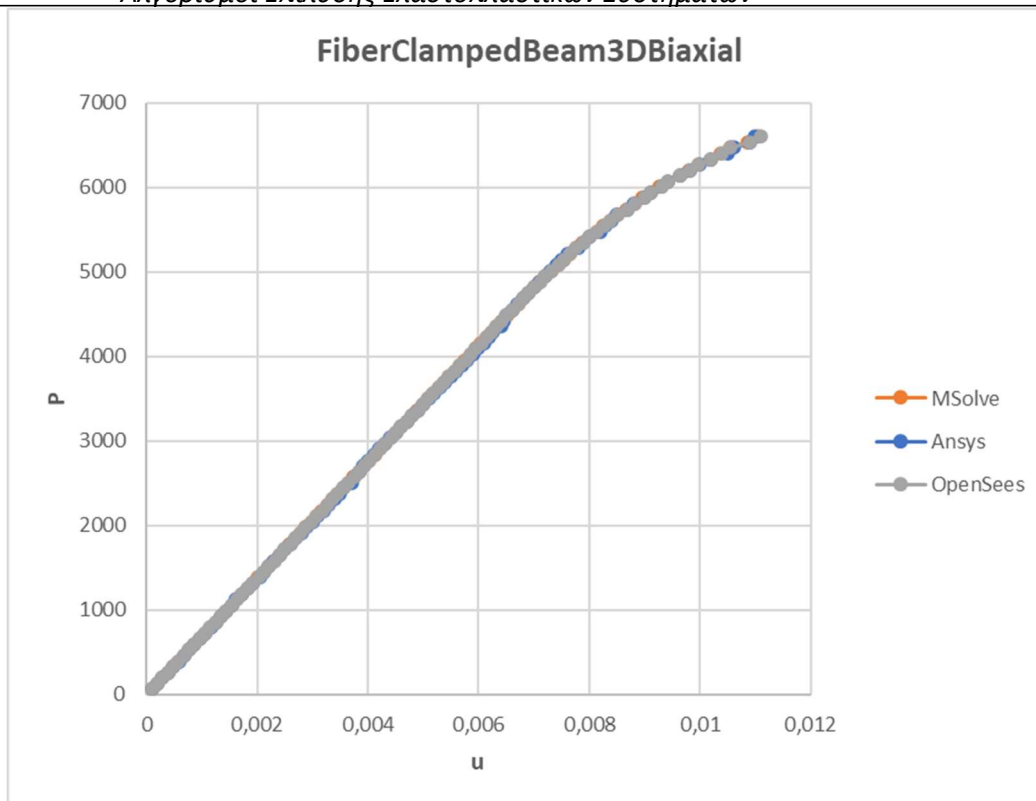
For the previous case of the clamped beam with rectangular shape $b \times h = 0,2 \times 0,4$ m. Fibers with thickness of b $t_b = 0.04$ (5 fibers) and Fibers with thickness of h $t_h = 0,016$ (25 Fibers). The discretization consists of two elements of 2,5 m each with Young's modulus $E = 210$ GPa, tangent Young's modulus $E_t = 21$ GPa, $\nu = 0,3$, $\sigma_y = 275$ MPa. Monotonic loading, biaxial in the upper surface of the clamped beam in the horizontal and vertical direction (100 increments) with magnitude of $P_z = 3300$ KN = P_y at its centre of the beam and cyclic loading of $P_z = 3300$ KN = P_y at its centre of the beam with 4×20 increments.

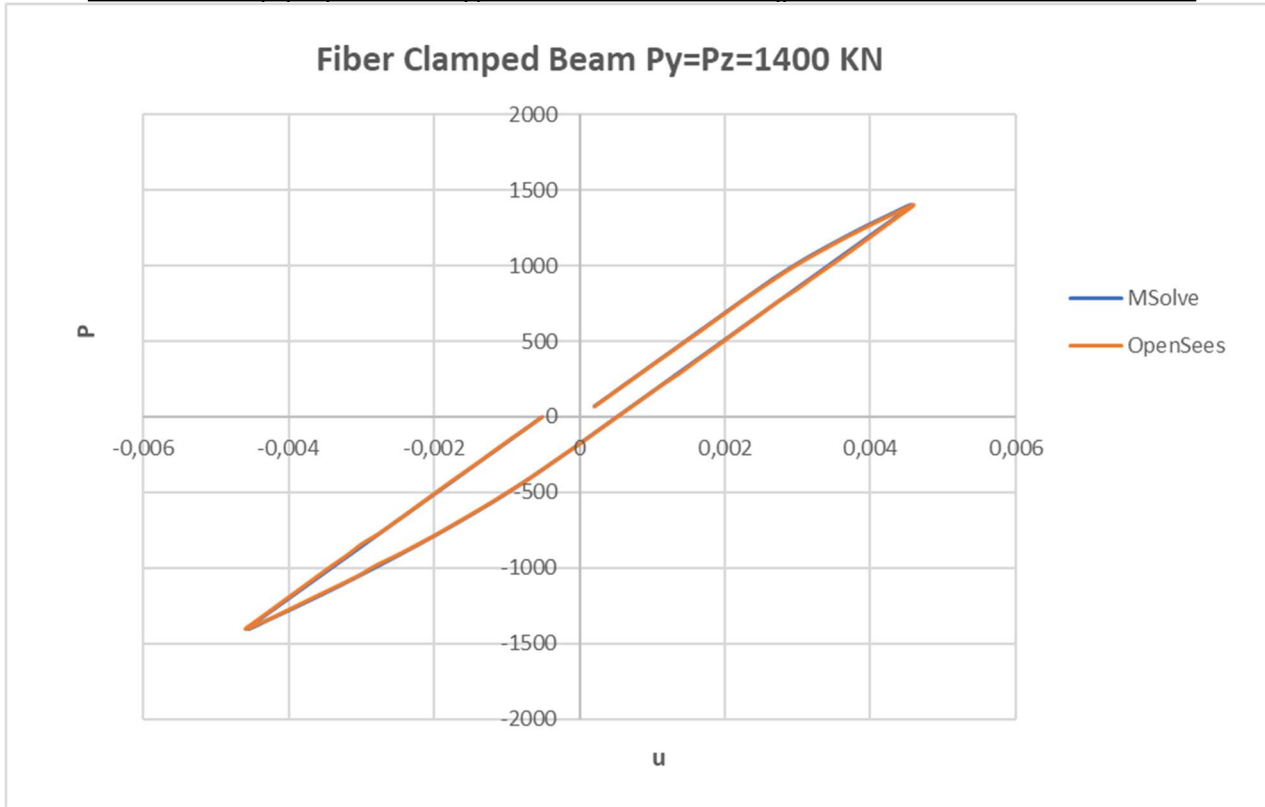
The Masing yield criterion is actually a pure kinematic hardening

Boundary conditions full fixed supports (i. e. for $x=0$ and $x=5$ m $u_x = u_y = u_z = 0$).

Also the same analysis was conducted with $P_z=1400\text{KN}= P_y$
Load Displacement Curve (Max Relative Divergence from Ansys 1,43% and 1,59% respectively found in comparison to MSolve less than 1% the corresponding errors for Openssees).





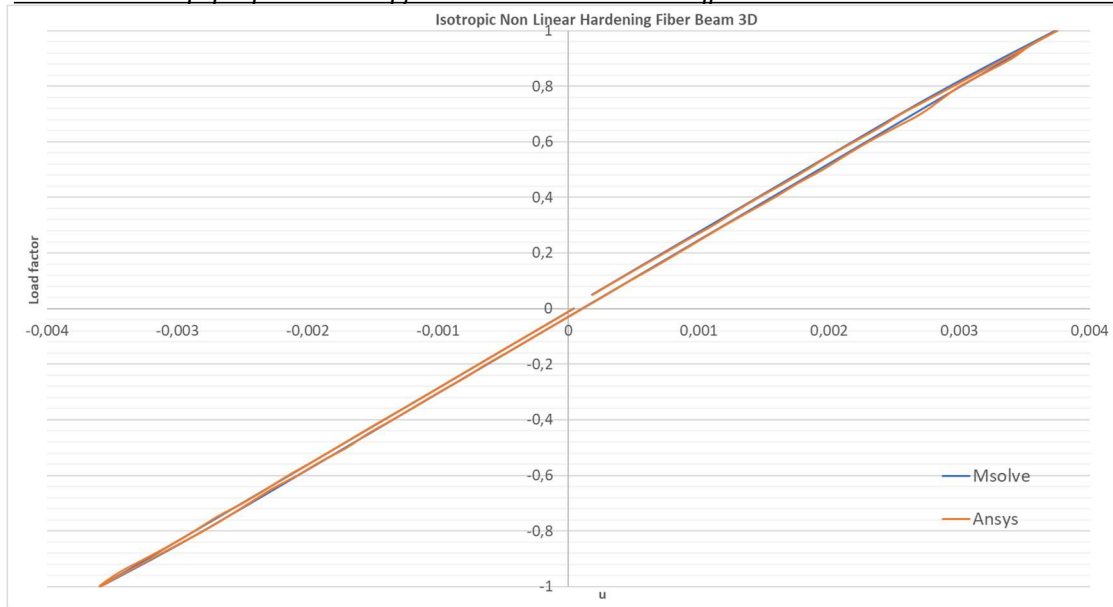


Example 5

For the previous case of the clamped beam with rectangular shape $b \times h = 0,2 \times 0,4$ m. Fibers with thickness of b $t_b = 0.04$ (5 fibers) and Fibers with thickness of h $t_h = 0,016$ (25 Fibers). The discretization consists of two elements of 2,5 m each with Young's modulus $E = 210$ GPa, tangent Young's modulus $E_t = 21$ GPa, $\nu = 0,3$, $\sigma_y = 275$ MPa. Cyclic loading, biaxial in the upper surface of the clamped beam in the horizontal and vertical direction (100 increments) with magnitude of $P_z = 1250$ KN = P_y at its centre of the beam and cyclic loading of $P_z = 1250$ KN = P_y at its centre of the beam with 4×20 increments.

Only isotropic hardening with curve $\sigma_y = \sigma_{y0} e^{\frac{\varepsilon_{pl}}{0,001}}$ discrete for values of ε_{pl} $[0,0,001]$ with step 10^{-6} . Boundary conditions full fixed supports (i. e. for $x=0$ and $x=5$ m $u_x = u_y = u_z = 0$).

Load Displacement Curve (Max Relative Divergence from Ansys 1,43% and 1,59% respectively found in comparison to MSolve less than 1% the corresponding errors for Ansys).

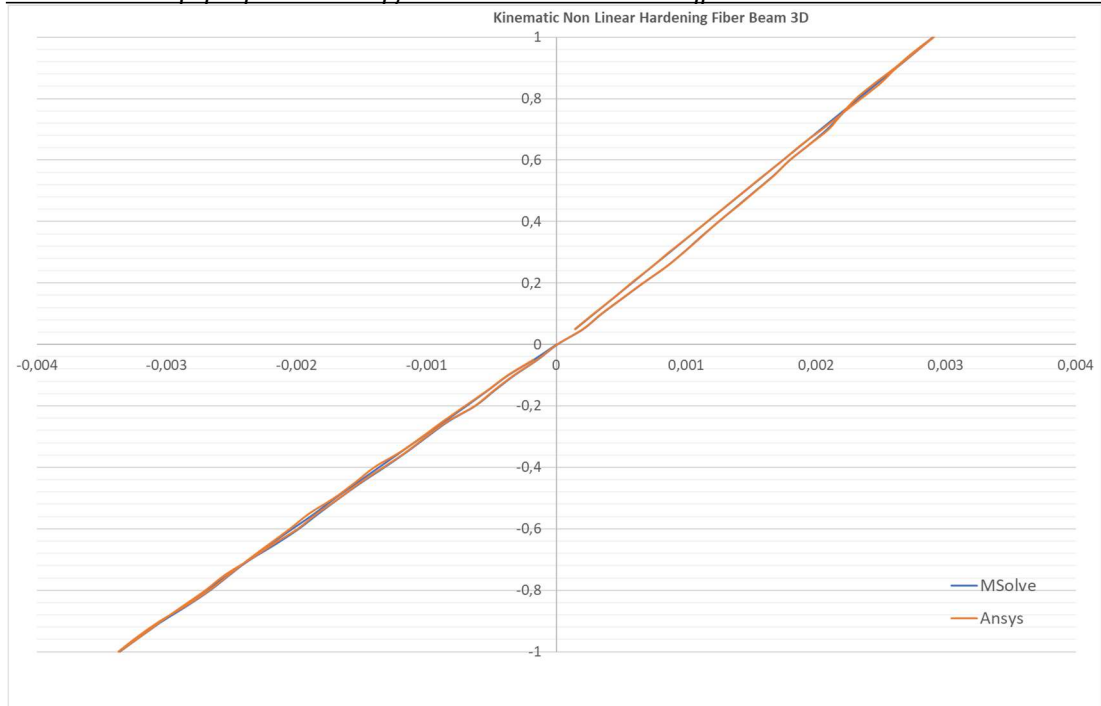


Example 6

For the previous case of the clamped beam with rectangular shape $b \times h = 0,2 \times 0,4$ m. Fibers with thickness of b $t_b = 0,04$ (5 fibers) and Fibers with thickness of h $t_h = 0,016$ (25 Fibers). The discretization consists of two elements of 2,5 m each with Young's modulus $E = 210$ GPa, tangent Young's modulus $E_t = 21$ GPa, $\nu = 0,3$, $\sigma_y = 275$ MPa. Cyclic loading, biaxial in the upper surface of the clamped beam in the horizontal and vertical direction (100 increments) with magnitude of $P_z = 1000$ KN = P_y at its centre of the beam and cyclic loading of $P_z = 1000$ KN = P_y at its centre of the beam with 4×20 increments.

Only kinematic hardening with curve $a(\text{Kpa}) = 275000(1 - e^{-8.97 \times 1000 \times \varepsilon_{pl}})$ discrete for values of ε_{pl} $[0, 0,001]$ with step 10^{-6} . Boundary conditions full fixed supports (i. e. for $x=0$ and $x=5$ m $u_x = u_y = u_z = 0$).

Load Displacement Curve (Max Relative Divergence from Ansys 1,43% and 1,59% respectively found in comparison to MSolve less than 1% the corresponding errors for Ansys).

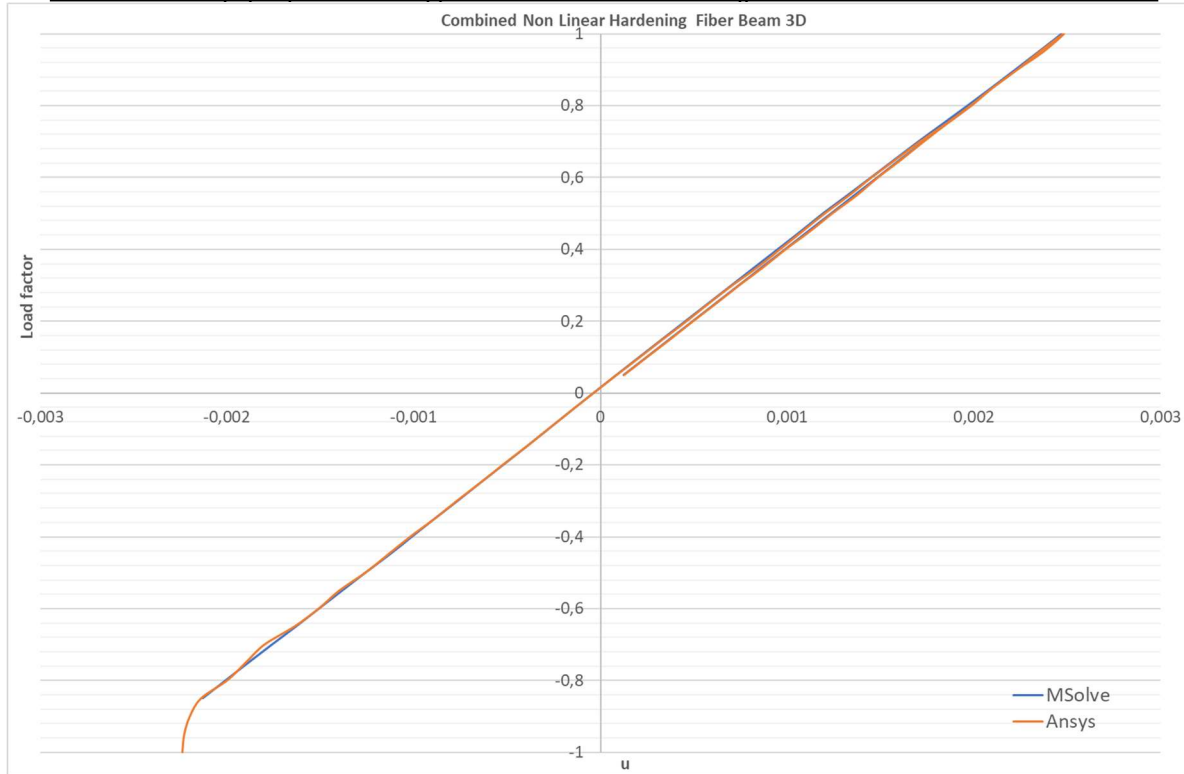


Example 7

For the previous case of the clamped beam with rectangular shape $b \times h = 0,2 \times 0,4$ m. Fibers with thickness of b $t_b = 0,04$ (5 fibers) and Fibers with thickness of h $t_h = 0,016$ (25 Fibers). The discretization consists of two elements of 2,5 m each with Young's modulus $E = 210$ GPa, tangent Young's modulus $E_t = 21$ GPa, $\nu = 0,3$, $\sigma_y = 275$ MPa. Cyclic loading, biaxial in the upper surface of the clamped beam in the horizontal and vertical direction (100 increments) with magnitude of $P_z = 850$ kN = P_y at its centre of the beam and cyclic loading of $P_z = 850$ kN = P_y at its centre of the beam with 4×20 increments.

Combined hardening with isotropic hardening curve $\sigma_y = \sigma_{y0} e^{\frac{\varepsilon_{pl}}{0,001}}$ discrete for values of ε_{pl} $[0,0,001]$ with step 10^{-6} and kinematic hardening curve α (Kpa) $= 275000(1 - e^{-8.97 \times 1000 \times \varepsilon_{pl}})$ discrete for values of ε_{pl} $[0,0,001]$ with step 10^{-6} . Boundary conditions full fixed supports (i. e. for $x=0$ and $x=5$ m $u_x = u_y = u_z = 0$).

Load Displacement Curve (Max Relative Divergence from Ansys 1,43% and 1,59% respectively found in comparison to MSolve less than 1% the corresponding errors for Ansys).



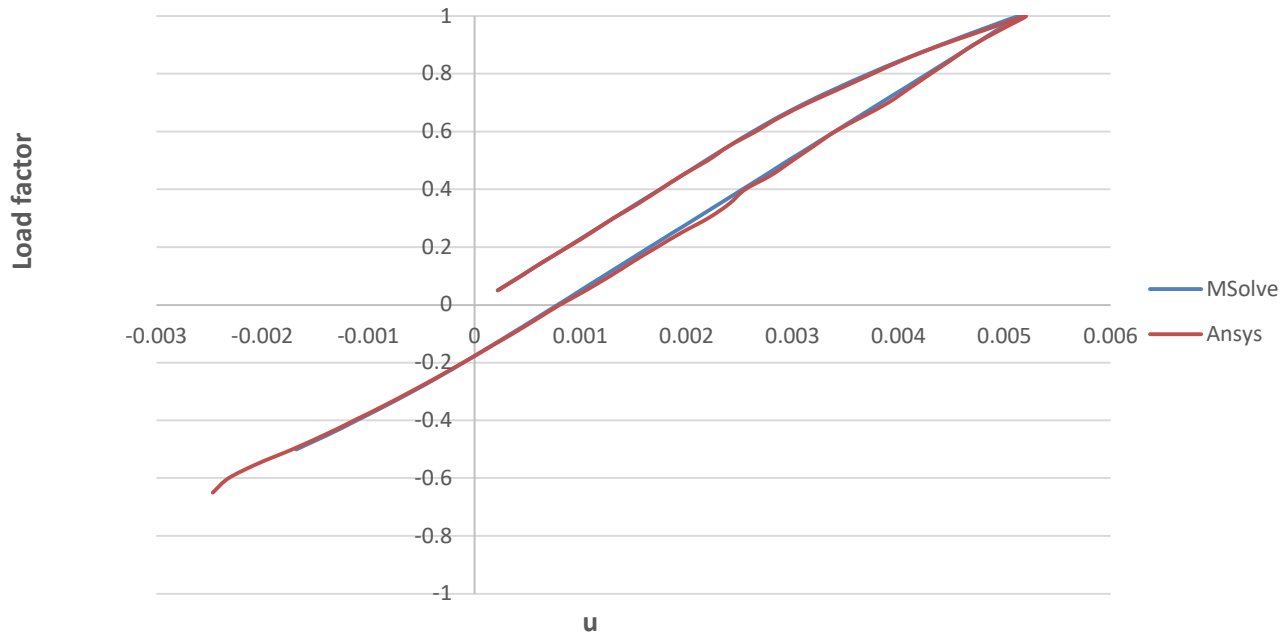
Example 8

For the previous case of the clamped beam with rectangular shape $b \times h = 0,2 \times 0,4$ m. Fibers with thickness of b $t_b = 0.04$ (5 fibers) and Fibers with thickness of h $t_h = 0,016$ (25 Fibers). The discretization consists of two elements of 2,5 m each with Young's modulus $E = 210$ GPa, Poissons coefficient $\nu = 0,3$, yield stress $\sigma_{y0} = 275$ MPa. Cyclic loading, biaxial in the upper surface of the clamped beam in the horizontal and vertical direction (100 increments) with magnitude of $P_z = 1500 \text{ KN} = P_y$ at its centre of the beam and cyclic loading of $P_z = 1500 \text{ KN} = P_y$ at its centre of the beam with 4×20 increments.

Only isotropic hardening with curve $\sigma_y = \sigma_{y0} e^{(\epsilon_{pl} * \lambda)}$, where $\lambda = 20$ (consistency parameter), discrete for values of ϵ_{pl} $[0, 0.1]$ with step 10^{-6} . Boundary conditions full fixed supports (i. e. for $x=0$ and $x=5$ m $u_x = u_y = u_z = 0$).

Load Displacement Curve (Max Relative Divergence from Ansys 5,08% respectively found in comparison to MSolve).

Isotropic Non Linear Hardening Fiber Beam 3D

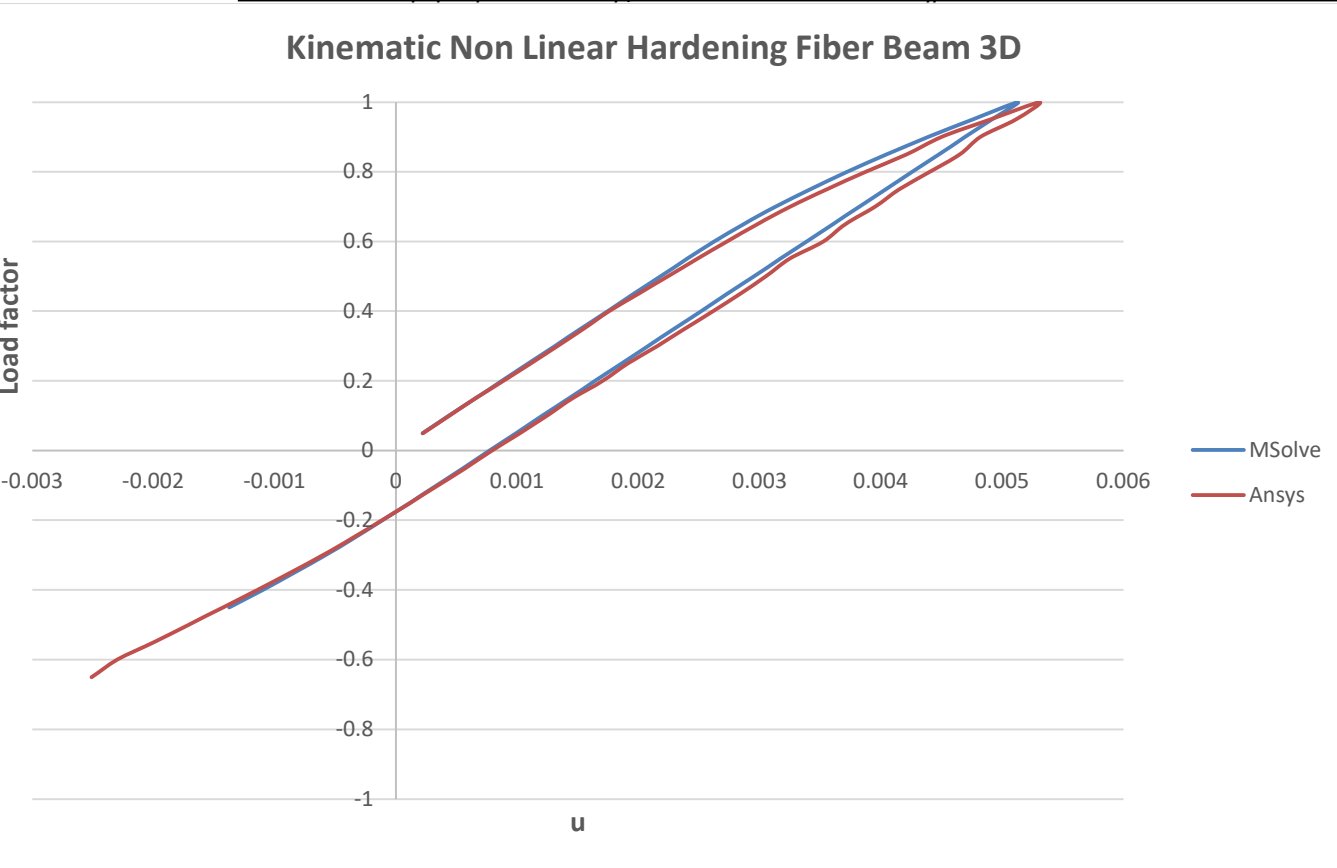


Example 9

For the previous case of the clamped beam with rectangular shape $b \times h = 0,2 \times 0,4$ m. Fibers with thickness of b $t_b = 0,04$ (5 fibers) and Fibers with thickness of h $t_h = 0,016$ (25 Fibers). The discretization consists of two elements of 2,5 m each with Young's modulus $E = 210$ GPa, $\nu = 0,3$, $\sigma_{y0} = 275$ MPa. Cyclic loading, biaxial in the upper surface of the clamped beam in the horizontal and vertical direction (100 increments) with magnitude of $P_z = 1500$ KN = P_y at its centre of the beam and cyclic loading of $P_z = 1500$ KN = P_y at its centre of the beam with 4×20 increments.

Only kinematic hardening with curve $a(\text{Kpa}) = \frac{C_1}{\gamma_1} (1 - e^{-\gamma_1 * \epsilon_{pl}}) = \frac{31638000}{277,32} (1 - e^{-277,32 * \epsilon_{pl}})$ where C_1, γ_1 parameters associated with the magnitude and rate of backstress component account for the decrease in the initial yield stress for mild structural steels, discrete for values of ϵ_{pl} $[0, 0.1]$ with step 10^{-6} . Boundary conditions full fixed supports (i. e. for $x=0$ and $x=5$ m $u_x = u_y = u_z = 0$).

Load Displacement Curve (Max Relative Divergence from Ansys 3,94% respectively found in comparison to MSolve).



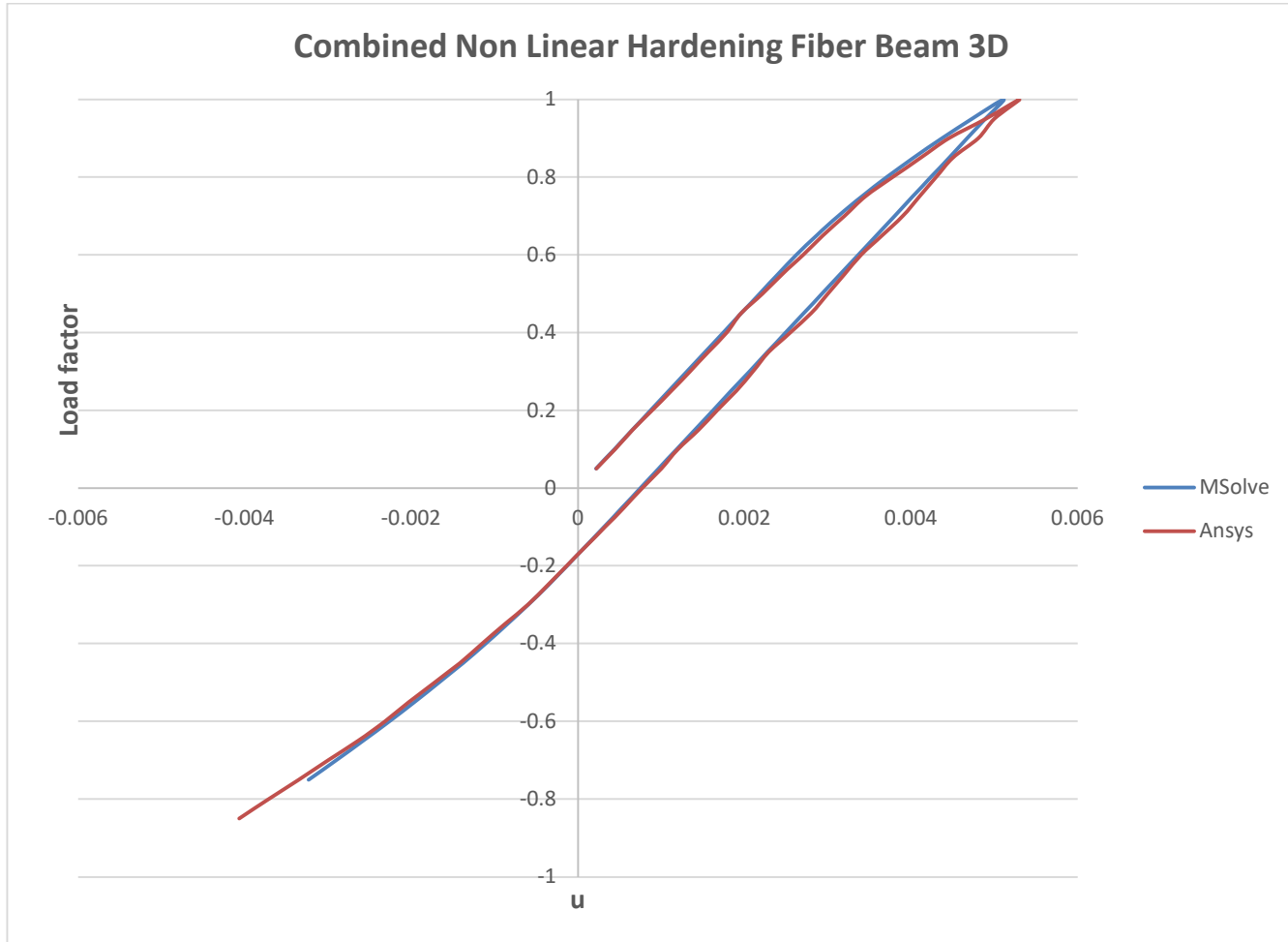
Example 10

For the previous case of the clamped beam with rectangular shape $b \times h = 0,2 \times 0,4 \text{ m} \times \text{m}$. Fibers with thickness of $b \text{ } t_b = 0,04$ (5 fibers) and Fibers with thickness of $h \text{ } t_h = 0,016$ (25 Fibers). The discretization consists of two elements of 2,5 m each with Young's modulus $E = 210 \text{ GPa}$, $\nu = 0,3$, $\sigma_y = 275 \text{ MPa}$. Cyclic loading, biaxial in the upper surface of the clamped beam in the horizontal and vertical direction (100 increments) with magnitude of $P_z = 1500 \text{ KN} = P_y$ at its centre of the beam and cyclic loading of $P_z = 1500 \text{ KN} = P_y$ at its centre of the beam with 4×20 increments.

Combined hardening with isotropic hardening curve $\sigma_y = \sigma_{y0} e^{(\varepsilon_{pl} * \lambda)}$, where $\lambda = 20$ (consistency parameter), discrete for values of $\varepsilon_{pl} [0,0.1]$ with step 10^{-6} and kinematic hardening curve $a(\text{KPa}) = \frac{C_1}{\gamma_1} (1 - e^{-\gamma_1 * \varepsilon_{pl}}) = \frac{31638000}{277,32} (1 - e^{-277,32 * \varepsilon_{pl}})$ where $C_1 (\text{KPa})$, γ_1 parameters associated with the magnitude and rate of backstress component account for the decrease in the initial yield stress for mild

structural steels, discrete for values of ε_{pl} [0,0.1] with step 10^{-6} . Boundary conditions full fixed supports (i. e. for $x=0$ and $x=5$ m $u_x = u_y = u_z = 0$).

Load Displacement Curve (Max Relative Divergence from Ansys 3,86% respectively found in comparison to MSolve).



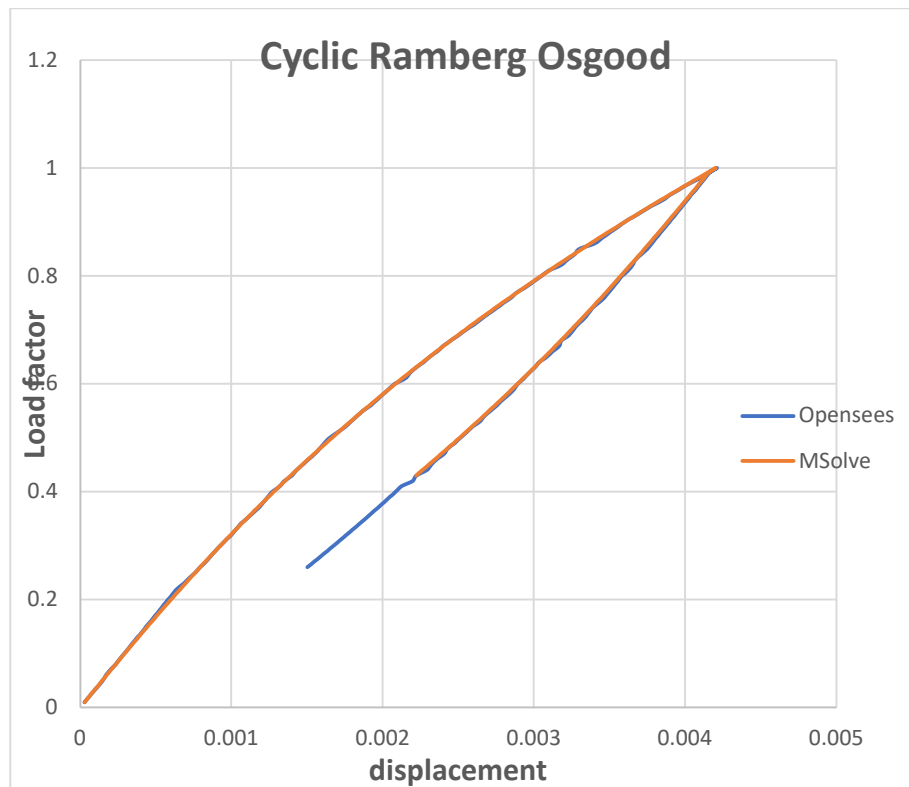
Example 11

For the previous case of the clamped beam with rectangular shape $b \times h = 0,2 \times 0,4$ m x m. Fibers with thickness of b $t_b = 0.04$ (5 fibers) and Fibers with thickness of h $t_h = 0,016$ (25 Fibers). The discretization consists of two elements of 2,5 m each with Young's modulus $E = 210$ GPa, $\nu = 0,3$, $\sigma_{yo} = 300$ MPa (initial yield stress). Cyclic loading, biaxial in the upper surface of the clamped beam in the horizontal and vertical direction (100 increments) with magnitude of $P_z = 1000$ KN = P_y at its centre of the beam and cyclic loading of $P_z = 1000$ KN = P_y at its centre of the beam with 4×100 increments.

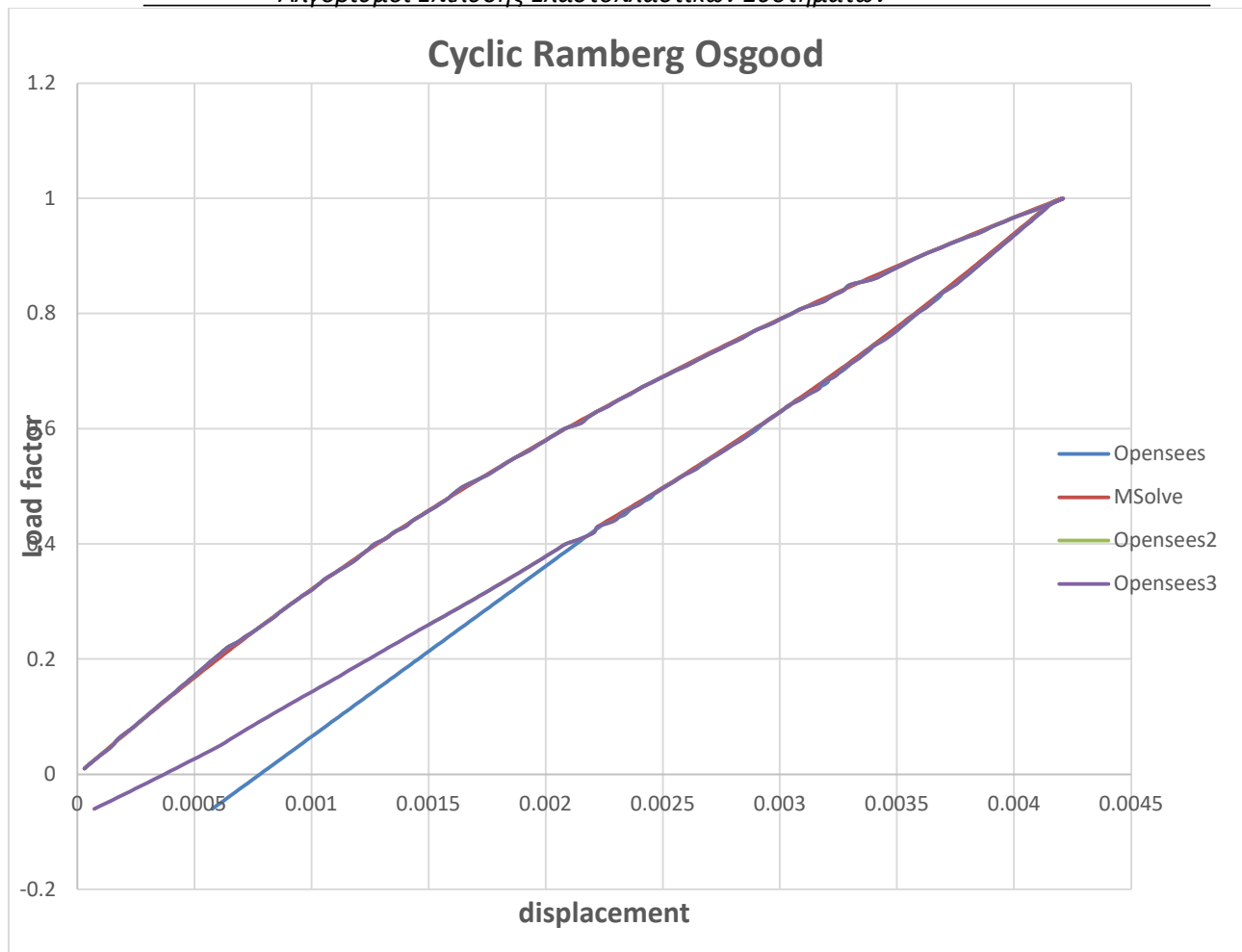
Ramberg Osgood curve $\varepsilon^{tot} = \frac{\sigma}{E} + \alpha \left(\frac{\sigma}{\sigma_{yo}} \right)^n$, where n is material strain-hardening

exponent and it is equal to $n = 2,821670429$, which controls the hardening of the material, as if “n” increases, the hardening ratio will be decreased respectively and $a = \alpha_{offset} = 0,2\% = 0,002$ (commonly used value) referred as “yield offset”. Boundary conditions full fixed supports at the left of the beam (i. e. for $Z=0$ $u_x = u_y = u_z = 0$).

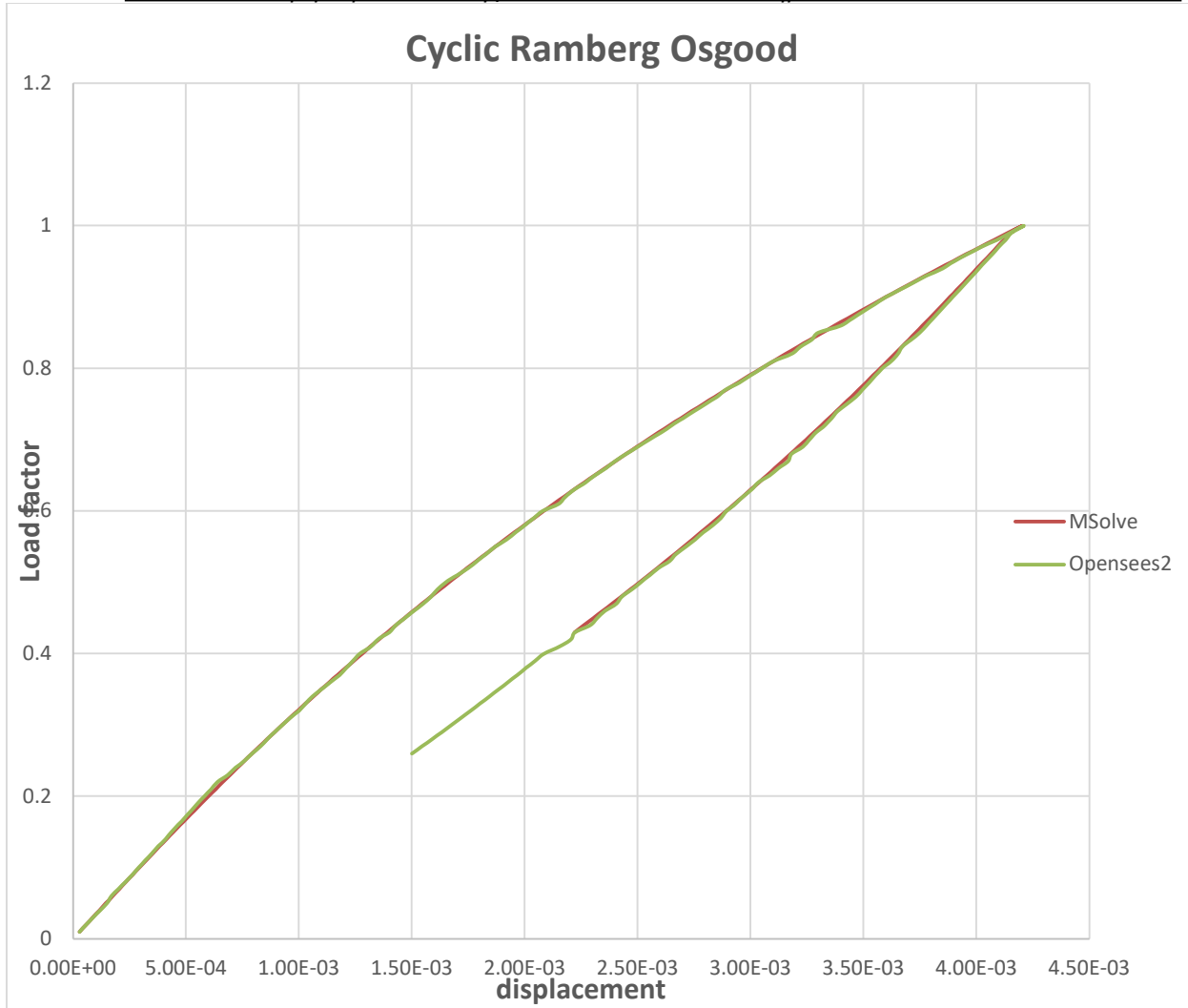
Load Displacement Curve (Max Relative Divergence from Ansys 1 % found in comparison to MSolve).



Comparison of MSolve and Opensees for a certain amount of the numerical damping value



Comparison of MSolve and Opensees for different values of the numerical damping ratio



Comparison of MSolve and Opensees for different values of the numerical damping ratio

ΚΕΦΑΛΑΙΟ 6th

6 CONCLUSIONS

6.1 GENERAL CONCLUSIONS

The purpose of this master's thesis is to describe in detail the numerical techniques used in the theory and analysis of small deformations of elastic and inelastic solids using the finite element method. Particular emphasis is placed on the derivation and description of various constitutive laws of the models due to material nonlinearity - based on phenomenological elasticity, elastoplasticity by using various cases of yield criteria where it is determined whether a material has fractured or exceeded yield strength - as well as for the associated numerical procedures and the practical issues that arise in them when solved computationally. The range covered goes from basic infinitesimal isotropic to more sophisticated finite strain theories, including anisotropy. These numerical techniques are implemented with the aid of the commercial software packages, Ansys Workbench, as well as the open-source software code, MSolve, and a comparative study and analysis is presented between Ansys Workbench and MSolve. The results were plotted graphically. For the finite element simulations in nonlinear constitutive relations, the fiber beam - column model for nonlinear analysis of reinforced concrete structures, the commercial software package Ansys Workbench was selected. Due to the complexity of the problem of material nonlinearity and the description of nonlinear constitutive relations as well as the cyclic loading incorporating plasticity and the Bauschinger effect, a powerful computational tool was used, MSolve software, which solved quite complex problems with higher accuracy in the results and less computational time and cost than other commercial software packages. Several numerical examples have been done utilizing Von Mises, Tresca, Mohr-Coulomb, Drucker Prager with nonlinear hardening especially the constitutive law has an exponential form both for monotonic and cyclic loading. Also, the second case has to do with force-based three-dimensional fiber beam utilizing Masing yield criterion, Ramberg Osgood, Menegotto Pinto and Kent Park model for both monotonic and cyclic loading. The third case that is examined is the soil interaction, Kavvadas Clays yield criterion, which it describes and evaluates a critical-state incremental-plasticity model for structured soils (MSS). The model simulates the engineering effects of processes causing structure development (pre-consolidation, ageing, cementation, etc.) and structure degradation (remoulding by volumetric and/or deviatoric straining), such as high stiffness and strength at the intact states, appreciable reduction of stiffness and strength during destructuring, and the evolution of stress-induced and structure-induced anisotropy. A novel feature of the model is the treatment of pre-consolidation as a structure-inducing process and the unified description of all such processes via the BSE. The proposed model

distinguishes the concepts of 'yielding' (i.e. the onset of irreversible deformation upon reaching the PYE) and the onset of major de-structuring which occurs when the BSE is engaged. Thus, the model avoids the large elastic domain of critical state models and permits the development of irreversible strains even for small variations of the stress levels.

✓ For the first case of yield criteria for monotonic and cyclic loading:

- i. Because of the material nonlinearity, which has to do with the hardening law that was used, and it was in an exponential form, we could conclude that if we use as input more and more tabular data as stress and strains the behavior of the constitutive law between the two software, Ansys and Msolve, coincides. Actually, the yield point, the critical load in monotonic and the reversal load in cyclic arises to be of the same magnitude.
- ii. Load Displacement Curve (Max Relative Divergence from Ansys 6% found in 1st step the rest are in the vicinity of 1%) for the von mises yield criterion of nonlinear isotropic hardening. As for nonlinear kinematic hardening, Load Displacement Curve (Max Relative Divergence from Ansys 12% found in 1st step the rest are in the vicinity of 4%) and for the case of mixed nonlinear hardening, we have that Load Displacement Curve (Max Relative Divergence from Ansys 13% found in 1st step the rest are in the vicinity of 2%)
- iii. The same behavior is observed for the transient analysis, the time history curve has :

Peak	Msolve	Ansys	
0,1	0,034404	0,035	1,703179
0,05	0,034404	0,034512	0,313358
End	Msolve	Ansys	
0,1	0,00134	0,001286	-4,17941
0,05	0,000868	0,000851	-1,94076

- iv. Load Displacement Curve (Max Relative Divergence from Ansys 13% found in 1st step the rest are in the vicinity of 5%)
- v. For the cyclic loading, the comparison between the Msolve and Ansys software for the constitutive law of nonlinear isotropic, kinematic and combined hardening are Load Displacement Curve (Max Relative Divergence from Ansys 19% found in Cyclic reverse the rest are in the vicinity of 1%), Load Displacement Curve (Max Relative Divergence from Ansys 10% found in 1st step the rest are in the vicinity of 4%) and the Load Displacement Curve (Max Relative Divergence from Ansys 13% found in 1st step the rest are in the vicinity of 5%) respectively.
- vi. As for Tresca model, we have Load Displacement Curve and Comparison with Mohr Coulomb with $\phi=\psi=0$ which should be very close referring to the

yield surfaces. (Max Relative Divergence from Ansys 7,5% found in 1st step the rest are in the vicinity of 1%) for monotonic loading and Load Displacement Curve. (Max Relative Divergence from Ansys 3%) for cyclic loading in the upper surface of the box in the vertical direction (100 Nonlinear increments/path total 400 increments) with Load-Unload-Reverse load-Reverse unload path.

vii. As for Mohr -Coulomb model, we have Load Displacement Curve (Max Relative Divergence from Ansys 7% found in 1st step the rest are in the vicinity of 1%) for monotonic loading and Load Displacement Curve. (Max Relative Divergence from Ansys 2%) for cyclic loading in the upper surface of the box in the vertical direction (100 Nonlinear increments/path total 400 increments) with Load-Unload-Reverse Load-Reverse unload path.

viii. As for Drucker Prager model, we have Load Displacement Curve (Max Relative Divergence from Ansys 7% found in 1st step the rest are in the vicinity of 4%) for monotonic loading and the Load Displacement Curve. (Max Relative Divergence from Ansys 1%) for cyclic loading in the upper surface of the box in the vertical direction (100 Nonlinear increments/path total 400 increments) with Load-Unload-Reverse load-Reverse unload path.

✓ For the case of 3D fiber-beam forced-based element the conclusions are: In the present master thesis, the limitations of the original Masing model and recent modifications of this model have been used to analyse the monotonic and cyclic stress–strain response. The following points same been demonstrated:

- i. Masing-type models correlate directly with the microstructure established in deformed materials, and the discrete yield levels can account for the Bauschinger effect.
- ii. The cyclic stress–strain response under variable amplitude loading conditions can be predicted from Masing-type models even for materials that show non-Masing behaviour in constant amplitude loading tests.
- iii. Relationships between the various Masing-type models and the Ramberg–Osgood interpretation of stress–strain response can be established which allow calculation of parameters such as the energy expenditure and the stored elastic energy during monotonic and cyclic loading, respectively. In particular, a link has been established between the Ramberg–Osgood strength (A) and cyclic hardening (b) parameters.

- iv. Load Displacement Curve (Max Relative Divergence from Ansys 0.9% found in comparison to MSolve) for the case of nonlinear isotropic hardening for monotonic loading. Load Displacement Curve (Max Relative Divergence from Ansys 0.9% found in comparison to MSolve) for the case of nonlinear kinematic hardening for monotonic loading. Load Displacement Curve (Max Relative Divergence from Ansys 1,43% and 1,59% respectively found in comparison to MSolve less than 1% the corresponding errors for Opensees) for the case of nonlinear mixed hardening constitutive law for Monotonic loading, biaxial in the upper surface of the clamped beam in the horizontal and vertical direction (100 increments) with magnitude of $P_z=3300KN= P_y$ at its centre of the beam and cyclic loading of $P_z=3300KN= P_y$ at its centre of the beam with 4*20 increments.
- v. Load Displacement Curve (Max Relative Divergence from Ansys 5,08% respectively found in comparison to MSolve) for Only isotropic hardening with curve $\sigma_y = \sigma_{y0} e^{(\varepsilon_{pl} * \lambda)}$, where $\lambda = 20$ (consistency parameter), discrete for values of ε_{pl} [0, 0.1] with step 10^{-6} . Boundary conditions full fixed supports (i. e. for $x=0$ and $x=5$ m $u_x = u_y = u_z = 0$) for cyclic loading, biaxial in the upper surface of the clamped beam in the horizontal and vertical direction (100 increments) with magnitude of $P_z=1500KN= P_y$ at its centre of the beam and cyclic loading of $P_z=1500KN= P_y$ at its centre of the beam with 4*20 increments.
- vi. Load Displacement Curve (Max Relative Divergence from Ansys 3,94% respectively found in comparison to MSolve) for only kinematic hardening with curve $a(Kpa) = \frac{C_1}{\gamma_1} (1 - e^{-\gamma_1 * \varepsilon_{pl}}) = \frac{31638000}{277,32} (1 - e^{-277,32 * \varepsilon_{pl}})$ where C_1, γ_1 parameters associated with the magnitude and rate of backstress component account for the decrease in the initial yield stress for mild structural steels, for cyclic loading, biaxial in the upper surface of the clamped beam in the horizontal and vertical direction (100 increments) with magnitude of $P_z=1500KN= P_y$ at its centre of the beam and cyclic loading of $P_z=1500KN= P_y$ at its centre of the beam with 4*20 increments.
- vii. Load Displacement Curve (Max Relative Divergence from Ansys 3,86% respectively found in comparison to MSolve) for Combined hardening with isotropic hardening curve $\sigma_y = \sigma_{y0} e^{(\varepsilon_{pl} * \lambda)}$, where $\lambda = 20$ (consistency parameter), discrete for values of ε_{pl} [0,0.1] with step 10^{-6} and kinematic hardening curve $a(Kpa) = \frac{C_1}{\gamma_1} (1 - e^{-\gamma_1 * \varepsilon_{pl}}) = \frac{31638000}{277,32} (1 - e^{-277,32 * \varepsilon_{pl}})$ where $C_1 (KPa), \gamma_1$ parameters associated with the magnitude and rate of backstress component account for the decrease in the initial yield stress for mild structural steels for cyclic

- loading, biaxial in the upper surface of the clamped beam in the horizontal and vertical direction with magnitude of $P_z=1500\text{KN}=P_y$ at its centre of the beam with 4*20 increments.
- viii. Load Displacement Curve (Max Relative Divergence from Ansys 1 % found in comparison to MSolve) for Ramberg Osgood curve $\varepsilon^{tot} = \frac{\sigma}{E} + \alpha\left(\frac{\sigma}{\sigma_{yo}}\right)^n$, where n is material strain-hardening exponent and it is equal to n= 2,821670429, which controls the hardening of the material for cyclic loading, biaxial in the upper surface of the clamped beam in the horizontal and vertical direction (100 increments) with magnitude of $P_z=1000\text{KN}=P_y$ at its centre of the beam and cyclic loading of $P_z=1000\text{KN}=P_y$ at its centre of the beam with 4*100 increments for three different numerical damping (amplitude decay factor), where it is concluded that in cyclic loading mainly we observe that there is a convergence in critical loading and the behavior of the constitutive law where there is difference in the duration of reverse loading and reverse unloading between MSolve and Ansys (17%).

Finally, it is worth recalling some considerations concerning the possible numerical dissipation produced by the algorithm. As long as the method is stable, $\gamma = \frac{1}{2}$ implies no numerical dissipation for physically undamped Newmark methods, whereas for $\gamma \geq \frac{1}{2}$ numerical dissipation is introduced reducing accuracy to first order. When parameters β and γ assume values 0.3025 and 0.6 respectively, the method is said to be damped.

- ix. For the case of Kavvadas clays yield criterion we have: the description and evaluation for a critical-state incremental-plasticity model for structured soils (MSS). The model simulates the engineering effects of processes causing structure development (pre-consolidation, ageing, cementation, etc.) and structure degradation (remoulding by volumetric and/or deviatoric straining), such as high stiffness and strength at the intact states, appreciable reduction of stiffness and strength during de-structuring, and the evolution of stress-induced and structure-induced anisotropy. A novel feature of the model is the treatment of pre-consolidation as a structure-inducing process and the unified description of all such processes via the BSE. The proposed model distinguishes the concepts of 'yielding' (i.e. the onset of irreversible deformation upon reaching the PYE) and the onset of major de-structuring which occurs when the BSE is engaged. Thus, the model avoids the large elastic domain of critical state models and permits the development of irreversible strains even for small variations of the stress levels. Other features of the MSS model include (a) a general-purpose damage-type mechanism which can model the structure degradation induced by volumetric and deviatoric strains (b) stress- and

bond-induced anisotropy as well as memory of the stress history, achieved by recording the offset of the two model surfaces from the isotropic axis-these characteristics are gradually erasable (fading memory) as the surfaces move and the material state adapts to more recent stressing (c) formulation in a tensorial space consisting of the isotropic axis and the deviatoric hyper-plane -this formulation ensures the generality required for incorporation in finite element codes without losing the geometrical insight of the triaxial p-q plane, and it facilitates the modelling of shear strength anisotropy by decoupling the shear strength parameters in the various shearing modes (triaxial, plane strain, simple shear, etc.), thus permitting independent control of the shear strength in these modes (d) downward compatibility with the MCC model when all structural and anisotropic features are turned off - furthermore, these features can be turned on and off according to the type of the available test data, thus adapting the level of predictive sophistication to the available data.

- x. Load Displacement Curve and Comparison with Mohr Coulomb with $\phi=\psi=0$ which should be very close referring to the yield surfaces. (Max Relative Divergence from Ansys 0.86% for monotonic loading.
- xi. Load Displacement Curve. (Max Relative Divergence from Ansys is about ~1%) for cyclic loading in the upper surface of the box in the vertical direction (100 Nonlinear increments/path total 400 increments) with Load-Unload-Reverse load-Reverse unload path.

To summarize that, for all the three cases that we examined, it was concluded that: Essentially, we had a verification and validation of the correctness of the results for all cases of nonlinear material hardening of all constitutive laws that are studied in this master thesis for both monotonic and cyclic loading case.

Exactly similar results were obtained through MSolve, which means that identification and absolute convergence of the results were achieved.

CHAPTER 7th

7 APPENDIX

7.1 CATALOGUE OF FIGURES

2.1.2.1	Απεικόνιση της υψηλής θερμικής αγωγιμότητας του CNT	11
2.1.2.2	Μετρήσεις θερμικής χωρητικότητας(θερμοχωρητικότητας) με θερμοκρασίες έως 12K	13
2.1.2.3	Μετρήσεις θερμικής αγωγιμότητας σε μεγαλύτερες θερμοκρασίες(0,400)K..	14
2.1.2.4	Νανოსωλήνας (συνεχής γραμμή), 2-D φύλλο γραφενίου (διακεκομμένη γραμμή με βούλα) και 3-D γραφίτη (διακεκομμένη γραμμή)	14
2.1.2.5	Θερμική αγωγιμότητα πολυφλοϊικού νανοςωλήνα	15
3.1.1.1	Γεωμετρικά χαρακτηριστικά του δισδιάστατου μοντέλου	35
3.1.2.1	Απεικόνιση των συνοριακών συνθηκών του προβλήματος	36
3.1.2.2	Μεταβολή του επιβαλλόμενου φορτίου συναρτήσει του χρόνου	37
3.1.2.3	Μεταβολή επιβαλλόμενης θερμοκρασιακής κατανομής συναρτήσει του χρόνου	37
3.1.2.4	Συνοριακές συνθήκες της κατασκευής στην πρώτη περίπτωση που εξετάστηκε με την επιβαλλόμενη θερμοκρασιακή μεταβολή στο κάτω τμήμα	38
3.1.2.5	Συνοριακές συνθήκες της κατασκευής στην δεύτερη περίπτωση με την εφαρμογή της θερμοκρασιακής κατανομής στο άνω όριο της	38
3.2.1.2.1	Μεταβολή της ειδικής θερμότητας του χάλυβα συναρτήσει της θερμοκρασίας	40
3.2.1.3.1	Μεταβολή της θερμικής αγωγιμότητας του χάλυβα συναρτήσει της θερμοκρασίας	41
3.2.1.4.1	Διάγραμμα μεταβολής του μέτρου ελαστικότητας (E) του χάλυβα σε σχέση με την αύξηση της θερμοκρασίας	42
3.2.1.4.2	Χαρακτηριστικό διάγραμμα τάσεων – παραμορφώσεων του χάλυβα και καμπύλωση του διαγράμματος υπό την έκθεση χάλυβα σε υψηλές θερμοκρασίες	43
3.2.1.4.3	Διάγραμμα τάσης – παραμόρφωσης χάλυβα S275 για διάφορες τιμές της θερμοκρασίας	43
3.4.1	Αρίθμηση των κόμβων του βασικού τριγωνικού πεπερασμένου στοιχείου και οι βαθμοί ελευθερίας του(TRIA 3)	47
3.4.2	Λεπτομέρεια του πλέγματος των πεπερασμένων στοιχείων στη διεπιφάνεια f, από τη δεύτερης έως την έκτη ανάλυση της κατασκευής	49

4.1.5.1 Συγκεντρωτικό διάγραμμα κατακόρυφου φορτίου – θερμικής αγωγιμότητας τη χρονική στιγμή $t = 60 \text{ sec}$	85
4.1.5.2 Συγκεντρωτικό διάγραμμα κατακόρυφου φορτίου – θερμικής αγωγιμότητας τη χρονική στιγμή $t = 200 \text{ sec}$	85
4.1.5.3 Συγκεντρωτικό διάγραμμα κατακόρυφου φορτίου – θερμικής αγωγιμότητας τη χρονική στιγμή $t = 400 \text{ sec}$	86
4.1.5.4 Συγκεντρωτικό διάγραμμα κατακόρυφου φορτίου – θερμικής αγωγιμότητας τη χρονική στιγμή $t = 600 \text{ sec}$	86
4.2.1 Διάγραμμα φορτίου – θερμικής αγωγιμότητας της τρίτης ανάλυσης f_3 των περιπτώσεων θερμικής φόρτισης που μελετήθηκαν, τη χρονική στιγμή $t = 60 \text{ sec}$	87
4.2.2 Διάγραμμα φορτίου – θερμικής αγωγιμότητας της τέταρτης ανάλυσης f_4 των περιπτώσεων θερμικής φόρτισης που μελετήθηκαν, τη χρονική στιγμή $t = 60 \text{ sec}$	87
4.2.3 Διάγραμμα φορτίου – θερμικής αγωγιμότητας της πέμπτης ανάλυσης f_5 των περιπτώσεων θερμικής φόρτισης που μελετήθηκαν, τη χρονική στιγμή $t = 60 \text{ sec}$	88
4.2.4 Διάγραμμα φορτίου – θερμικής αγωγιμότητας της έκτης ανάλυσης f_6 των περιπτώσεων θερμικής φόρτισης που μελετήθηκαν, τη χρονική στιγμή $t = 60 \text{ sec}$	88
4.2.5 Διάγραμμα φορτίου – θερμικής αγωγιμότητας της τρίτης ανάλυσης f_3 των περιπτώσεων θερμικής φόρτισης που μελετήθηκαν, τη χρονική στιγμή $t = 200 \text{ sec}$	89
4.2.6 Διάγραμμα φορτίου – θερμικής αγωγιμότητας της τέταρτης ανάλυσης f_4 των περιπτώσεων θερμικής φόρτισης που μελετήθηκαν, τη χρονική στιγμή $t = 200 \text{ sec}$	89
4.2.7 Διάγραμμα φορτίου – θερμικής αγωγιμότητας της πέμπτης ανάλυσης f_5 των περιπτώσεων θερμικής φόρτισης που μελετήθηκαν, τη χρονική στιγμή $t = 200 \text{ sec}$	90
4.2.8 Διάγραμμα φορτίου – θερμικής αγωγιμότητας της έκτης ανάλυσης f_6 των περιπτώσεων θερμικής φόρτισης που μελετήθηκαν, τη χρονική στιγμή $t = 200 \text{ sec}$	90
4.2.9 Διάγραμμα φορτίου – θερμικής αγωγιμότητας της τρίτης ανάλυσης f_3 των περιπτώσεων θερμικής φόρτισης που μελετήθηκαν, τη χρονική στιγμή $t = 400 \text{ sec}$	90
4.2.10 Διάγραμμα φορτίου – θερμικής αγωγιμότητας της τέταρτης ανάλυσης f_4 των περιπτώσεων θερμικής φόρτισης που μελετήθηκαν, τη χρονική στιγμή $t = 400 \text{ sec}$	91
4.2.11 Διάγραμμα φορτίου – θερμικής αγωγιμότητας της πέμπτης ανάλυσης f_5 των περιπτώσεων θερμικής φόρτισης που μελετήθηκαν, τη χρονική στιγμή $t = 400 \text{ sec}$	91
4.2.12 Διάγραμμα φορτίου – θερμικής αγωγιμότητας της έκτης ανάλυσης f_6 των περιπτώσεων θερμικής φόρτισης που μελετήθηκαν, τη χρονική στιγμή $t = 400 \text{ sec}$	9

7.2 NOTATION

BSE	bond strength envelope
c (or c_i)	eccentricity of the BSE and the PYE
dot (over a symbol)	infinitesimal increment of this quantity
e	void ratio
e (superscript)	elastic component of strain
G/K	elastic shear parameter in poro-elasticity
F	function of the BSE
f	function of the PYE
H	elasto-plastic modulus
I	unit second-order tensor
OCR	overconsolidation ratio
p (superscript)	plastic component of strain
PYE	plastic yield envelope
q	scalar stress deviator
R	auxiliary scalar quantity (defined in Appendix 2)
s	tensorial stress deviator
S_i	deviatoric stress components
T	auxiliary scalar quantity (defined in Appendix 2)
α	size of the BSE
α^*	elastic shear parameter in hyper-elasticity
γ	parameter controlling the variation of the elasto-plastic modulus (H)
Δu	excess pore pressure
ε	strain tensor
ε_v	volumetric strain
ε_q	scalar deviatoric strain
$\xi_v, \eta_v, \xi_q, \eta_q$	volumetric and deviatoric structure degradation parameters
θ_q	steady-state deviatoric structure degradation/hardening parameter
κ	poro-elastic compressibility
κ^*	hyper-elastic compressibility
λ	intrinsic compressibility
σ, p	mean effective stress
σ_{vmax}	maximum vertical pre-consolidation pressure
σ_{vo}	vertical consolidation pressure
σ	effective stress tensor
σ_K	coordinates of the centre of the BSE in the stress space
σ_L	coordinates of the centre of the PYE in the stress space
ξ	ratio of the sizes of the BSE and PYE
(χ, ψ)	parameters controlling the evolution of material anisotropy

CHAPTER 8th

8 REFERENCES

- [1] Addessi D., Ciampi V. (2007). "A regularized force based beam element with a damageplastic section constitutive law Int J Numer Methods Eng, 70(5), pp. 610629.
- [2] A. H. Buchanan, "Structural Design for Fire Safety", Wiley, Chichester, England, New York, 2001.
- [3] Almeida J.P., Das S., Pinho R. (2012). "Adaptive forcebased frame element for regularized softening response." Computers & Structures, 102103:113.
- [4] Bairan, G.J.M. and Mari, A.R. Shear-Bending-Torsion Interaction in Structural Concrete Members: A Nonlinear Coupled Sectional Approach. Arch Comput Methods Eng 2007; 14(249–278).
- [5] Ceresa, P., Petrini, L. and Pinho, R. Flexure-shear fiber beam-column elements for modeling frame structures under seismic loading - State of the art. Journal of Earthquake Engineering 2007; 11(46–88).
- [6] Ciampi, V., Carlesimo, L. (1986) A nonlinear beam element for seismic analysis of structures 8-th European Conf Earthquake Engrg Lisbon, 6.3/1986:73-80.
- [7] Coleman, J. and Spacone, E. Localization issues in force-based frame elements. J. Struct Eng 2001; 127(1257–1265).
- [8] De Borst, R. (1991) The zero-normal-stress condition in plane-stress and shell elastoplasticity Commun Appl Num Meth 1991; 7(29– 3).
- [9] Dvorkin, E. Pantuso, D. and Repetto, E. A formulation for the MITC4 shell element for finite strain elasto-plastic analysis. Comput Methods Appl Mech Eng 1995; 125(17–40).
- [10] EA de Souza Neto, Prof. D Periaë, Prof. DRJ Owen - Computational Methods for Plasticity Theory and Applications- Wiley (2009).
- [11] Eurocode 2, Design of Concrete Structures – Part 1-2: General Rules– Structural Fire Design, EN 1992 -1 -2, December 2004.
- [12] European Committee for Standardisation. Eurocode 2 (EC2) Design of Concrete Structures - Part 1: General Rules and Rules for Buildings 2000; Brussels, Belgium.
- [13] Filippou, F.C., Popov, E.P. and Bertero, V.V. (1983). "Effects of bond deterioration on hysteretic behavior of reinforced concrete joints." Report No. UCB/EERC-83/19, University of California,

- Berkeley.
- [14] Fragiadakis, M. (2001). "Nonlinear Material Modelling of Reinforcement Steel Bars Under Transient Loading", MSc Dissertation, Department of Civil Engineering, Imperial College London, UK.
 - [15] Karsan, I.D. and Jirsa, J.O. (1969). "Behaviour of Concrete under Compressive Loadings." *Journal of the Structural Division, ASCE* 95.
 - [16] Kavvadas, M. & Amorosi, A. (2000). *Geotechnique* 50, No. 3, 263-273
 - [17] Kent, D.C. and Park, R. (1971). "Flexural members with confined concrete." *Journal of Structural Division, ASCE* 97: 1964–1990.
 - [18] Klinkel S. and Govindjee S. Using finite strain 3D-material models in beam and shell elements. *Eng. Comput.* 2002; 19(902–921).
 - [19] Madas, P. and Elnashai, A.S. (1992). "A new passive confinement model for the analysis of concrete structures subjected to cyclic and transient dynamic loading." *Earthquake Engineering and Structural Dynamics*, 21: 409-431.
 - [20] Mander, J.B., Priestley, M.J.N. and Park, R. (1988), "Theoretical stress-strain model for confined concrete." *Journal of Structural Engineering, ASCE*, 114(8): 1804-1826.
 - [21] Marini, A. and Spacone, E. Analysis of reinforced concrete elements including shear effects. *ACI Struct. J.* 2006; 103(645–655).
 - [22] Menegotto, M. and Pinto, P.E. (1973) "Method of analysis for cyclically loaded RC plane frames including changes in geometry and nonelastic behavior of elements under combined normal force and bending", *Proc. IABSE Symposium, Lisbon, Portugal*.
 - [23] Mistakidis, E.S. and Panagouli, O.K. (2002), 'Strength evaluation of retrofit shear wall elements with interfaces of fractal geometry', *Engineering Structures*, Vol.24, pp. 649-659.
 - [24] Navarro, G.J., Miguel, S.P., Fernandez, P.M.A and Flippou, F.C. A 3D numerical model for reinforced and prestressed concrete elements subjected to combined axial, bending, shear and torsion loading. *Eng Struct* 2007; 29(3404–3419).
 - [25] Neuenhofer, A. and Filippou, F.C. Evaluation of nonlinear frame finite-element models. *J Struct Eng* 1997; 123(958-966).
 - [26] Papachristidis, A., Fragiadakis, M. and Papadrakakis, M. (2010). "A high performance shear-deformable fiber beam-column element for inelastic analysis", *Computational Mechanics*, 45:553–572.
 - [27] M. Papadrakakis, «Ανάλυση Φορέων με τη Μέθοδο των Πεπερασμένων Στοιχείων», Εκδόσεις Παπασωτηρίου, Αθήνα 2001.
 - [28] Petrangeli, M., Pinto, P.E., Ciampi, V. "A Fibre Element fir cyclic bending and Shear. I: Theory." *ASCE J Struct Eng* 1999; 125:994–1001.
 - [29] Petrangeli, M. and Ciampi, V. Equilibrium based iterative solutions for the non-linear beam problem. *Int J Numer Methods Eng* 1997; 40:423–437.

- [30] Ramberg R., Osgood W.R., Description of stress-strain curve by three parameters, Technical note. 902, NACA July 1943.
- [31] Saritas, A. and Filippou, F.C. (2004) Modelling of Shear Yielding Members for Seismic Energy Dissipation. Proceedings of the 13th World Conference on Earthquake Engineering, Vancouver, BC, Canada.
- [32] Scott H.M. and Hamutcuoglu O.M. (2008). "Numerically consistent regularization of forcebased frame elements." International Journal for Numerical Methods in Engineering, 76(10): 16121631.
- [33] Scott, B.D., Park, R. and Priestley, M.J.N. (1982). "Stress-strain behavior of concrete confined by overlapping hoops at low and high strain rates." ACI Journal, 79: 13–27.
- [34] Sheikh, S.A, Uzumeri, S.M. (1980). "Strength and ductility of tied concrete columns".Journal of Structural Division, ASCE 106(ST5): 1079–1102.
- [35] Spacone, E., Ciampi, V. and Filippou, F.C. Mixed formulation of nonlinear beam element. Comput Struct 1996; 58(71–83).
- [36] Spacone, E, Filippou, F.C. and Taucer, F.F. Fibre beam-column model for non-linear analysis of R/C frames: Part I. Formulation. Earthquake Eng Struct Dyn 1996; 25(711–725).
- [37] Stanton J.F., Mc Niven H.D. (1979). "The Development of a Mathematical Model to Predict the Flexural Response of Reinforced Concrete Beams to Cyclic Loads, Using System Identification", Earthquake Engineering Research Center, Report No EERC 79-2, Univ. of California, Berkeley
- [38] Vecchio, F.J. and Collins, M.P. Modified Compression-Field Theory For Reinforced Concrete Elements Subjected To Shear. ACI J 1986; 83:219–231.
- [39] Whitehouse, David (2012). Surfaces and their Measurement. Boston: Butterworth-Heinemann.
- [40] Yovanovich, M.M. & Anntonetti, V.W. (1988), Application of thermal contact resistance theory to electronic packages, in Bar-Cohen, A. & Kraus, A.D. (Eds), Advances in Thermal Modeling of Electronic Components and Systems, Chapter2. Vol.1, Hemisphere, New York, pp. 79-128.
- [41] Zeris, C.A. and Mahin, S. (1988) "Analysis of reinforced concrete beam-columns under uniaxial excitation" ASCE J Struct Eng 1988; 114:804–820.